Molecular mechanisms of the pressure-activation of Mrr, a Type IV restriction endonuclease, and induction of SOS response in Escherichia coli

Anaïs Bourges

▶ **To cite this version:**

Anaïs Bourges. Molecular mechanisms of the pressure-activation of Mrr, a Type IV restriction endonuclease, and induction of SOS response in Escherichia coli. Agricultural sciences. Université Montpellier, 2018. English. NNT : 2018MONTT051 . tel-01988126

HAL Id: tel-01988126
https://theses.hal.science/tel-01988126

Submitted on 21 Jan 2019

HAL is a multi-disciplinary open access archive for the deposit and dissemination of scientific research documents, whether they are published or not. The documents may come from teaching and research institutions in France or abroad, or from public or private research centers.

L'archive ouverte pluridisciplinaire **HAL**, est destinée au dépôt et à la diffusion de documents scientifiques de niveau recherche, publiés ou non, émanant des établissements d'enseignement et de recherche français ou étrangers, des laboratoires publics ou privés.

THÈSE POUR OBTENIR LE GRADE DE DOCTEUR DE L'UNIVERSITÉ DE MONTPELLIER

En Biophysique

École doctorale Sciences Chimiques et Biologiques pour la Santé

Unité de recherche Centre de Biochimie Structurale

Molecular mechanisms of the pressure-activation of Mrr, a Type IV restriction endonuclease, and induction of SOS response in *Escherichia coli*

Présentée par Anaïs BOURGES

Le 28 septembre 2018

Sous la direction de Nathalie DECLERCK

Devant le jury composé de

Dr Nathalie DECLERCK, Centre de Biochimie Structurale	Directrice
Dr Silvia ZORRILLA LOPEZ, Centro de Investigationes Biológicas	Rapporteur
Dr Benjamin EZRATY, Institut de Microbiologie de la Méditerranée	Rapporteur
Dr Edouard BERTRAND, Institut de Génomique Moléculaire de Montpellier	Président du Jury
Dr Julie PERROY, Institut de Génomique Fonctionnelle	Examinatrice
Dr Catherine ROYER, Rensselaer Polytechnic Institute	Marraine de thèse

UNIVERSITÉ DE MONTPELLIER

Table of contents

Acknowledgements

First of all, I would like to thank my supervisors: the official advisor Nathalie Declerck and the non-official Catherine Royer. I want to thank them both for their expertise in many domains and their support. It was a great opportunity that Cathy gave me to stay in her group for my thesis as a visiting scholar, after my Master 2 internship, which I could not refuse. She gave me the opportunity to present my works 3 years in a row at the Biophysical Society meeting as well as in Washington for the Deep Carbon Observatory meeting where I learned a lot about difficulties to study piezophilic organisms. Nathalie has been very helpful with always a lot of good ideas for the project and a lot of enthusiasm for the results.

I would like to thank Cathy's group (Savanna Dorsey, Martin Fossat, Kelly Jenkins, Siwen Zhang, Yi Zhang, Harish Balasubramanian xxv and Labe Black and my students) especially Martin Fossat who helped with the pressure part of my project and the organization of the lab during installation, and Savanna Dorsey. Savanna was a great labmate, officemate, roommate but more importantly a friend. It was great to spend all these years with her through all the good moments but also the hard times away from home. We shared our knowledge to progress in our respective projects and spend a lot of time dealing with our microscope in the dark.

I am also grateful for all the help I received during the summer at the CBS in particular from Angélique De Visch.

A special gratitude goes to all the people who help me in this project and to our collaborators of the Abram Aersten group, to the comity members of my PhD and to my jury especilally the two reviewers who have agreed to read this work. The Sloan Foundation provided part of the funding for this work, as well as the Rensselaer Polytechnic Institute and Pressure Bioscience which provided us with pressure equipment.

I would like to thank the French team, Mathieu and Damien, for their moral support far away from our country. I am also grateful to all the people I met in Troy especially the group of girls and my good friends/old roommates Katharina and Kathleen.

Finally, I would like to thank my parents, my sister Alizée, my brother Théophile and my friends who have supported me along the way. Delphine was a great moral support even though we were far away, we had great moments abroad each summer (your turn is coming soon!).

Thank you for all your encouragement!

Abstract/Resumé

The pressure encountered by organisms on Earth varies from the atmospheric pressure (0.1 MPa) to 110 MPa. Although *Escherichia coli* is not naturally resistant to high pressure, it is capable of acquiring pressure resistance and withstanding a pressure shock up to 2 GPa. When exposed to a sub-lethal pressure shock (100 MPa) *E. coli* induces a SOS response due to DNA double strand breaks, although pressure itself cannot generate such DNA damage. Genetic screens for pressure-resistant mutants have revealed that a Type IV restriction endonuclease, Mrr is the only factor responsible for DNA cleavage under pressure. This enzyme targets only methylated DNA and expression of a foreign methyltransferase, M.HhaII, is also capable of inducing an SOS response in strains harboring Mrr. Here, we demonstrate using fluorescence fluctuation microscopy techniques *in vivo* and *in vitro* that Mrr is present as a tetramer in unstressed cells and that pressure dissociates Mrr into active dimers that can bind DNA and cleave at some cryptic sites. In contrast, the M.HhaII MTase pulls the Mrr tetramer-dimer equilibrium to the dimer-bound DNA form probably due to the methylation of many high-affinity sites. Mutational analysis together with a 3D homology model of full-length Mrr suggests the probable structural basis for the switch from an inactive tetramer to an active dimer. We set up a system that allows microscopy experiments (*in vitro* and *in vivo*) under pressure and preliminary results have confirmed our model of Mrr activation.

Sur Terre les organismes vivants sont soumis à des pressions pouvant varier de la pression atmosphérique (0.1 MPa) à plus de 100 MPa. Bien que la bactérie Escherichia coli ne soit pas naturellement résistante aux fortes pressions, elle est capable de s'y adapter et de supporter un choc barotraumatique jusqu'à 2 GPa. L'exposition d'E. coli à un choc de pression sub-létal (100 MPa) induit une réponse SOS suite à l'apparition de coupures double brin dans l'ADN, bien que la pression elle-même ne soit pas capable de générer de telles lésions. Des criblages génétiques ont permis d'identifier le gène mrr codant pour une endonucléase de restriction de type IV comme seul facteur responsable du clivage de l'ADN à haute pression. Mrr cible uniquement l'ADN méthylé et son activité peut être aussi fortement stimulée en présence de méthylases (MTase) étrangères telles que M.HhaII de Haemophilus haemolyticus. Ici, nous démontrons en utilisant des techniques de microscopie de fluctuation de fluorescence, in vivo et in vitro que Mrr est présente sous la forme d'un tétramère dans les cellules non stressées et que la pression dissocie Mrr en un dimère capable de lier et cliver l'ADN au niveau de sites cryptiques. En revanche, l'induction de la MTase HhaII déplace l'équilibre tétramère-dimère vers la forme dimérique de Mrr interagissant plus efficacement avec l'ADN sur-méthylé. La caractérisation de mutants ainsi que la construction d'un modèle 3D de Mrr nous permettent de proposer le mécanisme structural de conversion du tétramère inactif en un dimère actif. Un système de microscopie bi-photonique sous pression a récemment été mis en place et les expériences préliminaires réalisées in vitro et in vivo confirment notre modèle d'activation de Mrr par la pression ou sur-méthylation de l'ADN.

List of figures

List of tables

Résumé

La vie sur Terre peut être soumise à des conditions extrêmes de pression, de température, de pH ou de concentrations en sel. Les organismes qui vivent dans des conditions aussi hostiles ou même léthales pour la plupart des autres organismes sont appelés extrémophiles. Ils peuvent être divisés en deux catégories : ceux qui peuvent soutenir ces conditions et ceux qui en ont besoin pour croitre. Comprendre comment ces organismes peuvent survivre et s'adapter aux conditions extrêmes, et comment leurs processus biologiques sont affectés, est important pour les connaissances fondamentales sur l'émergence de la diversité de la vie, et pour l'exploitation de leurs propriétés remarquables.

Dans ce travail, nous nous intéresserons à l'adaptation aux hautes pressions. La pression subie par les organismes vivants sur Terre varie de 0,1 MPa (pression atmosphérique) à 110 MPa dans la fosse océanique des Mariannes (Challenger Deep). Les organismes piézophiles (adaptés à la pression) doivent avoir évolué pour survivre dans ces environnements hostiles où, en plus d'une pression élevée, ils doivent aussi faire face au manque de lumière et d'oxygène, au peu de nutriments et à des températures extrêmes, soit très basses (2-3 °C en moyenne) dans les eaux profondes ou très hautes comme à proximité des sources hydrothermales. Bien que l'organisme modèle *Escherichia coli* soit sensible à la pression, cette bactérie potentiellement pathogène peut acquérir des propriétés de piézotolérance lui permettant de résister à de fortes pressions. Ceci peut compromettre l'efficacité des procédés de stérilisation par la pression (pascalisation) de plus en plus utilisés dans l'industrie agro-alimentaire. Chez *E. coli* K12, l'acquisition de cette résistance fait intervenir le système SOS induit pour réparer les dommages à l'ADN. Le but de cette thèse est de comprendre le mécanisme moléculaire d'induction de la réponse SOS par la pression chez *E. coli*.

D'une manière générale, la réponse SOS est activée chez les bactéries par tout type de stress provoquant des lésions importantes de l'ADN. Ce système SOS joue un rôle majeur car il constitue une stratégie de survie dans des conditions qui peuvent conduire à la mort cellulaire. Les bactéries tentent de réparer leur génome à tout prix, y compris par l'inclusion de mutations dues aux erreurs des mécanismes de réparation. Ces modifications génèrent de la variabilité génétique et peuvent permettre l'émergence de variants mieux adaptés. Chez *E. coli,* il a été montré que l'induction de la réponse SOS suite à un choc de pression de 100 MPa est dépendante du complexe RecBCD, impliqué dans la recombinaison homologue en cas de cassures de l'ADN double brin. La pression seule ne pouvant pas être responsable de ces cassures, un autre facteur doit être responsable des dommages à l'ADN et l'induction de la réponse SOS. Le criblage de mutants résistants à la pression a permis d'identifier le gène *mrr*, codant pour une enzyme de restriction (ER) de type IV. Contrairement aux ERs conventionnelles, les ERs de type IV reconnaissent l'ADN méthylé avec une faible sélectivité de séquence et ne possèdent de méthyltransférase (MTase)

spécifique associée. Mrr est l'une des enzymes de restriction d'*E. coli* K12 responsable du clivage d'ADN étranger entrant dans les cellules, réduisant fortement l'efficacité de clonage d'ADN hétérologues, en particulier l'ADN eucaryote fortement méthylé. Mrr restreint l'ADN modifié par diverses MTase méthylant des adénines ou des cytosines, mais aucune séquence consensus de reconnaissante n'a été déterminée à ce jour. L'expression dans *E. coli* K12 de MTase étrangères telles que M.HhaII d' *Haemophilus haemolyticus* affecte la croissance cellulaire et provoque l'induction de la réponse SOS en présence du gène *mrr* fonctionnel. Il a été montré par A. Aersten de l'Université de Leuven que, comme dans le cas de la pression, le système de réparation SOS est activé en présence de M.HhaII suite aux cassures d'ADN double brin générées par Mrr.

En collaboration avec le groupe d'A. Aersten, nous avons entamé la caractérisation à la fois *in vivo et in vitro* de la protéine Mrr afin de comprendre son mécanisme d'activation par la pression ou la méthylation de l'ADN par la MTase HhaII. Des études par microscopie classique de fluorescence ont été réalisées au laboratoire d'A. Aertsen avec des souches d'*E. coli* contenant un plasmide réplicatif permettant la surexpression de la protéine Mrr fusionnée à la GFP. Ces études ont fourni d'importantes informations sur la localisation de Mrr et son interaction avec le nucléoïde bactérien au cours du processus d'activation, révélant l'apparition de foci intenses associés à l'ADN condensé. Afin d'obtenir des données quantitatives sur le comportement de Mrr à des concentrations plus proches des conditions physiologiques, j'ai réalisé des expériences de microscopie bi-photonique au laboratoire de C. Royer à RPI (Troy, NY) aux Etats-Unis. J'ai notamment utilisé une méthode reposant sur l'analyse des fluctuations d'intensité de fluorescence, le *scanning Number and Brightness* (sN&B). Cette technique très sensible permet de mesurer directement dans des cellules vivantes les valeurs spatialement résolues de la concentration absolue de molécules fluorescentes et de leur brillance moléculaire. J'ai appliqué cette méthode pour caractériser la protéine GFP-Mrr exprimée à partir d'un gène de fusion intégré dans le chromosome bactérien. Ceci m'a permis notamment de mettre en évidence un changement de l'état oligomérique de la protéine après un choc de pression ou l'induction de M. HhaII. En parallèle j'ai entrepris au CBS à Montpellier la purification de la protéine GFP-Mrr ainsi que plusieurs mutants affectés dans le processus d'activation par pression ou sur-méthylation de l'ADN. Pour nous aider dans l'interprétation des résultats, nous avons construit un modèle par homologie de la structure tridimensionnelle de la protéine Mrr. Sur la base de ces résultats nous proposons un model structural du mécanisme d'activation de Mrr. Enfin, j'ai aussi mis en place un système de microscopie bi-photonique sous haute pression et j'ai pu tester ce système à la fois *in vitro* et *in vivo* pour observer le comportement de la protéine GFP-Mrr au cours d'un choc de pression.

L'ensemble de ce travail est détaillé essentiellement dans deux manuscrits, le premier ayant été publié dans la revue *Nucleic Acids Research* en 2017, le deuxième devant être soumis prochainement pour publication.

Manuscrit #1

L'activation de l'endonucléase de restriction Mrr par la pression chez *Escherichia coli* implique la dissociation de tétramères.

Résumé du manuscrit. Chez *Escherichia coli K12,* un choc sub-létal à haute pression hydrostatique (HP) d'environ 100 MPa déclenche le système SOS de réparation de l'ADN RecA-dépendant, bien que la pression ne puisse compromettre l'intégrité covalente de l'ADN. Le criblage de mutants a permis d'identifier Mrr (*methylated adenine recognition and restriction*), une endonucléase de restriction de type IV, comme étant responsable des cassures d'ADN double brin conduisant à la réponse SOS induite par la pression. Cette enzyme cible de manière peu spécifique des sites d'ADN méthylés, et son activité est fortement augmentée dans des souches d'*E. coli* exprimant la méthyltransférase (MTase) de type II M.HhaII. Dans ce travail, nous avons mesuré la concentration et la stœchiométrie de la protéine de fusion GFP-Mrr fonctionnelle en utilisant des techniques de microscopies de fluctuations d'intensité de fluorescence *in vivo*. Nos résultats démontrent que dans des cellules non stressées Mrr est un tétramère, qui devient dimérique après un choc HP ou la co-expression de M.HhaII. La comparaison de la protéine sauvage et d'un mutant catalytique a montré des différences dans la réversibilité de la dissociation du tétramère après un choc de pression ou l'induction de M.HhaII. Sur la base de ces résultats nous proposons un modèle selon lequel (i) la pression déclenche l'activité de Mrr en dissociant les tétramères inactives en dimères actifs, tandis que (ii) M.HhaII stimule l'activité de Mrr en créant des sites cibles de haute affinité sur le chromosome, déplaçant l'équilibre vers le dimère actif.

Manuscrit #2

Bases structurales du couplage entre oligomérisation et catalyse de l'endonucléase Mrr

Nous avons utilisé la même approche que celle développée dans le premier article pour caractériser des variants de GFP-Mrr affectés dans leur réponse à un choc HP et/ou à l'induction de la MTase HhaII. Ces mutants ont été isolés et caractérisés précédemment par nos collaborateurs du laboratoire d'A. Aertsen par microscopie conventionnelle utilisant des vecteurs d'expression inductibles plasmidiques. Ici, en utilisant la microscopie bi-photonique et la méthode d'analyse sN&B, nous avons comparé les protéines GFP-Mrr sauvage ou mutantes exprimées à très faible niveau à partir d'une insertion chromosomique et déterminé leur état oligomérique après exposition à un choc de pression ou la supra-méthylation de l'ADN chromosomique en présence de M.HhaII. Nous avons ensuite interprété nos données à la lumière d'un modèle structural du tétramère de Mrr inactif lié à l'ADN, réalisé en collaboration avec Gilles Labesse au CBS.

1. Introduction

Life on Earth can be subjected to extreme conditions of pressure, temperature, pH or salt concentrations (1, 2). Organisms that live in such hostile or even lethal conditions for most other organisms are called extremophiles. They can be divided into two categories: those which can support these conditions and those which require such conditions for survival. Understanding how these organisms can survive and adapt to extreme conditions and how their biological processes are adjusted is important not only for fundamental knowledge on the emergence of life diversity but also for potential exploitation of the remarkable properties of extremophiles. The study of the molecular basis of these mechanisms is called Extreme Biophysics. In this work, we will focus on high pressure.

Pressure encountered by living organisms on Earth varies from 0.1 MPa (atmospheric pressure) to 110 MPa in the Marianna trench (Challenger Deep). In spite of the very harsh conditions encountered in dark cold deep seas and hydrothermal vents, life forms with very high diversity have been discovered unexpectedly, probably thanks to the wide range of factors that can vary in such extreme environments (3, 4). In this chapter, some of the adaptive strategies developed by organisms living in the deep biosphere will be reviewed. Next, the model organism *Escherichia coli* (*E. coli*) will be discussed. This organism is sensitive to pressure but can resist high pressure shocks. Pressure affects many processes. Interestingly, in some strains of *E. coli*, pressure shock results in DNA damage that can compromise cell survival. In response to this stress, these strains of *E. coli* induce an SOS response which is essential for the adaptation and resistance of bacteria to pressure treatments used in some food processes (pascalization) (5). The purpose of this thesis is to understand the molecular mechanism of pressure-induced SOS response in *E. coli.*

1.1 Life under pressure

1.1.1 Pressure definition and units

Pressure is defined as a force per unit area applied perpendicularly to a surface. Two types of pressure stress can be distinguished: static (when the same pressure is maintained over a long time) and dynamic (when an important change of pressure is applied over a short time). For this work, we consider only the isostatic pressure (same pressure value applied in all directions) and more precisely hydrostatic pressure (in solution at pressure equilibrium). High pressure or high hydrostatic pressure will be called HP. The official pressure unit is Pascal (Pa) that corresponds to a force of 1 Newton (N) exerted on a surface of 1 m^2 (1 Pa=1 N/1 m2=10^{-5} bar). The hydrostatic pressure exerted by a water column of 1-meter height is 9.81 10^3 Pa. The Pascal is a very small pressure unit corresponding to about 1/100 000 of the atmospheric pressure on Earth at sea level. The MegaPascal (MPa)

is thus the usual unit in high pressure studies. Other commonly used pressure units are the Pound per Square Inch (PSI) in the US unit system (1 PSI=6895 N/M^2 or Pa), and the bar, mostly used in meteorology, equal to 0.1 MPa and close to the average atmospheric pressure (Table 1.1).

Table 1.1: Conversion of some units used for pressure (adapted from(6)).

	Atmosphere	**Bar**	**MPa**	**P.S.I.**
Atmosphere	1	0.987	9.901	0.068
Bar	1.013	1	10.000	0.069
MPa	0.101	1.021	1	0.00689
P.S.I.	14.696	14.504	145.038	1

1.1.2 The deep biosphere

Pressure is one of the thermodynamic parameters to which cells living in the oceans or under the earth's crust must adapt. Until the end of the 19th century, it was thought that the deep-sea environment was too extreme to support life (7). Improved equipment has allowed for proper sampling and study. In 1884, the French physiologist Regnard was the first to study the effect of pressure on living organisms (movement of various aquatic animals)(8). Since then, a large number of studies have addressed the effects of high pressure on biological systems and deep-sea organisms that must adapt to these extreme environments (2, 9, 10).

1.1.2.1 Definition

The deep biosphere (also termed piezosphere) was first defined by Jannasch and Taylor as oceanic waters below 1000 m, thus under a pressure exceeding 10 MPa (11) and was subsequently extended to all high pressure environments. It comprises more than half of the volume of the global biosphere (Figure 1.1). Indeed, oceans cover about 70% of the Earth's surface and have an average depth of 3800 m (38 MPa). The deep-sea piezosphere accounts for about 75% of the total ocean volume and hosts active and diverse biological communities (12). Life was also found in the subsurface of the earth's crust with a pressure up to 300 MPa (at 6.7 km inside the Earth's crust).

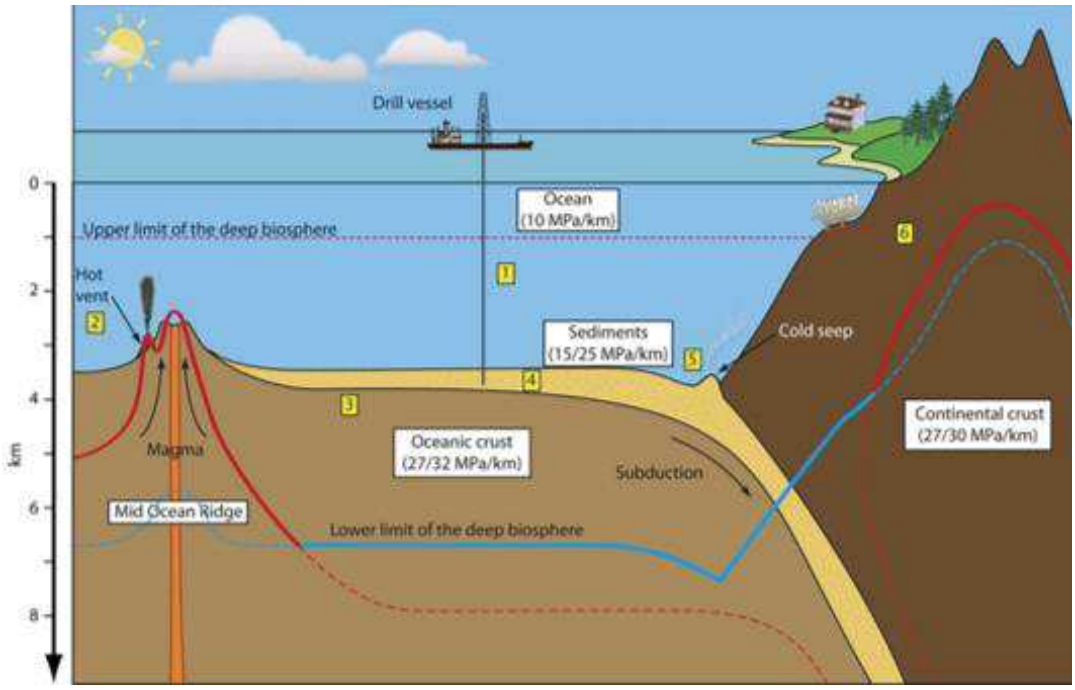

Figure 1.1: Schematic of a transversal section of the Earth. 1) deep-sea, 2) deep-sea hydrothermal vents, 3) deep oceanic crust, 4) sedimentary sub-seafloor, 5) deep-sea cold seep, 6) continental deep biosphere. The upper dashed red line symbolizes the 10 MPa arbitrary upper limit of the deep biosphere (from (13)).

Deep sea organisms must have evolved to survive in such hostile environments where besides high pressure, they also usually have to cope with the lack of sunlight and oxygen, scarce nutrients and extreme temperatures, either very low (with an average of 2-3 °C in deep waters) or very high temperatures, such as those in the vicinity of hydrothermal vents. Nevertheless, a wide variety of organisms inhabit the deep-biosphere, including the three kingdoms of life (bacteria, archaea and eukaryotes). The most significant process that takes place in the deep dark ocean is the use of chemosynthesis by micro-organisms instead of photosynthesis. Chemical oxidation, instead of light, is used as a source of energy for the biosynthesis of organic matter from CO_2 (9). Micro-organisms are very abundant and diverse in the deep biosphere, but their study is hampered by the fact that most of them cannot be cultivated in the laboratory. It is essentially thanks to the advent of genomics and metagenomics approaches that knowledge about the deep biosphere micro-flora has been acquired in recent years.

1.1.2.2 Piezophiles or pressure adapted organisms

First termed barophiles (14), piezophiles (from the Greek piezo=to press and philo=love) have optimal growth rates at pressure greater than atmospheric pressure and can survive up to about 100 MPa. Piezotolerant organisms have similar growth rates at atmospheric and high pressure but are not resistant to pressure exceeding 60 MPa.

Inversely, hyper-piezophiles or obligatory piezophiles are able to grow only at high pressure (Figure 1.2)(15).

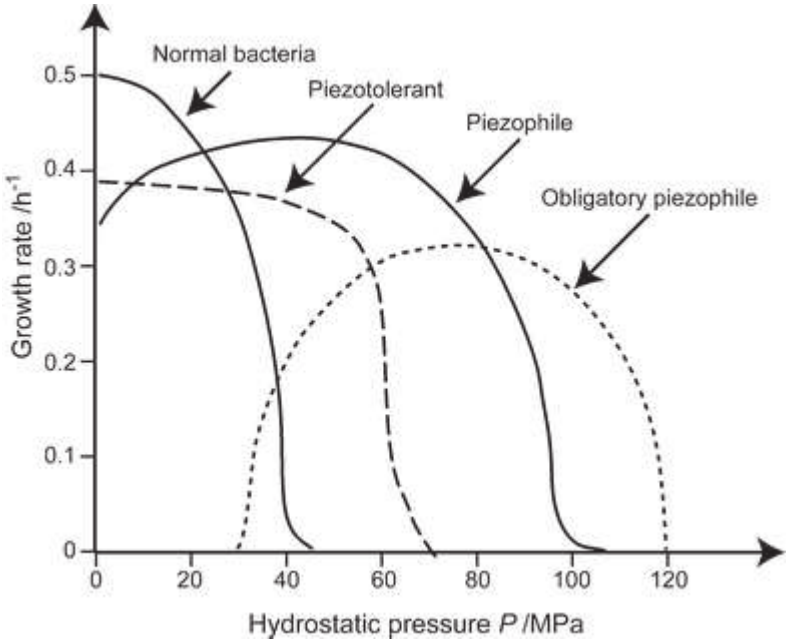

Figure 1.2: Relationship between growth rate of micro-organisms and pressure.The growth rate of bacteria decreases as pressure increases, while piezophiles grow optimally at high pressure (from (16)).

Most isolated piezo-adapted organisms are archaea from deep-sea hydrothermal vents and bacteria from cold deep-sea habitats (cold seeps). These latter are phylogenetically linked to psychrophilic bacteria from Antarctica able to grow at temperature close to 0°C, suggesting that the adaptation to high pressures derived from pre-existing adaptation to cold (17). Some deep-sea psychrophiles can grow at temperatures as low as -12°C (18). While the lower temperature limit is apparently set by the freezing temperature of intracellular water, the upper pressure limit for life is not known (19). Archaea from the *Pyrococcus* genus living in undersea hot vents are the most pressure resistant organisms discovered so far; they can survive at pressures up to 150 MPa with an optimal growth temperature of nearly 100°C (20). The large population of piezophilic prokaryotes plays an important role in the biogeochemical cycles of the global biosphere and their rapid growth allows a wide genetic diversity (21). They are considered as the most adaptive organisms that can survive in a variety of harsh environments (2).

1.1.3 Pressure effects on micro-organisms

Mesophilic micro-organisms that are not adapted to extreme conditions can rapidly suffer from an elevation of pressure, causing severe growth defects and eventually cell death. Indeed, macromolecular structures and their interactions are extremely pressure

sensitive, leading to the alteration of vital processes including cell motility, membrane fluidity and trafficking, DNA replication, cell division, protein synthesis and enzyme function (Figure 1.3)(22).

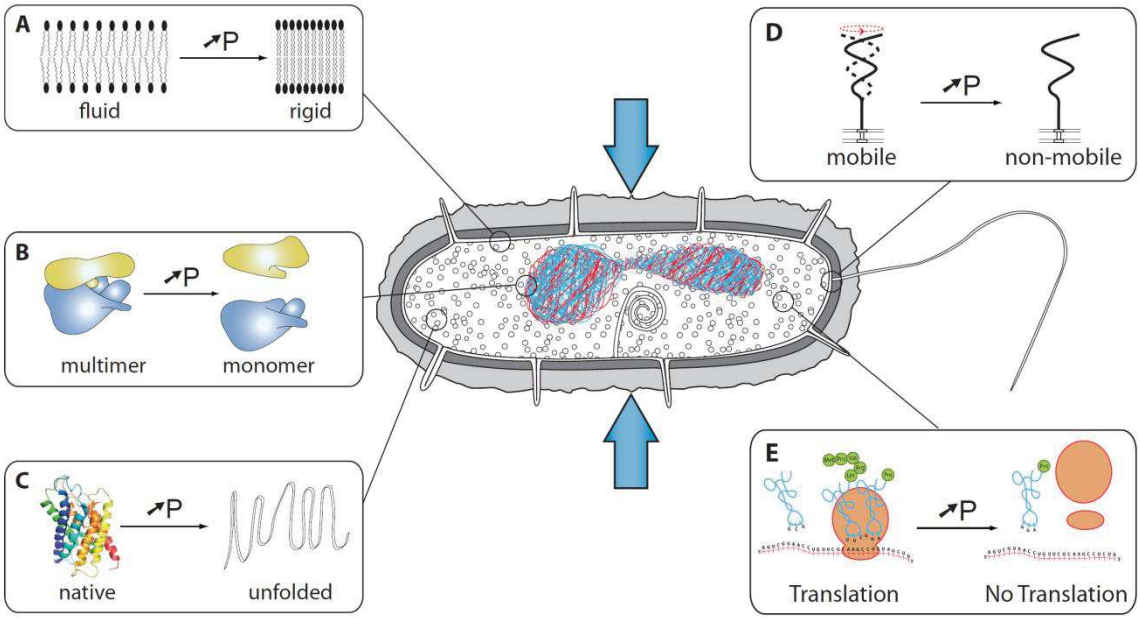

Figure 1.3: Effect of high pressure on cells and cellular components. A) lipids in membranes, B) multimeric protein assemblies, C) protein structure, D) cell motility and E) protein translation by ribosomes (from (13)).

1.1.3.1 Pressure adaptation of piezophiles

Life under pressure must either cope with or compensate for HP-induced perturbations of the many cellular functions mentioned above. Three adaptive mechanisms have been distinguished as strategies adopted by piezophilic organisms. The first one consists in tuning overall gene expression to compensate for the loss of biological activity. The second is the expression of specific genes involved in the resistance to pressure. The last one is a structural modification of biomolecules to sustain HP. Very few deep-sea micro-organisms have been studied in detail because of the problems inherent to their cultivation. A useful model organism for the study of life at HP is *Photobacterium profundum*, strain SS9 (SS9) and some of its pressure adaptation mechanisms will be presented in this section. This organism has the ability to grow over a wide range of pressure (0.1 to 90 MPa) with an optimal growth at 28 MPa and 15 °C, making it a moderate piezophile and psychrophile.

1.1.3.1.1 HP-dependent transcriptional tuning

Since the overall effect of pressure is to diminish the stability and hence activity of biomolecules, one way to overcome this reduction of activity is to increase the concentration of pressure-sensitive components. Indeed, transcriptomic studies in *E. coli* and yeast after exposure to sub-lethal HP shocks exhibit up-regulation of a large number of genes and operons involved in general cell metabolism, transport and signaling (23, 24). Interestingly, in the *P. profundum* strain SS9, decreasing pressure from the optimal growth pressure (28 MPa) to atmospheric pressure also leads to the up-regulation of most transport operons, metabolic enzymes, and signal sensing systems (25, 26). This indicates that in this moderately piezophilic organism, the transcriptome has been finely tuned for optimized activity at HP and that it is readjusted in response to pressure changes. Similarly, the proteome of the hyperthermophilic barophilic archaeon *Thermococcus barophilus* has been found to be highly pressure sensitive, with up to 378 genes being differently expressed in cells grown at sub- or supra- optimal pressure (40 MPa)(27).

1.1.3.1.2 Regulation of fatty acid membrane protein synthesis

To prevent the formation of gel-like membranes at low temperature and/or high pressure many deep-sea organisms modulate the fluidity of their lipid bilayers by adjusting their phospholipidic composition. Piezophiles and psychrophiles, do not produce specific lipids but rather increase the proportion of mono-unsaturated fatty acids which pack less tightly and thereby reduce the rigidity of the cell membranes (28, 29). Inversely, an increase in the proportion of saturated fatty acids that leads to more rigid membranes is observed in thermophilic micro-organisms living at high temperatures (30). Mutants of SS9 that produce less monounsaturated fatty acids are sensitive to pressure and sensitive to low temperatures (31). Deep-sea bacterial membranes also have a higher proportion of omega-3 polyunsaturated fatty acids that do not appear to contribute to piezo-adaptation, but are of interest because of reduced effects on the risk of human cardiovascular diseases (32). In addition to membrane lipids, some specific membrane proteins have been identified as being up-regulated under pressure. In SS9, the outer membrane porin-like protein OmpH is expressed at its highest level at 28 MPa, while the porin-like protein OmpL is preferentially expressed at ambient pressure (19, 33). These two genes are transcriptionally regulated by two proteins located in the inner membrane, ToxR and ToxS, a two-component system forming the only pressure sensor so far identified (34). Another documented example of HP specific gene expression is found in *Shewanella benthica*, a psychrophilic facultative piezophile which presents two different sets of respiratory chain components when growing at low or high pressure (35).

1.1.3.1.3 Piezo-stabilization of proteins

- By intrinsic factors

The fact that different proteins are produced in different pressure conditions suggests that structural adaptation of proteins takes place in piezophiles. However, compared to thermo-resistant proteins, there are so far very few studies demonstrating that proteins from piezophilic organisms are indeed more resistant to high pressure than their mesophilic counterparts (36), and the molecular features associated with the piezo-stabilization of protein structures are not yet clearly identified. So far, data point better packing to reduce the internal void volume as a likely feature of proteins that are more stable at HP.

One such studies is the comparison of the single-stranded DNA-binding (SSB) protein from 4 different strains of *Shewanella* with different pressure sensitivity (37). The dissociation of the SSB proteins by pressure monitored by fluorescence anisotropy have shown that the SSB proteins from the piezosentive strain were more sensitive to pressure than those from piezotolerant or deep-sea strains. The primary structure of the piezophilic SSB proteins contains significantly less glycine and proline residues that are known to be helix-destabilizing and helix-breaking residues, respectively. It was thus proposed that the piezophilic proteins are less flexible, making them less compressible (38) and possibly more stable (19). Indeed, it has been shown that a reduction in the flexibility of Staphylococcal nuclease chain (mutation of a proline to glycine) increases the stability of the protein under pressure (39).

- By extrinsic factors

In addition to modifying protein flexibility, extrinsic factors can have general protective properties against protein denaturation under extreme conditions. These include chaperone proteins and low molecular mass organic solutes (osmolytes) that accumulate in mesophilic organisms under stress conditions (33). The upregulation of genes encoding chaperone proteins has also been demonstrated in piezophiles. These proteins maintain the correct folding of proteins under pressure and at high temperature (13).

Osmolytes are small, highly soluble, charge-free molecules that do not disturb protein functions even at high concentrations. They play a favorable role on protein-solvent interactions by excluding water molecules from the surface of the proteins and thereby stabilize their structures. Marine animals and piezophiles show higher concentrations of different osmolytes such as trimethylamine-N-oxide (TMAO). The level of TMAO increases with depth in some deep-sea animals and helps to maintain the folding and function of proteins. In SS9, TMAO has been shown to act on substrate binding by decreasing the inhibitory effect of pressure. However, there are no such “piezolyte” (pressure-specific osmolyte) that would counteract the effect of high hydrostatic pressure on volume changes upon protein unfolding (40). Thus, the protein adaptation of piezophiles at HP seems to be secondary to their adaptations to both high and low temperatures (41).

1.1.3.2 Pressure effects on *E. coli*

E. coli is the model of Gram-negative bacteria. It is considered as a piezo-sensitive micro-organism although it has the ability to grow at pressures up to 50 MPa. Moreover, it can be evolved in test tube to survive pressure shocks up to 2 GPa (42). This makes *E. coli* an ideal model organism to investigate the effects of increased pressure on cellular processes and molecular structures.

1.1.3.2.1 Effect of HP on *E. coli* physiology

Cellular functions are differently affected when *E. coli* cells are abruptly exposed to increasing hydrostatic pressures (Table 1.2).

Table 1.2: Pressure sensitive processes detected in E. coli (adapted from (13)*).*

Process	Pressure abolishing process (MPa)	References
Motility	10	(43)
Substrate transport	26	(44)
Cell division	20-50	(45, 46)
Growth	50	(47)
DNA replication	50	(47)
Translation	60	(47, 48)
Transcription	77	(47)
Viability	200	(49)

Cell motility is one of the cellular processes most sensitive to pressure. A pressure of only 10 MPa affects cell motility by disrupting the polymerization and the rotation of the flagellar motor (43). Using a high-pressure cell implemented on a microscope, Nishiyama et al. showed that cell motility is completely abolished at 80 MPa and that above 120 MPa, the direction of rotation of the flagella filaments switches from counterclockwise to clockwise (50).

As noted above, lipid membranes are particularly exposed and sensitive to pressure. Perturbation of their properties directly interferes with many vital functions including nutrient transport and energy production. That is why they are considered as the main target of inactivation of micro-organisms by pressure (7), occurring below 30 MPa in the case of *E. coli*. As the pressure increases, the fluidity of the membranes decreases due to lipid compaction, which causes problems for the uptake of nutrients and cell signaling (51). Low temperatures have a similar impact on lipid bilayers, explaining why psychrophilic and piezophilic organisms adopt similar strategy to adapt their cellular membranes (39).

E. coli, like other mesophilic organisms, becomes filamentous under pressure, indicating that inhibition of cell division occurs before that of cell growth. Interestingly, piezophiles such as *P. profundum* SS9 filament when grown at pressure higher or lower than their optimum. Beyond pressure effects on DNA replication (see below), pressure has a direct impact on proteins involved in DNA segregation and in the formation of the division septum, in particular the tubulin homolog FtsZ. In *E. coli*, FtsZ forms a mid-cell ring structure (Z-ring) which is essential for the proper positioning of the septum and the division into two equal daughter cells. It was shown that the FtsZ polymers undergo dissociation *in vitro* at 50 MPa, presumably contributing to cell filamentation *in vivo*. This dissociation is reversible *in vitro* after decompression (52).

The growth rate of *E. coli* decreases with increasing pressure to a limit of about 50 MPa (Figure 1.4), a limit shared by many mesophilic organisms. This limit corresponds to a pressure where the synthesis of DNA is abolished (47). The initiation of DNA replication requires fluidization of the cell membrane and this could be the reason for the inhibitory effect of HP, although many other biochemical processes could be involved in or responsible for this pressure limit to growth.

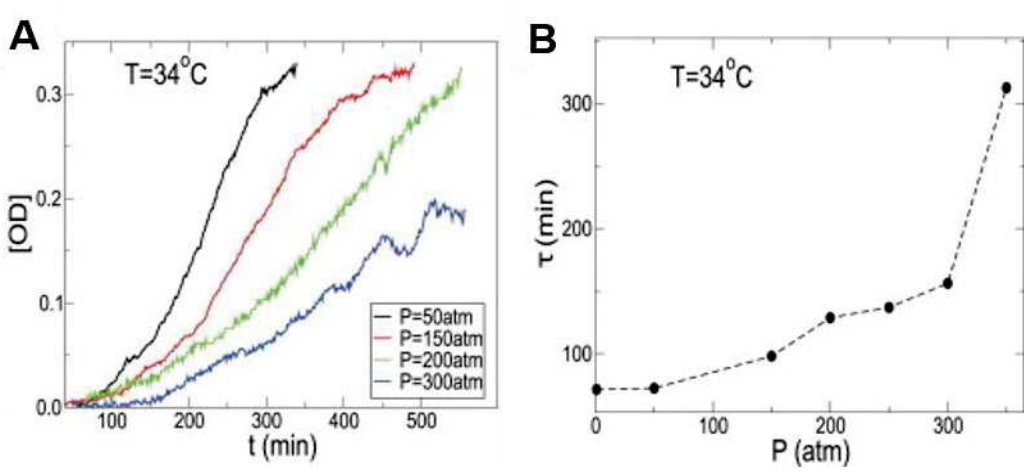

Figure 1.4: Effect of pressure on E. coli growth rate. A) Growth curves and B) doubling time of E. coli at increasing pressure (10 atm ~ 1 MPa) at 34°C (from (53).

The rate of protein synthesis decreases rapidly upon increasing hydrostatic pressure, although inhibition is reversible upon decompression. Dissociation of the ribosomal

subunits (70S -> 30S + 50S) observed *in vitro* (48, 54, 55) and *in vivo* (56, 57) seems to be the primary cause of the arrest of translation above 60 MPa, while transcription inhibition occurs 10 MPa above. The effect of HP on the structure of nucleic acids (see section 1.1.4.3) may also indirectly impact the efficacy of the transcription and translation processes (58).

Cell death occurs if pressure is further increased or maintained above 100 MPa over a long period of time. This appears to be mainly due to the disassembly of the ribosomal subunits and the arrest of protein synthesis. The bacterial cells survive until the amount of functional ribosomes decreases below a certain threshold that can no longer sustain vital cellular functions (56).

1.1.3.2.2 Response to pressure stress

The stress response of the *E. coli* proteome to elevated hydrostatic pressure was first reported by Welch et al. in 1993 (23). While the number of total proteins decreased with increasing pressure, the relative synthesis rate of many proteins is specifically enhanced 60 to 90 min after a pressure shock at 55 MPa. The authors observed 55 of these pressure-induced proteins (PIPs) among which the heat shock proteins, DnaK and GroEL, the major molecular chaperones that protect newly synthesized or stress-denatured polypeptides from misfolding and aggregation. A total of 11 heat shock and 4 cold shock proteins were identified among PIPs, more than for any other stress. The simultaneous induction of both heat and cold shock proteins is also unique. This apparent contradictory response could be explained by the fact that, both high pressure and high temperature destabilize protein structures and that high pressure and low temperature have similar inhibitory effect on many cellular processes, in particular membrane fluidity, DNA replication and protein synthesis. The role of chaperone proteins in the pressure resistance of *E. coli* has been demonstrated in a study in which disruption of the genes encoding the DnaK and DnaJ heat shock proteins, as well as the cold shock protein CspA and the IbpAB chaperone, increased the pressure sensitivity of *E. coli*. Heat shock pretreatment increases cell survival at 250 MPa by 100-fold compared to unheated cells (59). HP resistance mediated by heat shock proteins has also been reported in other organisms such as *Saccharomyces. cerevisiae* (60).

E. coli mutants that can survive at HP have been isolated. These mutants have high RpoS activity. RpoS is a RNA polymerase sigma factor that controls transcription of genes involved in starvation survival and other related stresses (5, 61, 62). Oxidative stress plays a role in the lethal effects of pressure on *E. coli* cells. Aertsen et al. demonstrated that *E. coli* mutants lacking reactive oxygen scavengers (ROS) were more sensitive to pressure than WT strains (63). Previous studies have also suggested that piezo-tolerance increases under osmotic stress, since an increase in the osmolarity of the growth medium increased the piezo-tolerance, a similar strategy adopted by *P. profundum* SS9. (64). It is thus likely that the ability to growth under HP is facilitated by preexisting adaptations to other environmental stresses.

1.1.4 Pressure effects on biomolecules

1.1.4.1 General effects of pressure

The thermodynamic consequence on biomolecular conformational equilibria of a change in hydrostatic pressure is to shift all biochemical equilibria to the side of the reaction that occupies the smallest molar volume. The dependence on the free energy of any such reaction on pressure can be expressed as:

$$\frac{\delta \Delta G}{\delta P} = \Delta V \qquad (1)$$

where P is the pressure, ΔV is the difference of the molar volume and ΔG is the difference of free energy between the two states of the reaction such as the folded and unfolded states of a protein. A small change in the molar volume due to pressure affects as well the rates of biochemical reactions (k_p) These rates depend exponentially on the free energy of the barrier and hence on the pressure-induced change in free energy of the barrier height as follows:

$$k_p = k_1 \exp(-\frac{P\Delta V}{RT}) \qquad (2)$$

where k_1 is the rate constant of the reaction (folding or unfolding for example) at atmospheric pressure and R is the gas constant. Because the relationship is logarithmic, small changes in volume can lead to large changes in rates. A volume change of +100 cm^3/mol leads to a 35% decrease in the rate at 10 MPa, and >99% decrease at 100 MPa. Since many biological processes are accompanied by volume changes in the range of 20-100 cm^3/mol, pressure increase can rapidly alter the conformational dynamics linked to the activity and structure of biomolecules (19).

1.1.4.2 Proteins

In 1914 Bridgman reported the coagulation of white egg at 700 MPa (65) and the reversible HP denaturation of serum albumin was described in 1963 (66). Since then, a small scientific community has been investigating the structure and dynamics of biomolecules upon changes of hydrostatic pressure which presents unique and interesting features compared to other thermodynamic parameters. However, because of the technical difficulties to set-up experiments for monitoring HP compared to temperature, pH or chemical denaturants, fewer studies have been performed to investigate HP-induced modifications of biological molecules.

The denaturation of proteins can be induced by different external factors such as temperature, chemicals and pressure. Temperature and chemical denaturants often lead to a complete and irreversible unfolding of proteins due to the disruption of non-covalent interactions that often cannot be reformed once disrupted due to off-pathway aggregation. Moreover, irreversible chemical modification of amino acid sidechains can also occur at high temperatures. In contrast, pressure-induced denaturation of proteins is much more gradual and gentle, allowing for reversible unfolding. Overall, high pressure in the range of 100 to 300 MPa has reversible effects on monomeric protein structures, while pressure greater than 300 MPa leads to irreversible reactions.

Unfolding of protein structures at increasing pressure is essentially due to the change in volume following the Le Chatelier's principle (67). This principle states that if any system at equilibrium is disturbed in terms of concentration, temperature, or pressure, the equilibrium shifts to a new equilibrium to counteract the change. According to this principle, a pressure increase shifts the equilibrium towards the state which occupies the smallest molar volume, which is the unfolded state of a protein. The volume of a protein is defined by the volume of the solvent molecules that hydrate the solvent accessible surface and the volume of the protein, itself defined by the volumes of constituent atoms and the solvent excluded internal void volume. At most temperatures, ΔV is negative so that pressure unfolds the proteins. Also, when temperature decreases, the absolute value of ΔV is larger. This is due to the difference in thermal expansion between the folded and unfolded states. Since the expansivity is larger for the unfolded state, its molar volume increases more with increasing temperature than that of the folded state, leading to a decrease in the difference in molar volume between the two states. This results in an enhanced effect of pressure on protein stability at lower temperature. Cold denaturation can occur near or below the freezing point of water, depending on the protein in question. Because of this limitation cold denaturation has not been as extensively studied as heat denaturation (68, 69). In any case, the combination of a more negative volume change and a lower stability leads to an enhancement of pressure-induced protein unfolding as temperature decreases.

The molecular mechanisms underlying the decrease in volume for the unfolding of proteins were for many years a subject of debate. Pressure has little effect on water itself because of its low compressibility (about 4% at 100 MPa). It was long thought that changes in water density at protein surfaces exposed to solvent concomitant with conformational changes such as unfolding contributed significantly to the volume changes implicated in pressure effects on protein structure and stability. However, recent experimental results demonstrate that this effect does not contribute significantly to the volume change of protein folding. In the work reported by Rouget et al. (70, 71), the authors first tested the effect of protein size on the value of the volume change associated to protein unfolding by pressure. If differences in density of water molecules hydrating surface area exposed upon unfolding were a major contribution to the volume change of unfolding, then larger proteins, which expose more surface area upon unfolding should have larger negative

values of ΔV. This is analogous to the m-value for chemical denaturation and the ΔCp for temperature denaturation, both of which result from interaction of water or denaturant molecules with the protein surface, and both of which are linearly dependent upon the protein size. Using a repeat protein (ankyrin domain of the Notch receptor) and deletion variants thereof, the authors found that the absolute value of ΔV did not decrease with decreasing size of the protein, even when nearly half of the protein had been deleted (70). This result was therefore not in support of protein hydration changes being the main factor contributing to the volume change of pressure-induced unfolding. Next the authors probed the effects of the introduction of internal cavities in a globular protein by mutation of large hydrophobic residues to alanine (71). In contrast to the limited effects of deleting nearly half of the protein repeats, single (iso)leucine to alanine substitutions resulted in up to two-fold increases of the volume change for folding. Finally, it is expected that when charged or ionizable sidechains that are buried inside protein cores are exposed to solvent upon unfolding, this will result in electrostriction of the charges by water molecules, a phenomenon that is accompanied by a decrease in volume. This was shown to be the case for mutants of a hyper stable variant of staphylococcal nuclease harboring buried ionizable residues.(72–74) However, outside of active sites (which are often hydrated in the folded state) there are very few ionizable residues found in protein interiors. The ensemble of these results clearly demonstrate that the major contribution of a volume change is due to the solvent-excluded internal void volumes present in the folded state of the protein that are largely eliminated (and therefore the volume occupied by water molecules) upon unfolding (see below).

In natural protein structures, internal solvent excluded void volume results from a combination of the constraints of the peptide backbone. The heterogeneity of the side chains leads to tertiary packing defects and the strong hydrophobic nature of protein interiors, which disfavors interaction with solvent. Generally, α helices, themselves, are not pressure sensitive (75–77) because they do not present internal solvent excluded volume. However, many peptides which are alpha helical in the context of folded proteins are often not stable on their own without the tertiary structural contacts. Thus, when the protein core is disrupted by the pressure, helices unfold as well. In contrast, β-sheets and barrels are highly constrained by the network of H-bonds, and tend to harbor significant void volume (78). Packing between helices and sheets, as well as loops can also harbor significant void volume. These regions must be sufficiently hydrophobic to exclude water molecules which is often the case (79–81). As mentioned above, proteins can be stabilized by osmolytes (such as sucrose and glycerol) but also destabilized by chemical compounds (such as urea) due to, respectively, unfavorable or favorable interactions with the protein surface. Osmolytes stabilize proteins against temperature and denaturants as well as pressure. This is because they are preferentially excluded from the protein surface, and the folded form has a smaller surface area than the unfolded form (82). However, these agents clearly do not alter the difference in volume between folded and unfolded states (71, 83, 84), in contrast to what has been previously suggested (85). It is likely that this discrepancy is due to a glycerol-induced deviation from two state behavior, combined with excessive

stabilization in this latter report, which resulted in erroneous values for the volume change of unfolding.

In contrast to other thermodynamic parameters such as temperature and pH, HP does not perturb other properties of a system besides its volume, leaving its internal energy and solvent composition unchanged. Moreover, pressure perturbation is based on the specific packing properties of the folded states of proteins, rather than on the amount of surface area exposed in the unfolded states, which is a global parameter. Hence the effects of pressure on protein structure are more local than those of temperature or denaturants, and as such can favor the population of intermediates which can hardly be detected upon unfolding by other denaturation methods. This makes pressure an interesting perturbation for monitoring fundamental thermodynamic states of biomolecules as well as for biotechnological applications (see section 1.1.4).

Importantly for the work in this thesis, protein oligomers and higher order assemblies are also disrupted by pressure (Figure 1.5). Much work has been carried out in this field over the past 50 years. Although the application of HP below 100 MPa does not generally lead to the complete unfolding of monomeric proteins, pressures in this range have been shown to destabilize many protein–protein interactions (86). Weber and collaborators (87), as well as the Jaenicke group (38) demonstrated decades ago that most oligomeric proteins can be dissociated by the application of hydrostatic pressure because the molar volume of this dissociated state is smaller than that of the oligomer, likely due to the existence of solvent excluded cavities at the interfaces between subunits. An increase glycerol concentration increases the stability of the pressurized Arc repressor. Indeed, There are many examples of oligomers dissociation by pressure such as enolase (87), lactate dehydrogenase (88), and ribosome subunits (54) Viruses are reversibly disassembled by HP as well (89, 90). While individual capsid proteins of P22 bacteriophage are rather sensitive to pressures below 150 MPa, assemblies in the procapsid are more resistant to pressure because of their stabilization by these higher order protein-protein interactions (91).

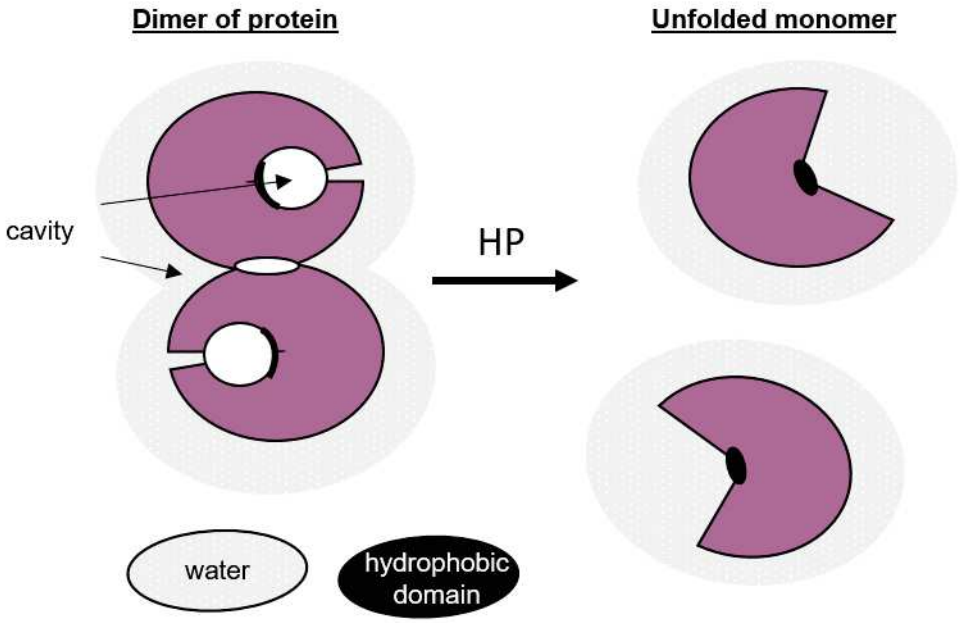

Figure 1.5: Pressure effects on a protein complex.

1.1.4.3 Nucleic acids

The effect of pressure on DNA/RNA is relatively small compared to that on proteins or lipids (58, 92–94). Indeed, in the tertiary structures of nucleic acids, almost all atoms are exposed to the solvent limiting the impact of pressure and there is no excluded void volume within a perfectly hydrolyzed DNA double helix. However, tertiary DNA/RNA structures such as hairpins are disrupted by pressure (95). Due to the stabilizing effect of HP on DNA hydrogen bonds, the melting temperature (T_m) of duplex DNA increases under pressure, which means that the pressure increases the stability of the dsDNA (96). Hydrophobic base stacking is accompanied by a decrease in molar volume, which also causes stabilization of the DNA double helix under pressure. T_m values also depend on the concentration of salt and the nature of the cations counteracting the interactions with water (96, 97). Increasing the concentration of various salts increases the T_m of DNA in response to pressure. Note that the increased stability of the DNA double helix under pressure can disturb fundamental processes (such as replication and transcription) by disturbing the transition from double to single strand (58).

1.1.4.4 Protein-nucleic-acid interactions

Pressure also acts on DNA-protein interactions (37), which are central to the work in this thesis as well. The protein-operator complex of the lactose repressor is destabilized by pressure (99, 100). Also, the increase in osmotic pressure, leads to cleavage by type II restriction enzymes at alternative sites (star sites) that differ from canonical recognition sequences. This has been observed for EcoRI but is completely reversed by HP (101, 102). It has been shown that a pressure of 70-130 MPa is sufficient to dissociate RecA-ssDNA interactions. RecA is involved in the SOS response (see section 1.2). It is likely that protein-

DNA interactions are disrupted not because of a change in DNA structure but because of the effect of pressure on protein oligomers or on the protein-DNA interaction interface often mediated by the insertion of protein helices in the major groove of the double helix (103). Ribosomes which involve RNA-protein and RNA-RNA interactions are also destabilized by pressure (56).

1.1.5 Pascalization

Pascalization is a promising non-thermal process used in the food industry since the early 1990s to inactivate foodborne pathogens and ensure food safety. The technique was named after Blaise Pascal, a French scientist of the 17th century who worked on the effects of pressure on fluids. HP treatments for food preservation was first instigated in 1899 by Hite (104). He demonstrated that 700 MPa increases the shelf life of milk and deteriorates less sensory properties than heat treatment. A typical pressure between 300 and 700 MPa is applied at a temperature below 45°C allowing a better preservation of vitamins and flavors, texture, colors, and nutrients than conventional heat treatments (6, 105). This process is used successfully on some products such as fruit juices (around 14% of HP treated food), meat and vegetables (27% each) and fish and seafood (13%) (106). Overall, the food maintains fresh-like characteristics with fewer or no additives.

The effectiveness of such treatment depends on many parameters, including the microbial population, the water activity of the system and the temperature. Micro-organisms have a different sensitivity to pressure. Gram negative bacteria are the most sensitive, then yeast/mold, Gram positive bacteria and finally spores. Bacterial endospores (a resistant form of some Gram-positive bacteria) cannot be inactivated by pressure at ambient temperature. *Bacillus* and *Clostridium* tolerate pressures over 1,000 MPa at 25 °C. For inactivation of these organisms, combinations of high pressure and heat are required (HPT). HPT is not yet used in the industry, but it is a promising technique for obtaining food without any additives and a longer shelf life. Inversely, *E. coli* is more efficiently inactivated by pressure at subzero temperature. Pressure has been shown as well to cause desirable effects. For example, the level of an antitumor called sulforaphane is increased after pressurization of broccoli (107). Unfortunately, some foodborne pathogens such as *E. coli* 0157:H7 and *Listeria monocytogenes* can acquire HP resistance, suggesting that pressure adaptation is an evolvable trait (42).

1.2 SOS response in *E. coli*

Different observations after UV irradiations of *E. coli* such as induction of prophage λ (108) and cell filamentation (109) led Miroslav Radman to discover and name the bacterial SOS response in 1975. SOS events are inhibition of cell division, DNA damage repair and mutagenesis. This SOS response is caused by various stresses in *E. coli* (Figure 1.6). The SOS response is typically induced by stress and agents that cause DNA damage or collapse of the replication forks, both of which result in exposure of ssDNA. The induction of the SOS

response occurs only in cells where DNA damage is detected. This system plays an important role in several of the most important strategies that bacteria use to survive stressful conditions. Bacteria work to repair their genome at any cost, including by mutations due to error-prone nature in repair mechanisms. In some cases, DNA modifications may result in adaptation to changing conditions in a wide range of environments. Overall, the SOS response can be beneficial for cell survival (110, 111).

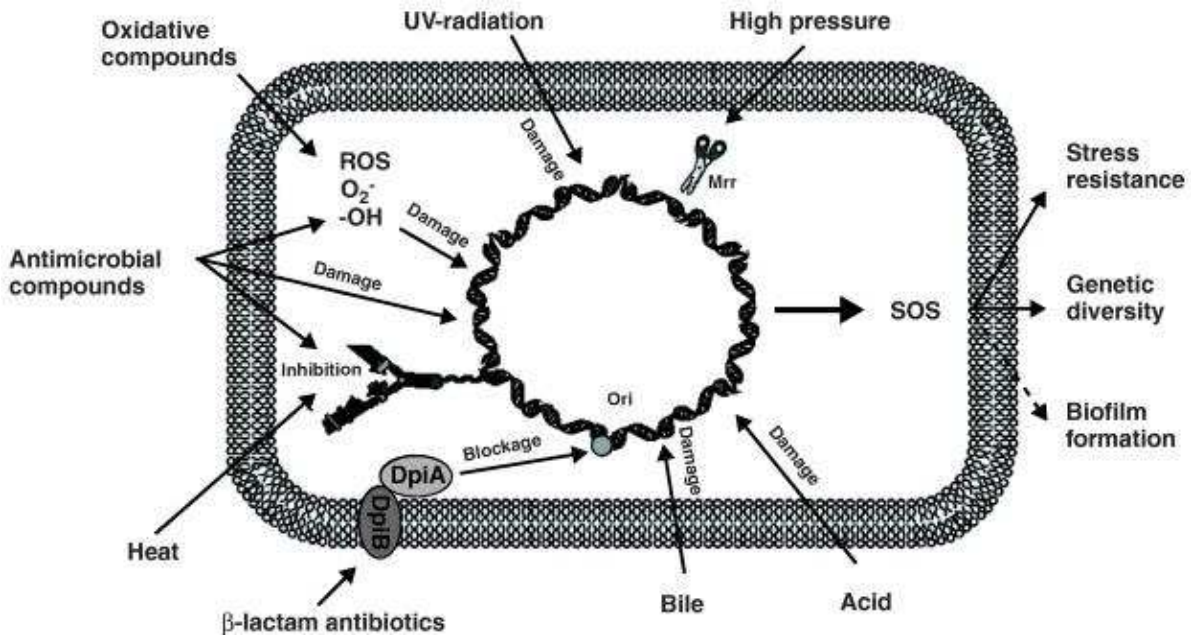

Figure 1.6: Stresses and other environmental factors that can trigger the bacterial SOS response (adapted from (112)*).*

The SOS response is a conserved pathway that is essential for DNA repair and restart of stalled or collapsed replication forks. It is regulated by the repressor LexA and the activator RecA (Figure 1.7). In healthy cells, the dimeric LexA protein binds to a 20-bp consensus sequence (the SOS box) thereby blocking RNA polymerase binding and transcription (Figure 1.7). The accumulation of single stranded (ssDNA) after DNA damage results in the activation of the SOS response. LexA has a cryptic auto-cleavage activity that is activated when LexA interacts with a RecA/ssDNA helical nucleoprotein filament. RecA oligomers formed on ssDNA in the presence of ATP with 5' -to- 3' assembly polarity (113). Thus, RecA is a positive regulator of this response and has a co-protease function. In normal growing cells, ssDNA is generated upon DNA replication. However, its level is really low and tolerated. The threshold level for inducing the SOS response can be reached by many factors, but the most common one is when the cell tries to replicate damaged DNA (114). Exposure of ssDNA can simply be reversed and the DNA returns to its original state. Other types of damage require the removal of a part of DNA around the damage (115). Then, the

bases can be resynthesized using the other strand as a template like the DNA repair system called base excision. Excision may be only a few nucleotides in the case of the nucleotide excision repair system or 1,000 nucleotides for the methyl-directed mismatch repair system. When the DNA is too damaged to repair itself, the SOS repair system is induced via either the RecFOR or RecBCD complexes that are part of the RecA of homologous recombination pathways.

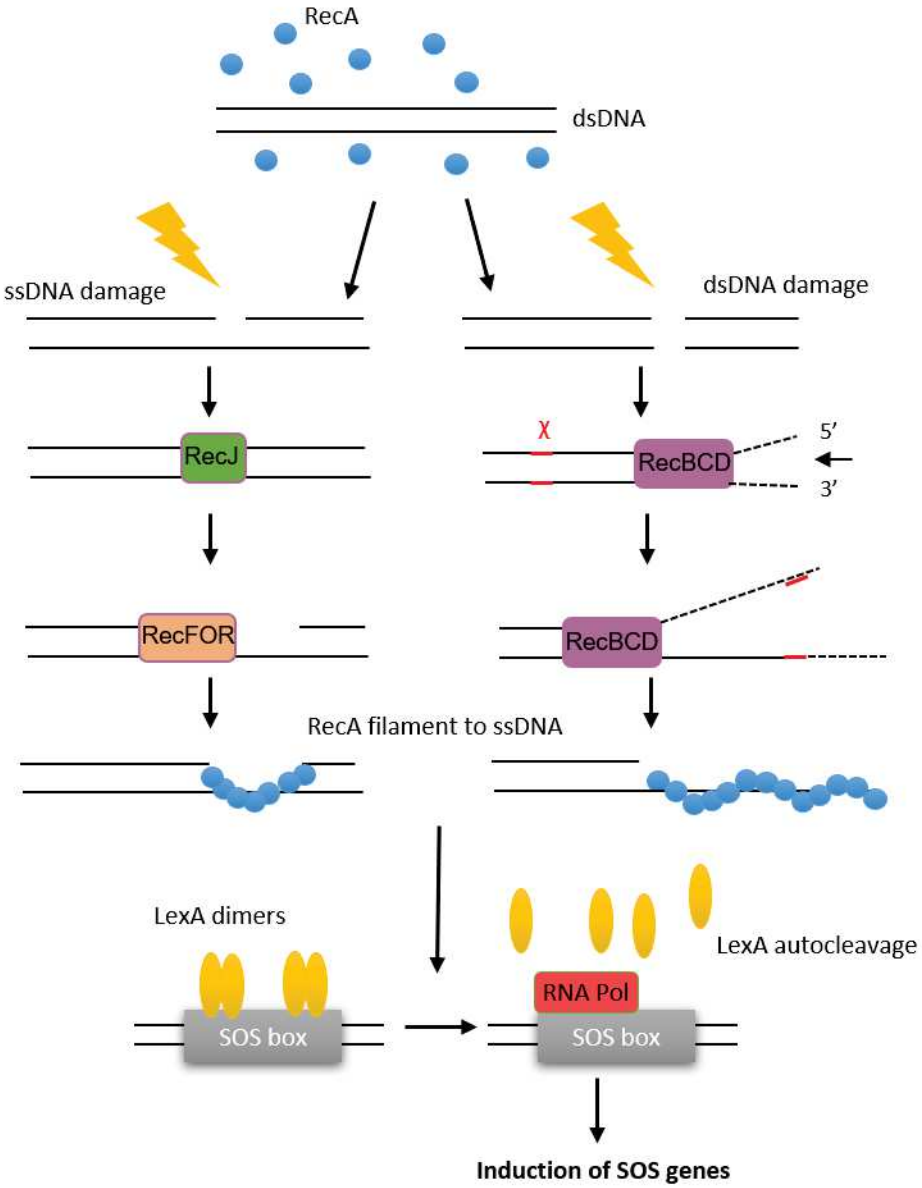

Figure 1.7: Induction of the SOS response regulon due to ssDNA or dsDNA damages. The DNA damages are sensed by either the RecFOR or RecBCD complex. The RecJ/RecFOR pathway is activated in the presence of ssDNA breaks where the RecA proteins binds and forms filament. In case of dsDNA breaks, the RecBCD complex is recruited to degrade one strand of the cleaved DNA until a specific sequence called the chi sequence (represented in red), generating ssDNA where the RecA polymers assemble. In both pathways formation of the RecA

nucleoprotein filaments activates the auto-cleavage of LexA repressor dimers bound at SOS boxes and thereby relieves the repression of SOS genes.

RecF pathway is involved in the ssDNA breaks repair system (Figure 1.7). ssDNA breaks are first recognized by the endonuclease RecJ which binds the single-strand gap and cleaves 5' to 3'. Then, the loading of RecA to form filaments on the ssDNA requires the complex RecFOR (116). RecFOR can also repair dsDNA breaks (DSBs) if the RecBCD complex, in charge of DSB, is mutated. The RecBCD pathway is explained in details in section 1.2.1. RecFOR complexes help to load RecA onto ssDNA generated during the replication of the damaged matrices (117).

The SOS regulon codes for more than 50 genes, expressed at a basal level, which significantly increase upon induction of the SOS response. SOS genes are not all activated at the same time. The first proteins expressed are involved in simple DNA damage repair. If the problem is not solved, low fidelity DNA polymerases are made. This provides an opportunity for bacteria suffering major DNA damage for creating mutations that may lead to cell survival under stress conditions. Cell filamentation observed upon induction of the SOS response is due to the alteration of the FtsZ proteins forming a Z-ring at the division septum. Besides pressure that can dissociate the FtsZ polymers (see section 1.1.3.2.1), the cell division inhibitor SulA is controlled by LexA and is up regulated following DNA damage. The direct binding of SulA dimers to FtsZ presumably prevents FtsZ polymerization into a Z-ring, resulting in filamentation (118, 119). Further in the interest of increasing the genetic repertoire of the bacteria population, the SOS response leads to the release of phage particles. Similar to the LexA repressor, the CI repressor, which maintains a lysogenic state, will cleave itself in the presence of the activated RecA. This will lead to the initiation of the lytic cycle (115).

1.2.1 The RecBCD pathway

Several exogenous genotoxic agents as well as introduction of foreign DNA, lead to DSBs. They are also generated during normal metabolism of DNA at a really low rate (120). Unrepaired DSBs are lethal to cells. The RecBCD complex is the major pathway to repair DSBs in *E. coli*. Deletion of the complex leads to an extreme sensitivity to DNA damage and low viability even in the absence of stress (30% of wild type *E. coli*). The complex senses and binds with high affinity DSBs. This complex is also a protection against viruses because it can degrade foreign DNA. Phage lambda produces a protein that inhibits the interaction between the complex and the DNA (121). Phage T4 and phage N15 develop similar protection against DNA degradation by RecBCD (122, 123). The RecBCD complex was discovered in the 1970's as an exonuclease activity in *E. coli*. RecBCD is a helicase-nuclease initiating the repair of DSBs by homologous recombination. These enzymes are not part of the SOS regulon. Their expression is strictly controlled and limited to a low copy number (about 10 copies per cells) (124). Overproduction impairs on DNA repair and homologous recombination (125).

RecB and RecD subunits participate in the helicase motor activity by using ATP hydrolysis while the nuclease activity is carried by RecB (126). Once the RecBCD complex recognizes blunt DNA ends, it rapidly separates the two DNA strands using its motor activity (RecC and RecD). Simultaneously, RecB degrades, through nucleolytic cleavage, the nascent strands until a specific sequence called Chi (5'-GCTGGTGG-3'). This sequence is recognized by RecB causing a short pause. Then, the up-regulation of the weaker 5'-to-3' exonuclease and down regulation of the 3'-to-5' exonuclease results in the production of a 3' tail capped by the Chi sequence. RecB interacts directly with RecA to facilitate its binding to the tail and form presynaptic filament to initiate the recombination or repair reaction.

1.2.2 SOS response induction by pressure

Activation of the SOS response by pressure was reported for the first time by Aertsen et al (127). Using a differential fluorescence induction screening, they first demonstrated the induction of a *uvr*A promotor that is part of the SOS regulon. Then, they studied the promotors of two key genes of the SOS response, *recA* and *sulA*. After exposure to 100 MPa, both P_{recA} and P_{sulA} are induced about 20 -fold increase in the expression. They further demonstrated the RecA and LexA dependent activation of the SOS response by HP (127). Note that Δ*recA* and Δ*lexA1* mutants are sensitive to pressure but not to UV treatment. In the same study, the authors observed that the induction of the lysogenic cycle of the lambda phage by pressure is depended on LexA as well as its induction by UV irradiation or treatment with mitomycin C. In contrast, the stability of the e14 element is not disturbed by pressure. This element is a lambdoid bacteriophage that excises itself from the genome after a UV treatment and the induction of the SOS response.

The Lon protease is an enzyme that decreases post-translationally the amount of SulA. Thus, Lon mutant *E. coli* cells are unable to degrade SulA, the cell division inhibitor. The severe filamentation makes the cells hypersensitive to the stress responsible of the SOS response (5). A stationary phase culture of the strain *E. coli* MG1655 lon::Kn was pressurized at 100 MPa for 15 min and was grown again to the stationary phase until a rescue mutant took over the population. Similar experiments were done with UV treatment. Two categories of mutants were identified. The first group contains mutants resistant to both pressure and UV which, in majority, compromise SulA function. The second category is the one of interest comprising mutants resistant to pressure only. These observations suggested a different pathway for the activation of the SOS response by pressure compared to other stresses.

In order to determine what kind of DNA breaks (SSB or DSB) trigger the SOS response following a pressure shock, the authors investigated whether HP-induced DNA lesion are sensed by the RecFOR or RecBCD complex (Figure 1.7). Although the absence of RecB had no effect on the SOS response induction by UV treatment, it fully abolished that induced by HP, indicating that dsDNA breaks are exclusively created. The formation of DSBs is rare under normal growth conditions and, unlike UV and mitomycin C pressure itself cannot

compromise the covalent integrity of the DNA (22). Thus, the authors concluded that a specific pathway producing DSBs elicits an SOS response when cells are exposed to high pressure.

The isolation of a spontaneous pressure resistant mutant in *E. coli* MG1655 lon::kn (no SOS response) but which was UV and mitomycin C sensitive, revealed a transposon insertion into the *mrr* gene. This gene codes for an endogenous type IV restriction endonuclease, Mrr. The *mrr* mutant gene was then transferred into wild-type *E. coli* MG1655 and RecA activity was followed by a GFP transcriptional fusion (5). The P_{recA} promotor was found to be induced after UV and mitomycin treatments but not following a pressure shock. Thus, Mrr appears to be the only effector of the HP-specific induction of the SOS response by directly cleaving dsDNA.

1.3 Restriction systems

Restriction systems are a primary defense mechanism against invading viruses (phages) or other infectious DNA molecules that may take over the cellular metabolism for their own replication. Restriction systems can be divided into two groups according to their enzymatic activities and DNA recognition: Restriction-Modification systems (RMs) and Modification-Dependent systems (MDs). Restriction systems allow bacteria to recognize as foreign an incoming DNA. Restriction endonucleases (REases) recognize short specific sequence in foreign DNA known as restriction sites and cleave the DNA into fragments. In order to prevent the cleavage of its own DNA, the host must protect it from the potentially lethal effects of REases. For this purpose, the DNA is modified, most often by a methyltransferase (MTase) which methylates specific nucleotides. One example of RM system is the EcoRI MTase system that methylates the EcoRI recognition sequence, GAATTC to GAm6ATTC. This modification completely protects the sequence from cleavage by EcoRI REase. On the opposite, MDs have only cleavage activity targeting modified DNA.

1.3.1 Classification of restriction endonucleases (REase)

There are four main types of REases that differ in their structures, cofactor requirements, recognition sequences and cleavage positions (128). All types of enzymes recognize short DNA sequences. Type II REases represent the largest group and they are widely used as tools for recombinant DNA technology. A much lower number of types I, III and IV have been characterized.

- Type I REases cut DNA at a random position far from their asymmetric recognition sequences (at least 1000 bp) (129). They are multifunctional proteins with 3 different subunits to accomplish both restriction and methylation activities (Figure 1.8.A).

- Type II REases recognize short palindromic DNA sequences, usually 4 to 8 base pairs, and make duplex cleavages at defined positions at or near their recognition sites. They form dimers that usually require Mg^{2+} as a cofactor (Figure 1.8.B) (130). Cleavage of both strands is either concerted or one strand at a time with dissociation of the enzyme in between scissions, depending on the DNA external structure and on reaction conditions. Type II enzymes do not have a methylase activity. There are many categories with different specificities.
- Type III REases cleave at a short distance (20-30 bp) from their recognition sites (131). They are part of a complex with a modification methylase that recognizes two separate inversely oriented non-palindromic sequences (Figure 1.8.C).
- Type IV REases recognize modified, typically methylated DNA (132). A sub category of Type II REases is type IIM that possesses similarities with Type IV REases. Indeed, they both cleave only modified DNA and are inactive on unmodified DNA. The main difference is that Type IV REases cleave at a long distance from their recognition sequences.

Recently, a new group of REases has been created, type V. They use guide RNAs to target the cleavage at specific non-palindromic sequences (133).

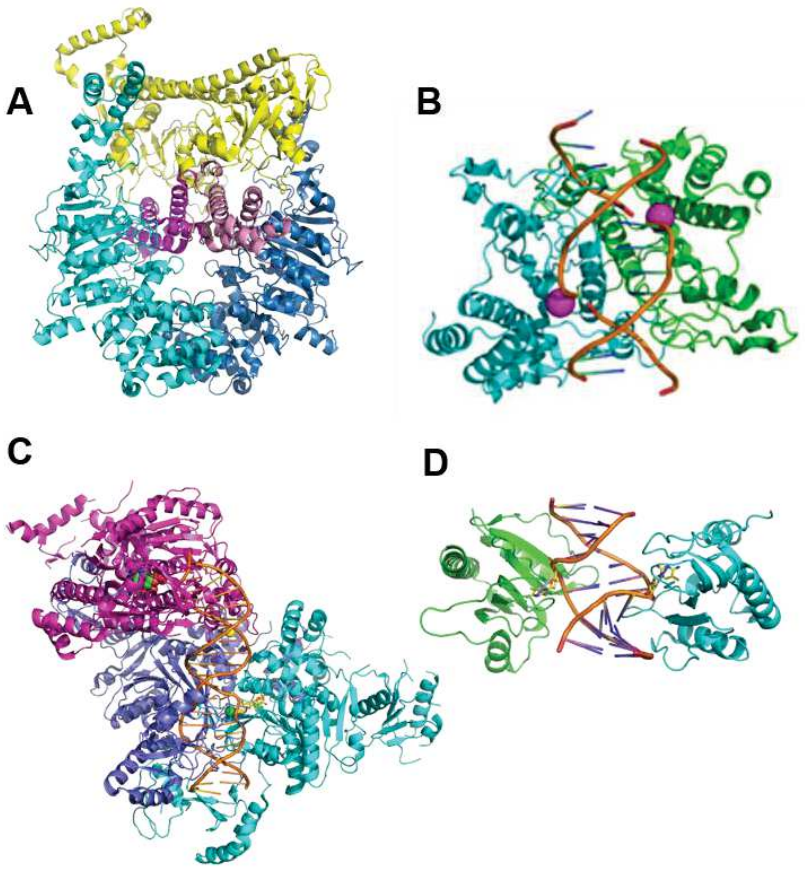

Figure 1.8: Structures of different types of E. coli restriction-modification (RM) enzymes. A) Type I RM EcoKI (pdb:2y7c). The complex is composed of two modification subunits (blue), two endonuclease subunits (magenta) and a

recognition subunit (yellow) (134). *B) Homodimer of the type II EcoRI restriction enzyme in complex with DNA (orange) and Mg2+ (magenta) (pdb:1ckq). C) Heterotrimer of the type III RM EcoP15I on DNA (pdb:4zcf)* (135). *The complex is formed of two methylation subunits (blue) and one restriction subunit (magenta). D) N-terminal binding domain of MrcBC, a type IV restriction enzyme from E. coli K12, interacting with methylated DNA (pdb:3ssc)* (136). *The REase recognizes a 5-methylcytosine which is extruded from the DNA double helix within a binding pocket of the recognition domain of the enzyme.*

1.3.2 Methyltransferase (MTase)

DNA MTases are a large group of enzymes that modify host DNA at specific sequences in order to protect it from cleavage by REases. The associated MTase and REase both have the same target sequence on DNA. MTase catalyzes the transfer of a methyl group to a specific nucleotide in the restriction site. This system provides protection against the entry of foreign DNA lacking the proper methylation signature. The bacterial DNA is methylated by the cognate MTase just after replication so that it will not be cleavable by the associated REase.

1.3.3 Type IV restriction enzymes

The modification-dependent type IV restriction enzymes are very diverse and only a few have been characterized in detail. In contrast with conventional REases, they recognize modified DNA with low sequence selectivity, they do not have a cognate MTase and they do not affect host DNA in the absence of modifications. Well known modified bases are m5C, m4C and m6A. In *E. coli* K12, three of these REases have been identified. McrA, McrBC (modified cytosine recognition) and Mrr (methylated adenine recognition and restriction). They are laterally acquired genetic elements. The *mrr*, *mcrB* and *mcrC* genes are located in the “Immigration Control Region” (ICR) characterized by a high density and variability of restriction function (137). The *mcrA* gene is encoded by the e14 element. McrA and McrBC are involved in restricting phage infection. These three enzymes recognize the modification m5C (Figure 1.9). McrA recognizes CmCCG sequence and McrBC recognizes pairs (A/G)mC separated by 30 to 3000 bp. As mentioned above, Type IV and Type IIM REases all recognize modified DNA. We are interested in two families in particular, DpnI and MspJI because they share structural similarities between their domains and those of Mrr (Figure 1.9 and section 1.4.4). Plasmids carrying heterologous genes are severely restricted in strains expressing Mrr (138). Thus, it is recommended when cloning in *E. coli* to use strains mutated for Mrr as well as McrA and McrCB (139).

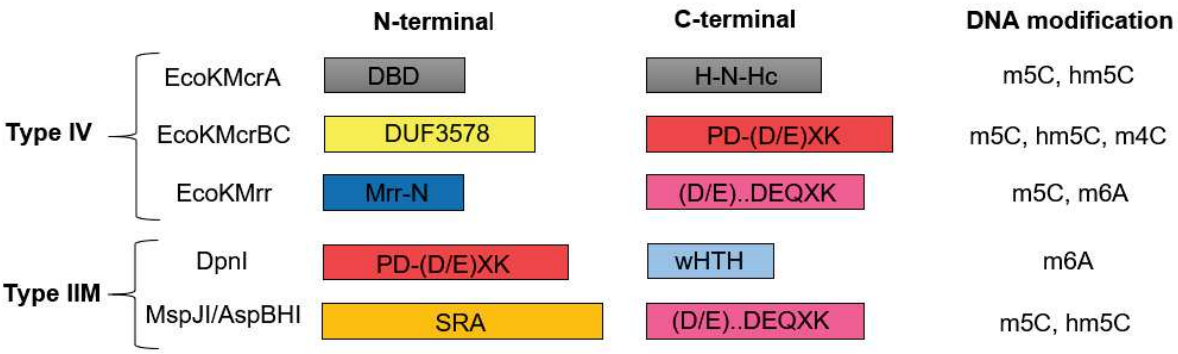

Figure 1.9: Modular structure of type IV REase from E. coli K12 and two different families of Type IIM REase. The N-terminal and C-terminal domains are colored according to their similarity and the size of the bar is relative to the size of the domain. The DNA modifications necessary for cleavage are 5-methylcytosine (m5C), 5-hydroxymethylcytosine (hm5C), N4-methylcytosine (m4C) and N6-methyladenine (m6A).

1.4 The Mrr protein

1.4.1 Discovery

In 1987, Heitman and Model discovered Mrr in *E. coli* K12 when they found that expression of a foreign MTase induced an SOS response due to DNA double-strand breaks (140). The authors were studying the HhaII system from *Haemophilus parahaemolyticus* that methylates adenine at specific DNA sequences. The expression of HhaII MTase in several *E. coli* K12 strains drastically inhibits growth due to DNA damage and thus the induction of the SOS response. They found that a mutation in the *mrr* gene blocked the effect of adenine methylation by the HhaII MTase. Thus, Mrr was initially recognized as an enzyme targeting the N6-methyladenine (m6A) modification. Later, it was shown that Mrr can also cleave certain DNA sequences containing 5 methylcytosine (m5C)(141). However, no specific sequence has so far been identified as Mrr recognition site. Although Mrr homologs have been found in many other organisms, their functions and characteristics remain mostly unknown (142).

1.4.2 Pressure activation of Mrr

The identification of Mrr as the only effector capable of sensing pressure and inducing DSBs has been described in section 1.2.2. A transcriptional promotor fusion of the *mrr* promotor with *gfp* was used to monitor *mrr* expression. After a sub-lethal pressure shock (15 min at 100 MPa), no increase in the transcription activity from the P_{mrr} promotor was observed, suggesting that *mrr* expression is constitutive in the cell. Thus, the nuclease activity of Mrr is somehow activated by pressure through a non-enzymatic modification or a change of the DNA structure that would make it more available for Mrr restriction (5).

The *mrr* coding sequence was translationally fused to the 3' end of *gfp* to study GFP-Mrr localization and its dynamic before and after a pressure shock using fluorescence microscopy in *E. coli* K12 MG1655 live cells (143). GFP-Mrr fusion was expressed from the arabinose inducible pBAD promotor on a low multi-copy plasmid (pBAD-gfp::mrr). Genotoxicity was not observed when Mrr was over-expressed without pressure treatment. In unstressed cells, GFP-Mrr is observed in a number of distinct foci on the DAPI-stained nucleoid indicating Mrr binding hotspots on the chromosome (Figure 1.10.A).

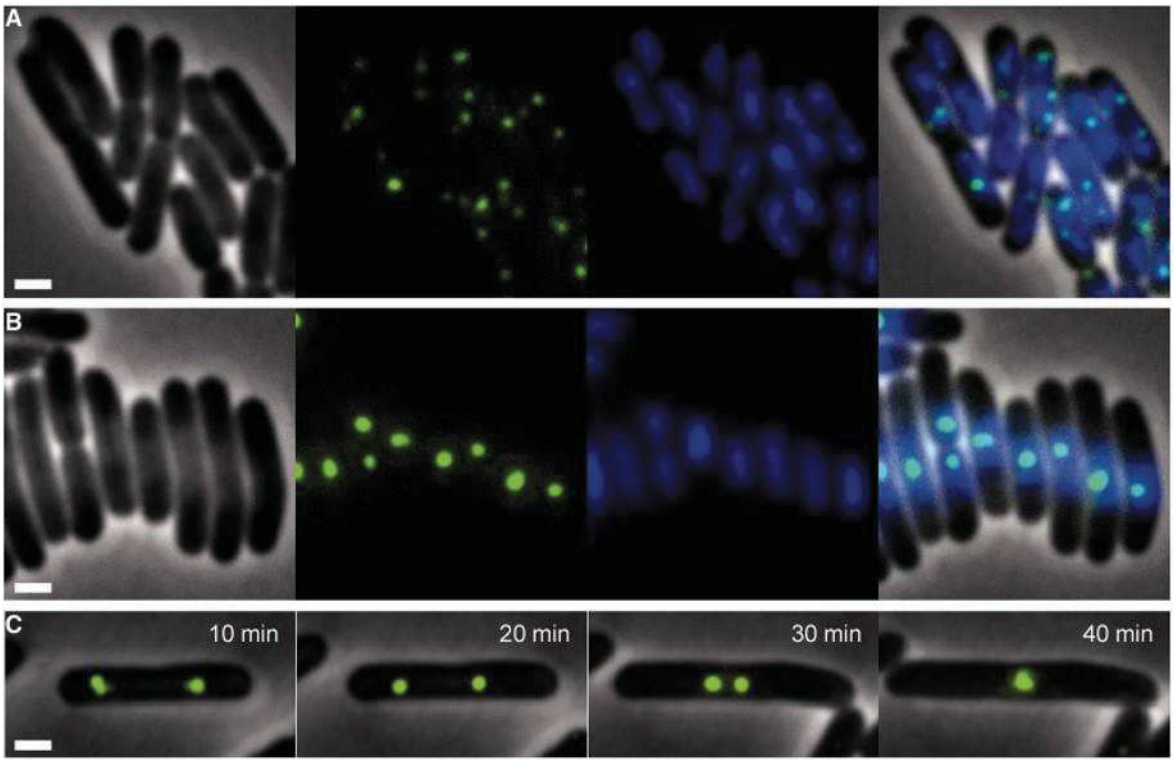

Figure 1.10: Fluorescence images of E. coli cells expressing GFP-Mrr. A) unstressed cells; B) cells after a pressure shock at 100 MPa for 15 min. Phase contrast, GFP, DAPI staining and merge images are respectively shown for the same cells. C) Coalescence of GFP-Mrr foci in a cell about to divide at indicated point time after pressure treatment. The scale bar corresponds to 1 µm. Figure from (143).

This observation might indicate that Mrr is a nucleoid-associated protein. After a HP treatment of 15 min at 100 MPa, GFP-Mrr foci coalesce in the middle of each bacterium with the condensed nucleoid (Figure 1.10.B). The nucleoid condensation is a typical result of DNA double-strand breaks (144). It has been shown that the ordered coalescence and realignment of two-sister chromosomes is mediated by two identical DSB to repair DNA. The interaction is initiated at replication forks and forms a robust complex independent of any proteins. Cells that are about to divide show two distinct foci at each extremity that move towards each other, indicating a retrograde transport between the two condensed nucleoids (Figure 1.10.C). At 60 min post-treatment, GFP-Mrr disperses in the cytoplasm, probably due to the loss of nucleoid integrity, leading to a drop in cellular viability. In the

absence of Mrr, cells recover from pressure shock and show normal viability and division as well as normal nucleoid segregation. After pressure, cells also suffer from some sort of cytoplasmic bleebbing (loss of cellular integrity) that is not observed in the absence of Mrr.

Further study revealed that not all Mrr homologues behave the same way. For example, the Mrr protein encoded by *Salmonella typhimurium* LT2 (LT2) cannot be activated by pressure (145). However, introduction of Mrr from *E. coli* MG1655 into LT2 conferred a constitutive activity in the absence of pressure activation (146). Interestingly, this genotoxicity is due to the activity of a Type III MTase present in LT2 (Mod^{LT2}). Another MTase Type III, Mod^{EDIA} from *E. coli* has the same effect. Thus, this study discussed an evolutionary antagonism between the activity of Mrr, a Type IV REase and Type III modification enzymes.

1.4.3 HhaII MTase activation of Mrr

It has been shown that Mrr reacts not only to the activity of M.HhaII, but also to the Type III Mod^{EDIA} and Mod^{LT2}. In this work, we will discuss in more detail the HhaII MTase activity. HhaII is a 26 kDa Type II MTase of *Haemophilus parahaemolyticus*. HhaII recognizes a short palindromic sequence (5'-G-A-N-T-C) in duplex DNA and causes specific methylation on the adenine nucleotide of both strands, thereby protecting the DNA from cleavage by the endogenous HhaII endonuclease. As previously described for pressure, GFP-Mrr localization was observed by fluorescence in *E. coli* MG1655 strains co-expressing a foreign the methyltransferase (M.HhaII, Mod^{EDIA} and Mod^{LT2}) (143). M.HhaII by itself is not toxic and does not cause nucleoid condensation. Its induction, in the presence of Mrr, leads to nucleoid condensation and coalescence of Mrr in the middle of the cells, similar to what is observed after a pressure shock. However, in case of M.HhaII induction, the nucleoid/Mrr complex appears to be more stable than the pressure-induced complex. Indeed, the GFP-Mrr foci remain very intense and the Mrr protein is not dispersed in the cytoplasm as seen 60 min after pressurization. Expression of Mod^{EDIA} and Mod^{LT2} both fail to impose nucleoid condensation, GFP-Mrr showing a cloud-like distribution on the nucleoid (143). In contrast to M.HhaII, these MTases tend to methylate only one DNA strand (hemimethylation). It is thus possible that the hemimethylated DNA does not constitute a high-quality substrate for Mrr, generating an insufficient number of double-stranded breaks for triggering nucleoid condensation.

1.4.4 Mrr structural properties

E. coli Mrr is a 33 kDa protein comprising 304 amino acids. The three-dimensional (3D) structure of Mrr has not been solved. However, sequence analysis reveals two domains, an N-terminal DNA binding domain (residues 1-95) proposed to be involved in the recognition of target (methylated) sites, and a C-terminal catalytic domain (CAT,139-304) for DNA

cleavage. The separation between the two domains is typical of REases that cut at a distance from their recognition site. They are connected with a variable linker.

No similarity was found with other protein families for the N-terminal DNA binding domain (DBD) of Mrr. Nevertheless, Orlowski et al., proposed a model of the monomeric N-terminal domain in interaction with DNA (Figure 1.11)(147). Sequence analysis of Mrr DBD revealed a variant of the helix-turn-helix motif, the wing-helix (wH), found in many other DNA-binding proteins (148). However, the overall organization of the Mrr DBD is unique to Mrr and its close homologs. It is composed of 3 wH, only one of which appears to be involved in DNA recognition (Figure 1.11). Some Type II REases also have a wH that recognizes modified DNA. The wH binds in the major groove and recognizes both strands at the same time.

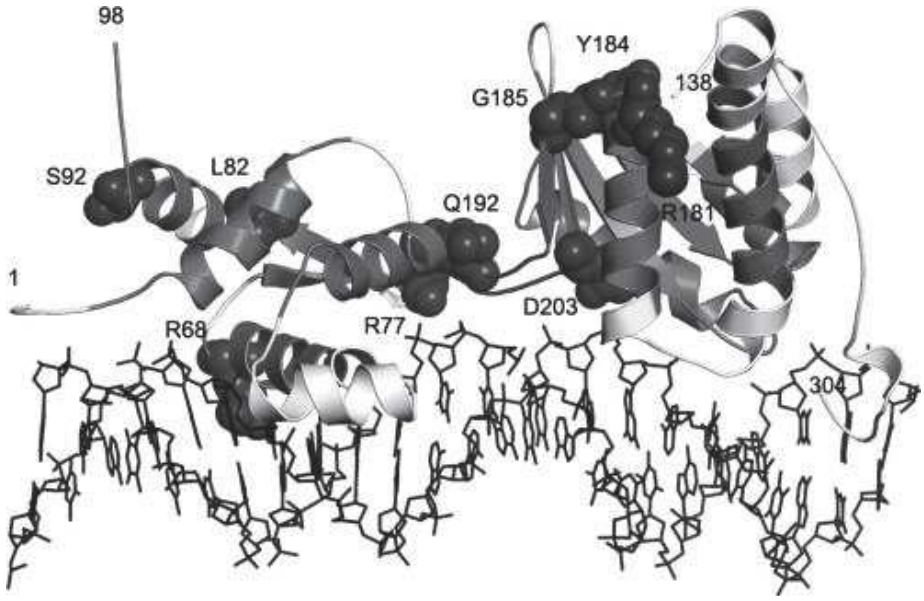

Figure 1.11: Structural model of full length monomeric Mrr. Labeled residues indicate positions where amino acid substitutions inactivating the enzyme have been found(from (147)*).*

The Mrr C-terminal domain corresponds to a catalytic domain (CAT) with a conserved core typical of Type II restriction enzymes from the PD-(D/E)XK superfamily. Mrr possesses a variant of the catalytic core, ID-QAK. Mrr CAT was modeled in 2001 (142) using the structure of the BgIII restriction enzyme (pdb:1Y88) from the same PD-(D/E)XK superfamily (147). The model of the full-length was evaluated with predicted mutations of conserved residues that prevent pressure-induced activation of the SOS response. These mutations were localized in the wH motif predicted to be involved in DNA recognition (R68 and R77) and in the catalytic domain (D203A, first "D" in the PD-(D/E)XK motif). The D203A mutation has also been found to prevent Mrr activation by M.HhaII-dependent DNA methylation. Overall, this study showed the functional importance of several conserved residues in Mrr although the mutational effects could not be fully understood from the proposed model of monomeric Mrr.

More recently was solved the crystal structure of two Types IIM modification-dependent endonucleases, MspJI (pdb:4FOP) and AspBHI (pdb:4OC8), that possess a catalytic core domain more closely related to that of Mrr (Figure 1.9). These restriction enzymes recognize methylated DNA (m5C) and introduce DSBs at a fixed distance from their binding site. However, their N-terminal DNA recognition domain is not structurally related to that of Mrr. MspJI and AspBHI both present an SRA (SET and RING Associated) methylcytosine-binding domain commonly found in eukaryotic regulatory proteins implicated in chromatin modification, transcriptional regulation and cell cycle. In the SRA/DNA complex, the methylated base is flipped out from the DNA helix into a conserved binding pocket of the SRA domain. It is interesting to note that a similar extrusion of the methylated base from the DNA helix has been seen in the complex with the non-structurally related N-terminal domain of the Type IV McrBC (149). These structures will be further discussed in the section describing our model.

1.4.5 Mrr catalytic mutants

Two genetic screens were temped in order to isolate *E. coli* MG1655 *mrr* mutant strains sensitive to either pressure or co-expression with the HhaII methyltransferase but not both. Interestingly, Ghosh et al. (143) identified such Mrr variants. The mutation V173A, substituting a valine for alanine 173, abolished the SOS response by pressure, but not by M.HhaII induction. As expected, the GFP-MrrV173A variant carrying the V173A mutation and the stained nucleoid showed no difference in unstressed and pressurized cells whereas M.HhaII induction provoked coalescence of MrrV173A with a condensed nucleoid in the middle of the cell. Inversely the H279Y mutation, substituting a tyrosine for histidine 279, reduced the SOS response in the presence of the MTase. While a condensation of the nucleoid was observed after pressure treatment, a cloud-like distribution was observed upon co-expression with M.HhaII. This suggests that MrrH279Y may be altered in its cleavage activity but still able to recognize and bind to target sites. Nevertheless, a 2-fold decrease in viability was observed (12-fold decrease for the WT Mrr).

1.5 Aim of this work

In this work, in collaboration with the Aersten's group, we investigated how Mrr is activated by pressure or DNA methylation by M.HhaII, and we propose a molecular model of activation based on our results. Our aim is to understand how the two pathways trigger the SOS response (by HP or M.HhaII) by characterizing the Mrr protein both *in vivo* and *in vitro*. The Aertsen's group already investigated Mrr localization by conventional microscopy at high concentration (from a low multi-copy plasmid expressing P_{BAD}-*gfp::mrr* fusion). Although these experiments gave important information on the Mrr/nucleoid interaction, they could not provide quantitative data that could enlighten the Mrr activation

process. We proposed the use of a quantitative fluorescence microscopy technique that relies on the fluctuations of fluorescence intensity called scanning Number and Brightness (sN&B). This sensitive technique allows measurement in living cells of spatially resolved values of the absolute concentration of fluorescent molecules (n) and their molecular brightness (e) informing on their oligomeric state. We performed these experiments before and after a pressure shock or the expression of the HhaII MTase. Instead of using a multi-copy plasmid, the P_{BAD}-*gfp::mrr* construct was inserted at the *mrr* locus and expressed in the chromosome. Thereby, GFP-Mrr was produced at a much lower concentration, closer to the native concentration and allowing N&B analyses. In parallel we purified the GFP-Mrr protein and studied its oligomeric properties *in vitro*. We also investigated the behavior of Mrr mutants that prevent activation of Mrr either by HP (V173A) or by the M.HhaII induction (H279Y) or both (D203A). A constitutively active Mrr mutant, although lethal for the cell, could also be characterized and confirmed our proposed model of activation switching an inactive Mrr tetramer into an active dimer. To help us in the interpretations of our *in vivo* and *in vitro* results, we constructed a structural homology model of the full-length Mrr tetramer. Another aim of my PhD work was to implement a high-pressure system on our microscope in order to investigate Mrr behavior not after but during a pressure shock. We succeeded in using fluorescence correlation spectroscopy (FCS) under pressure to study the purified GFP and GFP-Mrr and preliminary results will also be presented on sN&B performed on living bacteria under pressure.

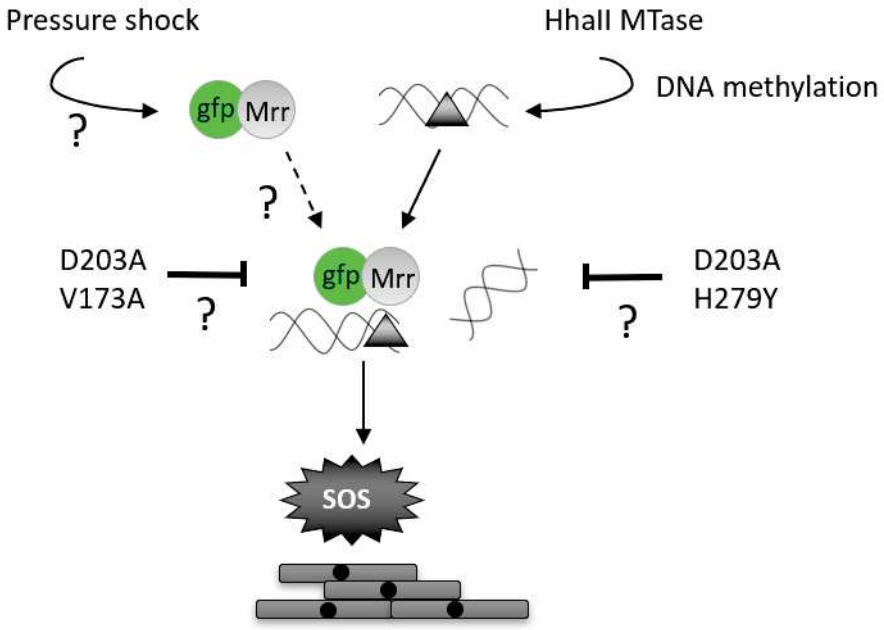

Figure 1.12: Summary of what we know and what we ought to answer about the SOS response mechanism induced via Mrr in E. coli after a pressure shock or DNA methylation by M.HhaII.

2. Materials and methods

This work was carried out mainly using microscopy techniques that rely on fluctuations in the intensity of fluorescence. Fluorescence Correlation Spectroscopy (FCS) and scanning Number and Brightness (sN&B) use the magnitude of fluorescence fluctuations to de-convolve the fluorescence intensity into the number of fluorescent particles (n) and their molecular brightness (e). These fluctuations come from fluorescents particles diffusing through the excited volume. They also can be used to extract the translational diffusion coefficient of the fluorescent molecules (D) on the microsecond to second time scale.

2.1 Fluorescence microscopy

Technological innovations led to the creation of the first optical microscopes during the 17th century. Thanks to their optical magnification, Robert Hooke observed and defined for the first time the term "cell". However, it was only at the beginning of the 19th century that cell biology was developed thanks to the improvement of microscopy techniques. Since then, new methodologies are constantly being developed to improve spatial resolution and contrast. The development of fluorescence probes in the middle of the 20th century, followed by confocal microscopy are the two major technical advances on which depends modern microscopy observation of specific structures within a cell. Over the past 20 years, there has been a remarkable growth in the use of fluorescence microscopy, which has become an essential tool to visualize biomolecular structures and monitor cell physiology (150). Both in 2008 and 2014 the Nobel Prize in Chemistry was awarded to important contributors in the field of fluorescence microscopy.

2.1.1 Fluorescence

2.1.1.1 Basic principles of fluorescence

Fluorescence is the ability of a molecule to emit light at a higher wavelength, and therefore a lower energy, than that of the light absorbed. The fluorescence phenomenon was first described in 1852 by George G. Stokes who observed blue luminescence in the mineral fluorite. He gave his name to the Stokes shift, corresponding to the fact that the emitted wavelength is longer than the incident wavelength (151). When a photon hits a molecule in its ground energy state, S0, if the energy of the photon corresponds to an energy difference between ground and excited states of the molecule, electrons from a ground state orbital undergo a transition to an excited state orbital, S1, S2 or more. This phenomenon, known as absorption is illustrated in the Jablonsky diagram (Figure

2.1)(152). It occurs on the femtosecond time scale. Once a molecule has absorbed energy in the form of electromagnetic radiation it can relax at S0 by various competing pathways. Fluorescence occurs when the molecule relaxes to its electronic ground state (S0) by emission of a photon. This emission occurs on the nanosecond time scale. The Stokes shift is due to the energy lost by the fluorescent molecule before the emission of photons. During this time (fs-~100 ps), the molecule relaxes to the lowest vibrational level (v0) of the lowest excited state (S1), from which emission occurs. The fluorescence process is cyclical, which means that the same fluorophore can be repeatedly excited unless the fluorophore is irreversibly destroyed (photo-bleaching). Relaxation can also occur via conversion to a triplet state, phosphorescence (10^{-3} to 10^{0} s), quenching or by a secondary non-radiative relaxation step (Figure 2.1).

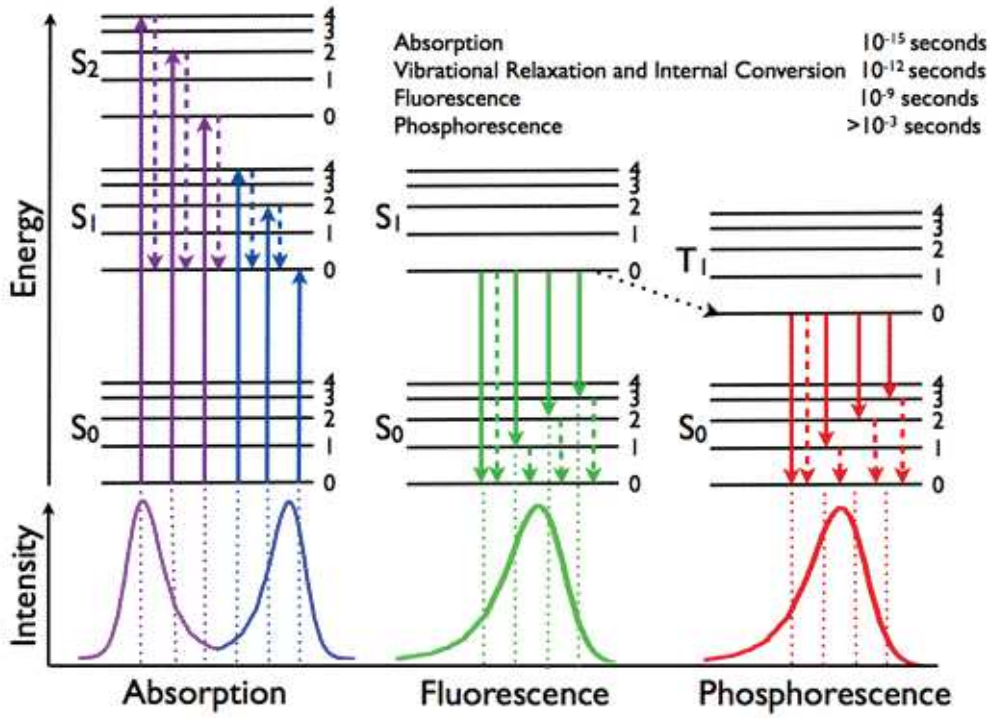

Figure 2.1: Jablonski diagram representing energy levels and spectra. Solid arrows indicate radiative transitions as occurring by absorption (violet, blue) or emission (green for fluorescence; red for phosphorescence) of a photon. Dashed arrows represent non-radiative transitions (violet, blue, green, red). Internal conversion is a non-radiative transition, which occurs when a vibrational state of a higher electronic state is coupled to a vibrational state of a lower electronic state. In the notation of, for example, S1,0, the first subscript refers to the electronic state (first excited) and the second one to the vibrational sublevel (v = 0). In the diagram the following internal conversions are indicated: S2,4→S1,0, S2,2→S1,0, S2,0→S1,0 and S1,0→S0,0. The dotted arrow from S1,0→T1,0 is a non-radiative transition called intersystem crossing, because it is a transition between states of different spin multiplicity. Below the diagram sketches of absorption, fluorescence and phosphorescence spectra are shown (from (153)*).*

2.1.1.2 Fluorescent probes

Most often, the (bio)molecules of interest are not naturally fluorescent. In this case, the molecules can be made fluorescent by chemically or genetically labeling a fluorescent molecule. A fluorescent probe is a fluorophore (or fluorochrome) with specific spectral properties(154). In addition to its extinction coefficient (= absorption cross-section) and its quantum yield (Q.Y. = number of photons emitted/number of photons absorbed), one of the most important properties of a probe is its photo-stability. Almost all fluorophores are photo-bleached during continuous illumination, especially in fluorescence microscopy where the light intensities are high.

Fluorophore probes can be divided in two categories:

- The first category includes organic dyes, such as rhodamine and fluorescein, which are the earliest and most conventional fluorescent probes used. These dyes have certain limitations that are critical to the quality of optical imaging: broad emission bands, short lifetime, low photochemical stability and photo-bleaching. Organic dyes can be chemically attached to a biological vector to target the proteins of interest. For example, in immunofluorescence a system is used with antibodies and their associated antigens to specifically label a molecule or structure in the living cell. Usually, these extrinsic antigens are labeled with small dyes (such as Alexa) that avoid interfering with the proper biological function.

- The second category regroups fluorescent proteins expressed genetically in living cells. An important addition to the probe library was the green fluorescent protein (GFP) from the bioluminescent jellyfish *Aequorea Victoria (*purified in 1962 (155), cloned in 1992 (156) and heterogeneously expressed in 1998 (157)). For this discovery, its application to biological research and improvement, Osamu Shimomura, Martin Chalfie and Roger Tsien were recently awarded of the Nobel Prize in Chemistry. This protein is a monomer of 27 kDa (Figure 2.2.A). Fluorescence is based on a fluorophore which results from the irreversible chemical maturation via a backbone cyclization reaction (Figure 2.2.B).

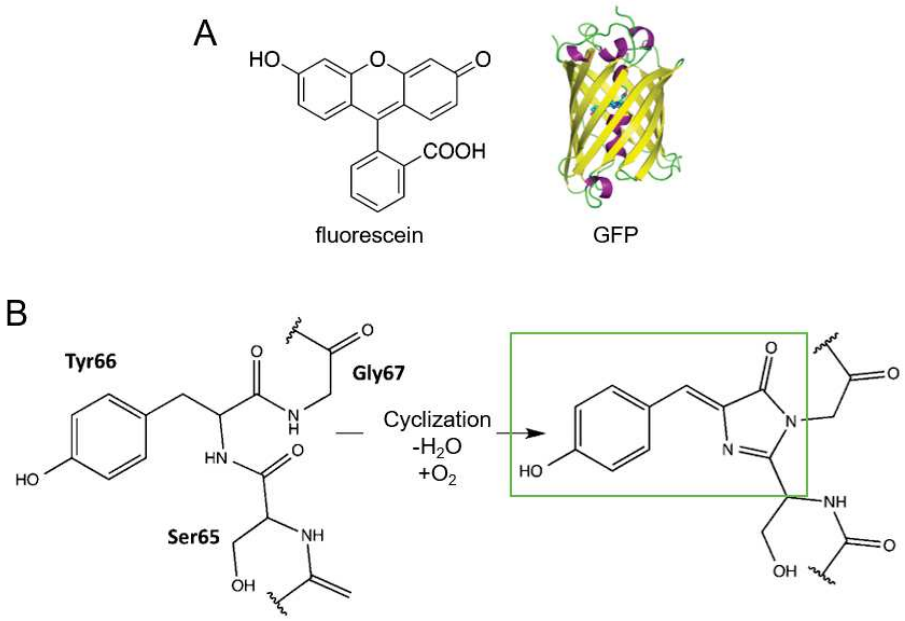

Figure 2.2: Structure of the fluorescent probes used in this work. A) Fluorescein used for calibration of the microscope and the Green Florescent Protein B) The ability of absorbing blue light by the GFP is accomplished by the adjacent serine 65, tyrosine 66 and glycine 67 (modified from (158)*).*

Wild-type GFP has two excitation peaks (396 nm and 475 nm) and an emission peak at 509 nm. GFP exhibits a reasonably high Q.Y. of 0.79 (159), yet a low extinction coefficient (22 000 $M^{-1}.cm^{-1}$), a slow maturation and a tendency to form dimers (157). GFPs with different spectral properties have been created by introducing mutations in the amino-acid sequence (160). In this work, we used a GFP variant, GFPmut2 which we will call GFP. This mutant has a higher quantum yield, a better photo-stability, and a much lower tendency to form oligomers compared to the commonly used eGFP (161). It is important to keep in mind that fluorescent proteins can change the normal biological function of the proteins to which they are attached and their photo-stability is generally not as good as fluorescent dyes.

2.1.1.3 Inherent limiting factors

2.1.1.3.1 Photobleaching and phototoxicity

Photobleaching happens when the fluorophore transfers from an excited singlet state to an excited triplet state (T, Figure 2.1) and undergoes an irreversible photochemical reaction that prevents molecules from fluorescing again. Bleaching depends on the exposure time and the intensity of the excitation light. This phenomenon is due to the generation of reactive oxygen species. The number of excitation/emission cycles before photo-bleaching depends on the fluorophore used and the environment. Another problem of using high intensity is the phototoxicity due to interactions between the excited

fluorophores and usually oxygen. The reaction produces free radical oxygen which can damage the fluorophore and cell structures. To prevent reactions with oxygens, there are antioxidant agents that reduce the amount of oxygen but many are toxic to living cells.

2.1.1.3.2 Background fluorescence

Fluorescence detection *in vivo* or in living cells can be compromised by background signals that are caused by unbound fluorescent probes that have not been removed or autofluorescence. Autofluorescence comes from the endogenous constituents of the cells (mainly from cofactors such as NAD(P)H and FAD). Their emission light can interfere with the signal of interest. Autofluorescence can be reduced with an appropriate emission filter and an excitation wavelength greater than 500 nm for 1-photon excitation. Indeed, these cofactors are respectively excitable at 340 nm and 450 nm (740 nm for 2-photon excitation) and the emission filter narrows the fluorescence detection. The reduction of photo-bleaching constitutes one of the main advantages of using infra-red 2-photon excitation for live-cell imaging as used in the present study. Moreover, the illumination volume inside cells is very much reduced. In addition, the use of a high-frequency illumination and filters reduce the scattering of light in dense media.

2.1.2 Confocal microscopy

Invented by Marvin Minsky in 1955 (162), confocal microscopy is an optical imaging technique to increase optical resolution and contrast by using focused light illumination (as opposed to wide-field illumination) and placement of a pinhole in the detection path (Figure 2.3). This pinhole eliminates the light out-of-focus and thus allows the reconstruction of three-dimensional structures from the images obtained. In order to form an image, the illuminated volume (Point Spread Function, PSF) is scanned through the sample while a point detector records the fluorescence signal. This technique has gained popularity for imaging live cells because of the increased optical resolution attained by confocal microscope. However, the signal intensity is decreased due to the pinhole, therefore requiring long exposures, and exposing the samples to photo-bleaching.

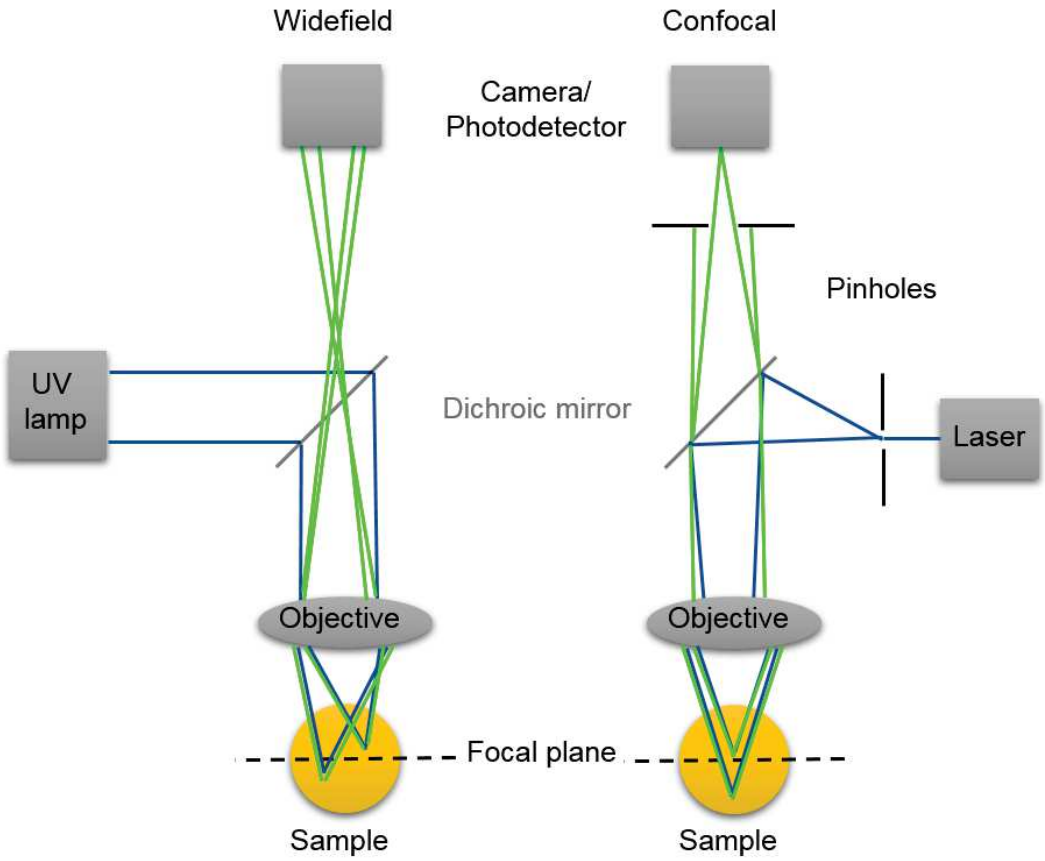

Figure 2.3: Configuration of a confocal microscope versus a wide-field microscope. Confocal microscopy increases optical resolution and contrast with a pinhole to block out-of-focus light in image formation.

2.1.3 2-photon microscopy

Biological tissues strongly scatter light, especially in visible wavelengths. While confocal microscopy can reject out of focus fluorescence using a pinhole, it fails to do so in deep tissue. Moreover, scattered light can contaminate the in-focus detection in confocal systems, leading to a loss of spatial resolution. Two-photon microscopy can overcome this limitation and provides an imaging depth greater than 500 µm in tissues.

2.1.3.1 2-photon excitation

The concept of two-photon excitation was first described by Maria Goeppert-Mayer (163) in 1931 but the first observation was done 30 years later by Wolfgang Kaiser (164). Two-photon excitation is a non-linear process in which two photons are simultaneously absorbed by a molecule. This excitation causes the excitation of a photon at a higher energy than either of the two excitatory photons (Figure 2.4.A). The probability of almost

simultaneous absorption of two photons is extremely low (165)(~10^{-50} cm^4s/photon, compared to 10^{-16} cm^2 for 1-photon absorption). Thus, a high flux of highly focused excitation photons is needed, usually from a femtosecond pulsed laser. The pulsing laser increases the probability of simultaneous excitation of 2 photons because an extremely high concentration of photons can be delivered to the sample in these very short (~100 fs) pulses. As a result, the axial propagation of the point spread function is much smaller than for single-photon excitation resulting in the improvement of the z-axis resolution (Figure 2.4.B). The double cone of the focused incident light is no longer observable. Only a small ellipsoidal region in the center is observed where the flux of photons is high enough for 2-photon excitation. This and the lower energy of photons are beneficial for intracellular measurements as they cause less damage to samples (cell destruction or photo-bleaching) and less autofluorescence. Indeed, excitation of the NAD(P)H fluorophores occurs by 3-photon excitation when 2-photon excitation is set at one micron, and this is even less probable than 2-photon excitation (~10^{-83} cm^6 $(s/photon)^2$).

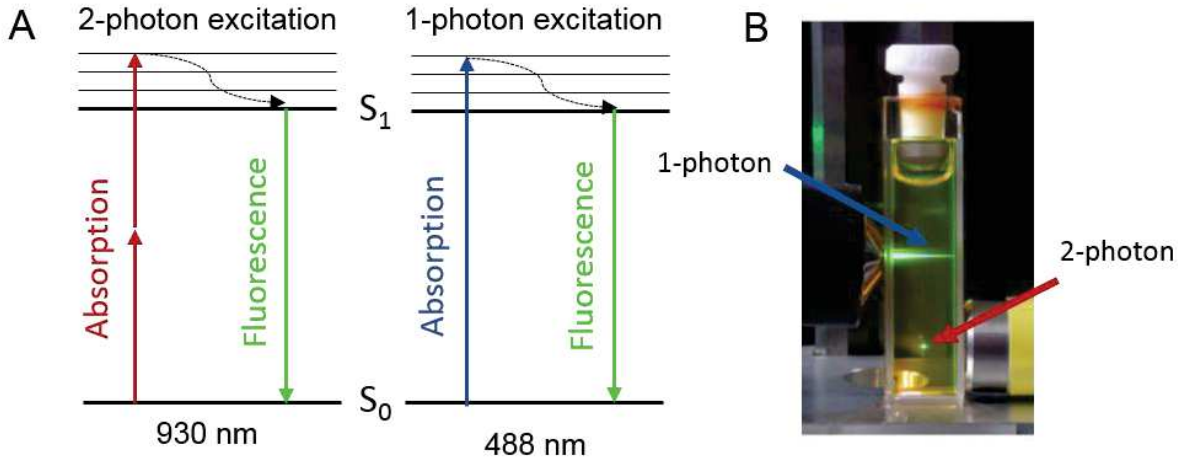

Figure 2.4: Comparison between one and two-photon excitation. A) Two-photon excitation of a fluorophore requires two photons of comparably lower photon energy than needed for one excitation. Each photon has the same energy corresponding to half the energy needed to excite the molecule. B) Improvement in the z- direction using a femtosecond laser compare to a mercury vapor lamp for one-photon excitation.

The 2-photon laser used in the present study, Sapphire Titan laser, has an excitation range of 740 nm to 1000 nm. This infrared excitation is less absorbed by the sample and can therefore penetrate deeper into sample. Compared to one photon excitation, it decreases the light contamination by the out-of-focus planes. Thus, two-photon excitation microscopy allows imaging of living tissues up to about 1 mm depth. Multiple photon excitation is beneficial for cross-correlation studies because two or more spectrally different fluorophores can be excited at the same wavelength. This is because the two-photon cross-sections are somewhat broader than those in one photon (165).

The point spread function (PSF) is the spatial distribution of incident light in the sample. Thanks to the development of confocal and 2-photon microscopy, the volume of the PSF is confined in 3D, so the excitation volume is small compared to 1-photon excitation (Figure 2.4.B) for a given wavelength, and similar for IR compared to visible light. It is important to know the size of the excitation volume to calibrate the system and calculate the concentrations of molecules. The volume of the two-photon PSF is well characterized by a 3D Gaussian-Lorentzian beam (Equation 3), where ω_0 is the beam waist and z_R is the Raleigh range.

$$V_{PSF} = \frac{\pi^2 {\omega_0}^2 z_R}{4} \tag{3}$$

The volume is underestimated by this equation because a physical volume is considered and not an open one. Thus, a gamma factor is introduced to take into account the variation excitation probability across the PSF. In two-photon microscopy, the probability of collecting a photon in all spaces of the excitation volume is not equal, so that the gamma factor Υ is less than 1. The effective volume (V_{eff}) is then defined by equation 4.

$$V_{eff} = \frac{V_{PSF}}{\gamma} \tag{4}$$

V_{eff} will be used to fit FCS curves.

2.1.4 Fluorescence Correlation Spectroscopy (FCS)

Fluorescence correlation spectroscopy was developed in the early 1970s by Madge, Elson and Webb with diffusion light scattering technique (DLS)(166). It is a technique widely used in Biophysics, first used in solution and more recently in cells (167, 168). FCS is one of many different modes of fluctuation analysis of fluorescent molecules diffusing freely through the excitation volume (V_{eff}) defined by a focused laser beam. The observed molecules are continuously replaced, allowing observation for long periods of time. The fluorophore does not undergo photo-bleaching while remaining in the excitation volume, but transitions to the triplet state may occur.

The parameter of primary interest is the time-depend fluctuations of the fluorescence intensity and not the average fluorescence intensity. Analyses of the rate and the amplitude of these fluctuations allow it to determine the local concentrations (c) and diffusion coefficients (D) of labeled molecules in the nanomolar concentration range. A small

observation volume can be obtained in confocal microscopy or in 2-photon microscopy. To get the most out of this technique, measurements should be made at a low concentration where only a few molecules are present in the observed volume. The data are interpreted in terms of correlation functions. Fluorescent molecules that diffuse trough the excitation volume create fluctuations in fluorescence intensity (δF).

$$\delta F(t) = F(t) - < F(t) > \tag{5}$$

These fluctuations are time correlated to extract from the correlation curve the diffusion coefficient and the number of particles. The autocorrelation curve is a representation of the self-similarity of a signal at some time point with itself at some time τ later. The autocorrelation function for the fluorescence intensities, normalized by the average intensity squared, is given by:

$$G(t) = \frac{< \delta F(t)\delta F(t+\tau) >}{< F(t) >^2} = G(0)\left(1 + \frac{\tau}{\tau_D}\right)^{-1}\left(1 + (\omega_0)^2\frac{\tau}{\tau_D}\right)^{-\frac{1}{2}} \tag{6}$$

where ω_0 is the dimension of the excitation volume to which detected fluorescence has dropped by a factor e^2 and τ is the diffusion time in case of two-photon excitation.

$$\tau_D = \frac{{r_0}^2}{8D} \tag{7}$$

For spherical particle, D is equal to:

$$D = KT/6\pi\eta R \tag{8}$$

where K is the Boltzmann constant, T is the temperature, η is the viscosity and R the hydrodynamics radius of the particle. The two main components of a correlation curve are its amplitude, G(0), and the mean decay time, τ. G(0) is inversely proportional to the number of fluctuating fluorescent particles. The average decay time gives the time scale of the fluctuation process. The concentration and size of the fluorescent particles influence both the fluctuations and thus the autocorrelation curve (Figure 2.5).

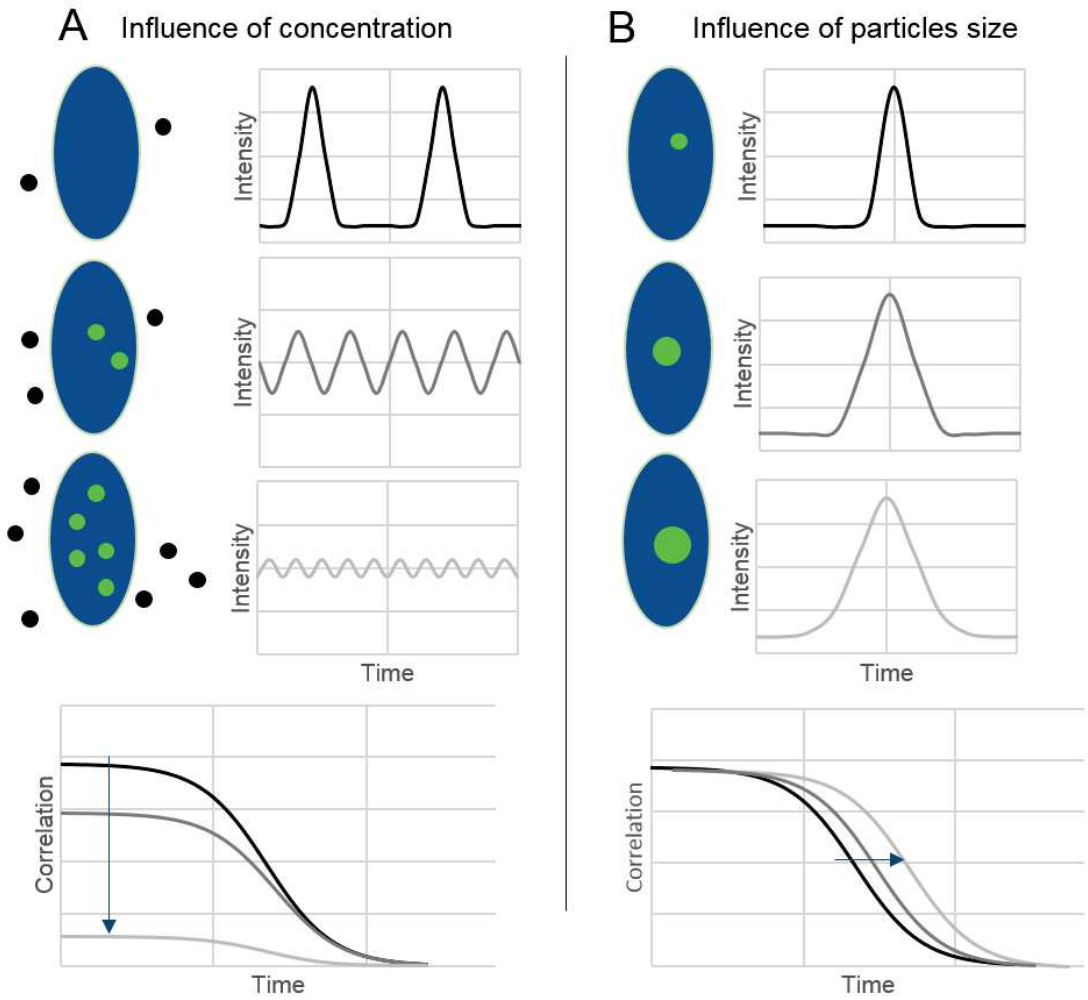

Figure 2.5: Principle of Fluorescent Correlation Spectroscopy. Influence of A) concentration and B) size of the fluorescent particles on the FCS measurements.

Two-photon excitation is very useful for FCS. Indeed, the excited volume is small because of the quadratic dependence of the light intensity. Importantly, the resolution of the z-axis is improved because the excited volume is less elongated. Fluorescence cross-correlation spectroscopy (FCCS) is a variant of FCS using two colors. Thus, it can monitor molecular interactions, enzymatic reactions and co-localization. Two spectrally distinct fluorophores are used to label two species. The signal detected on each detector is correlated to measure the cross signal. If the two species are bound, they diffuse together through the excitation volume, inducing a simultaneous fluctuation of the signal of the fluorescence intensity on their respective detector and thus a cross-correlation signal. Cross-correlation amplitude is a direct measure of the concentration of double-tagged particles diffusing together. The cross-correlation (Gx) of two populations of fluorescent particles, one green (G) and one red (R) is defined by the equation 9.

$$Gx(t) = \frac{< \delta F_G(t) \delta F_R(t+\tau) >}{< F_G >< F_R >} \qquad (9)$$

2.1.5 Principle of scanning Number and Brightness (sN&B)

A number of technics based on FCS have been published such as spot variation FCS (svFCS, (169, 170)), FRET-FCS (171), scanning FCS (172) with variant like RICS (see part 2.1.6.), TIRF-FCS (173), Image correlation spectroscopy (ICS, (174)) and brightness analysis (PCH (175)). The scanning Number and Brightness (N&B) analyses used in this work is also based on correlative fluorescence microscopy (176). However, unlike FCS, in which the laser beam is focused to a single spot in the sample, in sN&B, the laser beam scans the same field of view (FOV) multiple times. This provides multiple values for the intensity of fluorescence at each pixel in the image. N&B has been used in mammalian cells (177–185), neurons (186, 187), bacteria (188–190) and yeast (191) to calculate protein concentration and stoichiometry. Practically, in this approach, a series of raster scans (50-100 frames) is acquired using a pixel dwell time that is faster than the diffusion time to avoid averaging. This provides fluorescence intensity values over time for each pixel from which fluorescence fluctuations (variance, σ) and average intensity (<F>) can be calculated (Figure 2.6).

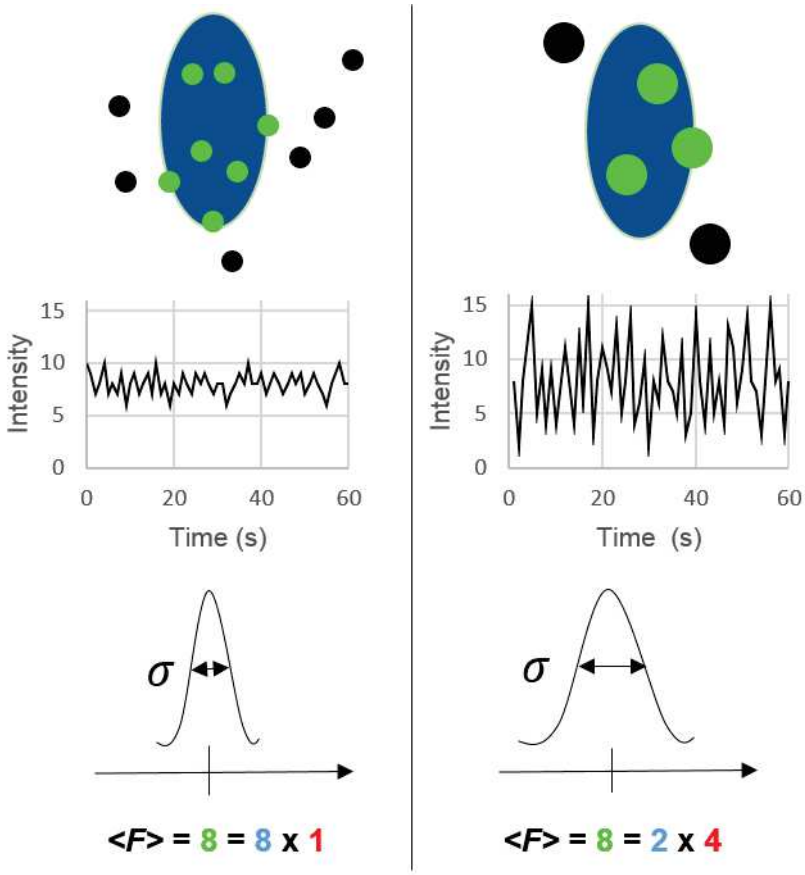

Figure 2.6: Principle of Number and Brightness (N&B) analysis. The variance of fluorescence fluctuations (σ) and the average intensity (<F>) depends on the number and the brightness of the fluorescent particles diffusing through the excitation volume. Thus, for the same average intensity a few bright particles can be distinguished from many dim particles.

As shown in Figure 2.6, this approach allows the distinction between a few bright particles and many dim particles, even if the average intensity is equal. Brighter particles cause larger fluctuations, and therefore a high variance. The fluorescence intensity can be deconvolved into the apparent brightness, B and number of particles in the effective volume, N, such that <F> = B x N. B is defined for each pixel as the ratio of the variance to the average intensity and N as the ratio of the total intensity to B.

$$B = \frac{\sigma^2}{< F >} \quad \text{and} \quad N = \frac{< F >}{B} = \frac{< F >^2}{\sigma^2} \tag{10}$$

The brightness values are shot noise corrected (176), meaning that the true brightness e = B – 1. Molecular brightness (e) is defined as the number of photons emitted per second per molecule when the molecule is in the middle of the excitation volume (Equation 11). Brightness depends on the intensity of the laser and the sensitivity of the detector. The true number, n, is the average of molecules present in the excitation volume (Equation 12).

$$e = \frac{< \delta F(t) >^2 - < F(t)}{< F(t) >} = B - 1 \tag{11}$$

$$n = \frac{< F(t) >^2}{< \delta F(t)^2 > - < F(t) >} = \frac{NXB}{e} \tag{12}$$

Thus, sN&B can provide information on the stoichiometry of the proteins of interest and their concentrations using the molecular brightness and the absolute number of fluorescent particles detected at each pixel of the image (see section 2.4.1).

2.1.6 Principle of Raster Image Correlation Scanning (RICS)

While N&B allows spatial information, RICS gives temporal information as described by Digman and Gratton (192). From the same raster scans used for N&B analyses, it is possible to extract information on the diffusion properties of the fluorescent molecules which can reveal interactions and binding events. The RICS analysis exploits the different time scales separating data acquisition between pixels on a series of raster-scanned images. For sN&B analysis, images of typically 256x256 pixels are recorded using a pixel dwell-time on the tens of microseconds time scale. Therefore, the time separating pixels on different lines of the same image is in the millisecond range, whereas the time separating pixels on different

frames are in the second range (Figure 2.7). Pixel-based fluorescence intensity fluctuations analysis such as sN&B and RICS can thus be performed even for very slow-moving particles such as DNA-binding proteins. In RICS the different time scales can be exploited to extract the diffusion coefficient of the fluorescent particles by fitting of the pixel pair spatio-temporal correlation function.

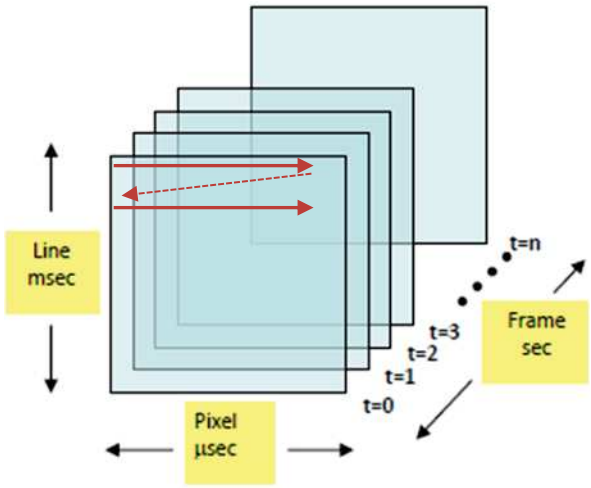

Figure 2.7: Different time scales of raster-scanning exploited by sN&B and RICS. The top left pixel is measured first, then the laser beam is moved to the right and travels to the next line. With a pixel dwell time of 40 µs and an image size of 256x256 pixels, the horizontal line is on the microsecond time scale and the vertical line is on the millisecond time scale. For the same pixel within the scans, the time scale between frames corresponds to seconds.

The intensity is acquired for each pixel ($i_{x,y}$) of each frame and the image autocorrelation is calculated for each frame using the equation 13.

$$G(\xi,\psi) = \frac{< \delta_i(x,y)\delta_i(x+\xi,y+\psi) >_{x,y}}{< i(x,y) >_{x,y} < i(x,y) >_{x,y}} \qquad (13)$$

with ξ and ψ the spatial correlation shift of x and y and δ_i=i-<i> and $<\ldots>_{x,y}$ the spatial average of the image. All the autocorrelations of each frame are averaged to allow background subtraction (see section 2.4.2) and increase the signal-to-noise ratio. The result is fitted using an equation relating the spatio-temporal correlation to the diffusion coefficient and particle concentration as described in (193, 194) such as the overall correlation (C(r,t)) is equal to the multiplication of equations 14 and 15.

$$S(x,y) = exp\left\{-\frac{\frac{1}{2}\left[\left(\frac{2x\delta r}{\omega_0}\right)^2 + \left(\frac{2y\delta r}{\omega_0}\right)^2\right]}{\left(1+\frac{4D(x+ny)\tau}{\omega_0}\right)}\right\} \quad (14)$$

$$G(x,y) = \frac{\gamma}{N}\left(1+\frac{4D(x+ny)\tau}{\omega_0^2}\right)^{-1}\left(1+\frac{4D(x+ny)\tau}{Z_0^2}\right) \quad (15)$$

where ω_0 is the beam waist and Z_0 the axial waist, δ is the pixel size, n is the sequential pixel number and τ is the pixel dwell time.

$$C(r,t) = \frac{1}{(8\pi DT)^{3/2}} exp\left(-\frac{r^2}{8Dt}\right) \quad (16)$$

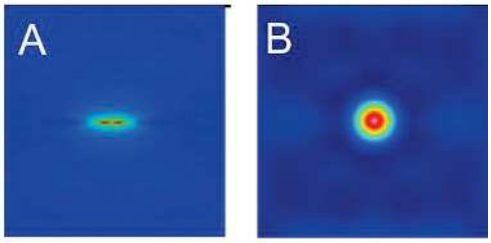

Figure 2.8: Example of RICS correlation image. Diffusion of A) a freely diffusing GFP protein (about 10 $\mu m^2/s$) or B) a GFP moiety fused to a membrane protein (0.1 $\mu m^2/s$).

The probability of seeing a molecule in the next line is higher if the molecule diffuses slowly (Figure 2.8.B). Thus, the correlation decreases rapidly on the vertical axis (ms time scale) if the molecule diffuses quickly (Figure 2.8.A). The autocorrelation function will correspond to the size of the PSF if the particle is immobile on the millisecond time scale.

2.2 Preparation bacterial samples for *in vivo* microscopy

Protocols for preparing samples for 2-photon scanning fluorescence microscopy are adapted from Ferguson et al. (188). A resumé is presented below and detailed protocols can be found in the annex.

2.2.1 *E. coli* MG1655 K12 strains

All strains were constructed by the A. Aertsen's group using *E. coli* K12 MG1655 (195) as the parental strain (for details see (196)). Fusions of GFPmut2 (called GFP in the manuscript) with Mrr wild-type (WT) as well as mutants were constructed. Expression from the natural P_{mrr} promotor being too low, the GFP-Mrr constructs were expressed under the control of the arabinose-inducible P_{BAD} promotor carried by a low multi-copy plasmid or insert at the natural chromosomal locus of the *mrr* gene. The gene coding sequence of the M.HhaII methylase was cloned on a high copy plasmid under the control of an IPTG (isopropyl β-D-thio-galactopyranoside) -inducible promotor.

Table 2.1: Resume of all E. coli strains used for microscopy experiments.

Strain	Chromosomal and/or plasmid	produces	Growth conditions
E. coli MG1655	-	-	-
E. coli MG1655 PBAD-*gfp-mrr*	Chromosomal	Free GFP and unlabeled Mrr	Induction arabinose 0.4%
E. coli MG1655 PBAD-*gfp-mrr* + pTrc99A empty	Chromosomal + empty plasmid	Free GFP and unlabeled Mrr	Induction arabinose 0.4% and IPTG 1 mM
E. coli MG1655 PBAD-*gfp-mrr* + pTrc99A hhaII	Chromosomal + plasmid	Free GFP and unlabeled Mrr and HhaII	Induction arabinose 0.4% and IPTG 1 mM
E. coli MG1655 PBAD-*gfp-mrr*	Plasmidic	Free GFP and unlabeled Mrr	Induction arabinose 0.002%
E. coli MG1655 PBAD-*gfp ::mrr*	Plasmidic	GFP-Mrr	Induction arabinose 0.002%
E. coli MG1655 Pmrr-*gfp ::mrr*	Chromosomal	GFP-Mrr	

Same strains for mutants GFP-Mrr D203A, GFP-Mrr V173A and GFP-Mrr H279Y	*E. coli* MG1655 P*BAD-gfp::mrr*	Chromosomal	GFP-Mrr	Induction arabinose 0.4%
	E. coli MG1655 PBAD-*gfp*::Mrr + pTrc99A empty	Chromosomal + empty plasmid	GFP-Mrr	Induction arabinose 0.4% and IPTG 1 mM
	E. coli MG1655 P*BAD-gfp::mrr* + pTrc99A-*hhaII*	Chromosomal + plasmid	GFP-Mrr and HhaII M.HhaII	Induction arabinose 0.4% and IPTG 1 mM
E. coli MG1655 PBAD-*gfp-mrr*		Plasmidic	GFP-Mrr$_{N111S/D124G/V175G}$	Growth on glucose 0.4% and induction arabinose 0.002%

2.2.2 Bacterial cultures

The day before an experiment, overnight cultures at 37 °C in LB were grown from -80°C glycerol stock with appropriate antibiotics. The next morning, the cultures were diluted into fresh LB medium (1/100 or 1/1000 for strains carrying the chromosomic or plamidic mrr constructs, respectively). After 1h at 37 °C at 200 rpm, cells were induced with arabinose 0.4 % and grown to the late exponential phase (optical density at 600 nm (OD_{600}) ~ 0.6). To avoid overexpression, plasmidic strains were induced for only 30 to 40 min. When appropriate, cultures at OD_{600} of ~ 0.15 were induced with 1 mM IPTG for induction of the MTase. In case of very low expression levels, e.g. in the strain expressing chromosomic GFP-Mrr from the natural P_{mrr} promotor, minimal media (M9) was used instead of LB in order to reduce the autofluorescent background contamination.

2.2.3 Sample preparation for microscopy

Microscopy samples were prepared as follows. A 500 µl - 1 mL cells culture at an OD_{600} ~ 0.6 was centrifuged at 850 × g for 2 min and re-suspended in LB to a final OD_{600} of ~ 25. This high density is important for imaging. A field of view (FOV) full of bacteria immobilized in a single layer is required for optimizing the quality of the data. A few microliters were deposed on a 2% agar pad sandwiched between two glass cover slips No1 (VWR) coated with poly-L-Lysine as depicted in annex 7.2. The pad was mounted in an attofluor (a stainless-steel) holder.

2.2.4 Pressure treatment

A volume of 500 µl of culture at an OD_{600} around 0.6 was centrifuged for 2 min and re-suspended in 50 µL of LB and transferred in a 50 µL Microtubes. Then, a computer-

controlled HUB440 high pressure generator equipped with the SW-16 pressure vessel was used to pressurize samples, typically for 15 min at 100 MPa. After the release of pressure, samples were centrifuged and re-suspended in a few µL of LB to prepare the microscopy sample. All pressure equipment is from Pressure BioSciences (Inc., South Easton, MA).

2.3 Data acquisition for *in vivo* microscopy

2.3.1 Two-photon scanning microscope set-up

A schematic of the two-photon microscope used in our studies is shown in Figure 2.9. Samples were raster scanned to image FOVs using a Titane:Saphir femtosecond mode-locked infrared laser (MaiTai, Newport/Spectra Physics, Mountain View, CA, USA) pulsed with a 80 MHz repetition rate. The small excitation volume obtained with a 2-photon excitation was focused through a 60x 1.2NA water immersive objective (Nikon APO VC). A 735 nm low pass dichroic filter (Chroma Technology Corporation, Rockingham, VT, USA) filtered the infrared light from detected light. Raster scans were performed with scanning mirrors (ISS, Champaign, IL). The emitted light was de-scanned and filtered with a 530/43 nm emission filter and photons were detected by avalanche photodiodes (Perkin Elmer).

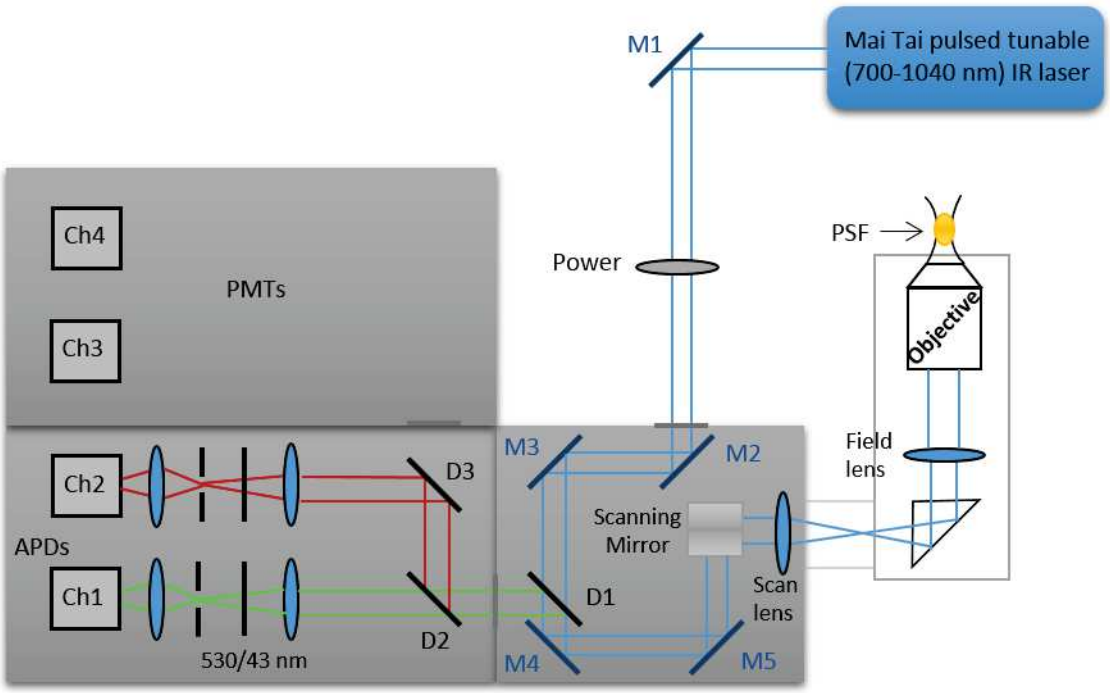

Figure 2.9: Schematic of our 2-photon scanning microscope.

2.3.2 FCS acquisitions

To ensure that our microscope was well aligned for correlation, each day of experiment we performed FCS measurements with a solution of fluorescein (Spectrum) at 45 nM. We acquired data at a frequency of 500 MHz for 100 s at 780 and 930 nm. We checked if the G(0) was as high as expected, corresponding to the diffraction limit. We also verified the fluorescein brightness at the beginning of each day. We fitted the fluorescein FCS data with the ISS Vista Vision software. Parameters for fitting were: 2-photon excitation, 3D Gaussian with 8Dt, one species with the concentration factor and gamma factor checked. On the software, G(t) curve and fluorescence intensity are displayed during the acquisition. It allows observation of bleaching or large fluctuations created by big aggregates that could impact the results. Some artefacts can occur from detector after pulsing (fast time scale) that we can prevent doing FCCS measurements instead of FCS.

2.3.3 Acquisitions for sN&B and RICS analysis

For each microscopy sample, series of raster scans were recorded for the same field of view (FOV). We typically recorded 50 scans of each FOV with the size of 20x20 µm and 256x256 pixels using a pixel dwell time of 40 µs. Thus, one raster scan series took 2 minutes and we usually recorded 5 to 8 FOVs for each sample. For time laps experiments however, we took only 25 frames instead of 50 in order to have enough time to record 4 FOVs at each time point. The excitation wavelength was set to 930 nm and the laser power to 11 mW to ensure a good GFPmut2 emission yet minimized autofluorescence of the cytoplasm and photo-bleaching. Although RICS analysis can be carried out on data acquired under these conditions, we also imaged FOVs of 13x13 µm to reduce the size of a pixel (78 to 51 µm), yielding better temporal resolution for RICS parameters. Each day, we performed acquisitions of the background strain MG1655 and a strain expressing the monomeric GFP under the same conditions using the same acquisition parameters. Indeed, the alignment of the microscope can slightly vary from day to day, changing the beam intensity and hence, molecular brightness of the fluorescent particles.

2.4 I*n vivo* microscopy data analyses

2.4.1 Number and brightness analyses

Ferguson et al. were the first to use the N&B approaches for quantitative studies of fluorescent proteins in live bacterial cells (197). We carried out similar analyses to those described in detail in that previous work (198) which use the PaTrack software implemented for bacterial cell tracking by P. Dosset (CBS, Montpellier). In PaTrack the bacterial cells of a FOV is automatically detected or manually tracked depending the fluorescence intensity using a map of the average fluorescence intensity (Figure 2.10). The

calculation of average fluorescence intensity, brightness and number is done for all bacteria in each FOV using only the central 50% of pixels in each bacterium. This avoids including pixels for which the PSF straddles the bacterial membrane and assures that all intensity measurements are entirely within each cell. Then, the PaTrack output data are transferred to an Excel file. All intensity and variance values at pixels within cells are averaged for each FOV and FOVs that differ greatly from the mean are eliminated. This can result be due to moving bacteria, sliding pad, or poor focusing. Then, from the values from all cells within the remaining FOVs are averaged to obtain ***F****sample,* ***e****sample* and ***n****sample* values that must be corrected for background contributions using the average fluorescence intensity and brightness values obtained from the background strain (***e****bg* and ***F****bg*) the same day under the same growth and imaging conditions as follows:

$$< \boldsymbol{e} > \ GFP\ sample = \frac{(\boldsymbol{e}sample * \boldsymbol{F}sample - \boldsymbol{e}bg * \boldsymbol{F}bg)}{\boldsymbol{F}sample - \boldsymbol{F}bg} \qquad (17)$$

$$< \boldsymbol{N} > GFP\ sample = \frac{(\boldsymbol{F}sample - \boldsymbol{F}bg)^{\boldsymbol{2}}}{(\boldsymbol{e}sample * \boldsymbol{F}sample - \boldsymbol{e}bg * \boldsymbol{F}bg)} \qquad (18)$$

GFP-Mrr stoichiometry was obtained by dividing the background corrected brightness values of GFP-Mrr by the brightness of the monomeric GFP measured the same day.

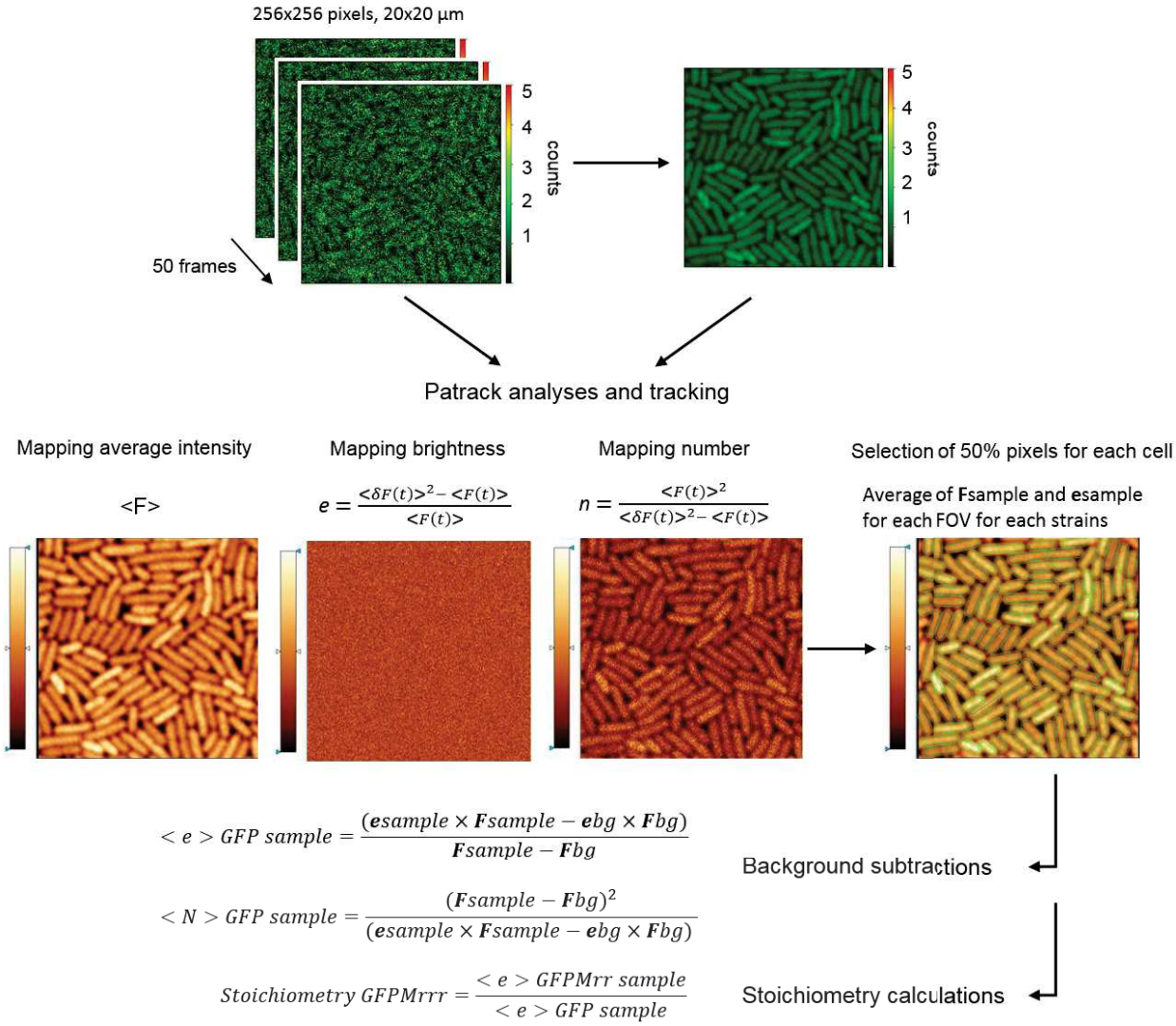

Figure 2.10: Calculation of Number and Brightness analyses in order to get GFP-Mrr stoichiometry using PaTrack.

To calculate the absolute concentration of GFP-Mrr, we divided the background corrected intensity (<F>GFP-Mrr) by the molecular brightness of the monomeric GFP ($<e>_{GFP}$), the excitation volume inside the bacteria (Vol_{ex}) and the Avogadro number (N_A)(Equation 19). Vol_{ex} is different from Vol_{eff} since the cross section of a bacterial cell is smaller than the PSF. It was previously estimated that for a rod-shape bacterial cell of about 1 µm in diameter, Vol_{ex} is about 0.07 fL (Figure 2.11)(198).

$$[GFP - Mrr](nM) = \frac{< F > GFPMrr}{< e > GFP\ *\ Vol_{ex}\ * N_A} \qquad (19)$$

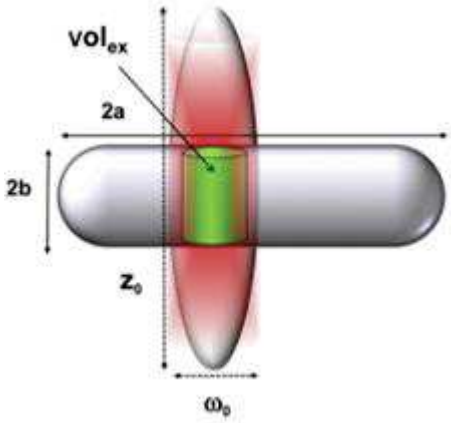

Figure 2.11: 2-photon fluorescence excitation volume inside a bacterium. The Vol_{ex} represented in green is the excitation volume inside the bacterial cell corresponding to the cross section of the PSF (in red) with the bacterial cytoplasm. It has been estimated at around 0.07 fL in E. coli cells.

2.4.2 RICS analyzing

SimFCS software (E. Gratton, LFD, University of California -Irvine) was used to analyze data according to equations 13-16 and extract horizontal and vertical spatial and temporal autocorrelation curves of the fluorescent signal. We performed a moving average background subtraction to remove stationary objects using 10 images. The average of 1 to 10 is subtracted to the frame 5. The time separating the acquisition at adjacent pixels is much shorter on the horizontal lines than on the vertical lines. So, the probability of detecting a particle in adjacent pixels is very high therefor the spatial autocorrelation function is high on the horizontal axe (Figure 2.12, in red), whereas on the vertical axe, if the particle is moving fast, such as freely diffusing GFP, it will usually be gone by the time the laser starts to record the next line so the autocorrelation function is low (Figure 2.12, in black).

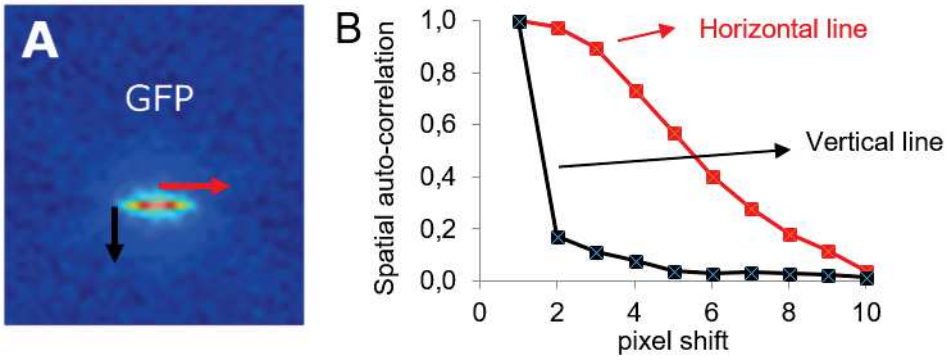

Figure 2.12: RICS analyze for free GFP. GFP is expressed in E. coli MG1655 under the control of the PBAD promotor in the chromosome. Data are analyzed with SimFCS using a moving average background subtraction with 10 frames. A) RICS

autocorrelation image and B) autocorrelation curves corresponding to the image with the horizontal line (red) and the vertical line (black). GFP diffuses freely in the cytoplasm and fast on the ms time scale so the autocorrelation function is low on the vertical axe.

2.5 *In vitro* characterization of StrepTagged GFP-Mrr

2.5.1 Strains used for purification

The *E. coli* strains used for the purification of GFP-Mrr WT and mutants were provided by the Aertsen's group. N-terminal Strep-tag® II fusions of GFP-Mrr were cloned into the pRSET B vector (Invitrogen) and expressed in *E. coli* BL21 (DE3) cells or T7 Express. The Strep-tag II is a sequence of 8 amino acids (WSHPQFEK) and 1 kDa (199). The total molecular weight of StrepTagged GFP-Mrr monomer is 61 kDa.

2.5.2 Purification and size exclusion chromatography

The protocol for the production and purification of StrepTagged GFP and GFP-Mrr can be found in annex. Strains were grown in minimum media and induced with 100 µM IPTG for 3h at 30 °C (Figure 2.13).

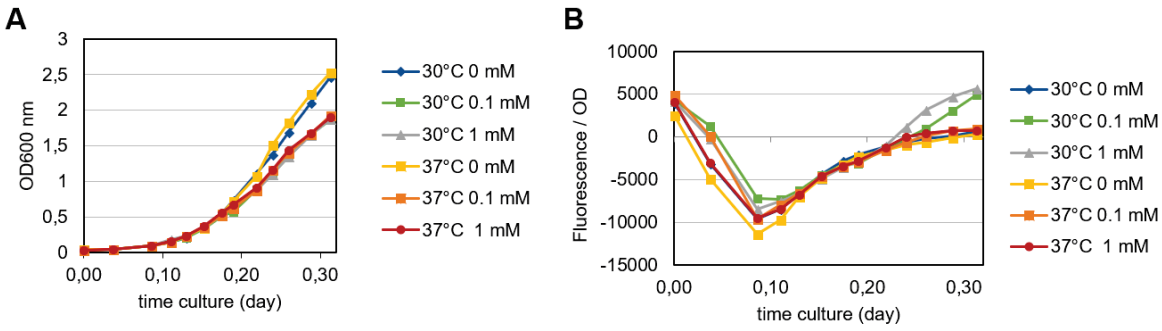

Figure 2.13: StrepTag-GFP-Mrr induced cultures. Cultures were grown in M9 synthetic medium at 37 °C to an OD_{600} of 0.7 and induced with different concentrations of IPTG (0, 0.1 or 1 mM). Cultures were then grown at 37°C or shifted to 30°C. At different time, we measured the OD_{600} and the fluorescence of the culture. A) OD_{600} and B) Ratio of the GFP fluorescence over the OD_{600}.

We encountered difficulties in purifying the protein. Although the StrepTag-GFP-Mrr induction level was good, the purification yield was rather low. As a restriction enzyme, Mrr is expected to have high affinity for DNA and indeed, after cell lysis and centrifugation, most of the GFP-Mrr protein remained in the pellet, probably associated to chromosomal DNA. Purification of the soluble fraction was performed on a high capacity Streptactin-

superflow resin (IBA). Analytical size exclusion chromatography was performed by injecting on a Superdex 200 10/300 column (GE Healthcare) pre-calibrated with Cytochrome C, Carbonic Anhydrase, Bovine serum albumin, Alcohol Dehydrogenase, β-amylase and dextran blue (Figure 2.14).

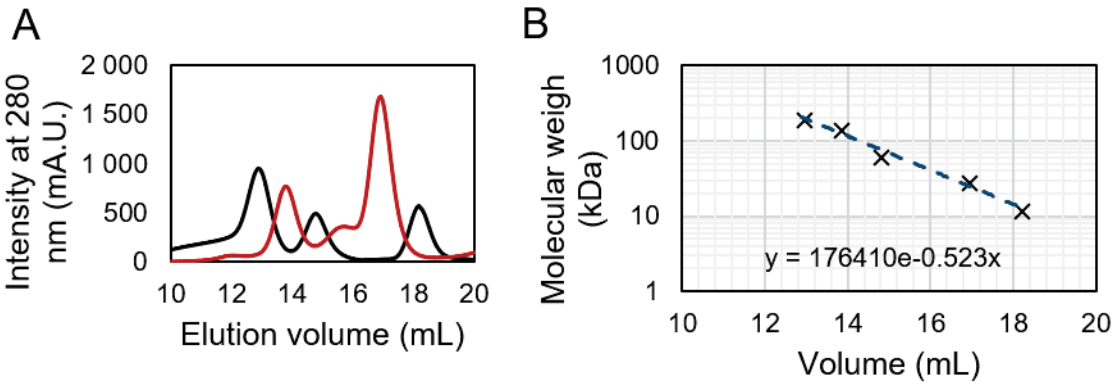

Figure 2.14: Calibration of the size exclusion chromatography Superdex 200 10/300 column. A molecular weight calibration kit (MWGF 200, Sigma) was used with a first injection (in black) of cytochrome C (12.4 kDa), β-amylase (200 kDa) and BSA (BSA, 66 kDa) and a second injection (in red) of carbonic Anhydrase (29 kDa), Alcohol Dehydrogenase (150 kDa) and dextran blue (2000 kDa). A) Elution profile at 280 nm and B) Calibration curve obtained using the molecular weights and the elution volumes of all compounds.

Due to the low concentrations, the relative amount of fluorescent proteins in the eluted was determined using an infinite M1000 PROplate reader (TECAN, Switzerland). The exciting/emission wavelengths were 488/15 nm and 528/20 nm. Measurements were done in 96-wells plate (Greiner) with 100 µL from each elution fraction.

2.6 High pressure microscopy

Fluorescence intensity fluctuation techniques allow the measurements of the stoichiometry of proteins. Hence, they are useful to measure protein interactions and dissociation under pressure. We decided to use FCS to investigate the *in vitro* behavior of purified GFP-Mrr as a function of pressure. Quantitative microscopy studies under pressure are challenging. The first microscopy chamber was developed in 1970's and was only able to sustain a pressure of 80 MPa, with a few applications to measure fluorescence of a calcium dye under pressure. Subsequently, several chambers were developed to sustain high pressure using quartz, sapphire and diamond windows, which have high refraction indexes. Thus, the quality was neglected and the resolving power of the images was decreased. The main improvement is the use of a thin capillary as a pressure vessel

developed by Müller and Gratton (200) and used to study giant unilamellar vesicles (201). Müller and Gratton used a fussed silica circular capillary (Polymicro, Phoenix, AZ) that can withstand, in theory, pressures up to 700 MPa. The capillary has an inner diameter of 50 µm and an outer diameter of 350 µm (Figure 2.15 A). Thus, the thickness of the walls of 150 µm matches the thickness a regular coverslip. This allows the use of high N.A. immersion objectives. One end of the capillary was threaded through a drilled pressure plug, while the other was sealed with a blow torch. To avoid heating the sample, (which was already loaded prior to heat sealing) a very long capillary, 30-50 cm, was required. Unfortunately, the cylindrical geometrical shape of the capillary leads to refraction of the laser beam and a distortion of the optical point spread function. Nonetheless these authors showed that reasonably high-quality FCS measurements could be made using this capillary system under pressure using 2-photon excitation.

We used a system similar to that of Müller and Gratton(200). However, we made some adjustments to aid in sample loading. Rather than sealing one end with a blow torch, we used the drilled plug system for both ends. Following Müller and Gratton, the capillary is inserted in pressure plug drilled to the appropriate diameter and sealed with epoxy glue as shown in Figure 2.15.B.

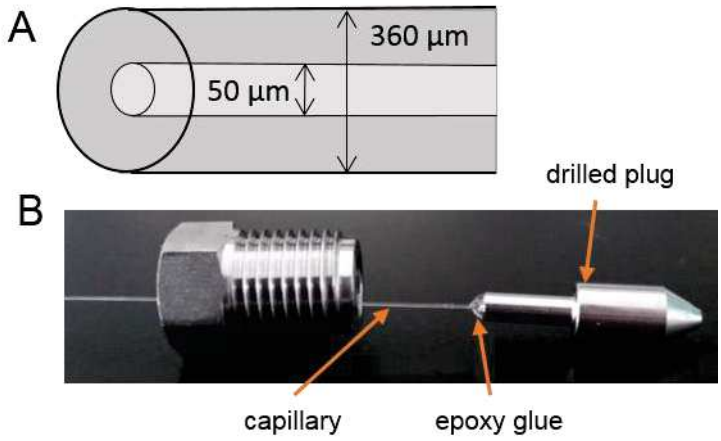

Figure 2.15: Representation of the fused silica circular capillary used for microscopy experiment under pressure. A) A schematic cross section of the capillary. B) The capillary is glue into a small hole drilled in a pressure plug.

Because both ends were connected to the pressure system via the drilled plugs, we could use a peristaltic pump to load the sample into the capillary (Figure 2.16). Pressure experiments are performed by closing a valve located at one end of the capillary (V5 on Figure 2.16.A). The other end of the system is disconnected from the peristaltic pump and connected to an automated pressure pump. Our current setup used an automated, modified HPLC pump from Pressure Bioscience (Waltham, MA) with a maximum pressure of 15,000 psi (~ 100 MPa).

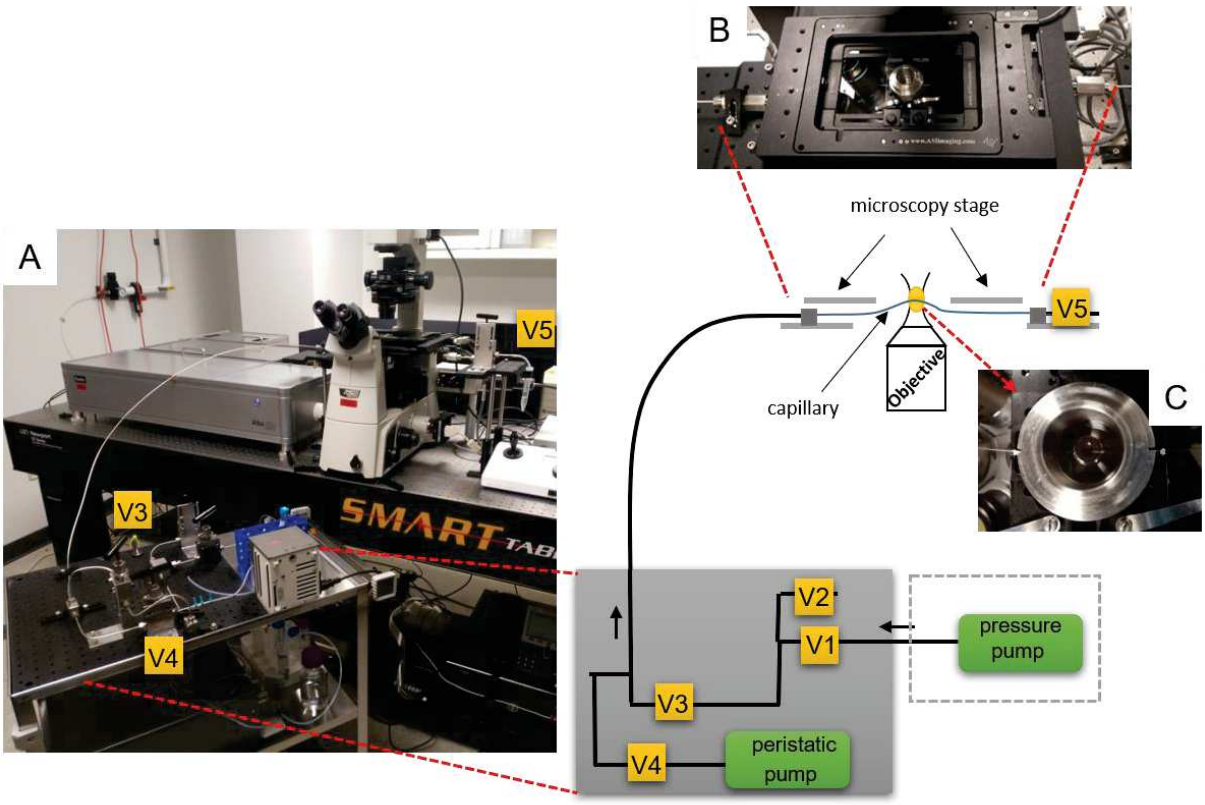

Figure 2.16: High pressure set-up for microscopy experiments. A) Overall image and schematic of the set up showing the pressure pump and the peristatic pump. Two valves allow switching with either one of the pumps to load the sample or apply pressure (V3 and V4). B) Microscopy stage showing the capillary immobilized in a holder. C) Zoom of the capillary in sandwich between a coverslip and the objective with glycerol as a coupling media.

The capillary is immobilized in a stainless-steel holder the size of an attofluor coverslip holder used for the agar pad (Figure 2.16.C). To perform HP-FCS experiments, we used the same microscope set-up as previously described in section 2.3.1, except that the water objective was replaced by a 60X 1.4 NA oil immersion objective (Nikon APO, VC). To match the fused silica capillary refraction index, oil was replaced by glycerol as the coupling medium. A coverslip is used to rigidly support the capillary and avoid bending upon contact with the objective. Similar to Müller and Gratton, we performed a characterization of the capillary using a solution of fluorescein at a concentration of 18 nM. Fluorescence was recorded at 930 nm for 100 s at a 500 kHz frequency on two detectors. FCCS allows better autocorrelation curves with elimination of after pulsing. We fitted data using Vista vision software.

3. Investigating Mrr behavior in response to pressure shock and HhaII MTase induction.

To investigate the mechanism underlying the Mrr-mediated pressure-induced SOS response in *E. coli* strain MG1655, we used fluorescence intensity fluctuation spectroscopy to characterize the behavior of GFP-Mrr fusion before and after a pressure shock, or due to DNA hyper-methylation by the HhaII methyltransferase. A previous study (143), carried out by our collaborators of the Aertsen group revealed by epifluorescence the appearance of bright GFP-Mrr foci in the middle of each bacterium co-localized with a condensate nucleoid after HP treatment or induction of M.HhaII (Figure 1.10). Using the 2-photon sN&B approach, and because of the low levels of autofluorescence at the IR excitation wavelengths, we were able to perform these experiments at a much lower concentration of GFP-Mrr expressed from a chromosomal insertion inducible by arabinose instead of the multi copy plasmid used in the prior work. As described in section 2.1.5, the pixel-based analysis of the fluctuations of fluorescence signal of raster-scanned images of immobilized live cells allows the direct measurement of the molecular brightness (*e*) and the absolute number (*n*) of fluorescent proteins. Molecular brightness corresponds to the photon counts per measurement time for a single molecule. Knowing the value of *e* for monomeric GFP molecules measured under the same conditions, one can calculate the average stoichiometry of oligomers of the fusion protein. For instance, a dimer of a protein fused to GFP will present a value of *e* that is twice that of monomeric GFP. In addition, these experiments provide information on Mrr localization, intracellular concentration and diffusion properties.

Measurements were made in unstressed *E. coli* cells and in living cells after a high-pressure shock or induction of the foreign methyltransferase HhaII. Results of the sN&B analysis revealed an unexpected oligomeric switch behind Mrr activation by HP or M.HhaII induction. We expected to measure a higher stoichiometry of GFP-Mrr in the bright foci observed after HP treatment, due for instance to the formation of aggregates upon protein denaturation. We found that in unstressed cells, GFP-Mrr was evenly distributed throughout the cells and diffused on average as a tetramer. Surprisingly, we found that the stoichiometry of Mrr in the foci observed after HP or M.HhaII induction was in fact 2-fold lower than that in unstressed cells, *i.e.,* dimer instead of tetramer. We could also confirm this result in strains expressing a chromosomal *gfp-mrr* gene at very low level from the natural promotor. Based on these results we have proposed a model for the activation of the SOS response by pressure or DNA hyper-methylation. Such a model would never have been developed without the knowledge on the oligomeric state of intracellular proteins afforded by sN&B. No other single molecule techniques allow for the measurement of the stoichiometry of Mrr in living bacterial cells at a low expression level. The timescale and simplicity of the efficiency of sN&B measurements demonstrate its utility for obtaining detailed molecular insight into the behavior of proteins in living systems.

3.1 *In vivo* characterization of GFP-Mrr by fluorescence fluctuation microscopy

Most of the results obtained *in vivo* to characterize Mrr were carried out using sN&B analyses. We studied the behavior of GFP-Mrr WT and a catalytic mutant (GFP-MrrD203A) which abolishes the induction of the SOS response HP- or M.HhaII-dependent. This mutation is located in the proposed catalytic loop of Mrr based on homology with other Type IV REases. We have proposed a model where the pressure dissociates the inactive tetramers into active dimers which are able to recognize, bind and cleave dsDNA. Dimers not bound to DNA would re-associate into tetramers when the pressure is released. In contrast, the hyper-methylation of DNA upon M.HhaII induction would create a large number of high affinity sites for Mrr, pulling the equilibrium between inactive tetramers to active dimers that irreversibly cleave and stay bound to the DNA. As expected, HP has no effect on the behavior of GFP-MrrD203A, except that the stoichiometry in unstressed cells is decreased probably due to a destabilization of the tetrameric form. However, the methylation of many high affinity sites by MTase leads to results similar to those of WT, even if no cleavage and therefore no induction of the SOS response occurs. We presume this is due to the high affinity, nearly irreversible interaction of Mrr with the methylated sites.

3.2 Purification and *in vitro* characterization of GFP-Mrr

Part of my PhD work was aimed at the purification and *in vitro* characterization of the GFP-Mrr protein in order to compare its behavior with that measured *in vivo* by fluorescence fluctuation microscopy. Unfortunately, in spite of many attempts, we did not succeed in purifying sufficient amounts of the protein for extensive *in vitro* studies. Although the protein could be expressed at rather high level using inducible expression systems, most of the fusion protein remained in the cell pellet. The small amount of soluble protein that could be recovered after StrepTag affinity purification was always highly contaminated with DNA (precluding accurate estimation of protein concentration by conventional methods) as well as with free GFP (probably due to proteolytic cleavage) in spite of the use of DNase and anti-proteases. The typical profile of the size exclusion column that we observed by monitoring fluorescence intensity after GFP-Mrr purification showed several peaks (Figure 3.1.A). The first and second peaks both contained proteins with the expected size for GFP-Mrr tetramers and dimers, while the last peak shows free GFP as confirmed by SDS gel (Figure 3.1.B). Nevertheless, our results confirmed that *in vitro* GFP-Mrr is in equilibrium between a tetrameric and dimeric form.

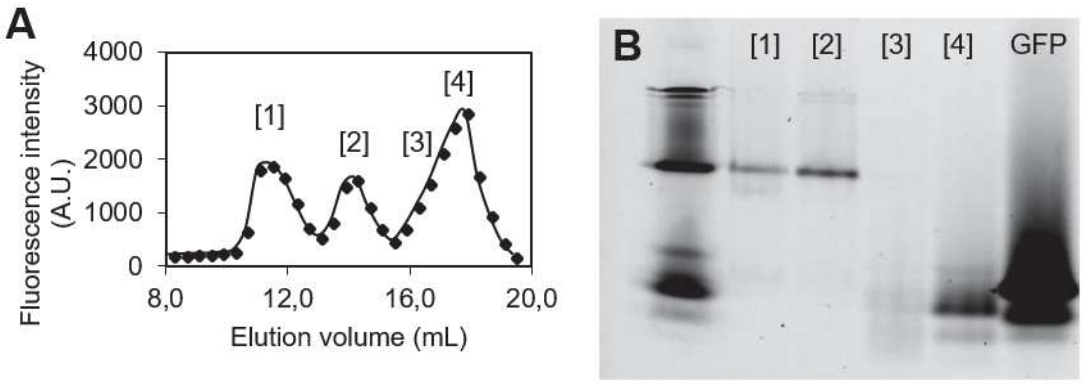

Figure 3.1: Size exclusion chromatography of purified StrepTag-GFP-Mrr. A) Fluorescence intensity measured in 400 µL elution fractions recovered from size exclusion chromatography (SEC) on Superdex 200 HR10-300 column. B) SDS-PAGE analysis of the sample loaded on the SEC column (first row), four elution fractions and purified GFP detected by fluorescence excitation of the gel at 473 nm.

We were somewhat disappointed to observe no difference in the size exclusion chromatography elution profiles of purified GFP-Mrr after a pressure shock (Figure 3.2). Thus, if pressure is indeed able to dissociate the Mrr tetramers *in vitro*, they rapidly re-associate when the pressure is released. Pressure effects on oligomeric subunit interactions are indeed expected to be reversible in the pressure range we applied (see section 1.1.4). In order to establish that pressure is indeed able to dissociate the GFP-Mrr tetramers into dimers, we decided to set-up a 2-photon microscope with a pressure-control device that will allow *in vitro* FCS experiments under pressure. The results are presented in the second paper and the results section on microscopy under pressure.

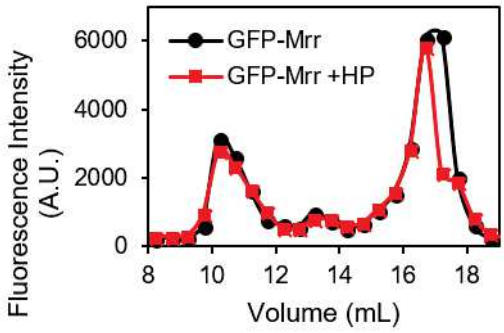

Figure 3.2: Fluorescence intensity of the elution profile of purified StrepTag-GFP-Mrr before (black circle) and after (red square) exposure to pressure for 15 min at 100 MPa.

Published online 21 March 2017

Nucleic Acids Research, 2017, Vol. 45, No. 9 ***5323–5332***
doi: 10.1093/nar/gkx192

High pressure activation of the Mrr restriction endonuclease in *Escherichia coli* involves tetramer dissociation

Anaïs C. Bourges[1,2,†], Oscar E. Torres Montaguth[3,†], Anirban Ghosh[3], Wubishet M. Tadesse[3], Nathalie Declerck[2], Abram Aertsen[3,*] and Catherine A. Royer[1,*]

[1]Department of Biological Sciences, Rensselaer Polytechnic Institute, Troy, NY 12180, USA, [2]Centre de Biochimie Structurale, CNRS UMR5048, INSERM U1054, Université Montpellier, 34000 Montpellier, France and [3]Department of Microbial and Molecular Systems, Laboratory of Food Microbiology, KU Leuven, B-3001 Leuven, Belgium

Received February 07, 2017; Revised March 07, 2017; Editorial Decision March 08, 2017; Accepted March 14, 2017

ABSTRACT

A sub-lethal hydrostatic pressure (HP) shock of ∼100 MPa elicits a RecA-dependent DNA damage (SOS) response in *Escherichia coli* K-12, despite the fact that pressure cannot compromise the covalent integrity of DNA. Prior screens for HP resistance identified Mrr (Methylated adenine Recognition and Restriction), a Type IV restriction endonuclease (REase), as instigator for this enigmatic HP-induced SOS response. Type IV REases tend to target modified DNA sites, and *E. coli* Mrr activity was previously shown to be elicited by expression of the foreign M.HhaII Type II methytransferase (MTase), as well. Here we measured the concentration and stoichiometry of a functional GFP-Mrr fusion protein using *in vivo* fluorescence fluctuation microscopy. Our results demonstrate that Mrr is a tetramer in unstressed cells, but shifts to a dimer after HP shock or co-expression with M.HhaII. Based on the differences in reversibility of tetramer dissociation observed for wild-type GFP-Mrr and a catalytic mutant upon HP shock compared to M.HhaII expression, we propose a model by which (i) HP triggers Mrr activity by directly pushing inactive Mrr tetramers to dissociate into active Mrr dimers, while (ii) M.HhaII triggers Mrr activity by creating high affinity target sites on the chromosome, which pull the equilibrium from inactive tetrameric Mrr toward active dimer.

INTRODUCTION

The Mrr (Methylated adenine Recognition and Restriction) protein of *Escherichia coli* K-12 is a laterally acquired Type IV restriction endonuclease (REase) with specificity for methylated DNA (1,2). Contrary to Type I-III REases, Type IV enzymes are not found in conjunction with their cognate methyltransferases (MTases) (3). Typically, MTases modify the bacterial chromosome at specific sequences to protect it from cleavage by the cognate REase. Such restriction modification (RM) systems constitute a primitive immune system for bacteria to protect against phage infection or lateral acquisition of foreign DNA, since the latter lack the proper protective methylation signature (4). Type IV REases, on the other hand, recognize and cleave modified DNA (5). Indeed, while genotoxic Mrr activity in *E. coli* K-12 was originally discovered to be elicited upon the heterologous expression of foreign methyltransferases (MTases) such as the Type II M.HhaII methyltransferase from *Haemophilus haemolyticus* (6), it was recently demonstrated that Mrr could be activated as well, by the expression of Type III MTases (Mod proteins) acquired from *E. coli* ED1A and *Salmonella Typhimurium* LT2 (6). To date, the sequences of the target sites for Mrr binding and cleavage have not been established.

Surprisingly, it was documented previously as well, that a sub-lethal hydrostatic pressure shock (HP∼100 MPa for ∼15 min) is also able to trigger Mrr-dependent DNA damage in its *E. coli* K-12 (strain MG1655) host (7,8). While Mrr can harmlessly be expressed in cells under atmospheric conditions, fluorescence microscopy has shown that its activation by HP causes nucleoid condensation and concomitant confinement of nucleoid associated Mrr proteins (9). HP activation of Mrr triggers a RecA-dependent SOS response, underscoring that active Mrr causes double strand

*To whom correspondence should be addressed. Tel: +1 518 276 3796; Fax: +1 518 276 4233; Email: royerc@rpi.edu
Correspondence may also be addressed to Abram Aertsen. Tel: +32 16 32 17 52; Fax: +32 16 32 19 60; Email: abram.aertsen@kuleuven.be
†These authors contributed equally to the paper as first authors.
Present address: Anirban Ghosh, Department of Cell and Molecular Biology, Uppsala University, Uppsala, 75124, Sweden.

© The Author(s) 2017. Published by Oxford University Press on behalf of Nucleic Acids Research.
This is an Open Access article distributed under the terms of the Creative Commons Attribution License (http://creativecommons.org/licenses/by-nc/4.0/), which permits non-commercial re-use, distribution, and reproduction in any medium, provided the original work is properly cited. For commercial re-use, please contact journals.permissions@oup.com

d from https://academic.oup.com/nar/article-abstract/45/9/5323/3076221
- IGH user
e 2018

breaks in the host nucleoid (8). Furthermore, HP/Mrr-mediated activation of the SOS response was shown to result in typical SOS-mediated phenotypes such as prophage activation and SulA-mediated filamentous growth after pressure release (8,10–12).

Here, we sought to determine the molecular mechanisms of the HP shock-induced activation of Mrr and how it differs from that of MTase-mediated activation. More specifically, we determined the localization, absolute concentration and stoichiometry of Mrr fused with a green fluorescent protein (GFPmut2) in live *E. coli* cells before and after HP or M.HhaII exposure using a quantitative fluorescence fluctuation microscopy approach called scanning Number and Brightness (sN&B) (13). Our results reveal that Mrr is tetrameric in unstressed cells, but dissociates into a dimer after HP shock or co-expression with M.HhaII. We suggest that, given the well-documented ability of pressure to dissociate protein oligomers (14), the activation of Mrr by HP shock results from direct dissociation of the inactive tetramer to an active dimer which recognizes and cleaves the *E. coli* chromosome at cryptic, low affinity sites. In contrast to this HP *pushing* model, we also propose that expression of the MTase leads to the creation of numerous high affinity methylated sites on the chromosome, *pulling* the Mrr DNA binding equilibrium toward the active, dimeric, bound form, which then cleaves the DNA. These models provide a detailed example of understanding the multiple and varied molecular mechanisms underlying the response and adaptation of living organisms to pressure.

MATERIALS AND METHODS

Strains and construction of mutants

Escherichia coli K-12 MG1655 was used as parental strain (15), and a summary of all the strains and plasmids used in this study is provided in Table 1. The various GFP-Mrr expressing MG1655 derivatives were constructed by scarless λ-red based recombineering (16). Briefly, the MG1655 chromosomal *mrr* locus was first replaced by a *tetA-sacB* cassette (yielding MG1655 *Δmrr::tetA-sacB*) obtained from a polymerase chain reaction (PCR) amplicon (using primers 5′-TAGTGCTATA GTAGCCGAAAAACATCTACCTGATTCTGCAAG GATGTACTTCCTAATTTTTGTTGACACTCTATC-3′ and 5′-AAGGGGTTATGGGCCGGATAAGGCGC AGCCGCATCCGGCCTGATATTTCAATCAAAGG GAAAACTGTCCATATGC-3′ on genomic DNA of *E.coli* T-Sack (17)), after which this *tetA-SacB* cassette was replaced by the *gfp-mrr* construct of interest using Tet/SacB counter-selection media (17). For construction of the *E. coli* MG1655 P_{mrr}-*gfp::mrr* strain, chromosomally expressing the GFP-Mrr fusion protein from the native *mrr* promoter, the chromosomal *Δmrr::tetA-sacB* allele was replaced with the *gfp::mrr* allele obtained from a PCR amplicon prepared on the pBAD-*gfp::mrr* vector ((9); using primers 5′-ATTTTTGTAGTGCTATAGTAG CCGAAAAACATCTACCTGATTCTGCAAGGA TGTACTATGAGTAAAGGAGAAGAAC-3′ and 5′-CGAT AAGCTTG CGTTTGCGGGGTTGAGG -3′). For construction of the *E. coli* K12 MG1655 P_{BAD}-*gfp::mrr* strain, chromosomally expressing the GFP-Mrr fusion protein from an arabinose inducible promoter, the chromosomal *Δmrr::tetA-sacB* allele was replaced with the P_{BAD}-*gfp::mrr* allele obtained from a PCR amplicon prepared on the pBAD-*gfp::mrr* vector (9) (using primers 5′-ATTTTTGTAGTGCTAT AGTAGCCGAAAAACATCTACCTGATTCTGCAA GGATGTACTTTATGAC AACTTGACGGCTA-3′ and 5′-CGATAAGCTTGCGTTTGCGGGGTTGAGG-3′). For construction of the *E. coli* K12 MG1655 P_{BAD}-*gfp-mrr* strain, chromosomally co-expressing GFP and Mrr as separate proteins from a bicistronic mRNA driven by an arabinose inducible promoter, the chromosomal *Δmrr::tetA-sacB* allele was replaced with the P_{BAD}-*gfp-mrr* allele obtained from a PCR amplicon prepared on the pBAD-*gfp-mrr* vector (9) using primers 5′-ATTTTTGTAGTG CTATAGTAGCCGAAAAACATCTACCTGATTCTGC AAGGATGTACTTTATGACAACTTGACGGCTA-3′ and 5′-CGATAAGCTTGCGTTTGCGGGGTTGAG G-3′).

Similar to the pBAD-*gfp::mrr* and pBAD-*gfp-mrr* plasmids constructed earlier (9), the pBAD-*gfp::*mrr^{D203A} plasmid was constructed by digesting a PCR amplicon of the mrr^{D203A} allele (obtained using primers 5′-ATCGCTGCAGACGGTTCCTACCTATGAC-3′ and 5′-CGATAAGCTTGCGTTTGCGGGGT TGAGG-3′ on the pACYC184-mrr^{D203A} vector; (18)) with PstI and HindIII, prior to ligation in the low copy number pBAD33-gfp_mut2-T7tag plasmid (19), digested with same enzymes. Subsequently, for construction of the *E. coli* K12 MG1655 P_{BAD}-*gfp::*mrr^{D203A} strain, chromosomally expressing a catalytically compromised version of the GFP-Mrr fusion protein from an arabinose inducible promoter, the chromosomal *Δmrr::tetA-sacB* allele was replaced with the pBAD-*gfp::*mrr^{D203A} allele obtained from a PCR amplicon prepared on the pBAD-*gfp::*mrr^{D203A} vector (using primers 5′-ATTTTTGT AGTGCTATAG TAGCCGAAAAACATCTACCTGATTCTGCAAGG ATGTACTTTATGACAACTTGACGGCTA-3′ and 5′-CGATAAGCTTGCGTTTGCGGGGTTGAGG-3′). When required, the pTrc99A-*hhaII* plasmid (9), expressing the M.HhaII MTase from an IPTG (isopropyl β-D-thiogalactopyranoside) inducible promoter and corresponding pTrc99A control backbone (20) were introduced into *E. coli* MG1655 or its derivatives by electroporation.

Cell growth conditions and sample preparation

Cells from −80°C glycerol stock were grown overnight at 37°C in LB medium with antibiotics if necessary, at final concentrations of 100 μg/ml ampicillin, 30 μg/ml chloramphenicol or 50 μg/ml kanamycin. Cells were then 100-fold diluted in LB, induced with arabinose 0.4% and grown until late exponential phase (optical density at 600 nm (OD_{600}) ∼ 0.6). When appropriate, the MTase was induced with 1 mM IPTG from the moment the cell culture reached an OD_{600} of ∼ 0.15. A 500 μl aliquot of cells at OD_{600} 0.6 was subsequently centrifuged at 850 × *g* for 2 min and re-suspended in fresh LB to a final OD_{600} of ∼ 25. This high density was important for obtaining a field of view (FOV) full of bacteria in a single layer. All chemicals and media used are from AMRESCO (OH, USA).

led from https://academic.oup.com/nar/article-abstract/45/9/5323/3076221
: - IGH user
ine 2018

Table 1. *E. coli* K12 MG1655 strains used for this work

Strain	Chromosomal and-or plasmid	Produces	Growth conditions
***E. coli* MG1655**			
E. coli* MG1655 mrr::Kn P_{BAD}-*gfp-mrr	Plasmid	Free GFP and unlabeled Mrr	Induction arabinose 0.002%
E. coli* MG1655 P_{BAD}-*gfp-mrr	Chromosomal	Free GFP and unlabeled Mrr	Induction arabinose 0.4%
***E. coli* MG1655 P_{BAD}-*gfp*-mrr + pTrc99A empty**	Chromosomal + empty plasmid	Free GFP and unlabeled Mrr	Induction arabinose 0.4% and IPTG 1 mM
E. coli* MG1655 P_{BAD}-*gfp-mrr* + pTrc99A-*hhaII	Chromosomal + plasmid	Free GFP and unlabeled Mrr and HhaII MTase	Induction arabinose 0.4% and IPTG 1 mM
E. coli* MG1655 P_{mrr}-*gfp::mrr	Chromosomal	GFP-Mrr	Native promotor
E. coli* MG1655 P_{BAD}-*gfp::mrr	Chromosomal	GFP-Mrr	Induction arabinose 0.4%
***E. coli* MG1655 P_{BAD}-*gfp*::Mrr + pTrc99A empty**	Chromosomal + empty plasmid	GFP-Mrr	Induction arabinose 0.4% and IPTG 1 mM
E. coli* MG1655 P_{BAD}-*gfp::mrr* + pTrc99A-*hhaII	Chromosomal + plasmid	GFP-Mrr and HhaII MTase	Induction arabinose 0.4% and IPTG 1 mM
***E. coli* MG1655 P_{BAD}-*gfp::mrr*^{D203A}**	Chromosomal	GFP-MrrD203A	Induction arabinose 0.4%
***E. coli* MG1655 P_{BAD}-*gfp::mrr*^{D203A}**	Chromosomal + plasmid	GFP-MrrD203A and HhaII MTase	Induction arabinose 0.4% and IPTG 1 mM
E. coli* BL21 (DE3)+ pBAD-*strep::gfp::mrr	Plasmid	STREP-tagged GFP-Mrr	Induction arabinose 0.2%

Microscopy samples and high pressure treatment

Sample preparation for microscopy were made on agar pads (2% UltraPureTM LMP Agarose, Invitrogen) sandwiched between two glass cover slips No1 (VWR) coated with poly-L-Lysine and mounted in a stainless-steel holder as described in details in Ferguson *et al*. (21). For pressure treatment, 500 μl of culture was centrifuged at 3500 rpm for 2 min and re-suspended in 50 μl of LB. Then a computer-controlled HUB440 high pressure generator equipped with the SW-16 pressure vessel) was used to pressurize samples in 50 μl MicroTubes (both from Pressure BioSciences, Inc., South Easton, MA, USA). After pressure release, samples were centrifuged and re-suspended in a few microliters of LB to prepare the microscopy sample.

Fluorescence fluctuation microscopy

Two-photon fluorescence fluctuation imaging was performed using an Avalanche Photo Diode-based detector (ISS, Champaign, IL, USA). Excitation from a femtosecond pulsed infrared laser (MaiTai, Newport/Spectra Physics, Mountain View, CA, USA) was focused through a 60×1.2NA water immersion objective (Nikon APO VC) onto coverslip N1 (VWR). Calibration of the volume of the two-photon point spread function (PSF) was carried out using 40 nM fluorescein solutions (Spectrum) and 780 and 930 nm excitation at a laser power 12 and 43 mW, respectively. An excitation wavelength of 930 nm was used for the measurement of the GFP. The average power exciting laser was 11 mW. The wavelength was selected to simultaneously optimize GFP emission and minimize cellular autofluorescence. The excitation power was chosen to maximize the signal, while avoiding saturation and photo-bleaching effects. Infrared light was filtered from detected light by using a 735 nm low-pass dichroic filter (Chroma Technology Corporation, Rockingham, VT, USA). Emitted light was filtered with a 530/43 nm emission filter and detected by avalanche photodiodes (Perkin Elmer).

Number and brightness analyses

sN&B allows the measurement in living cells of the spatially resolved values of absolute concentration of fluorescent molecules (n) and their molecular brightness (e), in counts per dwell-time per molecule (22). In this approach, one performs a series of raster scans (50 in this case, with a two-photon excitation beam) using a pixel dwell-time (40 ms) that is faster than the diffusion time. This provides 50 values of fluorescence intensity at each pixel of the FOV from which fluorescence fluctuations (variance) and average can be calculated. In the case of bacteria this provides 256 × 256 pixel-based values in a 20 × 20 μm FOV of the molecular brightness of the diffusing fluorescent molecules and their concentration as previously described (21,23). The average molecular brightness of the particles is obtained from the ratio of the variance to the average intensity at each pixel. To obtain the average number (n) of diffusing particles, we divide the average intensity (F) at one pixel by the brightness (e):

$$e = \frac{\langle \delta F(t) \rangle^2 - \langle F(t) \rangle}{\langle F(t) \rangle} \quad (1)$$

$$n = \frac{\langle F(t) \rangle^2}{< \delta F(t)^2 > - \langle F(t) \rangle} = \frac{F}{e}. \quad (2)$$

We note that the timescale (t) of fluctuations in sN&B corresponds to the frame-time (the time it takes to return to a given pixel) and this is several seconds. Hence, unlike traditional point FCS in which acquisition is on the millisecond timescale, even very slowly moving particles can be studied by sN&B. sN&B analyses were performed with the Patrack (24) and Simfcs (E. Gratton, LFD, University of California, Irvine, CA, USA) software packages. Due to the low levels of expression, even in the case of the induced expression, sN&B data were contaminated by background auto-fluorescence (bg). First, each individual bacterium was identified and sized in each of the 5–8 FOV acquired per experiment (using the Patrack software, as previ-

ıd from https://academic.oup.com/nar/article-abstract/45/9/5323/3076221
- IGH user
ıe 2018

ously described). Calculation of the average fluorescence intensity, brightness and number were done for all bacteria in each FOV using only the central 50% of pixels in each bacterium as described by Ferguson *et al.* (21). Next, these average values from all the FOV were averaged for each sample (*F*sample, *e*sample and *n*sample) and corrected for bg contributions using the average fluorescence and brightness obtained from the background strain (*ebg* and *Fbg*) the same day under the same growth and imaging conditions as follows (21):

$$\langle e\rangle \text{ GFP sample} = \frac{(e\text{sample}*F\text{sample} - ebg*Fbg)}{F\text{sample} - Fbg} \quad (3)$$

$$\langle N\rangle \text{ GFP sample} = \frac{(F\text{sample} - Fbg)^2}{(e\text{sample}*F\text{sample} - ebg*Fbg)}. \quad (4)$$

Molecular brightness depends upon microscope alignment and excitation intensity, and hence the free monomeric GFP brightness was measured as a control each day for all experiments. Using this value we obtained the stoichiometry of GFP-Mrr by dividing the brightness of the Mrr sample (<e> GFP-Mrr sample) by the brightness of monomeric GFP measured the same day. Mrr absolute concentration was calculated by dividing the background corrected intensity by the molecular brightness of monomeric GFP (<e>GFP (counts per dwell-time per molecule) by the excitation volume inside the bacteria and Avogadro number (N_A).

$$[\text{GFP} - \text{Mrr}]\,(\text{nM}) = \frac{\langle F\rangle \text{ GFPMrr (counts per dwell time)}}{\langle e\rangle \text{ GFP (counts per dwell time per molecule)} * \text{ Vol } (l) * N_A\,(mol^{-1})}. \quad (5)$$

RICS analysis of diffusion dynamics of GFP-Mrr

The multiple raster scans obtained in the N&B imaging can also be analyzed to extract diffusion information as described by Digman and Gratton (25,26). This approach allows one to extract the diffusion coefficient of the fluorescent particles via fitting of the pixel pair spatio-temporal correlation function derived from the image size, the x-y gaussian PSF dimensions and the pixel dwell-time. Image size was 256 × 256 pixels for 13 × 13 μm. In the N&B images, pixel dwell-time was 40 μs, corresponding to a line time of 11.26 ms and a frame time of 2.61 s. In this analysis, spatial information is not retained, contrary to N&B. The SimFCS software (E. Gratton, LFD, University of California, Irvine, CA, USA), was used to fit the imaging data for the average diffusion coefficient for all the pixels in the FOV as described in the above cited work.

GFP-Mrr *in vitro* biochemistry

To obtain purified GFP-Mrr, the corresponding *gpf::mrr* fusion gene was equipped with a sequence encoding a Strep-tag and expressed from the pBAD33 plasmid (27) in *E.* coli BL21 (DE3) cells to produce N-terminal Strep-tag® II protein fusions. The Strep-*gfp::mrr* amplicon was obtained using the primers, 5'-ACGTGGTACCCGGGGATCCTCTAGAGGA GGGAGTAATGTGGAGCCACCCGCAGTTC GAAAAAAGTAAAGG AGAAGAACTTTT-3′ and 5′-CGATAAGCTTGCGTTTGCGGGGTTGAGG-3′, on the plasmid pBAD-*gfp::mrr* (9)) digested with with KpnI and HindIII, and ligated to pBAD33, digested with the same enzymes. For protein production, *E.* coli BL21 (DE3) cells equipped with the resulting pBAD-*strep::gfp::mrr* vector were grown in 700 ml LB at 37°C until OD_{600} reached ∼0.7, after which they were incubated with 0.2% arabinose for 3 h at 30°C. The cell pellet was kept at −80°C until resuspension in 15 ml of lysis buffer (100 mM Tris pH8, 150 mM NaCl, 1 mM ethylenediaminetetraacetic acid (EDTA), 1 mM Dithiothreitol (DTT) and 2 mM benzamidine). The cell suspension was supplemented with 1 mM lysozyme, 2 mM DNase and 12.5 mM Na_2HPO_4, left on ice for 30 min, sonicated then centrifuged for 25 min at 18 000 rpm. The Strep-tagged fusion protein was purified from the supernatant on a 5 mL Streptactin-superflow high capacity resin (IBA) equilibrated in 100 mM Tris pH 8, 150 mM NaCl, 1 mM EDTA. The protein fusion was eluted with the same buffer containing 2.5 mM desthiobiotin. The most concentrated fractions were pooled, protein concentration was estimated by the Bradford assay and aliquots were kept at −80°C. Analytical gel filtration was performed on Superdex 200 10/300 (GE Healthcare) equilibrated in 20 mM Tris pH 8, 150 mM NaCl and 1 mM EDTA at 0.5 ml/min. Samples of 500 μl were injected and elution fractions of 400 μl were collected. The presence of GFP-Mrr in the elution fractions was detected by measuring the fluorescence intensity of 100 or 200 μl aliquots on an infinite M1000 PRO plate reader (TECAN, Switzerland), exciting at 488 (±15) nm and collecting emission at 528 (± 20) nm.

RESULTS

Mrr is a tetramer in unstressed cells

As a first step to understand the mechanisms of Mrr activation by pressure shock, we sought to establish the localization and organization of Mrr inside *E. coli* cells. To visualize Mrr in live *E. coli* MG1655 cells we expressed it as a GFP-fusion. The GFP-Mrr fusion protein was previously shown to retain the known functionalities of the wild-type (WT) Mrr protein (9). To obtain robust signal to autofluorescent background ratios, the chromosomal *mrr* locus was replaced with a P_{BAD}-*gfp::mrr* construct expressing the GFP-Mrr fusion protein from an arabinose inducible promoter (Figure 1C). We also examined strains expressing the *gfp::mrr* allele under control of the natural *mrr* promoter (P_{mrr}) at the natural locus on the *E. coli* MG1655 chromosome (Figure 1B) and in a strain equipped with a plasmid containing the P_{BAD}-*gfp::mrr* allele (not shown). In the MG1655 P_{mrr}-*gfp::mrr* strain, GFP fluorescence levels were very low, although measurably above the levels of the autofluorescence (Figure 1A and B).

As a control, the *mrr* locus in MG1655 was similarly replaced with a P_{BAD}-*gfp-mrr* construct co-expressing GFP and Mrr as separate proteins from a bicistronic mRNA driven by an arabinose inducible promoter. Induction of both MG1655 P_{BAD}-*gfp-mrr* and MG1655 P_{BAD}-*gfp::mrr* with arabinose therefore allowed direct comparison of the

aded from https://academic.oup.com/nar/article-abstract/45/9/5323/3076221
PE - IGH user
June 2018

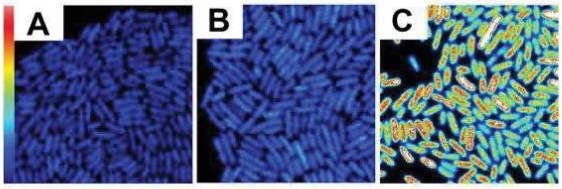

Figure 1. GFP fluorescence intensity maps of unstressed cells of (**A**) the parental *Escherichia coli* K12 MG1655 wild-type strain (MG1655 WT), (**B**) the MG1655 P_{mrr}-*gfp::mrr* strain producing GFP-Mrr from the native *mrr* promoter and (**C**) the MG1655 P_{BAD}-*gfp::mrr* strain producing GFP-Mrr from the arabinose inducible P_{BAD} promoter (arabinose 0.4%). Scale 20 × 20 μm FOV and maximum intensity is 1.5 counts per 40 μs pixel dwell-time. Cells were grown in a minimal media to avoid background auto-fluorescence.

properties of free GFP to that of the GFP-Mrr fusion. Images of untreated cells expressing the free GFP (along with unlabeled Mrr) (Supplementary Figure S1Aa) revealed a homogenous distribution of the GFP throughout the cells. Analysis of the diffusion of the free GFP in these untreated cells using Raster Scanning Image Correlation Spectroscopy (RICS) (Supplementary Figure S2A and D) yielded a diffusion coefficient of 4.14 ± 0.01 $\mu m^2/s$, consistent with the diffusion of free monomeric GFP in bacteria (28). Although the intracellular concentration of the free GFP averaged over multiple fields of view (FOV) was much higher (i.e. 788 ±167 nM) when the P_{BAD}-*gfp-mrr* construct was expressed with arabinose 0.002% from the pBAD-*gfp-mrr* plasmid compared to its expression from the chromosomal locus (i.e. 115 ± 9 nM) with arabinose 0.4%, the average molecular brightness of the free GFP was similar in both cases (0.082 +/− 0.004 counts/per molecule/pixel dwell time). We therefore conclude that the association state of free GFP does not change over this concentration range. Due to differences in microscope alignment, the GFP molecular brightness calculated by N&B analysis as well as the auto-fluorescence of the parental MG1655 strain (i.e. not expressing any GFP; Figure 1A) could vary from day to day (Supplementary Figures S1B and 3E). Accordingly, auto-fluorescent background and free GFP control measurements were performed for each experiment. The GFP-mut2 variant used has been demonstrated to be a monomer (29). Hence we assign the daily brightness value measured for the free GFP to correspond to that of GFP monomer.

The average concentration of GFP-Mrr in unstressed MG1655 P_{BAD}-*gfp::mrr* cells (0.4% arabinose), calculated from the average corrected intensity and the monomeric GFP molecular brightness using Equation (5) was 185 ± 56 nM, expressed in monomer units (∼120 monomers per cell). Calculation of the molecular brightness for the GFP-Mrr fusion on multiple FOV of this strain using Equation (3) yielded brightness values 4-fold higher than those found for the monomeric GFP controls. Hence the GFP-Mrr fusion exhibits a stoichiometry of four GFP units per complex, indicating that Mrr is tetrameric in unstressed cells (Figure 2B). The concentration calculations reveal that Mrr is present at ∼45 tetramers per cell under these conditions. Interestingly, RICS analysis of the N&B stacks for the translational diffusion of the GFP-Mrr fusion from this strain

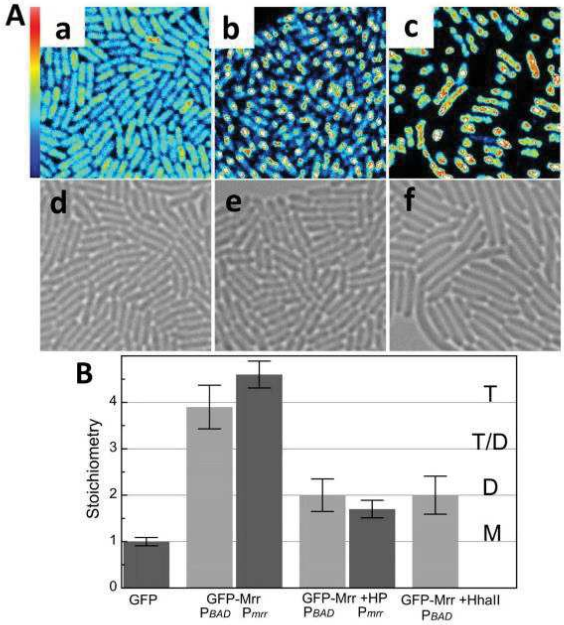

Figure 2. Effect of HhaII MTase and pressure on GFP-Mrr localization and molecular brightness. GFP-Mrr is expressed under the control of P_{BAD} promotor with induction by arabinose (P_{BAD}) or is native promotor (P_{mrr}) in the chromosome. (**A**) Fluorescence intensity maps of (a) P_{BAD}-*gfp::mrr* in unstressed cells (GFP-Mrr) (b) P_{BAD}-*gfp::mrr cells after 20 min at 100 MPa (+HP)* and (c) P_{BAD}-gfp::mrr + pTrc99A-HhaII after 60 min induction of the MTase HhaII by IPTG (+HhaII). Scale is 20 × 20 μm. Maximum intensity scale is 2 counts per 40 μs pixel dwell-time. Bright-field images of (d) P_{BAD}-*gfp::mrr* in unstressed cells, (e) P_{BAD}-*gfp::mrr* cells after 20 min at 100 MPa and (f) P_{BAD}-*gfp::mrr* + pTrc99A-HhaII after 60 min induction of the M.HhaII by IPTG. (**B**) Stoichiometry values of fluorescent proteins corresponding to GFP monomers (M), dimers (D), tetramers (T) or a possible equilibrium between dimer and tetramer (T-D) as deduced from the background corrected molecular brightness of fluorescent proteins in strain P_{BAD}-*gfp-mrr* (GFP), P_{BAD}-*gfp::mrr* yielding GFP-Mrr expressed from the P_{BAD} promoter at the natural chromosomal locus (GFP-Mrr, P_{BAD}) or from the natural promoter P_{mrr}-*gfp::mrr* (GFP-Mrr, P_{mrr}) in unstressed cells or after pressure treatment (HP) and P_{BAD}-*gfp::mrr* + pTrc99A-HhaII after induction of the HhaII MTase by IPTG.

(Supplementary Figure S2B and D) indicated significantly slower diffusion than free GFP, with the GFP-Mrr protein being immobile on a timescale of tens of milliseconds. Slower dynamics could be due in part to the difference in size between monomeric GFP and the GFP-Mrr tetramer. However, due to the cube root dependence of diffusion time on molecular weight, the ∼10-fold difference in size would only decrease the diffusion coefficient by a factor of ∼2.2 to ∼1.7 $\mu m^2/s$. Hence, non-specific interactions with the chromosome likely contribute significantly to slow diffusion of GFP-Mrr compared to free GFP. In agreement with the notion that GFP-Mrr interacts with the chromosome in unstressed cells, the chromosomally expressed GFP-Mrr appeared somewhat localized in cell center (Figures 1C and 2Aa). Moreover, a previous study in *E. coli* cells expressing the same GFP-Mrr fusion protein at much higher levels from a low-copy plasmid revealed nucleoid-bound Mrr foci

ıd from https://academic.oup.com/nar/article-abstract/45/9/5323/3076221
- IGH user
ıe 2018

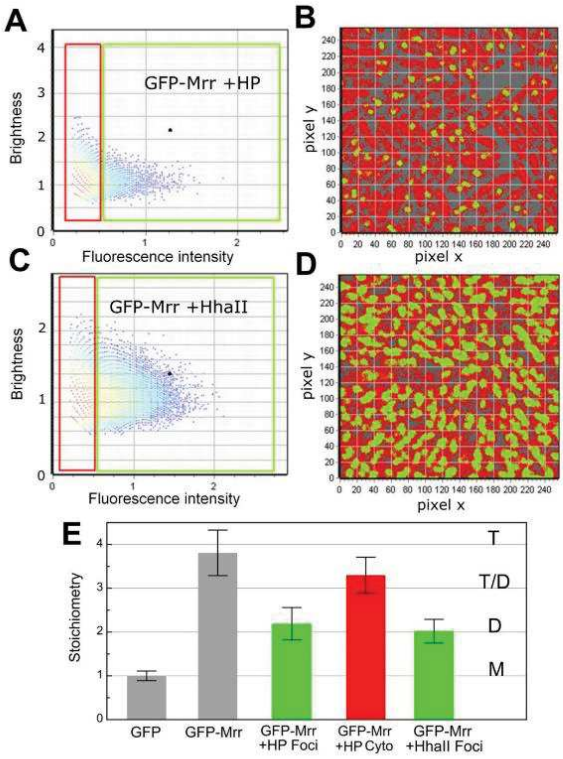

Figure 3. Localization dependent effect of pressure or MTase induction on GFP-Mrr stoichiometry. Images were obtained after pressure shock of 20 min at 100 MPa or M.HaII induction by IPTG. (**A** and **B**) Example of image after HP shock. (A) Brightness versus intensity pixel histogram from an example image obtained after HP shock. All the pixels in the FOV in (B) are plotted in (A) according to the molecular brightness (counts per pixel dwell-time per molecule) and the average intensity (counts per pixel dwell time) calculated for each pixel. In the red rectangle those pixels with intensity values below 0.5 counts per dwell time have been selected, where as in the green square, all pixels with intensity values above 0.5 counts per dwell time have been selected. Intensity values below 0.2 were eliminated by thresholding. (B) Intensity-based pixel selections from (A) mapped to the image obtained after HP shock. Green pixels correspond to those selected with the green square in (A). They exhibit a high intensity but lower brightness and they localize to the foci, while red pixels with a lower intensity but higher brightness localize in the cytoplasm (outside of the foci). (**C** and **D**) Example of image obtained after M.Hhall induction. (C) Brightness versus intensity pixel histogram for an example image obtained after M.Hhall induction. All the pixels in the FOV in (D) are plotted in C according to the molecular brightness (counts per pixel dwell-time per molecule) and the average intensity (counts per pixel dwell time) calculated for each pixel. In the red rectangle those pixels with intensity values below 0.5 counts per dwell time have been selected, where as in the green square, all pixels with intensity values above 0.5 counts per dwell time have been selected. Intensity values below 0.2 were eliminated by thresholding. (D) Intensity-based pixel selections from (C) mapped to the example image obtained after M.Hhall induction. Green pixels correspond to those selected with the green square in (C). They exhibit a high intensity but lower brightness and they localize to the foci, while red pixels with a lower intensity localize in the cytoplasm (outside of the foci). (**E**) Stoichiometry values of fluorescent proteins corresponding to GFP monomers (M), dimers (D), tetramers (T) or a possible equilibrium between dimer and tetramer (T-D) as deduced from the background corrected molecular brightness of fluorescent proteins in strains P_{BAD}-*gfp-mrr* (GFP), chromosomal P_{BAD}-*gfp::mrr* + pTrc99A-*hhaII* (GFP-Mrr +HhaII) after M.HhaII induction and chromosomal P_{BAD}-*gfp::mrr* in unstressed cells (GFP-Mrr) or after pressure treatment (GFP-Mrr +HP) for pixels inside of the foci (green, Foci) and outside of the foci (red, cytoplasm).

(9). At the present expression levels, cell morphology was not strongly altered as a result of GFP-Mrr expression (9), underscoring the inactive nature of Mrr under control conditions.

Mrr becomes a dimer organized into foci when triggered by HP or M.HhaII

To investigate the molecular basis for the puzzling pressure-induced SOS response, we examined the behavior of GFP-Mrr after HP shock, by exposing arabinose induced MG1655 P_{BAD}-*gfp::mrr* to 100 MPa for 20 min. Pressure shock resulted in the formation of GFP-Mrr foci and some cellular elongation (the extent of which depends upon time after pressure shock) (Figure 2Ab and e), in agreement with the previous study (9). Interestingly, although the existence of such foci suggested GFP-Mrr had aggregated on the nucleoid, N&B calculations on the foci actually revealed that tetrameric GFP-Mrr had dissociated to dimer after HP treatment (Figures 2B and 3A and B). However, not all of the total cellular GFP-Mrr content became focally organized after HP shock. The remaining cytoplasmic GFP-Mrr exhibited a stoichiometry between tetramer and dimer (Figure 3A and B), perhaps due to a decrease in concentration and the contribution of background fluorescence. No large change in the average translational diffusion coefficient of GFP-Mrr after pressure treatment was observed.

We succeeded as well, in quantifying the molecular brightness for GFP-Mrr expressed from its natural promoter (MG1655 P_{mrr}-*gfp::mrr*) by reducing autofluorescence via growth on minimal media (Figure 1B). N&B analysis revealed that GFP-Mrr in this strain was tetrameric prior to HP treatment and dimeric after pressure release, as observed for the GFP-Mrr produced from the P_{BAD} promoter (Figure 2B). Likely due to the low expression levels of Mrr under control of its native promotor (6-12 nM Mrr in monomer units, or 1–2 tetramers per cell on average) no foci were observed after pressure treatment. HP shock had no effect on the auto-fluorescence of control cells not expressing any GFP (Supplementary Figure S3). Nor did it change the molecular brightness (stoichiometry) of free GFP in the P_{BAD}-*gfp-mrr* strain, which expressed free GFP and untagged Mrr from the arabinose inducible promoter at the Mrr natural chromosomal locus (Supplementary Figure S1).

Mrr has been shown to promote DNA damage in response to expression of the foreign methyl transferase, M.HhaII (6). Hence, we sought to determine if M.HhaII expression would modify the stoichiometry of GFP-Mrr, as in the case of HP shock. The MG1655 P_{BAD}-*gfp::mrr* strain was equipped with the pTrc99A-*hhaII* plasmid expressing the M.*hhaII* gene under the control of the IPTG responsive P_{trc} promoter. Co-expression of GFP-Mrr and M.HhaII resulted in filamentous cells and the appearance of pronounced GFP-Mrr foci in the center of the cells (Figure 2Ac and f), in agreement with previous observations (9).

ided from https://academic.oup.com/nar/article-abstract/45/9/5323/3076221
?E - IGH user
June 2018

As in the case of HP shock, M.HhaII induction led to dissociation of tetrameric GFP-Mrr to dimer (Figures 2B and 3C and D). The fluorescence intensity and molecular brightness outside the foci in MG1655 P_{BAD}-*gfp::mrr* upon IPTG induction of M.HhaII were found to be at auto-fluorescent background levels, indicating that nearly all of the GFP-Mrr molecules were present in the foci (Figure 2Ac). Interestingly, in contrast to HP shock, the apparent mobility of the dimeric GFP-Mrr in the foci after M.HhaII induction increased compared to that of dimeric GFP-Mrr after HP shock or tetrameric GFP-Mrr in unstressed cells either bearing the empty pTrc99A plasmid or not (Supplementary Figure S2B and C).

The changes in GFP-Mrr stoichiometry upon HP shock or MTase induction cannot be ascribed to the presence of the empty plasmid, pTRC99A, as arabinose and IPTG treatment of the MG1655 P_{BAD}-*gfp::mrr* strain equipped with the empty pTrc99A plasmid backbone yielded normally growing cells with tetrameric GFP-Mrr (Supplementary Figure S4). Moreover, no effect on cell morphology, auto-fluorescence intensity or molecular brightness was observed upon IPTG induction of M.HhaII, when GFP-Mrr expression was suppressed (MG1655 P_{BAD}-*gfp::mrr* strain bearing the pTrc99A-*hhaII* plasmid, in presence of IPTG, but in absence of arabinose and in presence of glucose to ensure the lack of Mrr expression) (Supplementary Figure S3). Furthermore, the N&B results of free GFP produced in the MG1655 P_{BAD}-*gfp-mrr* strain did not significantly differ in brightness or concentration between unstressed control cells and M.HhaII exposed cells (Supplementary Figure S1), although the latter cells (due to the M.HhaII mediated activation of Mrr) displayed a similar filamentation as MG1655 P_{BAD}-*gfp::mrr* (Figure 2Af).

Purified Mrr is in a tetramer dimer equilibrium *in vitro*

Since the brightness values for GFP-Mrr obtained by N&B indicated that Mrr is tetrameric in unstressed *E. coli* cells and dimeric after HP shock or MTase induction, we sought to determine the oligomeric state of purified GFP-Mrr *in vitro.* A Strep-tagged version of GFP-Mrr was produced in *E. coli* BL21 (DE3) cells, purified and subjected to analytical size exclusion chromatography (SEC). Elution of the protein injected at 155 nM (Figure 4, black curve) was monitored by fluorescence intensity, revealing a large major peak of 257 kDa, consistent with a tetramer, followed by a minor peak at 112 kDa consistent with a dimer. Sodium dodecyl sulphate-polyacrylamide gel electrophoresis analysis of the eluted fractions showed that both peaks contained purified Strep-tagged GFP-Mrr at the expected size (61 kDa), suggesting the presence of different oligomeric states for the native protein (data not shown). When the protein was injected on the SEC column at 35 nM, the relative intensity of the tetramer and dimer peaks was inverted (Figure 4, red curve). Moreover, when the peak from the injection at 155 nM, corresponding to the tetramer was collected and re-injected onto the SEC column, the relative intensity of the tetramer peak compared to the dimer decreased as well (Figure 4, gray curve). This demonstrates that purified GFP-Mrr forms tetramers *in vitro* that dissociate into dimers at lower concentration.

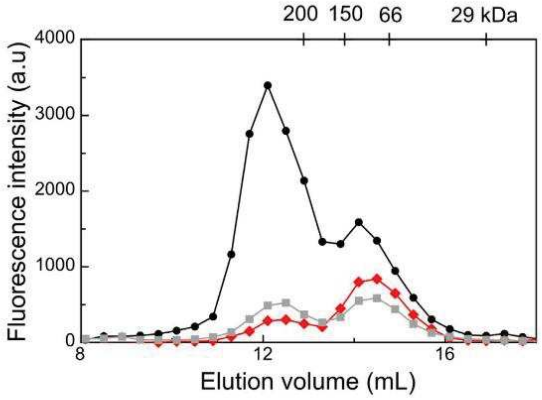

Figure 4. Size exclusion chromatography of purified Strep-Tagged-GFP-Mrr injected at 155 nM (black circles) or 35 nM (red diamonds), and of the fractions collected between 11.7–12.5 ml re-injected on the column (gray squares). Fluorescence intensity in the elution fractions was detected in a fluorescence plate reader using and 488–528 nm excitation-emission. The elution volume of the molecular weight markers used for calibrating the column is indicated on top.

In vivo properties of an Mrr catalytic mutant

Further investigation focused on the behavior of an engineered Mrr mutant with a D203A substitution in the putative catalytic loop, which was previously shown to be resistant to HP activation (18), strain MG1655 P_{BAD}-*gfp::mrr*^{D203A}. The average stoichiometry values calculated from N&B analysis of this strain revealed that in unstressed cells Mrr^{D203A} exhibited a slightly lower stoichiometry than WT GFP-Mrr (Figure 5), indicating that the protein was present in equilibrium between dimer and tetramer. Since the GFP-Mrr^{D203A} protein was expressed from the P_{BAD} promoter at concentrations equivalent to WT GFP-Mrr (218 +/− 114 nM), the lower average stoichiometry of the D203A mutant indicates a lower affinity between dimers for the GFP-Mrr^{D203A} mutant. Indeed the WT is tetrameric even at the low concentrations expressed from the WT promoter, further supporting the conclusion that the D203A mutation results in a large decrease in affinity between dimers. After pressure shock, a slight accumulation of GFP-Mrr^{D203A} was observed in the cell center, in the vicinity of the chromosome, but no *bona fide* foci formation occurred (Figure 5). Unlike the results obtained for WT GFP-Mrr, no change in average stoichiometry was observed for the GFP-Mrr^{D203A} mutant after pressure treatment, suggesting either that HP does not disrupt the tetramer or that HP-dissociated dimers can re-associate rapidly to tetramers after pressure release. Depending upon the exact expression levels of the GFP-Mrr^{D203A} mutant, the average stoichiometry values calculated for unstressed cells varied from day to day due to the concentration dependence of the tetramer-dimer equilibrium. However, for a given expression level, these values were equal before and after a pressure shock (Supplementary Figure S5). In contrast to HP treatment, plasmid-borne M.HhaII expression in the strain expressing GFP-Mrr^{D203A} resulted in filamentation, robust formation of foci, and dissociation of the GFP-Mrr^{D203A} to dimer

d from https://academic.oup.com/nar/article-abstract/45/9/5323/3076221
- IGH user
e 2018

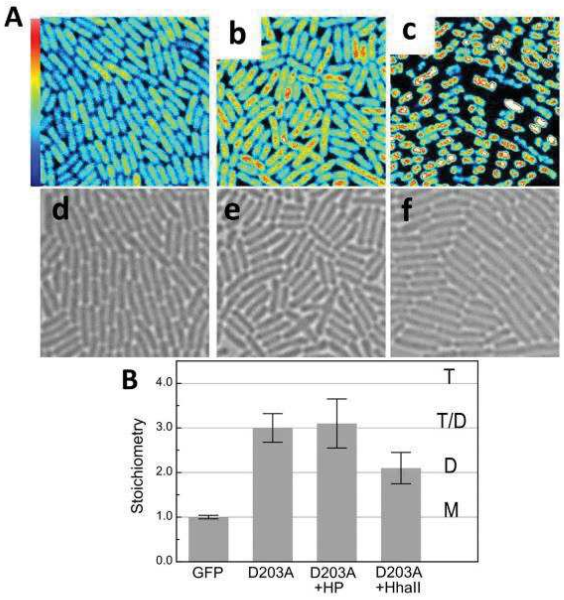

Figure 5. N&B results from Mrr mutant strains P_{BAD}-*gfp::mrr*^{D203A} and P_{BAD}-*gfp::mrr*^{D203A} + the pTrc99A-*hhaII* plasmid after pressure treatment or induction of the MTase HhaII. (**A**) Fluorescence intensity maps of GFP-Mrr^{D203A} (a) without treatment, (b) after 20 min at 100 MPa (HP) and (c) after induction of M.HhaII with IPTG for 60 min (20 × 20 μm). Maximum intensity scale is 2 counts per 40 μs pixel dwell-time. Bright-field images of P_{BAD}-*gfp::mrr*^{D203A} (d) without treatment, (e) after 20 min at 100 MPa (HP) and (f) after induction of M.HhaII with IPTG for 60 min. (**B**) Stoichiometry values of fluorescent proteins corresponding to GFP monomers (M), dimers (D), tetramers (T) or a possible equilibrium between dimer and tetramer (T-D) as deduced from the background corrected molecular brightness of fluorescent proteins in P_{BAD}-*gfp-mrr* (GFP), P_{BAD}-*gfp::mrr*^{D203A} without (D203A) or after pressure treatment (D203A +HP) and P_{BAD}-*gfp::mrr*^{D203A} + pTrc99A-*hhall* after induction of MTase expression (D203A +HhaII).

(Figure 5 Ac and f and B). Like the WT GFP-Mrr, mobility of the catalytic mutant increased after M.HhaII induction (Supplementary Figure S2), suggesting that this effect does not require cleavage.

DISCUSSION

In *E. coli* K-12 MG1655, the DNA damage (SOS) response can be mounted by activating the endogenous Mrr Type IV REase through HP shock or through expressing the M.HhaII Type II MTase (7,30). Based on sequence homology with the MspII Restriction endonuclease (31), Mrr is putatively composed of a DNA binding domain that recognizes specific methylated DNA sequences, and a catalytic domain responsible for DNA cleavage (32). The average stoichiometry and dynamics of GFP-Mrr in the absence of HP or MTase triggers indicated that the protein forms tetramers that are immobile on a timescale of tens of milliseconds. In contrast, the protein is dynamic on a timescale of seconds, since intensity fluctuations are observed in N&B (22). Consequently, we conclude that the protein is in reversible interaction with the chromosome, although these interactions may be non-specific. Even non-specific protein–DNA interactions can appear immobile on a timescale of tens of milliseconds (33). Most importantly, since Mrr is inactive in unstressed cells (8,9), no DNA cleavage occurs.

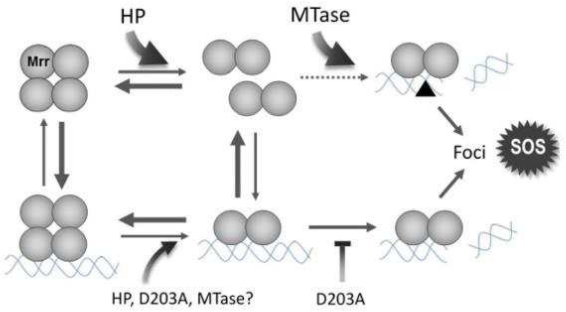

Figure 6. Schematic of the proposed mechanism of Mrr activation by a high pressure shock (HP) or by expression of the M.HhaII methyltransferase (MTase). HP is proposed to dissociate the inactive tetrameric Mrr to an active dimer which recognizes low affinity sites on the chromosome and cleaves them. Dimeric Mrr would remain bound at the DNA cleavage site and form foci while triggering the SOS response. By favoring the dimer, pressure would thus *push* Mrr toward activation. The MTase is proposed to function by methylating the DNA, thus creating a large number of high affinity sites for Mrr (black triangle). Any infinitesimal amount of active dimer in equilibrium with inactive tetramer would be readily captured at these high affinity sites and cleave them, thus irreversibly *pulling* Mrr toward activation. The Mrr D203A catalytic site mutation would inhibit cleavage of non-methylated DNA, reducing foci formation and precluding the HP-induced SOS response. It is likely that the DNA-bound Mrr tetramer is also subjected to the effect of high pressure, DNA methylation or the D203A mutation.

Upon pressure shock and release, or induction of MTase expression, we observed that Mrr forms foci, shown previously to be associated with the chromosome (9). N&B analysis reveals that the Mrr present in these foci is dimeric. Interestingly, while HP shock has no effect on GFP-Mrr mobility, MTase induction leads to increased dynamics. The origins of this increased mobility are unclear. One possibility is that cleavage of the DNA at the multiple methylated sites created by the MTase leads to greater mobility of the fragmented chromosome. However, this increase in mobility upon MTase induction is observed for the catalytic mutant of Mrr as well, although residual activity cannot be ruled out. Another possibility is that the existence of a large number of specific target sites on the chromosome leads to increased Mrr migration between target sites, even in the absence of cleavage.

Overall, the results from Number and Brightness measurements suggest distinct molecular mechanisms of Mrr activation by HP and M.HhaII expression (Figure 6). We propose that pressure *pushes* the Mrr tetramer-dimer equilibrium toward the active, dimeric form. The catalytic sites of Mrr may be masked in the tetrameric form, and exposed upon dissociation to dimer. While it is possible that the effect of HP could result from a structural perturbation of the *E. coli* nucleoid, thereby exposing cryptic Mrr sites, rather than a direct effect on Mrr oligomerization state, the effect of pressure on protein oligomerization equilibria (34) has been known for decades (14,35,36). Upon release of pres-

aded from https://academic.oup.com/nar/article-abstract/45/9/5323/3076221
PE - IGH user
June 2018

sure some proportion of GFP-Mrr dimers, perhaps those not specifically bound to the chromosome, re-associate to tetramer. However, the observation that GFP-Mrr present in the foci after pressure release is dimeric suggests that cleavage at the cryptic sites present in the chromosome leads to an increase in affinity between active, dimeric Mrr and the target sites, which prevents its re-association to tetramer. We assume that Mrr does not remain bound to a single target site on the chromosome, but rather remains statistically in interaction with the chromosome, migrating between these cryptic target sites. Hence the small number of Mrr molecules produced from the natural Mrr promoter can cleave at multiple sites after dissociation/activation by pressure. Increased affinity could arise from a change in conformation at the cleaved sites, nucleoid condensation or the recruitment of other SOS factors to the foci. In the absence of cleavage, as is likely the case for the catalytic mutant, the affinity of Mrr for the un-cleaved cryptic sites is not high enough to prevent, in a dynamic equilibrium, its re-association to tetramer after pressure release. In support of our model in which pressure *pushes* the Mrr tetramer-dimer equilibrium toward the active dimer, we note that oligomerization appears to be linked to function in the case of Mrr, since the catalytic D203A mutant exhibits a lower affinity between dimers in unstressed cells.

In contrast to pressure *pushing* the Mrr toward active dimer, we propose that M.HhaII MTase activity *pulls* the tetramer-dimer equilibrium to an active, dimeric state. Upon expression of the MTase, a large number of highly specific, high affinity methylated sites for Mrr are generated on the chromosome. The small amount of Mrr dimer in equilibrium with the tetramer binds to these specific sites. Alternatively, tetrameric Mrr could bind to these sites and then dissociate to dimer. In either case, this *pulls* the tetramer-dimer equilibrium toward active dimer. In the case of WT Mrr, extensive cleavage of the chromosome ensues. Interestingly, the effects of MTase expression on Mrr localization, stoichiometry and dynamics are identical for the catalytic mutant. One interpretation of this observation is that the large increase in affinity of the active, dimeric form of Mrr for the methylated DNA sites, stabilizes the dimer in the foci, even in the absence of cleavage.

N&B analysis has revealed strong coupling between Mrr oligomerization and its function *in vivo*, further supported by *in vitro* analytical biochemistry. The oligomerization and activity are perturbed via distinct mechanisms by pressure shock and MTase induction, both resulting in an SOS response. These studies highlight the importance of quantitative molecular measurements for deciphering functional mechanisms in live cells.

SUPPLEMENTARY DATA

Supplementary Data are available at NAR Online.

ACKNOWLEDGEMENTS

The authors would like to express their appreciation to Pressure BioSciences, Inc. of South Easton MA for their loan of the HUB440 high pressure generator used in this study.

FUNDING

Rensselaer Polytechnic Institute; Alfred P. Sloan Foundation 2015-14088 (to C.A.R.); KU Leuven Research Fund [DBOF/12/035, DBOF/14/049, GOA/15/006 to A.A.]. Funding for open access charge: RPI internal funds.
Conflict of interest statement. None declared.

REFERENCES

1. Aertsen,A. and Michiels,C.W. (2006) Upstream of the SOS response: figure out the trigger. *Trends Microbiol.*, **14**, 421–423.
2. Heitman,J. and Model,P. (1987) Site-specific methylases induce the SOS DNA repair response in Escherichia coli. *J. Bacteriol.*, **169**, 3243–3250.
3. Loenen,W.A.M. and Raleigh,E.A. (2014) The other face of restriction: modification-dependent enzymes. *Nucleic Acids Res.*, **42**, 56–69.
4. Bickle,T.A. and Kruger,D.H. (1993) Biology of DNA restriction. *Microbiol Rev.*, **57**, 434–450.
5. Roberts,R.J., Belfort,M., Bestor,T., Bhagwat,A.S., Bickle,T.A., Bitinaite,J., Blumenthal,R.M., Degtyarev,S.K., Dryden,D.T.F., Dybvig,K. *et al.* (2003) SURVEY AND SUMMARY A nomenclature for restriction enzymes , DNA methyltransferases, homing endonucleases and their genes. *Nucleic Acids Res.* **31**, 1805–1812.
6. Tesfazgi Mebrhatu,M., Wywial,E., Ghosh,A., Michiels,C.W., Lindner,A.B., Taddei,F., Bujnicki,J.M., Van Melderen,L. and Aertsen,A. (2011) Evidence for an evolutionary antagonism between Mrr and Type III modification systems. *Nucleic Acids Res.*, **39**, 5991–6001.
7. Aertsen,A., Van Houdt,R., Vanoirbeek,K. and Michiels,C.W. (2004) An SOS response induced by high pressure in Escherichia coli. *J. Bacteriol.*, **186**, 6133–6141.
8. Aertsen,A. and Michiels,C.W. (2005) Mrr instigates the SOS response after high pressure stress in Escherichia coli. *Mol. Microbiol.*, **58**, 1381–1391.
9. Ghosh,A., Passaris,I., Tesfazgi Mebrhatu,M., Rocha,S., Vanoirbeek,K., Hofkens,J. and Aertsen,A. (2014) Cellular localization and dynamics of the Mrr type IV restriction endonuclease of Escherichia coli. *Nucleic Acids Res.*, **42**, 3908–3918.
10. Aertsen,A. and Michiels,C.W. (2005) SulA-dependent hypersensitivity to high pressure and hyperfilamentation after high-pressure treatment of Escherichia coli lon mutants. *Res. Microbiol.*, **156**, 233–237.
11. Ghosh,A. and Aertsen,A. (2013) Cellular filamentation after sublethal high-pressure shock in Escherichia coli K12 is Mrr dependent. *Curr. Microbiol.*, **67**, 522–524.
12. Aertsen,A., Faster,D. and Michiels,C.W. (2005) Induction of shiga toxin-converting prophage in Escherichia coli by High hydrostatic pressure induction of shiga toxin-converting prophage in Escherichia coli by high hydrostatic pressure. *Appl. Environm. Microbiol.* ,**71**, 1155–1162.
13. Digman,M.A., Wiseman,P.W., Choi,C., Horwitz,A.R. and Gratton,E. (2009) Stoichiometry of molecular complexes at adhesions in living cells. *Proc. Natl. Acad. Sci. U.S.A.*, **106**, 2170–2175.
14. Silva,J.L., Foguel,D. and Royer,C.A. (2001) Pressure provides new insights into protein folding, dynamics and structure. *Trends Biochem. Sci.*, **26**, 612–618.
15. Blattner,F.R., Plunkett,G. III, Bloch,C.A., Perna,N.T., Burland,V., Riley,M., Collado-vides,J., Glasner,J.D., Rode,C.K., Mayhew,G.F. *et al.* (1997) The complete genome sequence of Escherichia coli K-12. *Science*, **277**, 1453–1462.
16. Datsenko,K.a and Wanner,B.L. (2000) One-step inactivation of chromosomal genes in Escherichia coli K-12 using PCR products. *Proc. Natl. Acad. Sci. U.S.A.*, **97**, 6640–6645.
17. Li,X.T., Thomason,L.C., Sawitzke,J.A., Costantino,N. and Court,D.L. (2013) Positive and negative selection using the tetA-sacB cassette: recombineering and P1 transduction in Escherichia coli. *Nucleic Acids Res.*, **41**, 1–8.
18. Orlowski,J., Tesfazgi,M., Michiels,C.W., Bujnicki,J.M. and Aertsen,A. (2008) Biochemical and Biophysical Research Communications Mutational analysis and a structural model of

d from https://academic.oup.com/nar/article-abstract/45/9/5323/3076221
- IGH user
e 2018

methyl-directed restriction enzyme Mrr. *Biochem. Biophys. Res. Commun.*, **377**, 862–866.
19. Hallez,R., Geeraerts,D., Sterckx,Y., Mine,N., Loris,R. and Van Melderen,L. (2010) New toxins homologous to ParE belonging to three-component toxin-antitoxin systems in Escherichia coli O157:H7. *Mol. Microbiol.*, **76**, 719–732.
20. Amann,E., Ochs,B. and Abel,K.J. (1988) Tightly regulated tac promoter vectors useful for the expression of unfused and fused proteins in Escherichia coli. *Gene*, **69**, 301–315.
21. Ferguson,M.L., Le Coq,D., Jules,M., Aymerich,S., Declerck,N., Royer,C.A., Le,D., Jules,M., Aymerich,S., Declerck,N. *et al.* (2011) Absolute quantification of gene expression in individual bacterial cells using two-photon fluctuation microscopy. *Anal. Biochem.*, **419**, 250–259.
22. Digman,M.A., Dalal,R., Horwitz,A.F. and Gratton,E. (2008) Mapping the number of molecules and brightness in the laser scanning microscope. *Biophys. J.*, **94**, 2320–2332.
23. Ferguson,M.L., Le Coq,D., Jules,M., Aymerich,S., Radulescu,O., Declerck,N., Royer,C.a, Le,D., Jules,M., Aymerich,S. *et al.* (2012) Reconciling molecular regulatory mechanisms with noise patterns of bacterial metabolic promoters in induced and repressed states. *Proc. Natl. Acad. Sci. U.S.A.*, **109**, 155–160.
24. Espenel,C., Margeat,E., Dosset,P., Arduise,C., Le Grimellec,C., Royer,C.a, Boucheix,C., Rubinstein,E. and Milhiet,P.-E. (2008) Single-molecule analysis of CD9 dynamics and partitioning reveals multiple modes of interaction in the tetraspanin web. *J. Cell Biol.*, **182**, 765–776.
25. Digman,M.A., Brown,C.M., Sengupta,P., Wiseman,P.W., Horwitz,A.R. and Gratton,E. (2005) Measuring fast dynamics in solutions and cells with a laser scanning microscope. *Biophys. J.*, **89**, 1317–1327.
26. Digman,M.A., Stakic,M. and Gratton,E. (2013) Raster image correlation spectroscopy and number and brightness analysis. *Methods in Enzymol.*, **518**, 121–144.
27. Guzman,L.M., Belin,D., Carson,M.J. and Beckwith,J. (1995) Tight regulation, modulation, and high-level expression by vectors containing the arabinose PBAD promoter. *J. Bacteriol.*, **177**, 4121–4130.
28. Elowitz,M.B., Surette,M.G., Wolf,P.E., Stock,J.B. and Leibler,S. (1999) Protein mobility in the cytoplasm of Escherichia coli. *J. Bacteriol.*, **181**, 197–203.
29. Cormack,B.P., Valdivia,R.H., Falkow,S., Cormack,B.P., Valdivia,R.H. and Falkow,S. (1996) FACS-optimized mutants of the green fluorescent protein (GFP). *Gene*, **173**, 33–38.
30. Waite-Rees,P.A., Keating,C.J., Moran,L.S., Slatko,B.E., Hornstra,L.J. and Benner,J.S. (1991) Characterization and expression of the Escherichia coli Mrr restriction system. *J. Bacteriol.*, **173**, 5207–5219.
31. Horton,J.R., Mabuchi,M.Y., Cohen-karni,D., Zhang,X., Griggs,R.M., Samaranayake,M., Roberts,R.J., Zheng,Y. and Cheng,X. (2012) Structure and cleavage activity of the tetrameric MspJI DNA modification-dependent restriction endonuclease. *Nucleic Acids Res.* **40**, 9763–9773.
32. Zheng,Y., Cohen-karni,D., Xu,D., Chin,H.G., Wilson,G., Pradhan,S. and Roberts,R.J. (2010) A unique family of Mrr-like modification-dependent restriction endonucleases. *Nucleic Acids Res.* **38**, 5527–5534.
33. Wang,A.C., Revzin,A., Butler,A.P. and Von Hippel,P.H. (1977) Binding of E.coli lac repressor to non-operator DNA. *Nucleic Acids Res.*, **4**, 1579–1594.
34. Royer,C.a (2002) Revisiting volume changes in pressure-induced protein unfolding. *Biochim. Biophys. Acta*, **1595**, 201–209.
35. Paladini,A.A. and Weber,G. (1981) Pressure-induced reversible dissociation of enolase. *Biochemistry*, **20**, 2587–2593.
36. Schmid,G., Ludemann,H.-D. and Jaenicke,R. (1979) Dissociationand aggregation of lactic dehydrogenase by high hydrostatic pressure. *Eur. J. Biochem.*, **97**, 407–413.

oaded from https://academic.oup.com/nar/article-abstract/45/9/5323/3076221
IPE - IGH user
June 2018

SUPPLEMENTARY DATA

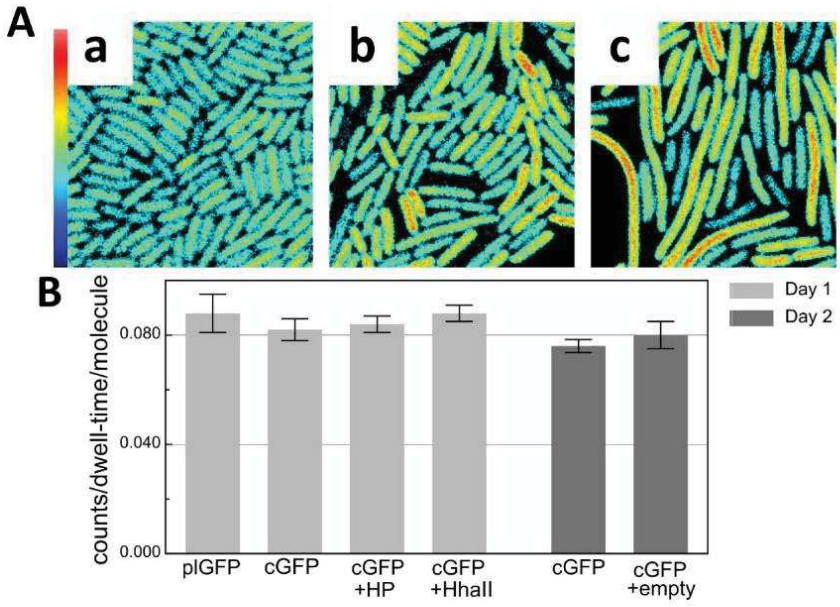

Figure S1. Brightness properties of free GFP in unstressed cells and after HP shock or MTase induction. A) Fluorescence intensity map of cells expressing free GFP from the P_{BAD} promotor at the *mrr* chromosomal locus in strain P_{BAD}-*gfp-mrr* which expresses GFP and Mrr from the natural chromosomal locus and which has a stop codon between the GFP coding sequence and Mrr, such that both proteins are produced, but the GFP is not covalently linked to the Mrr protein. A) before treatment (a), after 20 min at 100 MPa (b), or together with the M.HhaI methyltransferase in strain P_{BAD}-*gfp-mrr* + pTrc99A-*hhaII* (c) (Scale is 20X20 µm). Maximum intensity scale is 2 counts per 40 µs pixel dwell-time. B) Molecular brightness values (background corrected) of free GFP expressed from the plasmid-borne P_{BAD}-*gfp-mrr* (plGFP) or chromosome-borne P_{BAD}-*gfp-mrr* (cGFP) in unstressed cells or after pressure treatment (cGFP +HP), and in the presence of the M.HhaII MTase (cGFP +HhaII) or pTrc99A empty (cGFP +empty). The color corresponds to two different experiment days.

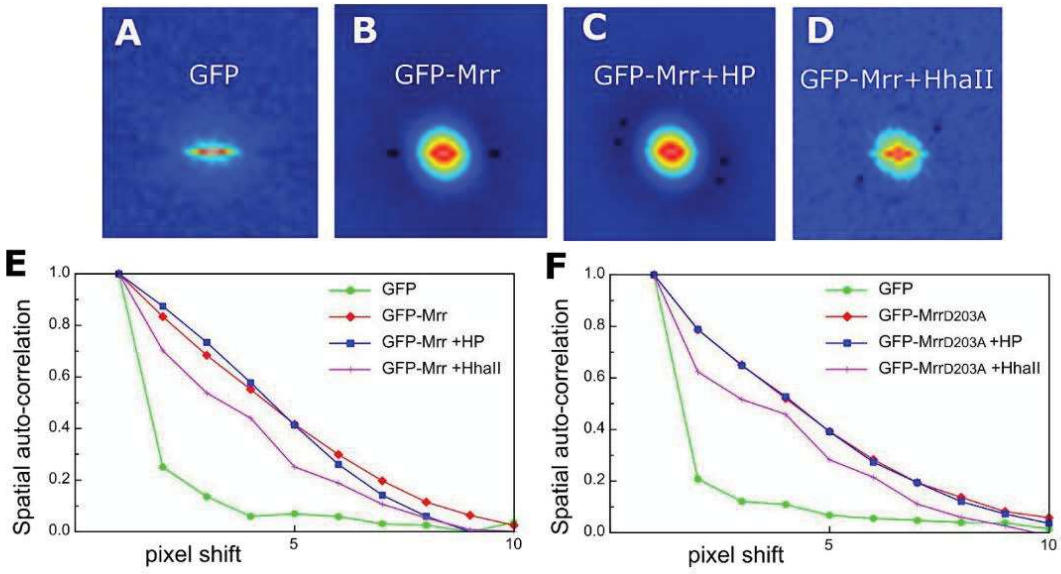

Figure S2. RICS analysis of raster scans acquired by sN&B imaging of GFP-Mrr and GFP-Mrr^{D203A} under different conditions. A-D). 2D plots generated by SimFCS of spatial auto-correlation retrieved from fluorescence intensity maps of *E. coli* strains containing A) chromosomal P_{BAD}-*gfp/mrr*, expressing free GFP in unstressed cells, B) chromosomal P_{BAD}-*gfp-mrr*, expressing the GFP-Mrr fusion in unstressed cells, C) chromosomal P_{BAD}-*gfp-mrr*, expressing the GFP-Mrr fusion in cells after 20 minutes of pressure shock at 100 MPa, D) P_{BAD}-*gfp-mrr* + pTrc99A-*hhaII*, expressing the GFP-Mrr in the presence of MTase M.HhaII. E-F Comparison of the vertical auto-correlation profile of GFP-Mrr (E) and GFP-MrrD203A (F) in unstressed cells, after HP or HhaII induction using chromosomal P_{BAD}-*gfp-mrr*, and P_{BAD}-*gfp-mrr* + pTrc99A-*hhaII* strains.

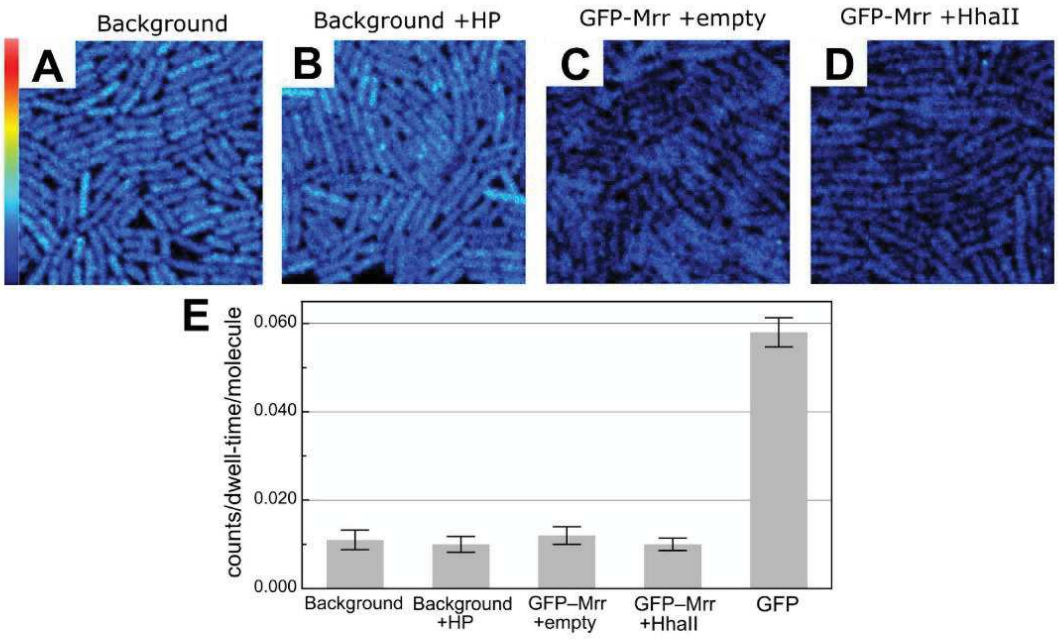

Figure S3. Fluorescence intensity maps and molecular brightness of auto-fluorescent background. A) Parental background strain *E. coli* K12 MG1655 before and B) after a pressure shock. C) Un-induced GFP-Mrr in strain chromosomal P_{BAD}-*gfp::mrr* + pTrc99A empty but in presence of IPTG and D) Un-induced GFP-Mrr in chromosomal P_{BAD}-*gfp::mrr* + pTrc99A-*hhaII* with M.HhaII induction by IPTG. Scale 20 µmX20 µm FOV and maximum intensity is 1.5 counts per 2 ms scan time per pixel. E) Molecular brightness values of parental background strain (Background) in unstressed cells or after a pressure treatment (HP) and non-induced GFP-Mrr in strains with chromosomal P_{BAD}-*gfp::mrr* + pTrc99A empty (GFP-Mrr +empty) and P_{BAD}-*gfp::mrr* + pTrc99A-*hhaII* in absence of arabinose and in presence of glucose to ensure lack of GFP-Mrr expression (GFP-Mrr +HhaII) after induction of MTase and P_{BAD}-*gfp-mrr* (GFP).

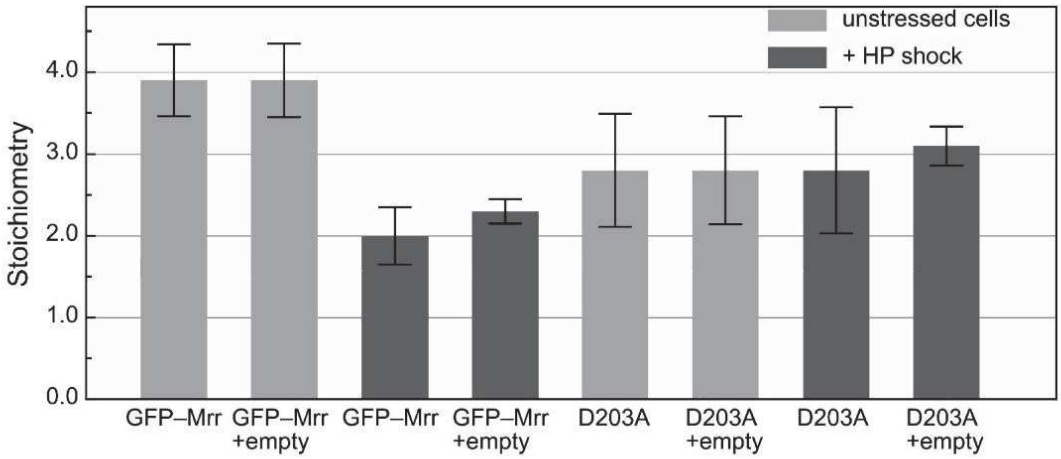

Figure S4. Stoichiometry values of unstressed cells (light grey) or after a pressure shock of 15min at 100MPa (HP, dark grey) in chromosomal strains P_{BAD}-*gfp::mrr* (GFP-Mrr), P_{BAD}-*gfp::mrr* + pTrc99A empty (GFP-Mrr +empty), P_{BAD}-*gfp::mrr*^{D203A} (D203A) and P_{BAD}-*gfp::mrr*^{D203A} + pTrc99A empty (D203A +empty).

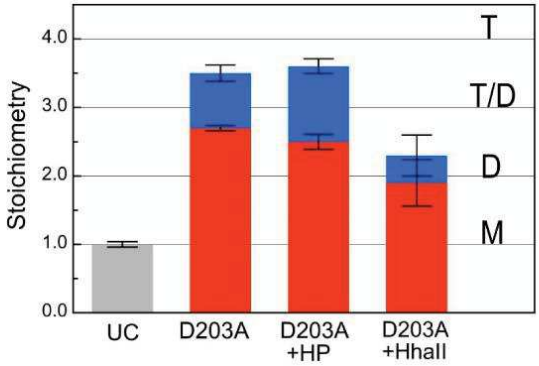

Figure S5. N&B results from Mrr mutant strains P_{BAD}-*gfp::mrr*^{D203A} and P_{BAD}-*gfp::mrr*^{D203A} +pTrc99A-*hhaII* after pressure treatment or induction of the MTase, M.HhaII. Stoichiometry values correspond to two different days of experiments (blue and red). GFP monomers (M), dimers (D), tetramers (T) or a possible equilibrium between dimer and tetramer (T/D) as deduced from the back-ground corrected molecular brightness of fluorescent proteins in chromosomal P_{BAD}-*gfp-mrr* (GFP), P_{BAD}-*gfp-mrr*^{D203A} in unstressed cells (D203A) or after pressure treatment (D203A +HP) and P_{BAD}-*gfp-mrr*^{D203A} + pTrc99A-*hhaII* after induction of the MTase (D203A + HhaII).

4. The structural basis for the coupling between oligomerization and catalysis of the Mrr endonuclease

In this manuscript that will be submitted soon for publication we have employed the same approach as the one developed in the first paper to characterize GFP-Mrr variants affected in their response to a HP shock and/or induction of HhaII MTase. These mutants have been isolated and previously characterized by our collaborators in Aertsen laboratory by conventional epifluorescence microscopy using plasmidic inducible expression vectors (143, 147). Here, using our 2-photon sN&B analysis method, we have compared the wild-type and mutant GFP-Mrr proteins expressed at very low level from a chromosomal insertion and determined their oligomeric state after exposure to high pressure or hyper-methylation of chromosomal DNA in the presence of M.HhaII. We next interpreted our data in the light of a 3D-homology model of the inactive Mrr tetramer bound to DNA that we constructed in collaboration with Gilles Labesse at the CBS.

4.1 Introduction

We have characterized a total of four GFP-Mrr mutant proteins:

- The variant carrying the D203A mutation located in the catalytic site (GFP-MrrD203A) is resistant to both HP- and M.HhaII-dependent activation. This variant had already served for validating our sN&B approach in our first paper (196). We confirmed that this variant is not responding to high pressure but found that, similar to the wild-type, the protein is dissociated into dimers in the presence of the HhaII methyltransferase although the SOS response is not elicited.

- The V173A and H279Y mutations have been isolated by screening variants where the activation of GFP-Mrr by high pressure and M.HhaII-dependent DNA methylation is decoupled, that is mutants responding to either HP or M.HhaII induction but not both (143). In good agreement with the observations made previously by epifluorescence (Figure 4.1.A), we found that GFP-MrrV173A was much less sensitive than the WT to a HP shock, whereas it still dissociated into dimers and formed foci in M.HhaII induced cells similar to what we observed for the WT by 2-photon scanning microscopy (Figure 4.1.B).

- As expected, the GFP-Mrr variant carrying the H279Y mutations still responded to pressure by forming foci, but our N&B analysis revealed that it remained essentially as a tetramer when observed after pressure release. Moreover, although this mutant

Mrr appeared less sensitive than the wild-type to M.HhaII induction in the experiments performed by our collaborators, we observed dimer dissociation as well as foci formation after HhaII-induction. As discussed later, this discrepancy could be due to the lower protein concentration in the strain we used, expressing the chromosomal version of the *gfp-mrr*H279Y mutant gene inserted as single copy at the *mrr* locus.

- Finally, we succeeded in characterizing a constitutively-activated GFP-Mrr variant in spite of the very high toxicity of the triple mutation it carries (N111S/D124G/V175G). As we expected, this variant associates as a dimer under all conditions, corroborating our finding that tetramer dissociation into dimers is at the basis of the molecular mechanism of Mrr activation by increased pressure or DNA methylation.

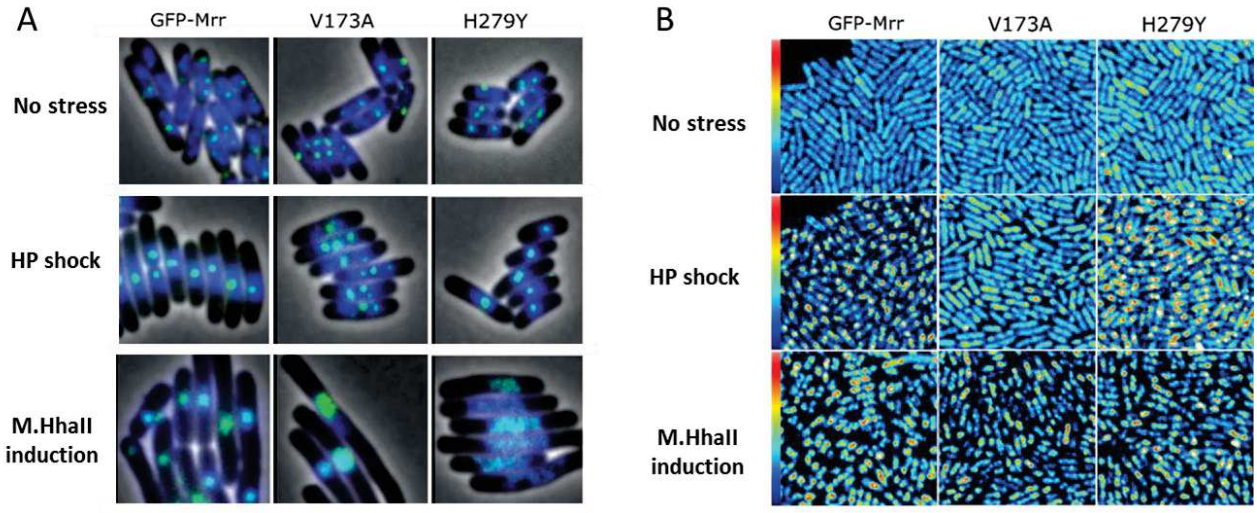

Figure 4.1: Comparison of the fluorescence images of E. coli MG1655 expressing wild-type or mutant GFP-Mrr by A) conventional epifluorescence microscopy in Aertsen laboratory or by B) 2-photon scanning fluorescence microscopy as observed in this work. Cells expressing the wild-type or mutant gfp-mrr fusion carried by a A) replicative plasmid or B) chromosomal insertion were observed before and after pressure treatment or induction of the M.HhaII methyltransferase. Panel A adapted from (143) *shows the merged images of the cells in phase contrast, GFP (green) and DAPI staining (blue). Panel B shows the average fluorescence intensity maps of fifty 20x20 µm scanned images. Maximum intensity is 2.5 counts per 40 µs pixel dwell-time. (Figure 2 in the following manuscript).*

The structural basis for the coupling between oligomerization and catalysis of the Mrr endonuclease

Anaïs Bourges[1,2], Oscar E. Torres M.[3], Anirban Ghosh[3], Wubishet M. Tadesse[3], Gilles Labesse[2], Catherine A. Royer[1], Abram Aertsen[3] and Nathalie Declerck[2*]

[1] Department of Biological Sciences, Rensselaer Polytechnic Institute, Troy, NY, 12180, USA
[2] Centre de Biochimie Structural, CNRS-Université Montpellier UMR 5048, 34000 Montpellier, France
[3] Department of Microbial and Molecular Systems, Laboratory of Food Microbiology, KU Leuven, B-3001 Leuven, Belgium

ABSTRACT

We have already demonstrated using scanning Number and Brightness microscopy that HP shock activation of the RecA-dependent SOS response in *Escherichia coli* K12 via the action of the Type IV RE, Mrr, is due to the dissociation of Mrr inactive tetramers into dimers capable of recognizing, binding and cleaving dsDNA at some cryptic sites on *E. coli* chromosome. In addition, we demonstrated that triggering of Mrr activity by the expression of the foreign methyltransferase HhaII which also leads to the induction of an SOS response, involves as well tetramer dissociation to dimer. We proposed a model for Mrr activation which the equilibrium coupling of oligomerization and activity is pushed from the inactive tetramer to the active dimer by pressure, and pulled by the creation of a large number of high affinity methylated sites by the methyltransferase. Using the same approach that we used to study the behavior of wild type Mrr and a catalytic mutant that abolished the response, we next investigated another set of mutant Mrr constructs that decouple the pressure response from the MTase induced response. In order to facilitate the interpretation of our *in vivo* and *in vitro* results and to gain insight into the structural basis of Mrr activation, we propose a 3D homology-based structural model of the full length of Mrr inactive tetramer bound to DNA.

INTRODUCTION

High pressure (HP) represents an important environmental factor for understanding bacterial adaptation. It has been suggested that the biomass in HP environments, such as in the oceans or under the Earth's crust, exceeds that on the surface (1). Moreover, HP is routinely used in food processing, a practice which has led to the appearance of HP-resistant bacterial strains. Indeed, strains of *E. coli* resistant to 2 GPa pressure have been obtained by directed evolution in only a few generations (2). It has previously been shown that HP shock of 100 MPa for 15 minutes to *E. coli* K12 strain MG1655 elicits an SOS response, with typical SOS-mediated phenotypes such as prophage activation and SulA-mediated filamentous growth upon return to atmospheric pressure (3). The bacterial SOS response allows for rapid adaptation to challenging environments by triggering mutagenesis and recombination (4). This HP-dependent SOS response was shown to depend on RecB, not RecF, indicative of HP-induced double stranded breaks in the chromosome (5). Moreover, in the same study, an HP screen in *Lon* deficient mutants revealed the pressure response to depend on a Type IV restriction endonuclease (RE), Mrr, which is constitutively present in cells in an inactive form, and which is activated by pressure. Type IV Res are not present in conjunction with a cognate Methyl Transferase (MTase) (6). Indeed, Type IV REs target modified DNA (7, 8), and Mrr activation can also be triggered by expression of the Type II M.HhaII methyltransferase from *Haemophilus haemolyticus* (9).

We recently proposed a model for HP and MTase activation of Mrr based on the observation using Number and Brightness analysis of GFP fusions of Mrr in live single *E. coli* cells (10) that Mrr exists a tetramer at atmospheric pressure or in absence of the MTase but is present as a dimer in chromosome-bound foci after either HP shock or induction of MTase expression (11). In our model, HP, which is known to lead to oligomer dissociation, pushes the Mrr tetramer-dimer equilibrium toward the active dimer, which binds to cryptic sites present in the chromosome, irreversibly cleaves the DNA, and induces the SOS response. In this case, after pressure release, the Mrr protein remains dimeric and localized to foci associated with DNA damage. In contrast, expression of the MTase pulls the tetramer-dimer equilibrium to the active dimer via the creation of a large number of high affinity methylated sites on the *E. coli* chromosome. Likewise, recognition and cleavage by the active dimer is irreversible. The structure of the Mrr monomer consists of an N-terminal winged helix turn helix DNA binding domain (DBD) and a C-terminal catalytic domain (12). Recognition of specific (or cryptic) sites is thought to be carried out by the DBD, whereas cleavage occurs at some distance to the recognition site, as is typical for Type IV REs (6). Alanine substitution of an aspartic acid (D203A) in the putative active site of the catalytic domain resulted in resistance to HP shock (12). A linkage between function and oligomeric state was revealed in our previous N&B study, as we showed the tetramerization capacity of the D203A mutant to be compromised.

In the present work we investigate the structure-function relationships between tetramerization and cleavage by determining the stoichiometry of a series of Mrr mutants, and the effects of pressure and MTase expression thereon. Scanning Number and Brightness (sN&B) is a particle counting technique in which the amplitude of fluorescence

intensity fluctuations in the two-photon excitation volume are measured relative to the average fluorescence in each pixel of a Field of View (FOV) over multiple rapid raster scans. We measured as previously described in detail (11), the molecular brightness (in counts per pixel dwell-time per particle) of GFP-fusions of Mrr variants expressed at the natural locus in the *E. coli* chromosome under control of an arabinose inducible promoter. We also measured the molecular brightness of free, monomeric GFP expressed in the same strain from an inducible plasmid. The ratio of the molecular brightness of GFP-Mrr over that of free monomeric GFP yields the stoichiometry of the Mrr-GFP complex. As predicted by our previously published model for Mrr activation, we find that a GFP fusion of a constitutively active mutant of Mrr, GFP-Mrr$^{N111S/D124G/V175G}$ is dimeric when expressed in single live *E. coli* cells. Two other mutants of Mrr, Mrr^{V173A} and Mrr^{H279Y}, which appeared to decouple the response to HP shock from that induced by MTase expression were isolated in a recent screen (13). Mrr^{V173A} could only be activated by expression of M.HhaII, but was resistant to HP shock. In contrast, the Mrr^{H279Y} mutant could only be activated by pressure, but not MTase expression. The stoichiometry of GFP fusions of these mutants determined here also in live single *E. coli* cells by N&B analysis was found to be slightly lower than tetramer on average for both proteins in unperturbed cells. As expected, the Mrr^{V173A} mutant was found to dissociate to dimer upon MTase expression, while no significant effect of pressure was observed. Surprisingly, similar behavior was observed for the Mrr^{H279Y} mutant. Size exclusion chromatography of purified Strep-Tag-GFP fusions of these variants revealed decreased tetramer-dimer affinity for the Mrr^{V173A} mutant relative to WT Mrr. Finally, using a high-pressure capillary system we demonstrate that *in vitro* purified WT Mrr-GFP tetramer dissociates under pressure. To aid in the interpretation of the effects of these mutations in terms of the structure-function relationships between the dimer-tetramer equilibrium of Mrr and its DNA cleavage activities we constructed a homology model of the tetrameric catalytic domain. In this model, the catalytic loop was found to be adjacent to the interface between dimers, providing insight into the linkage between tetramer dissociation and activation. Valine 173 is in the helix that packs up against the catalytic loop, and its mutation to alanine could destabilize this interaction. Histidine 279 is distant from both the catalytic loop and the dimer/dimer interface in the tetrameric homology model.

MATERIAL AND METHODS

Strains and construction of mutants

MG1655 was used as a parental strain (14). A screen was realized by Anirban Ghosh to find Mrr variants with altered activity. The aim was to get an Mrr mutant that is not answering to pressure but still activated by Mod^{LT2} or HhaII and vice versa. To accomplish those mutants, they used the parental strain expressing Mrr and HP shocks to select HP resistant with Mrr mutation and on the other hand, they used *S. Typhimurium* LT2 K2 to look at Mod^{LT2} and HhaII activity. A mutation triggered to no response to HP but react to HhaII induction, V173A and a second mutation H279Y did not respond to HhaII induction but it was still activated by pressure. All strains used for this work are resume in the Table 1.

Table 1. Escherichia coli strains used for this work.

Strain		Chromosomal and/or plasmid	Produces	Growth conditions
***E. coli* MG1655**				
E. coli* MG1655 PBAD-*gfp-mrr		Chromosomal	Free GFP and unlabeled Mrr	Induction arabinose 0.4%
E. coli* MG1655 PBAD-*gfp-mrr		Plasmidic	Free GFP and unlabeled Mrr and M.HhaII	Induction arabinose 0.002%
E. coli* MG1655 PBAD-*gfp ::mrr		Plasmidic	GFP-Mrr	Induction arabinose 0.002%
E. coli* MG1655 PBAD-*gfp-mrr		Plasmidic	GFP-$Mrr_{N111S/D124G/V175G}$	Growth on glucose 0.4% and induction arabinose 0.002%
Same strains for mutants GFP-Mrr D203A, GFP-Mrr V173A and GFP-Mrr H279Y	***E. coli* MG1655 P*BAD-gfp::mrr***	Chromosomal	GFP-Mrr	Induction arabinose 0.4%
	***E. coli* MG1655 PBAD-*gfp*::Mrr + pTrc99A empty**	Chromosomal + empty plasmid	GFP-Mrr	Induction arabinose 0.4% and IPTG 1 mM
	E. coli* MG1655 P*BAD-gfp::mrr* + pTrc99A-*hhaII	Chromosomal + plasmid	GFP-Mrr and HhaII M.HhaII	Induction arabinose 0.4% and IPTG 1 mM

Growth conditions and sample preparation

As previously described (11), bacteria are grown in LB with the appropriate antibiotic if needed (ampicillin) and cells are induced with 0.4% arabinose. If required, the MTase HhaII was induced with 1 mM IPTG (isopropyl β-D-thio-galactopyranoside) when cells reached an OD_{600}~ 0.15. Late exponential phase bacteria are centrifuge (OD_{600} is around 0.6) and the pellet is resuspended in LB to a final OD_{600} of 25 for good microscopy sampling. Sample preparation for microscopy was made on a 2% agar pad sandwiched between two coverslips No1 (VWR) with a poly-L-Lysine coating. A computer-controlled HUB440 high pressure generator is used to pressurized sample in 50 µL MicroTubes (Pressure BioSciences, Inc., South Easton, MA).

Fluorescence Fluctuation Microscopy

Fluorescence fluctuation imaging was performed using a femtosecond pulsed infrared laser (MaiTai, Newport/Spectra Physics, Mountain View, CA, USA) focused through a 60X 1.2NA water immersion objective (Nikon APO VC). Photons were detected by avalanche photodiodes (Perkin Elmer). For the measurement of the GFPmut2, infrared light was

filtered from detected light by using a 735nm low-pass dichroic filter (Chroma Technology Corporation, Rockingham, VT) and emitted light was filtered with a 530/43 nm emission filter. The wavelength and the laser power were optimized for a good GFPmut2 emission without cellular autofluorescence and photo-bleaching. Thus, fluorescence fluctuation imaging was performed using an exciting power laser of 11 mW at 930 nm. Calibration of the excitation volume was done using a 40 nM fluorescein solutions (Spectrum).

Number and brightness analysis

Number and brightness analysis is a fluctuation approach much like fluorescence correlation spectroscopy. Diffusion of fluorescent particles in and out of the small effective volume (V_{eff}) of the 2-photon point spread function of the microscope leads to fluctuations in the fluorescence intensity relative to the average. In scanning number and brightness (sN&B) acquisitions of a series of raster scans (50 frames) of a field of view (FOV) using a pixel dwell-time (40 µs) that is faster than the diffusion time provides 50 values of fluorescence intensity at each pixel in the FOV from which variance (σ^2) and the average intensity ($\langle F \rangle$) can be calculated. These are used to calculate a pixel-based map of the molecular brightness (B) and number of particles (N). According to Poisson statistics, B is defined for each pixel as the ratio of the variance over the average intensity

$$B = (\sigma^2 / \langle F \rangle) \quad (1).$$

and the number of molecules in the V_{eff}, N, as the ratio of the square of the total intensity over the variance

$$N = (\langle F \rangle^2 / \sigma^2) \quad (2).$$

The shot-noise corrected brightness, e, is

$$e = B - 1 \quad (3).$$

and the shot noise corrected number of particles (n) in V_{eff} is

$$n = NXB/(B-1) \quad (4).$$

Thus, $\langle F \rangle = e \times n$. Values are corrected for the autofluorescence background contribution as previously described (11). To do so, the autofluorescent background of the parent MG1645 strain are determined each day. For each FOV the central 50% of pixels inside all bacteria (minus the edge pixels) are selected by intensity thresholding. Next, these average values from all the FOV were averaged for each sample (F_{sample}, e_{sample} and n_{sample}) and corrected for background (bg) contributions using the average fluorescence and brightness obtained from the background strain (e_{bg} and F_{bg}) the same day under the same growth and imaging conditions as follows:

$$e_{GFP}\,(sample) = (e_{sample} * F_{sample} - e_{bg} * F_{bg})/(F_{sample} - F_{bg}) \quad (5)$$

$$n_{GFP}\ (sample) = (F_{sample} - F_{bg})^2/(e_{sample} * F_{sample} - e_{bg} * F_{bg}) \quad (6)$$

This correction assumes that the brightness in the sample is a linear combination of the brightness of the GFP in the sample, e_{GFP} (sample), and the brightness of the background, weighted for their fractional contributions, which together add up to unity. The brightness of free GFP is also measured daily using a strain expressing free GFP and unlabeled Mrr (P_{BAD}-*gfp-Mrr*) as described previously (11). Then the stoichiometry of the Mrr variants is calculated by dividing their background and shotnoise corrected brightness value, e_{GFP} *(sample)*, by the brightness of the free monomeric GFP.

In vitro FCS measurements

Like N&B, Fluorescence correlation spectroscopy (FCS) is a single molecule sensitive technique that is based on the time correlation of fluorescence intensity fluctuations (δF) due to fluorescent molecule diffusing through the excitation volume. When those fluctuations are time correlated, it is possible to extract from the correlation curve information about diffusion (D) and concentration (N, number of particles). The autocorrelation curve is a representation of the self-similarity of a signal at some time point with itself at some time τ later. The autocorrelation function for the fluorescence intensities, normalized by average intensity squared, is given by:

$$G(t) = \frac{<\delta F(t)\delta F(t+\tau)>}{<F(t)>^2} = G(0)\left(1+\frac{\tau}{\tau_D}\right)^{-1}\left(1+\left(\frac{r_o}{z_o}\right)^2\frac{\tau}{\tau_D}\right)^{\frac{-1}{2}} \quad (7).$$

Where the diffusion time, $\tau_D = \frac{r_o^2}{4D}$, with a diffusion coefficient, D, and r_o and z_o corresponding to the dimensions of the excitation volume. G(0) is inversely proportional to the number of particles (N) in the volume.

High pressure FCS set up

High pressure microscopy is challenging, but Gratton and Mueller (15) developed a pressure cell made of a glass capillary of internal diameter 50 μm, and total dimeter 400 μm which could resist several thousand bar of pressure. We used a similar capillary system, but rather than seal one end using a blow torch and the other by fixing it into a pressure nipple drilled to the appropriate diameter with epoxy glue, we used the glued nipple connections on both ends to facilitate sample loading. The capillary was mounted in a stainless-steel holder the size of an attofluor coverslip holder with slits for the capillary, and the nipple/seal ensemble on either end of the capillary was connected to a high-pressure line. A peristaltic pump is used to load the sample in a thin fused silica capillary. For high pressure experiments the HP line was blocked by closing the valve on one end of the capillary and connected to an automated high-pressure pump from Pressure Biosciences (Waltham, MA) on the other. To perform high pressure FCS, the same

microscope set up as in the sN&B experiments was used, except that the water objective that was replaced by a 60X 1.4NA oil immersion objective (Nikon APO VC), and glycerol, rather than oil was used as the coupling medium. This matched the capillary refraction index better than oil and minimized the distortion due to the capillary curvature. For each sample we recorded the fluorescence signal for 100 s at a 500 kHz frequency. Clean samples are critical for FCS acquisitions because any fluorescent aggregates will contaminate the signal.

GFPmut2-Mrr in vitro biochemistry

In order to purify GFPmut2-Mrr and GFPmut2-Mrr mutants, N-terminal Strep-tag® II fusions were cloned into the pRSET B vector (Invitrogen) and expressed in *E.* coliBL21 (DE3) cells or T7 Express. StrepTag-GFP-Mrr fusions were purified on a Streptactin-superflow high capacity resin (IBA) using an elution buffer (20 mM Tris pH8, 150 mM NaCl and 1mM EDTA). Size exclusion chromatography was performed on a pre-calibrated Superdex 200 10/300 in a different buffer (100mM Tris pH8, 150mM NaCl and 1mM EDTA). Due to the low amount of the proteins, protein levels in all fractions were measured using an infinite M1000 PROplate reader (TECAN, Switzerland) for GFPmut2 fluorescence at exciting and emission wavelengths, 488/15 nm and 528/20 nm.

Structure modeling

Due to important sequence divergence, comparative modeling of Mrr relied on fold-recognition to identified optimal templates for the N-terminal and C-terminal domains using the server @TOME-2 (16). Various templates sharing with Mrr sequence identity in the range of 15-25%, were detected for both domains and no known structure contains both domains precluding modeling of the complete target. Sequence-structure alignments were refined using a dedicated editor Vito (17) to maximize coverage and optimally place insertions/deletions. Then MODELLER (18) was used to build full model of each domain. The catalytic domain was modeled as a tetramer using PDB4OC8 (19) and PDB4F0Q (20) in combination. In parallel, coevolution was predicted using Gremlin (21) in order to point potential role of the mutated positions V173 and H279.

RESULTS

A constitutively active variant of Mrr is dimeric

We have proposed previously (11) that the active form of Mrr is a dimer, and that the mechanism of pressure-activation is based on the pressure-induced dissociation of the inactive tetrameric form to active dimer. Here, we investigate the structure-function linkages between oligomerization of Mrr and its activity. First, we determined by sN&B in live *E. coli* cells, the oligomeric state of a GFP fusion of WT Mrr and a constitutively active mutant of Mrr ($Mrr^{N111S/D124G/V175G}$) expressed under control of the P_{BAD} promoter in a plasmid to ascertain whether constitutive activity could be linked to a constitutively dimeric form of the protein. Upon induction by arabinose (at very low levels) this mutant formed large immobile foci in the cells (Figure 1A), without application of pressure or induction of M.HhaII compare to WT Mrr which formed small very mobile foci. Moreover, expression of the mutant led to a strong cell filamentation response. We found by sN&B analysis that the foci were composed of tetrameric Mrr for the WT which confirmed our previous observation done at lower a concentration (11) whereas the constitutive mutant is dimeric (Figure 1B). Only at much later times after induction (> 80 min) at a high concentration the mutant protein aggregates in one large foci localized in the middle of each bacterium. The observation that a constitutively active variant of Mrr is dimeric strongly supports our model for Mrr activation based on the dissociation of inactive tetramer to active dimer.

Mrr mutations uncouple oligomerization and activation

The structural basis for the activity of the dimer, with respect to inactive tetramer could involve conformational unmasking of the active site or increased DNA binding upon dissociation. Two recent genetic screens revealed Mrr mutants in which activation by MTase expression and pressure shock were decoupled (13). A strain expressing one of the mutant Mrr proteins, Mrr^{V173A}, exhibited a significant decrease in viability after expression of the MTase, but only a modest effect of pressure shock. In contrast, the viability of a strain expressing the other variant, Mrr^{H279Y}, was significantly decreased after pressure shock, but was only modestly affected by expression of the MTase. As in the case of WT GFP-Mrr, we expressed GFP fusions of these two mutant Mrr variants from the natural chromosomal locus of Mrr under the control of a P_{BAD} promoter. While no significant foci were apparent in unstressed cells, MTase induction led to the formation of foci by both variants, and, as previously shown (11), by WT Mrr and the catalytically inactive mutant, Mrr^{D203A}. Significant foci formation after pressure shock was observed for the Mrr^{H279Y} variant, but not the Mrr^{V173A} variant (Figure 2A). We next examined by sN&B in live *E. coli* cells the oligomeric properties of these two mutants before and after perturbation by either pressure or the expression of the MTase. The variant V173A showed slightly lower stoichiometry (3.5) than tetrameric (4.0) WT GFP-Mrr before perturbation, but not as low as the catalytically inactive mutant, D203A (3.0) previously reported (11)(Figure 2B). This indicates that the tetramer-dimer affinity of these Mrr variants is slightly diminished by the mutations. Expression of the MTase resulted in the dissociation of both mutant Mrr

variants to dimer, while pressure had only a small effect on the stoichiometry of both variants. These effects of pressure and MTase expression were expected for the Mrr^{V173A} variant, as it had been shown previously to be strongly activated by MTase expression, yet less responsive to pressure (13). However, we were surprised that the Mrr^{H279Y} variant exhibited the same oligomerization responses to the perturbations as the Mrr^{V173A} variant, since the viability of cells expressing Mrr^{H279Y} was greatly diminished by pressure shock, while only slightly modified by MTase expression. For this mutant, dissociation to dimer and interaction with methylated DNA resulting from MTase expression is insufficient for activation, whereas dissociation to dimer by pressure appears to be sufficient for some degree of activation of Mrr^{279Y} bound to unmethylated cryptic sites in the *E. coli* chromosome.

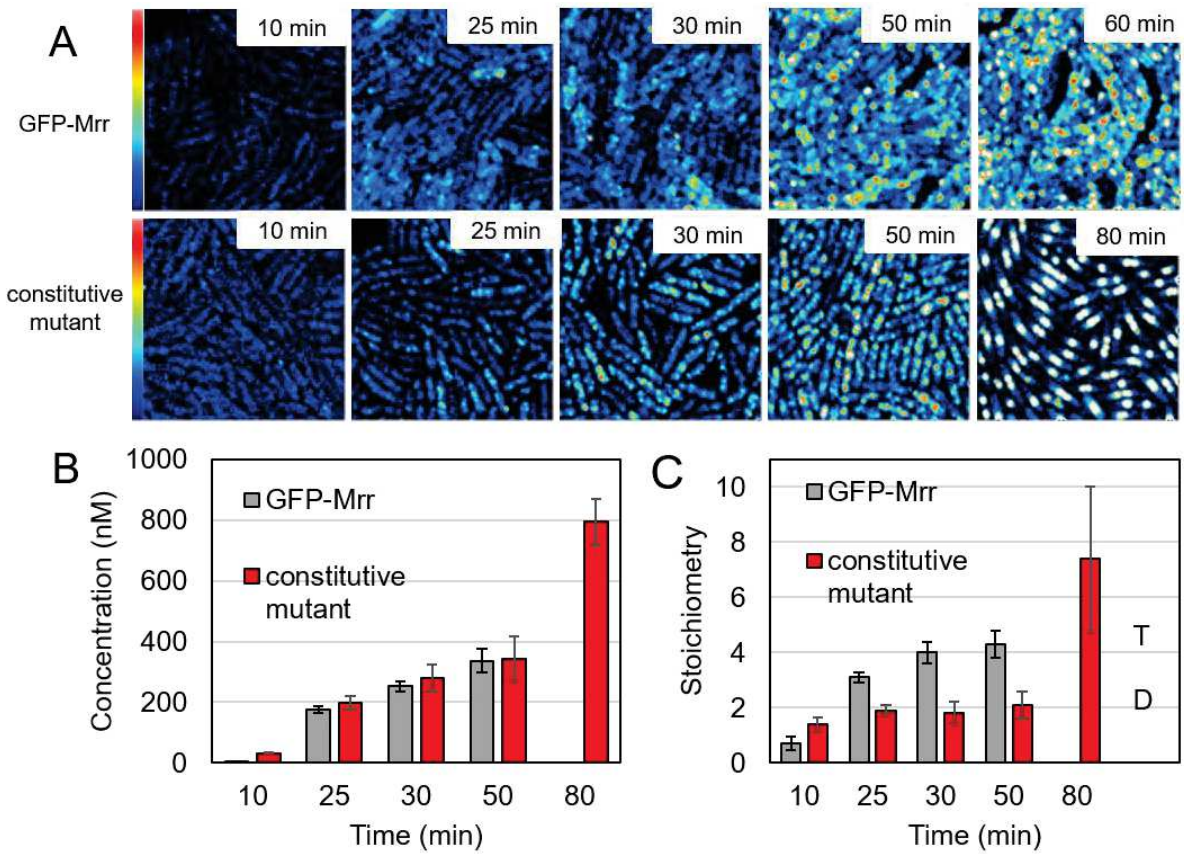

Figure 1. Effect of Mrr constitutive activity on Mrr stoichiometry. (A) Fluorescence intensity map of GFP-Mrr WT and constitutive mutant expressed under the control of the plasmid-based promotor P_{BAD}-gfp::mrr as a function of time after a switch from glucose to arabinose pad. Bacteria are grown in LB with 0.4% glucose, wash in LB and immobilize on 2% agar pad implemented with 0.4% arabinose for microscopy acquisition (Scale is 20X20 µm). Maximum intensity is 2.5 counts per 40 µs pixel dwell-time. B) Concentration values and C) Stoichiometry values of fluorescent proteins corresponding to GFP dimers (D) or tetramers (T) over as deduced from background corrected molecular brightness of GFP-Mrr WT and constitutive mutant expressed from a plasmid P_{BAD}-gfp::mrr over time after induction on pad with arabinose.

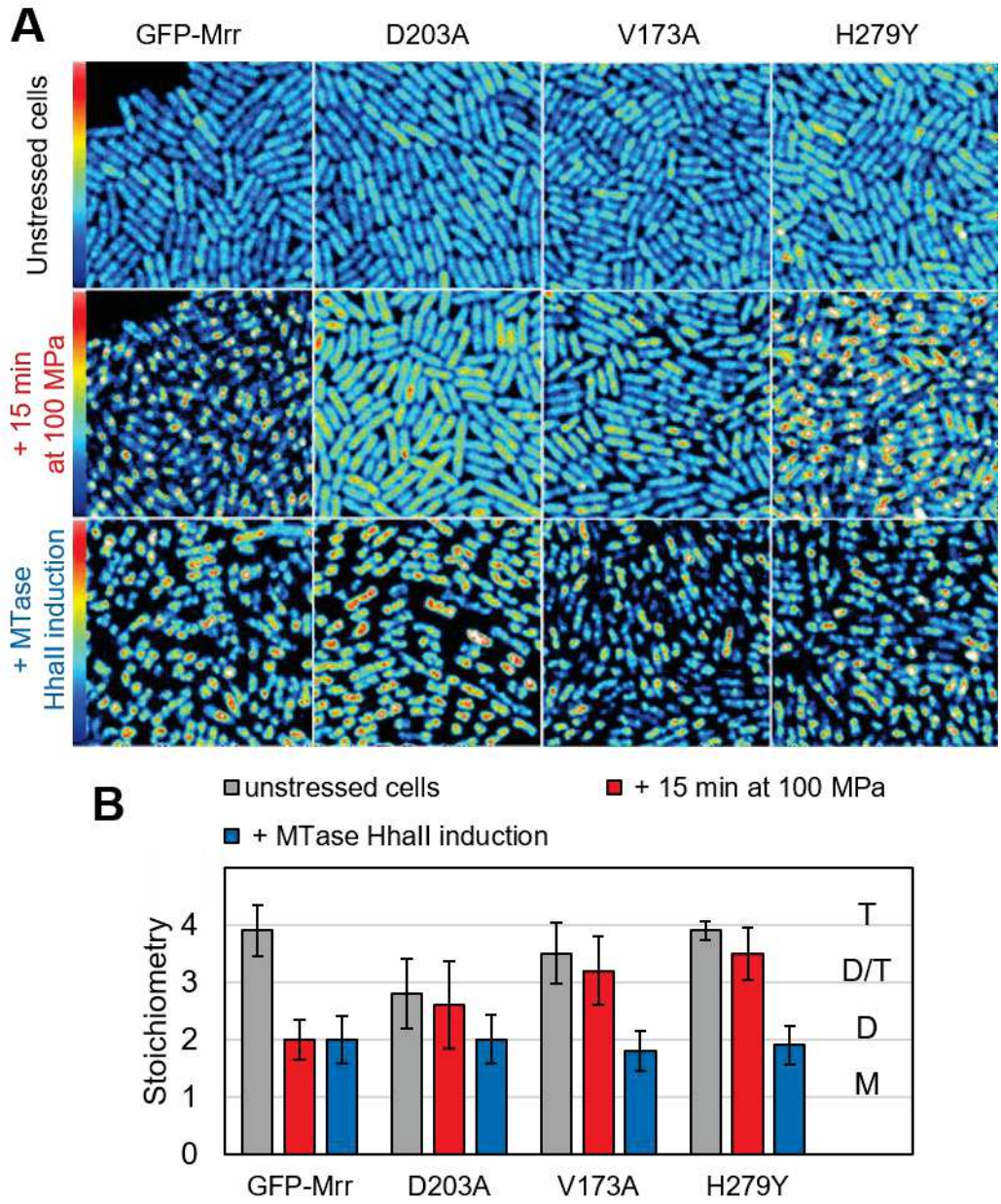

Figure 2. Effect of pressure and HhaII MTase expression on the stoichiometry of GFP-Mrr and mutants. GFP-Mrr is expressed under the control of P_{BAD} promotor with induction by arabinose in the chromosome. Fluorescence intensity maps of P_{BAD}-gfp::mrr WT (GFP-Mrr) and mutants D203A (GFP-Mrr^{D203A}), V173A (GFP-Mrr^{V173A}) and H279Y (GFP-Mrr^{H279Y}) in A) unstressed cells and after pressure treatment 15 min at 100 MPa or P_{BAD}-gfp::mrr +pTrc99A-HhaII after the induction of HhaII MTase by IPTG (20X20 µm). Maximum scale is 2.5 counts per 40 µs pixel dwell-time. B) Stoichiometry values of fluorescent proteins corresponding to GFP monomers (M), dimers (D), tetramers (T) or a possible equilibrium between dimer and tetramer (D/T) as deduced from background corrected molecular brightness of fluorescence proteins in strains P_{BAD}-gfp::mrr WT (GFP-Mrr) and mutants GFP-Mrr^{D203A} (D203A), GFP-Mrr^{V173A} (V173A) and GFP-Mrr^{H279Y} (H279Y) in unstressed cells (grey) and after pressure treatment (red) or P_{BAD}-gfp::mrr +pTrc99A-HhaII after the induction of HhaII MTase by IPTG (blue).

GFP-Mrr variants are in equilibrium between tetramers and dimers at atmospheric pressure in vitro

Two of the variants, carrying the D203A and V173A mutations, exhibited stoichiometry values that were somewhat lower than that of WT GFP-Mrr, suggesting that the affinity between dimers might be lower in the mutants than in the wild-type. Hence, we sought to investigate their oligomerization properties *in vitro*. To do so we purified StrepTag-GFP-Mrr fusion proteins for the WT and the three variants expressed in *E. coli* BL21 cells. The proteins were subjected to analytical size exclusion chromatography with fluorescence detection. Three peaks were observed for all variants of Mrr (Figure 3). The last, low molecular weight peak corresponded to free GFP and suggested that some proteolytic cleavage occurred during the production/purification procedure. The other two peaks had apparent molecular weight values consistent with the StepTag-GFP-Mrr dimeric and tetrameric forms. All four Mrr variants exhibited similar fluorescence intensities, and hence were present in these experiments in the same range of concentrations. Concentrations were very low and could not be accurately assessed by absorption measurements. Using fluorescence, by comparison with free GFP concentrations, we estimate the concentrations to be in the nanomolar range. Under these conditions, all variants appeared to be in equilibrium between tetramer and dimer. However, due to variable levels of proteolytic cleavage comparison of the affinities between the variants was not feasible.

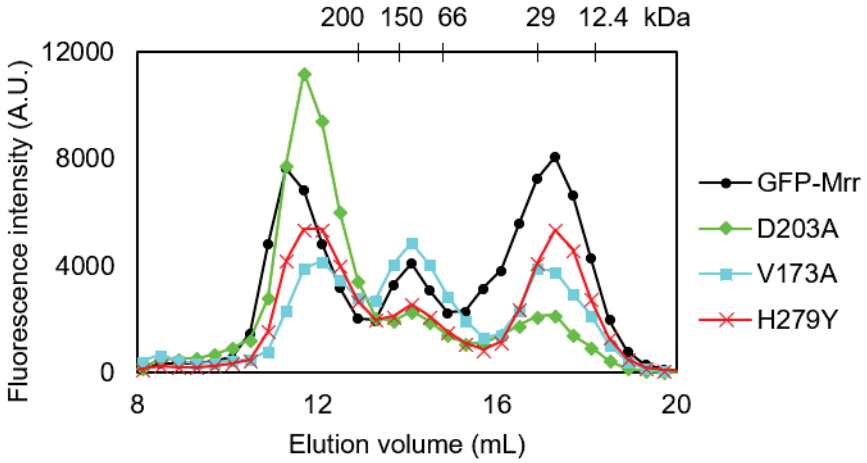

Figure 3. Size exclusion chromatography of purified StrepTag-GFP-Mrr (black circle), StrepTag-GFP-Mrr^{D203A} (green diamonds), StrepTag-GFP-Mrr^{V173A} (cyan squares) and StrepTag-GFP-Mrr^{H279Y} (red crosses). Fluorescence intensity in the elution fractions was detected with a fluorescence plate reader using 488-528 nm excitation-emission wavelength. The position of the elution peak for molecular weight markers used for the calibration of the column is shown on the upper axis.

Pressure leads to GFP-Mrr tetramer dissociation in vitro

The previous determinations of GFP-Mrr stoichiometry by sN&B *in vivo* were performed after a pressure shock and after pressure release to one bar. However, these prior results did not conclusively demonstrate that GFP-Mrr dissociates while under pressure. For example, pressure could conceivably change the conformation of the nucleoid, thereby increasing Mrr affinity and pulling the protein toward dimer, much as occurs upon methylation of DNA after MTase expression. It was thus important to demonstrate that pressure leads directly to the dissociation of Mrr tetramers. We subjected the purified WT StrepTag-GFP-Mrr using the fused silica capillary system derived from Mueller and Gratton (15), as described in the Methods section, and measured FCS profiles in 2-photon excitation mode. As a control we carried out the same experiment for purified GFP. The G(0) value of the FCS curves (corresponding to the plateau value of G(τ) at short times) is inversely proportional to the number of particles in V_{eff} and directly proportional to their brightness. Dissociation of a higher order oligomer would lead to both an increase in the number of particles and a decrease in their brightness, and hence a lower value for G(0). As expected pressure had no effect on the G(0) value obtained for free monomeric GFP (Figure 4A). In contrast, we observed a pressure dependent decrease in the G(0) value for the purified WT StrepTag-GFP-Mrr, with the largest effect observed between 85 and 100 MPa, the pressure limit of our capillary system (Figure 4B and S2). Proteolytic cleavage of the GFP in the StrepTag-GFP-Mrr leads to lower brightness values for the tetrameric form. In addition, after purification using the gel filtration column, the protein is diluted, and while the dissociation is slow on the time scale of the chromatography, the diluted sample eventually equilibrates to a lower proportion of tetramer. Both of these phenomena limit the dynamic range of the experiment. Nonetheless, these results demonstrate that Mrr dissociates under pressure.

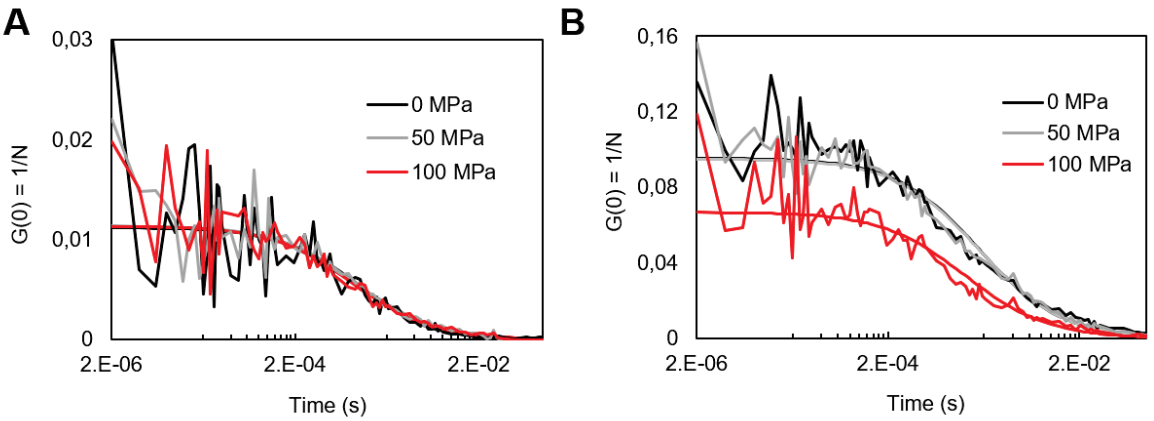

Figure 4. Pressure-induced dissociation of purified GFP-Mrr *in vitro* using high pressure FCS. Purified Strep-Tagged- A) GFP or B) GFP-Mrr samples were loaded into a thin fused silica capillary tube and hydrostatic pressure was applied up to 100 MPa. FCS measurements were acquired after 5 minutes of stabilization. G(0) corresponds to the inverse of the number of fluorescent particles diffusing in and out of the excitation volume.

Structural insights into the linkages between Mrr oligomerization and activity

To aid in the structure-function interpretation of the effects of mutation on the linkages between Mrr activity and stoichiometry, we constructed a homology model of the tetrameric Mrr catalytic domain (Figure 5) based on sequence alignment to the catalytic domain of two distantly related restriction enzymes MspJI and AspBHI. Despite, the low sequence identity (~18% over 170 residues), the overall fold and the tetrameric organization are predicted to be similar with rather well conserved monomer-monomer interfaces. The catalytic site seems also to be rather conserved and to contain several acidic amino acid residues such as D203. Interestingly, in the two templates, this aspartate and the surrounding residues (especially the glycine-rich loop 195-201) adopt two different conformations that might correspond to distinct activity states.

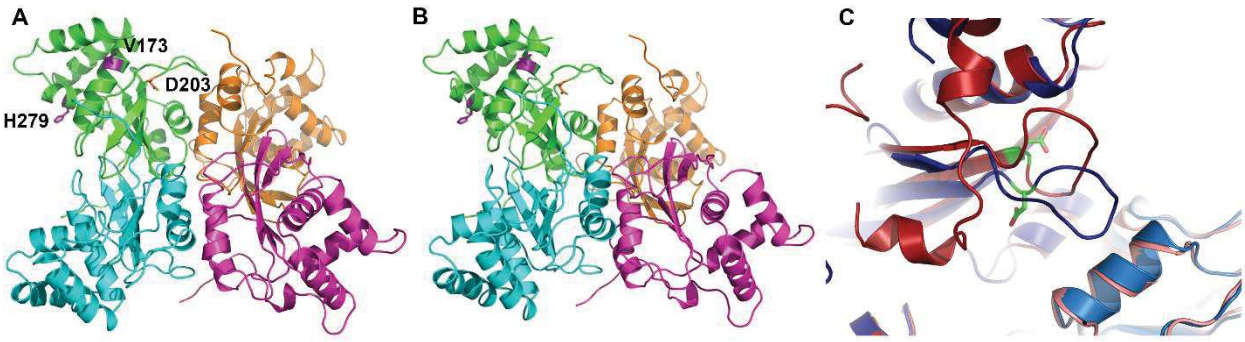

Figure 5. Structural homology models of the catalytic domain of the Mrr tetramer based on the crystal structure of A) MspJI (pdb:4foq) and B) AspBHI (pdb:4oc8). The amino acid side-chain of mutated residues are shown as stick. C) Zoom of the overlay of the catalytic loop from the two models showing the D203 sidechain in stick representation.

In this model, the catalytic loop was found to be adjacent to the interface between dimers, suggesting a direct structural linkage between tetramer dissociation and activation. Access of the active site residues to their target DNA would likely be partially or totally blocked in the tetrameric form of the enzyme. Dissociation to dimer would expose the active sites and allow for cleavage to occur. The V173A variant of Mrr was shown in previous screens to respond strongly to MTase expression but was significantly less sensitive to pressure shock. In our structural model, valine 173 is found in a helix that packs against the catalytic loop, and its mutation to alanine could destabilize this interaction. Furthermore, this helix harbors also the phenylalanine F271 and the glutamate E272 two highly conserved residues pointing into the hydrophobic core and the catalytic site, respectively. The mutation may directly affect their important role. In addition, the same helical segment is in direct contact with the C-terminal helix that wraps over valine 173 and the nearby arginine 173 that lies at the stem of the catalytic loop. The mutation could impact drastically the local network of interactions. Therefore, introduction of a cavity in the core of the protein by the V to A mutation could lead to pressure induced full or partial unfolding, such that the dimeric form populated under pressure would not be active. In *in*

vitro measurements, this variant was shown to actually favor the dimeric form of the enzyme, which should increase activity. However, if the pressure dissociated state were also unfolded, this could diminish or abrogate the pressure-induced SOS response. On the other hand, tight binding to methylated sites could stabilize the protein, leaving the MTase response intact. The viability of cells expressing Mrr^{H279Y} variant after MTase induction not strongly decreased, in contrast to a large effect of pressure shock (13). In the present work we found that Mrr^{H279Y} formed foci, as in the case of WT, after both pressure shock and MTase expression. However, unlike WT Mrr, this variant was found to be nearly tetrameric in the foci observed after pressure treatment, indicating reversibility of the pressure effect on tetramer dissociation and a more stable tetramer, despite a loss of viability in the cells. Moreover, the dimers present in the foci obtained upon MTase expression must be inactive. These observations suggest that interactions with the cryptic or methylated DNA target sites are distinct for this variant with distinct consequences for oligomerization and activity. Histidine 279 is distant (~22 Angstroms) from both the catalytic loop and the dimer/dimer interface in the tetrameric homology model, suggesting that the uncoupling of oligomerization and activity after pressure or MTase induction may involve the linkers between the DNA binding and the catalytic domains. Alternatively, it may also impact catalysis or the activation mechanism indirectly. Indeed, the histidine is harbored by a helix (273-287) in direct contact with a helix (152-164) running toward the active site. Indeed, co-evolution predicts a structural and/or functional connection between H279 with alanine A154 (Ca-Ca distance in the model ~ 11 A). Accordingly, the mutation toward a larger and more hydrophobic tyrosine may perturb the local conformation which may propagate toward the active site and induce the observed dysfunction.

Interestingly, the DNA binding domain could be also modeled despite the important divergence using various winged HTH as templates (e.g.: PDB1F5T; PMID: 10956029). These domains adopt a fold totally different from that of the DNA binding domains of the REs used to model the catalytic domain of Mrr. Meanwhile, the long and highly divergent connecting segment (residues 90-135) cannot be modeled accurately. In addition, the varying domain organization between Mrr and the distantly related RE precluded proper estimate of the co-evolution between the N- and C-terminal domains. So, the potential interactions between them cannot be established, yet.

Discussion

We observed in the present study that a constitutively active mutant of Mrr is dimeric in live *E. coli* cells in absence of any perturbation. We showed that the other Mrr variants, like WT Mrr, exist *in vitro* in equilibrium between tetramers and dimers. We also demonstrated by high pressure FCS experiments that pressure directly dissociates purified Mrr. These observations provide strong support for our previously published model for Mrr activation by pressure and MTase expression (11). In this model we proposed that pressure directly dissociates tetrameric Mrr into dimers that then bind to cryptic sites on the *E. coli* chromosome and cleave the DNA. Hence pressure *pushes* the tetramer dimer equilibrium toward the active, dimeric form. In contrast, MTase expression produces a

large number of high affinity methylated DNA sites. Since Mrr is in equilibrium between tetramers and dimers, the dimeric form, despite being not highly populated, binds to these sites and cleaves them. Since this reaction is irreversible, this eventually *pulls* all of the Mrr to the dimeric, active form. A three-dimensional structural model of the tetrameric Mrr catalytic domain provides possible structural explanations for the effects of mutations on Mrr activity and oligomerization and the linkages between them. First of all, the catalytic loop is located adjacent to the interface between Mrr dimers in the model of the tetramer, suggesting that partial occlusion of the active site in the tetramer could explain why it is inactive. Mutations that uncouple activity from oligomeric state and pressure and MTase effects can also be better interpreted in light of the structural model. Valine 173 is found in a helix that is packed against the catalytic loop. Its mutation to alanine could conceivably destabilize this region, particularly in the dimeric form which has lost the stabilizing contacts at the dimer-dimer interface. Such a destabilization would be expected to have more important consequences under pressure, where the protein is dissociated to its dimeric form yet not tightly bound to DNA, compared to MTase expression where the protein spends little time as a free dimer, and is either tetrameric or tightly bound to DNA in a dimeric form. The effects of the H279Y mutant could conceivably derive from modifications of the interactions between the DNA binding and catalytic domains by the mutation. Overall these studies validate the model for pressure and MTase effects on Mrr activity and provide an example of how proteins use oligomeric interaction surfaces for allosteric modulation of activity.

SUPPLEMENTARY DATA

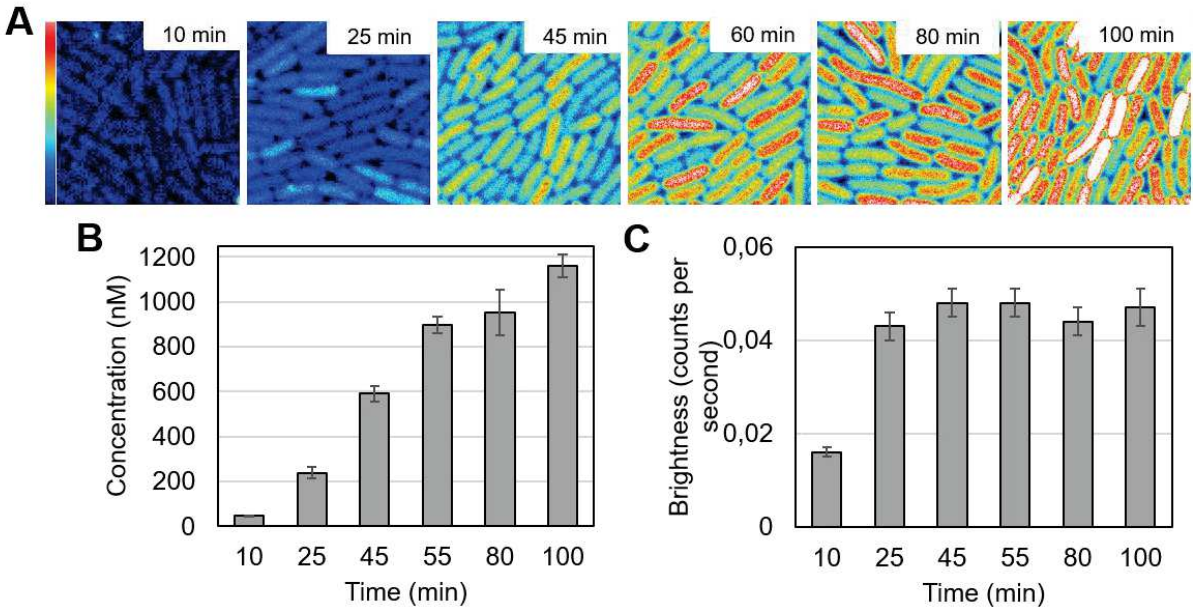

S1. Effect of protein concentration on the molecular brightness of GFP. (A) Fluorescence intensity maps of free GFP expressed under the control of the plasmid-based promotor P_{BAD}-*gfp* as a function of time after a switch from glucose to arabinose pad. Bacteria were grown in LB with 0.4% glucose, washed and immobilized on 2% agar pad supplemented with 0.4% arabinose for microscopy acquisition (scale is 13X13 µm). Maximum intensity is 2.5 counts per 40 µs pixel dwell-time. B) Concentration and C) molecular brightness values of the diffusing fluorescent molecules calculated after background correction.

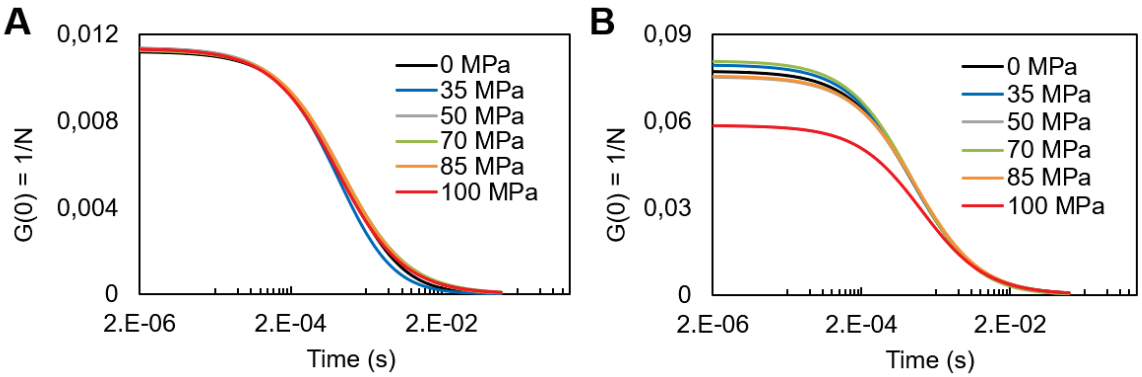

S2. FCS fits of purified Mrr-GFP in vitro under pressure. Purified Strep-Tagged- A) GFP or B) GFP-Mrr Samples were loaded into a thin fused silica capillary tube (50 µm I.D.). Hydrostatic pressure was applied from 0 to 100 MPa and FCS measurements were acquired after 5 minutes of stabilization. Fits were calculated using SimFCS. G(0) corresponds to the inverse of the number of fluorescent particles diffusing in and out of the excitation volume.

4.2 Homology model of the full-length Mrr tetramer

In order to better interpret and further understand the structural basis of Mrr activation, we constructed a homology model of full length Mrr bound to DNA. A structural model of a full length Mrr monomer in complex with a DNA fragment have already been published by our collaborators in 2008 (147)(see section 1.4.4). Since then, new structural information has been acquired on Mrr structural homologs that served as templates for improved 3D modeling using the @TOME server of the CBS (http://atome.cbs.cnrs.fr).

4.2.1 Model construction

A number of templates were detected sharing 15-25 % sequence identity with Mrr but no known structures containing both domains were found. Thus, each domain was modeled using a different template. The Mrr catalytic domain (CAT, residue 135-304) was first built as a tetramer using low sequence identity templates from two REases, MspJI (pdb:4fop), and AspBHI (pdb:4oc8) (Figure 4.2 and Figure 5 of Manuscript #2) (202–204). The organization of the dimer-dimer interaction forming a tetramer is well conserved as well as the catalytic loop rich in glycine residues. At their N-terminal part, these Type IIM REases possess an SRA motif also involved in the recognition of methylated DNA but structurally different from that of Mrr, characterized by a winged helix motif commonly found in DNA binding proteins. Another template, from the Diphteria toxine repressor (DTXR, pdb:1f5t) (205), was thus used for the modeling of the Mrr N-terminal DNA binding domain (DBD, residue 1-96). Interestingly, for the long linker connecting the two domains (residue 97-134) our predictions suggest that it contains two alpha helices (α6 and α7 in Figure 4.2) that are also present in the structure of MspJI and AspBHI. Moreover, similar to Mrr, the MspJI tetramer interacts with DNA in an inactive configuration. In the crystal structure of the MspJI/DNA complex (pdb:4r28), each dimer presents a distinct conformation, one is called the “open” conformation and the second is called the “closed” conformation. The position of the SRA domain relative to the CAT domain is very different in the open and closed configuration (Figure 4.3.A). The switch between these two conformations is accomplished by the re-positioning of the long linker region represented in red in Figure 4.3.A.

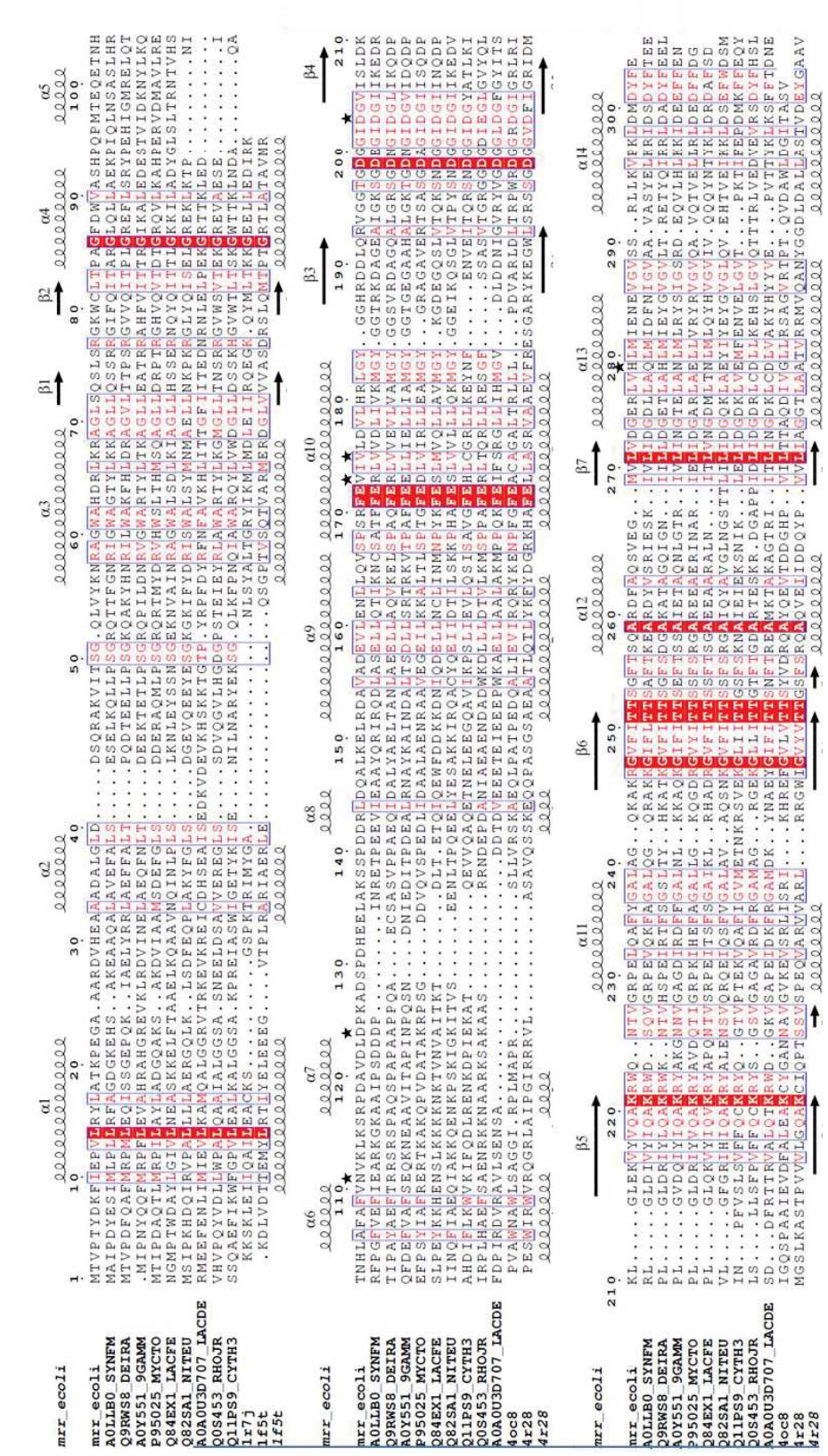

Figure 4.2: Sequence alignment of E. coli Mrr with its homologs and with sequences of the templates used for modeling. Mrr secondary structures were obtained from the homology model. In red are represented the conserved residues.

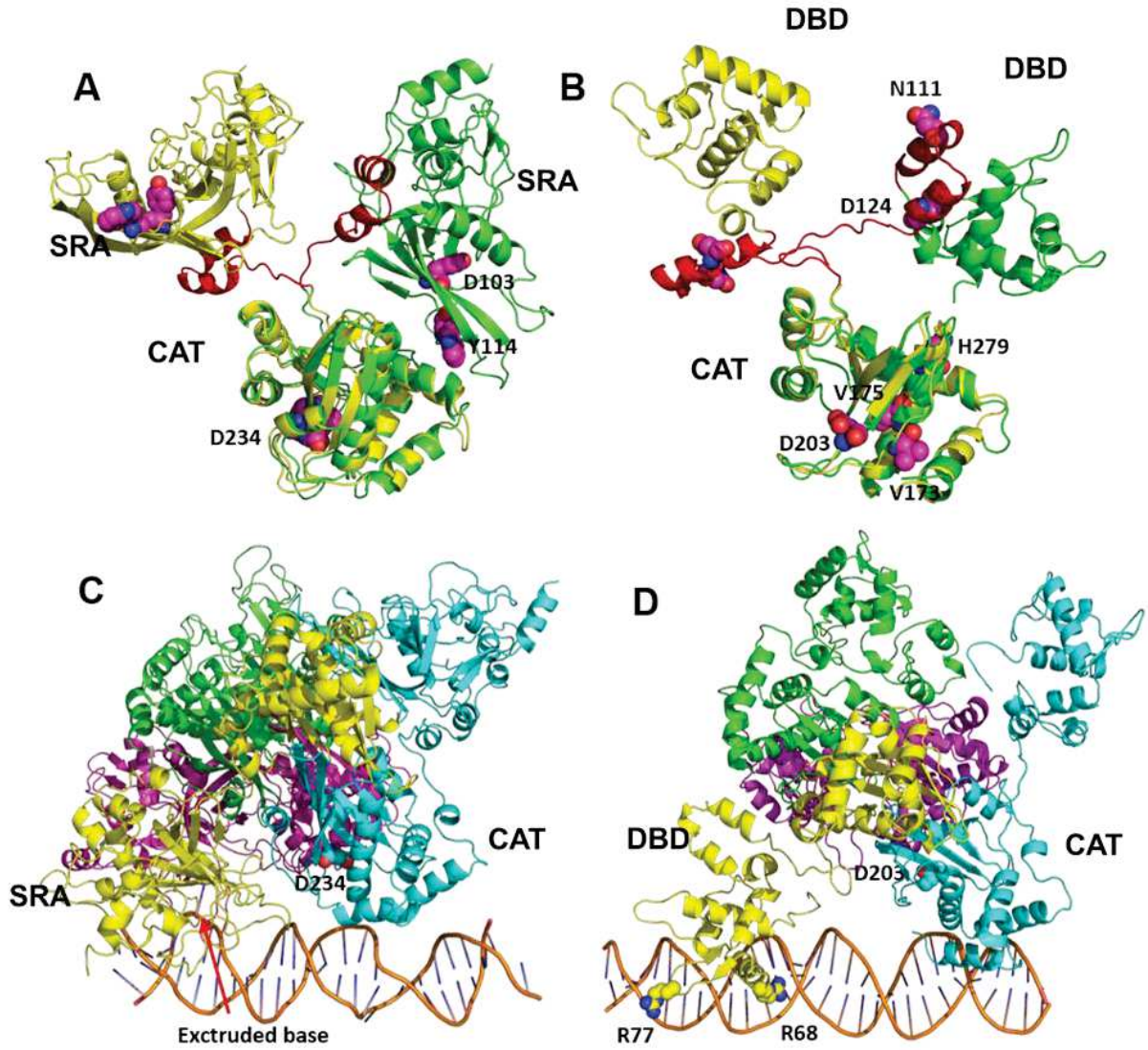

Figure 4.3: Homology model of Mrr . A) structure of the MspJI monomer and B) of the homology model of the full-length Mrr monomer in the "open" conformation (yellow) and the "closed "conformation (green). The switch between the two conformations involves the linker region (red) connecting the N-terminal DNA binding domain (SRA in MspJI, DBD in Mrr) and the C-terminal catalytic domain (CAT). For each protein, the conserved catalytic domains are superimposed. C) Structure of the MspJI tetramer bound to DNA and D) homology model of a tetrameric Mrr/DNA complex. In both figures, the "open" dimer is shown in cyan and yellow) and the "closed" dimer in green and magenta.

We retained the same two configurations of the linker for constructing the full-length Mrr monomers (Figure 4.3.B) and model an inactive tetramer bound to DNA using the MspJI/DNA complex structure (Figure 4.3.C.D). One dimer is composed of two monomers in the "closed" conformation (green and magenta) and a second dimer that interacts with the DNA is in an "open" conformation (yellow and blue). Note that the methylated cytosine

specifically recognized by the SRA domain is extruded from the DNA helix in the MspJI complex (Figure 3C). This feature is not present in the Mrr/DNA complex since the DNA fragment from the DTXR/DNA structure used for modeling is not methylated. For better visualization we have represented separately the two conformations of the dimers present in the tetrameric form of Mrr (Figure 4.3.E and F). In the closed conformation, the two DBD of the dimer are packing against the catalytic core domain. In the "open" dimer, the DBD of one monomer (yellow) interacts with the putative specific DNA recognition sequence through the winged helix motif, whereas the CAT domain of the second monomer (blue) interacts non-specifically with the DNA for cleavage. However, as in the MspJI/DNA template, the position of the DNA helix in this tetrameric form does not allow cleavage of the DNA strands, as visualized by the position of the conserved catalytic residue D203 (D234 in MspJI).

4.2.2 Structural interpretation of mutational effects

To validate our model of the Mrr tetramer bound to DNA, we have examined the predicted position of residues where mutations affecting Mrr activity have been found (Figure 4.4). Two residues located in the N-terminal winged helix motif, R68 and R77, abolish Mrr activity when mutated to alanine (Figure 4.3.D, (147)). In our model, these two residues are in direct contact with the DNA and their mutation presumably disrupts these key interactions. The D203A mutation leads to inactive Mrr, as expected for this catalytic residue located in the glycine-rich catalytic loop at the dimer-dimer interface. Similarly, the Val173 is predicted to be located in a α-helix that packs against the catalytic loop at the dimer-dimer interface, therefore the V173A mutation which reduces Mrr activity could alter hydrophobic interactions and create a cavity in this critical region. Other mutations that abolish Mrr activity have been identified in a previous work but no structural explanation could be proposed based on the monomeric model of Mrr (147).

In our model of the Mrr tetramer, the residues carrying these mutations (R181, Y184, G185 and Q192) are located in a loop region involved in monomer/monomer interaction in both conformations of the dimer. Mutations in this loop are likely to disrupt these interactions and destabilize the Mrr tetramer and dimers. Moreover, in the "closed" conformation, this loop would contact the long linker between the DBD and CAT domain which is expected to be a key region for the Mrr active-inactive conformational switch. Interestingly, a constitutive mutant of Mrr has been identified with two mutations (N111S and D124G) located in this linker that both introduce amino acid side-chains smaller than in the wild-type. These side-chain substitutions could impair interactions or create cavities at the DBD/CAT interfaces that may shift the linker conformational equilibrium towards the "open" configuration and the active dimer, resulting in constitutive activity. This constitutive Mrr mutant harbors a third mutation (V175G), which is located very close to the catalytic loop and , as the V173A mutation, is likely to reduce the stability (206) and

hence the activity of Mrr. This decreased activity may avoid the lethality of this constitutively active Mrr mutant, allowing for its isolation by genetic screening.

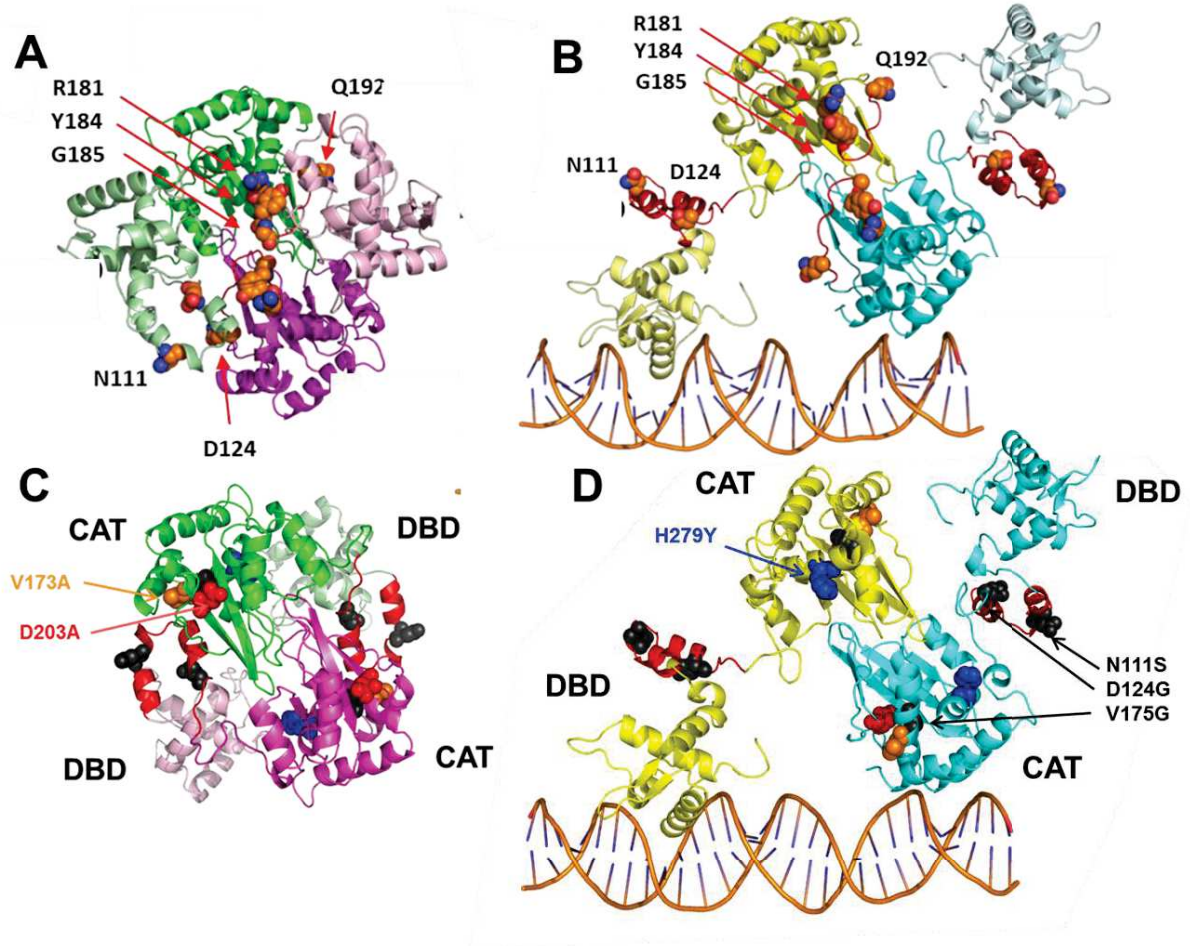

Figure 4.4: Cartoon representation of the Mrr dimer in the "closed" (A/C) and "open" (B/D) configuration, showing the CAT domains (bright colors) in similar orientation and the DBD (pale colors) either packed against the CAT domain (E) or interacting with one molecule of DNA (F) Spheres shows the amino acid side chains of residues where mutations altering Mrr activity have been identified.

Mrr harboring the H279Y mutation has been shown to respond to pressure but not to the expression of the MTase. Residue H279 is located distant from the catalytic loop and the dimer/dimer interface, but according to our model it appears to interact with the linker in the "closed" conformation (Figure 4.4). Replacement of the histidine side chain by a large aromatic tyrosine side chain could stabilize this conformation and thereby the tetrameric form due to the increase of hydrophobic or stacking interactions. Pressure may still be able to dissociate the tetramers into dimers allowing cleavage, but when the pressure is released all the dimers re-associate into tetramers that can bind to the DNA. However, the SOS response is not induced by MTase even though a small decrease in viability has been observed. Thus, the proteins in the foci must be inactive. The fluorescence images reveal the presence of foci as in the WT strain while Ghosh et al. observed a cloud-like distribution (Figure 4.1). An explanation could be the different concentration of the protein and in

particular the ratio between the number of tetramers and the number of methylated sites. In the strains used by Ghosh et al., Mrr and the mutants were strongly over-expressed from a multi-copy plasmid. High concentration of Mrr would favor the tetrameric and inactive form of the enzyme and the high number of methylated DNA site created upon induction of the MTase would not be sufficient to "tear" apart the large number of tetramers. In contrast, in our experiments or when expressed from its natural promoter at its natural locus when there are only a few copies of Mrr, the dissociation of the tetramers into dimers bound to DNA is favored because of the large number of available sites. This could explain why we observed foci after M.HhaII induction in our experiments, whereas they were rather attenuated in the experiments reported by Ghosh et al. (143).

4.3 Putative active form of the Mrr dimer

As described in the article, the catalytic loop adopts two different conformations that could correspond to two distinct activity states. Because this loop is found near the interface between the dimer and the linker, we have suggested a structural link that couples the dissociation of tetramers and the activation of Mrr. The catalytic site is hidden in the inactive tetrameric form. Tetramer dissociation to dimer would expose the active site to target DNA sites for cleavage. Although we do not know the conformation of the dimers, the dissociation of the tetramers either by pressure or by binding to high affinity sites upon induction of M.HhaII could trigger a rearrangement of the catalytic domain allowing the correct positioning and cleavage of the DNA. Once the pressure is released, these dimers remain bound to the DNA, while the non-associated dimers can re-associate to inactive tetramers. In case of M.HhaII induction, hypermethylation of the DNA by the methylase creates many high affinity sites that might favor the DNA-bound dimeric form compared to the tetrameric form because the affinity of the dimer for methylated DNA would be higher than the affinity between dimers.

In our model of the Mrr tetramer bound to DNA, the DNA helix is positioned too far from the active site and cleavage cannot occur (Figure 4.5.B). The dissociation of Mrr into dimers can allow a reconfiguration of the dimers that would expose the active sites that are buried in the inactive, tetrameric form of the enzyme. Given the impact of a few mutations in or near the linker, we suggest a "closed" to "open" conformational change. Based on the structure of Mrr and MspJI homologues containing the conserved (D/E)..DEQXK, the active site capable of cleaving the DNA in the dimeric configuration is likely to be located near what we at first assumed to be the weaker interface between dimers (Figure 4.5.B). The scissors shown in the figure indicate where the DNA must be positioned to be cleaved by the enzyme. In this figure, the active dimer would be formed by the two monomers colored yellow and green (or magenta and cyan) that interact through helices, whereas the other dimer interface involves β sheets. Given the structural backbone-based constraints of β sheet orientation, they generally exhibit significant packing defects which would render the interface more pressure sensitive. In fact, the search for internal cavities using POCASA

(207) indicates the presence of void volumes in the vicinity of the active site loop, as well as at the interface between the dimers which would participate in the "open" conformation (cyan and yellow on Figure 4.5.B). Hence, pressure may dissociate the tetramer specifically to active dimers. The V173A and V175A mutations could enlarge the cavity already present near the catalytic site and destabilize this region under pressure and thus inactivate the enzyme.

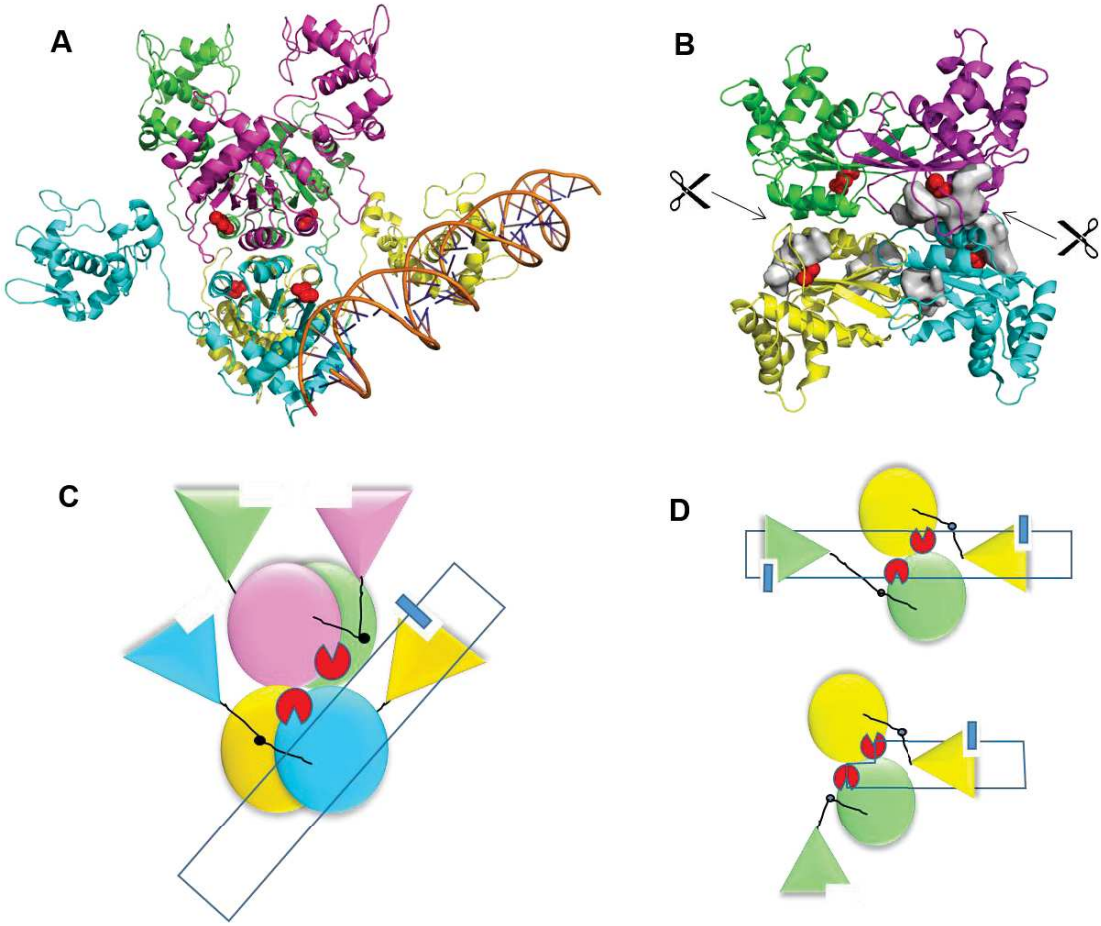

Figure 4.5: Possible model of the oligomeric switch leading to Mrr activation. Structural model of tetrameric full-length Mrr bound to DNA (A) or the catalytic domains showing internal cavities at the dimer-dimer interface where DNA cleavage is predicted to take place. The catalytic D203 residue is shown with red spheres. C) Schematic representation of the inactive Mrr tetramer bound to DNA and D) of the active dimer capable of DNA cleavage. The N-terminal DNA recognition domains are represented as triangles and the C-terminal catalytic domains as spheres. In the Mrr tetramer, the dimer in the open configuration (yellow and cyan monomers) can interact with DNA at a methylated recognition site (blue rectangle) but the DNA is not properly orientated for cleavage at the dimer-dimer interface or binding of a second DNA recognition domain. High pressure or the presence of numerous methylated recognition sites would disrupt dimer-dimer interactions, allowing reorientation of the DNA and formation of a

complex where each catalytic site (in red) is in position to cut one strand of the DNA. After cleavage, the Mrr dimer would stay bound to one end of the restricted DNA fragment.

A different view of the tetrameric model of Mrr associated with DNA is shown (Figure 4.5.A) in order to schematize the tetrameric form binding DNA (Figure 4.5.C). The yellow and cyan monomers are in "open" conformation interacting with the DNA and the green and magenta are in a "closed" conformation. Using the representation of the active MspJI dimers proposed in (208), we made a schematic of what might be the active dimer form of Mrr. Two monomers are bound back to back to the DNA and each of the monomers can cleave one strand of the DNA. Their conformations do not correspond to an "open" and "closed" conformation. When cleavage occurs, one of the monomers stays bound to the DNA with the second monomer attached thereto (Figure 4.5.D). Reconfiguration of the binding domain which does not bind to the DNA does not allow the formation of tetramers with the exception H279Y mutant after pressure treatment. Thus, H279Y mutation could interact with the linker and allow the association of a dimer.

5. Experiments under pressure

All experiments presented above were carried out by exposing the bacterial cells to high pressure for a define time, and imaging them after the release of pressure. To study what happens to Mrr during the pressure treatment, we implemented our microscope with a system allowing FCS and N&B experiments inside a glass capillary. It was developed and tested *in vitro* by Muller and Gratton (200) but we were able to obtain images of living bacteria immobilized inside a square capillary at 100 MPa.

5.1 Characterization of capillaries

We tested the performance of our set-up for quantitative 2-photon microscopy. We first tested the effect of using round capillaries instead of flat coverslips for fluorescence fluctuation measurement. A reference solution of fluorescein at 18 nM was loaded in the capillary and the system was closed with the valve. Then, FCCS curves were recorded at different z position to determine the amplitude of the signal, G(0), inversely proportional to the number of molecules (Figure 5.1). The z position when the objective was moved up to the sample was adjusted for the best focus, which is the position of the maximum intensity, arbitrarily set as z=0. Results were compared with the same solution of fluorescein deposited on a regular coverslip (150µm thickness) (Figure 5.2).

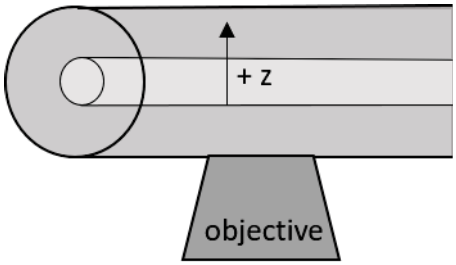

Figure 5.1: Representation of the fused silica capillary. Position z = 0 is the maximum intensity (bottom of the capillary). Thus, the arrow direction corresponds to positive values.

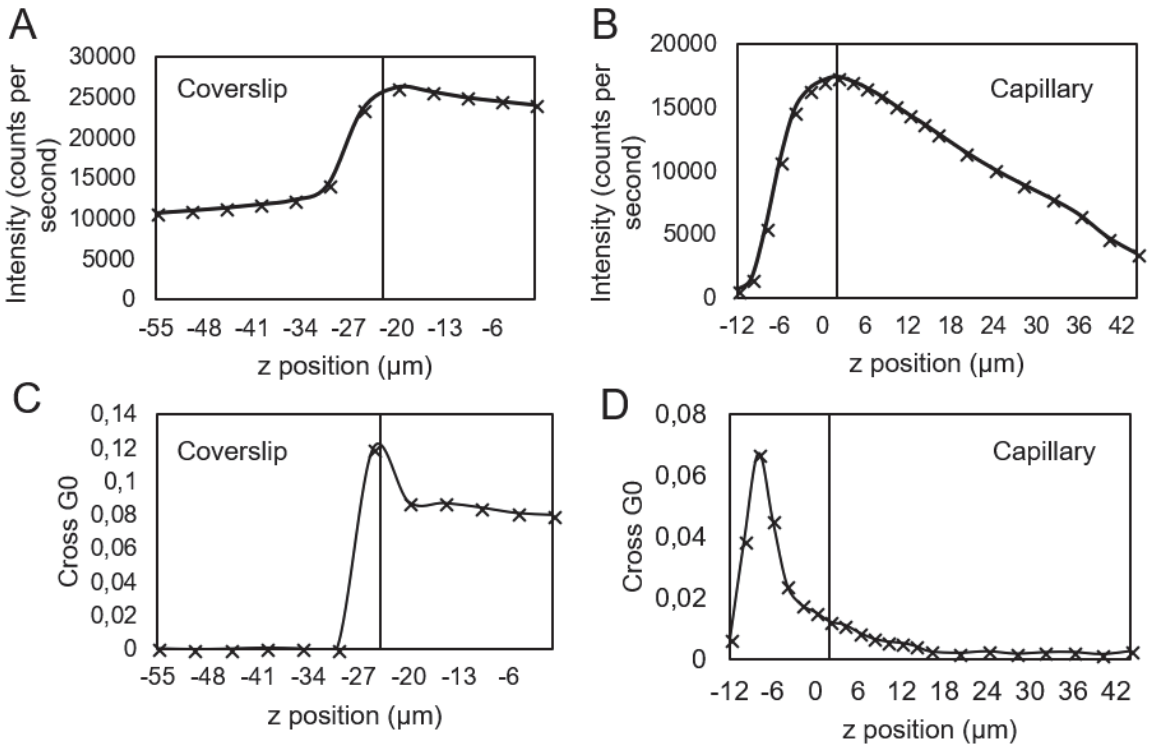

Figure 5.2: Characterization of a circular fused silica capillary. A solution of fluorescein at a concentration of 18 nM was used to compared the intensity (A and B) and the cross G(0) (C and D) versus the z position. Measurements were done on a coverslip N°1.5 or into a capillary.

Under the same imaging conditions, the intensity of the fluorescein solution was found to be around 30 % lower in the capillary compared to that measured on the coverslip. The intensity increased quickly with increasing z, then it decreases gradually. The maximum of fluctuation (higher cross G(0)) is reached when the intensity is about the half of its maximum. This z position will be used for future measurements. In contrast, the cross G(0) value for the fluorescein solution on the coverslip is the highest at maximal intensity. The G(0) retrieved for the fluorescein solution in the capillary is about 25 % lower than that on the coverslip. In conclusion, performance of the capillary is slightly lower compared to the measurements done on a coverslip.

We also tested the effect of pressure on fluorescence fluctuation measurements. Increasing pressure was applied to the fluorescein solution and acquisition was done after 5 min of equilibration at each point. Cross G(0) and diffusion coefficient did not change upon increasing pressure, similar to what was observed for purified GFP (Figure 5.4). The molecular brightness of purified GFP was calculated by sN&B and it did not change neither under pressure (0.029 at 0 MPa and 0.028 at 100 MPa) but it is twice lower than the one on the coverslip (0.064). The main problem of the round capillaries is the curved surface that changes the PSF of the incoming light. That is why we used glycerol as a coupling media with a refraction index similar to the one of the quartz. Nevertheless, the inner surface has

a different refraction of the aqueous media used for samples. This problem explains the z position dependence of the capillary (200).

To improve the optical quality of the setup and obtain higher G(0) values, we tested a square capillary with an inner diameter of 50 µm and an outer diameter if 360 µm (Figure 5.3.A). Due to its shape, the capillary is less solid than the circular one. According to the supplier (Polymicro Technologies), the square capillary with an external polyimide coating can sustain pressure in our range of observation (up to 1 kbar). This coating is removed by burning the the capillary with a flame for a few second on a small area for the observation (Figure 5.3.B). The capillary is cleaned with a lens paper and methanol.

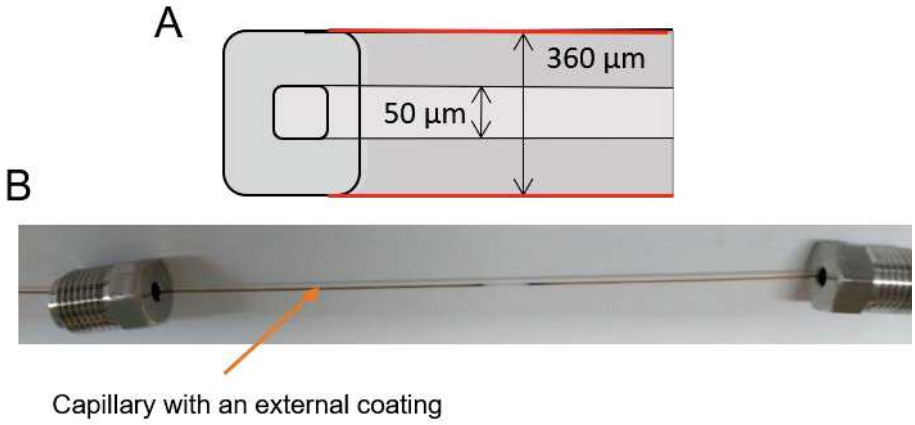

Figure 5.3: Representation of the square capillary. A) Schematic and B) Picture of the capillary with an external polyimide coating.

The same controls as for the round shape capillary were done with the fluorescein solution in the square capillary. Such a system has been recently used by others (209). Although the fluorescence intensity of the fluorescein decreases in the capillary, the maximum G(0) obtained is higher than that obtained on a coverslip (0.059 vs 0.046). In contrast, the maximum G(0) in the circular capillary was lower than the one on a coverslip. Thus, the square capillary improves the signal and reduces distortion problems compared to the circular capillary.

5.2 Behavior of purified proteins upon increasing pressure

Prior to testing the square capillary, we used the round one to test the effects of pressure on purified wild-type GFP-Mrr *in vitro*. We demonstrated that purified WT GFP-Mrr tetramer dissociates under high pressure. FCS curves are presented and explained in details in the second paper. Below are shown diagrams of the corresponding G(0) values for StrepTag-GFP and StrepTag-GFP-Mrr at increasing pressures (Figure 5.4).

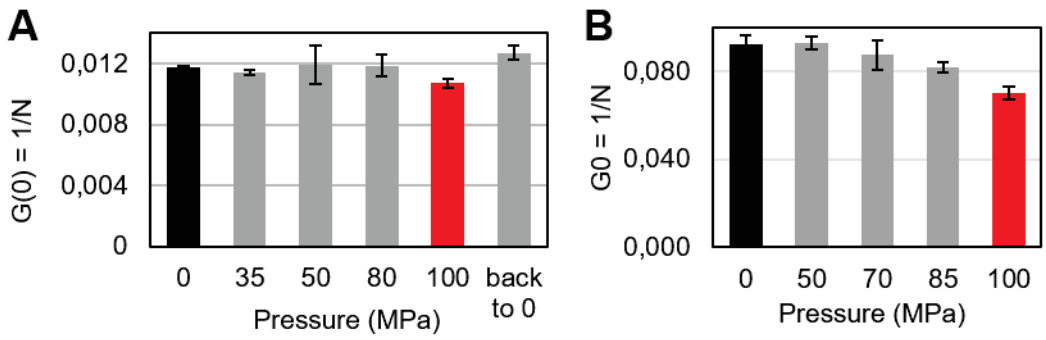

Figure 5.4: In vitro effects of pressure on purified GFP and GFP-Mrr. FCS data were fitted and G(0) values are reported upon increasing pressure of purified A) StrepTag-GFP and B) StrepTag-GFP-Mrr.

The G(0) value for free GFP is independent of pressure, demonstrating as expected that neither brightness, nor number of this monomeric protein is pressure dependent. In contrast, the G(0) value of Mrr-GFP decreases with pressure, consistent with a decrease in brightness and an increase in particle number correlated with tetramer dissociation. The dissociation is clearly incomplete by 100 MPa, the limit of the pump in this case. Oligomer dissociation is protein concentration dependent, and hence the pressure range for the observed dissociation depends on the concentration of the protein.

5.3 Number and Brightness under pressure

5.3.1 Pressure effects on free GFP in live *E. coli* cells

Recently, we were able to immobilize live *E. coli* K12 cells expressing free GFP and a fusion of GFP-Mrr in a square capillary to carry out sN&B at atmospheric and high pressure. To achieve immobilization, the capillary was coated with a solution of concanavaline A at 0.2 mg/ml for a few hours and rinsed with water. Cells were grown in LB medium as described in section 2.2.2. for the *in vivo* experiments observing Mrr-GFP before and after exposure to high pressure. After centrifugation, the bacteria were resuspended at a high OD_{600} (around 25) and loaded into the capillary using the peristaltic pump. We let them settle for 15 min. A very slow flow rate was used to wash out the bacterial cells that did not adhere to the surface. Once, the valve is closed and the high-pressure pump connected, we used brightfield illumination to find an area with enough bacteria for imaging (density is low). Scanning N&B acquisitions were then performed on these areas containing immobilized cells as a function of pressure. Similar to *in vitro* high-pressure experiments, we waited 5-10 min after a pressure shift (Figure 5.5).

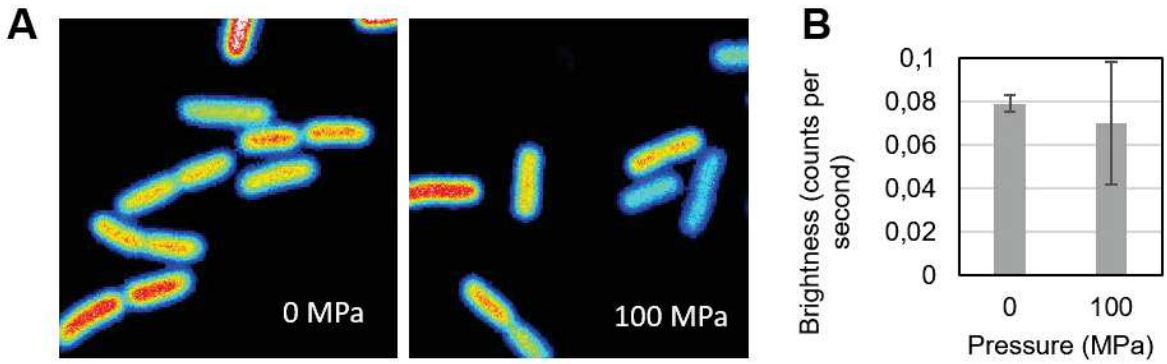

Figure 5.5: In vivo free GFP behavior under pressure. GFP is expressed in E. coli cells under the control of the PBAD promotor (induced by arabinose) in a low copy plasmid. A) Fluorescence intensity maps at ambient and 100 MPa (13x13 µm). Minimum scale is 0.6 counts per 40 µs dwell time. B) Molecular brightness values retrieved from sN&B analysis inside cells at 0 and 100 MPa.

The brightness of the GFP expressed under the control of the P_{BAD} promotor from a plasmid was not significantly different at 100 MPa as compared to ambient pressure. This is consistent with a lack of pressure effect on monomeric GFP brightness G(0) *in vitro*. In addition, the brightness value observed for the monomeric GFP was similar to that obtained on an agarose pad. The bacterial cells, which are not expressing Mrr, do not appear to present any obvious phenotype after 15 minutes pressure shock at 1 kbar.

5.3.2 Pressure effects on GFP-Mrr in live *E. coli* cells

Similar high pressure sN&B experiments were carried out in the square capillary using the MG1655 strain expressing GFP-Mrr from the natural locus under the control of the P_{BAD} promoter as used in our prior experiments. We observed that the molecular brightness of GFP-Mrr in living cells decreases by nearly a factor of 2 at 100 MPa (Figure 5.6).

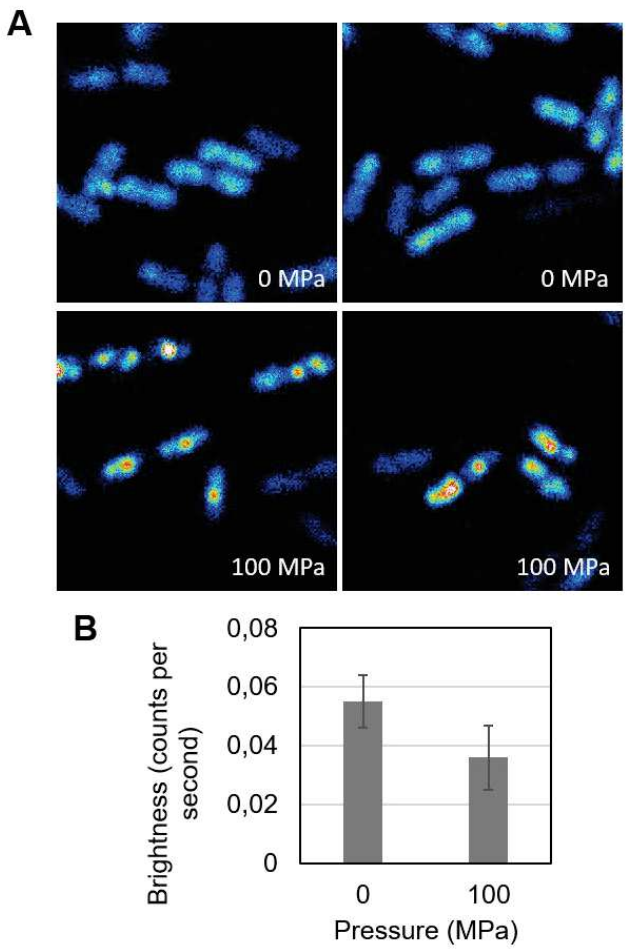

Figure 5.*6: In vivo Mrr behavior under pressure. GFP-Mrr is expressed under the control of the PBAD promotor with induction by arabinose in the chromosome. A) Fluorescence intensity maps of PBAD-gfp::mrr at 0 and 100 MPa (13x13 µm). Minimum scale is 0.2 counts per 40 µs dwell time. B) Molecular brightness values of PBAD-gfp::mrr at 0 and 100 MPa.*

The brightness is relatively low due to a low intensity and thus a contamination of the signal by autofluorescence. To date we have not yet acquired data on the MG1655 background strain under similar conditions. Such data would be required to carry out accurate background subtraction calculations. Nevertheless, these results are consistent with a dissociation of Mrr tetramers into dimers at high pressure. They strongly support the results in part 3 showing that GFP-Mrr was tetrameric before application of pressure and dimeric after the pressure shock and return to atmospheric pressure. This indicates that indeed the tetramer-dimer switch is the result of direct dissociation of Mrr by pressure. In addition, we observed the presence of foci like those we observed on agarose pads after the release of pressure, appeared in the middle of the cells at high pressure. We have presented here preliminary results on sN&B under pressure that we believe are the first high-resolution microscopy images of live cells under pressure. These preliminary experiments demonstrate the proof of principle for high pressure, high resolution live cell imaging. A manuscript describing these results is in preparation.

6. Conclusion

Pressure is an important environmental factor (oceans cover 70 % of the Earth) to which bacteria must adapt. Although *E. coli* is not subjected to pressure variation in its natural environment, pressure is used to kill food pathogens by pascalization. In this context, it has been shown that *E. coli* is able to rapidly acquire a resistance to pressure. *E. coli* was able to grow at a higher pressure than usual and even survive pressure shock up to 2 GPa by direct evolution, which may compromise the efficiency of pascalization treatments. Some *E. coli* strains induce an SOS response after a pressure shock of 15 min at 100 MPa. This system bypasses the conventional DNA repair system when there is too much DNA damage. Through homologous recombination, cells can mutate and acquire resistance to different stresses in order to adapt to harsh environments. The HP-dependent SOS response is induced due to double stranded DNA breaks created directly by a Type IV restriction endonuclease, Mrr. The mechanisms by which Mrr is activated by pressure have remained unknown. Earlier, Mrr was also identified as inducing such a response after induction of a foreign methyltransferase to *E. coli*, HhaII. Using techniques that rely on fluctuations of fluorescence intensity, we have been able to determine the oligomerization state of Mrr WT and its mutants in living *E. coli* cells before and after HP or M.HhaII induction. Our results reveal the importance of the coupling between the state of oligomerization of enzymes such as Mrr, and their function.

The activation of Mrr by pressure or by M.HhaII occurs via two distinct pathways. We found that pressure *pushes* the tetramer/dimer equilibrium of Mrr to the active dimeric form of Mrr. This active dimeric form is able to bind to and cleave the methylated cryptic sites of *E. coli* DNA. In contrast the methylation of the DNA by the foreign methyltransferase, M.HhaII, *pulls* the equilibrium to the DNA-bound dimeric form due to the creation of many methylated, high affinity sites recognized by the small amount of dimeric Mrr present at equilibrium (Figure 6.1). These sites act as a thermodynamic sink, pulling the tetramer to active dimers. Once bound to DNA, cleavage by Mrr occurs at a distance from the recognition site, which is typical of Type IV REase. Without this characterization of Mrr stoichiometry *in vivo* using N&B analyses, we would never have suspected this coupling between oligomerization and activity. Moreover, we would not have been able to provide an explanation for the intriguing effects of point mutations on the pressure and MTase responses of Mrr using the homology model based on the structure of another highly homologous Type IV RE, MspJI.

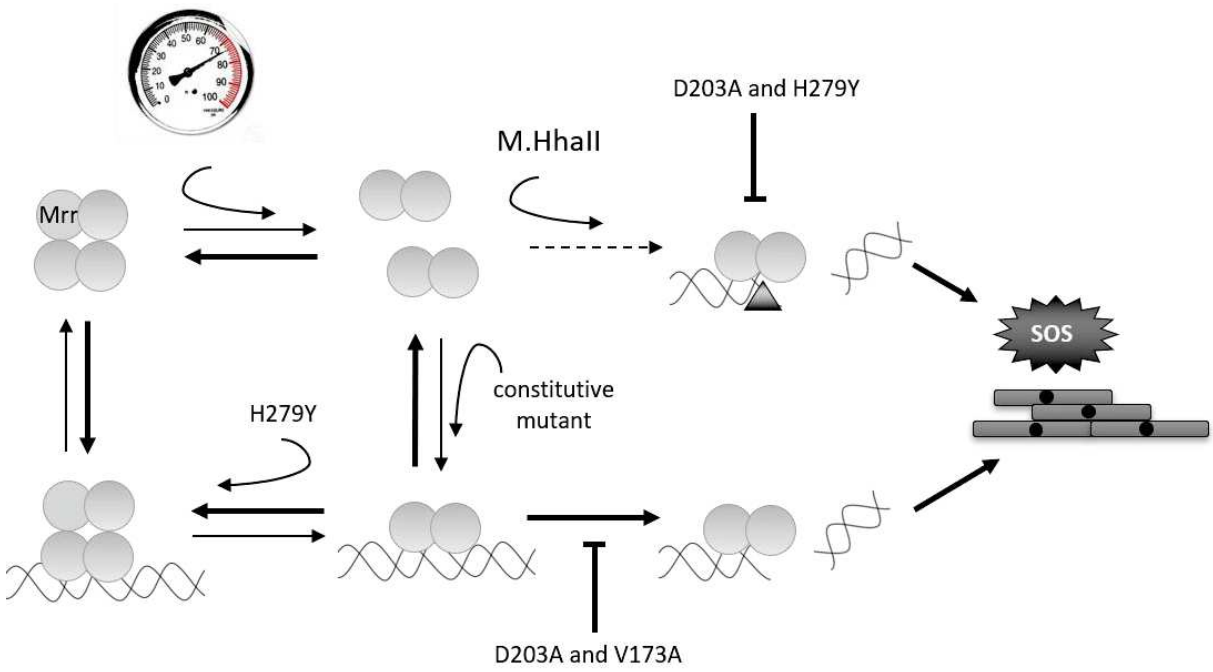

Figure 6.1: Proposed model for Mrr activation and induction of the SOS response by pressure or induction of M.HhaII.

Although most of the experiments were performed after the release of pressure, our preliminary *in vitro* and *in vivo* results under pressure appear to confirm pressure-induced dissociation of inactive Mrr tetramers to dimers. The dimers are then able to bind the cryptic site and cleave the DNA leading to the formation of foci at 100 MPa. Based on this model, we suggest that Mrr can adopt two conformations (Figure 6.2). The tetramer cannot cleave DNA because the active site is buried in the folded tetramer. To cut both DNA strands at the same time, two monomers must form an active dimer that can bind methylated DNA sites and cleave the double strand thanks to tetramer dissociation coupled with a conformational rearrangement that exposes the active sites.

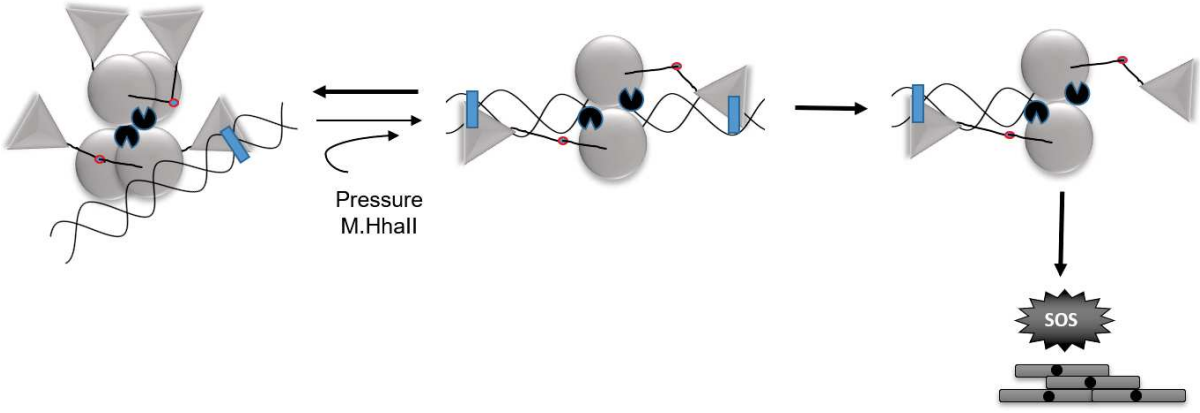

Figure 6.2: Schematic of Mrr structures from an inactive tetramer to an active dimer.

It is likely that Mrr dissociation by pressure constitutes the major basis for the pressure-induced SOS response. However, we cannot eliminate the possibility that pressure acts on the conformation of DNA as well making cryptic sites more available for recognition and cleavage of Mrr. The effects of pressure on methylated DNA have not been extensively studied. A publication from 1989 demonstrated local stabilization of the double helix due to methylation of cysteine (212). However, the known compaction of the double helix under pressure could favor the extrusion of the methylated base allowing specific recognition by Mrr dimer. In fact, we do not have information on the sequence and structural determinants of the Mrr binding site. Base extrusion of the m5C methylated base is observed in the structure MspJI-DNA complex as well as in other DNA modifying enzymes containing SRA binding domain (210, 211). However, there is no evidence that this could be also the case upon binding of Mrr to its methylated DNA target sites. It can also be hypothesize that the methylation of a large number of sites could favor base extrusion and thereby facilitate Mrr binding and cleavage. Note that the methylation of DNA by M.HhaII in the absence of Mrr does not affect the growth rate at atmospheric pressure. In future work, it would be interesting to perform HP NMR experiments of unmethylated and methylated DNA to determine the impact of the methylations on the structure of the DNA helix at high pressure. Such experiments could be performed with the specific recognition sequence of MspJI (methylated and unmethylated). Furthermore, it would be of interest to determine whether HP is also able to activate this homologous enzyme via dissociation of MspJI tetramers, possibly coupled to extrusion of the methylated bases. A final perspective for future work would be to obtain super resolution images of the Mrr foci formed under HP and after expression of the MTase. This would provide insight into the number and orientation of Mrr cleavage sites.

7. Annex

7.1 Abbreviations

3D = 3 dimensional
APD = Avalanche Photo Diode
ATP =adenosine trisphosphate
bp = base pair
BSA = Bovine Serum Albumin
D = Dimer
Da= Dalton
DNA = Deoxyribose Nucleic Acid
DSB= Double-strand DNA Break
dsDNA= double-strand DNA
FCS = Fluorescence Correlation Spectroscopy
FCCS = Fluorescence cross correlation Spectroscopy
FAD = Flavin Adenine Dinucleotide
FOV = Field of View
FP = Fluorescent Protein
GFP = Green Fluorescent Protein
HHP = HP = High Hydrostatic Pressure
HPT =High Pressure Temperature
IPTG = isopropyl β-D-thio-galactopyranoside
IR = Infra-Red
LB = Lysogeny Broth
M = Monomer
MD = Modification Dependent
MPa = MegaPascal
MTase = methyltransferase
NA = Numerical Aperture
NADH = reduced Nicotinamide Adenine Dinucleotide
N&B = Number and Brightness
OD = Optical Density
ON = Over-Night
PSF = Point Spread Function
PSI = Pound per Square Inch
REase = restriction endonuclease
RM = Restriction Modification system
RNA = ribonucleic acid
SDS= sodium dodecyl sulfate
SRA =Ring Finger Associated
SSB = single stranded DNA binding
ssDNA = single-stranded DNA
T = Tetramer
T_m= melting temperature
TMAO = trimethylamine-N-oxide

UV = Ultra-Violet
wH = winged Helix
WT = Wild Type
Microscopy techniques:
DLS = Diffusion Light Scattering
FCCS = Fluorescence Cross Correlation Spectroscopy
FCS = Fluorescence Correlation Spectroscopy
FRET = Föster Resonance Energy Transfer
ICS = Image Correlation Spectroscopy
PCH = Photon Counting Histogram
RICS = Raster Image Correlation Scanning
sN&B =scanning Number and Brightness
TIRF = Total Internal Reflection Fluorescence

7.2 Protocol for microscopy

All chemicals are from AMRESCO.

Coverslips N°1 (VWR)

Plates (Greiner)

Pressure equipment (BioSciences)

Glycerol stock:

- Re-isolate the strains from a plate or previous glycerol stock on LB-agar with appropriate antibiotics. Grow at 37°C ON.
- Inoculate 2 mL of LB medium antibiotics.
- When the culture is well grown (6-8 hours), add 1 mL of sterile glycerol 50% and mix well. *Use sterile filtered tips to avoid any risk of contamination.*
- Make 2-3 aliquots of 1 mL and store at -80°C.

Overnight pre-cultures:

- Fill a sterile culture tube with 2 mL of LB supplemented with the appropriate antibiotics.
- Inoculate from glycerol stock. Grow at 37°C.

Culture (24 (or 6) wells plate):

- Fill a 24 (or 6) wells plate with 1.5 mL (or 4 mL) of LB.
- Inoculate a well with 15 µL (or 30 µL) of ON culture.
- Incubate at 37°C and 200 rpm in a plastic box with a wet tissue into the bottom and a lid (with some holes for aeration).
- After 30 min, induce if necessary, with 35 µL (or 80 µL) of arabinose 20%.
- Remove 200 µL from each cultures and place into a Grener flat bottom 96 well plate and measure the OD and Fluorescence with the TECAN plate reader.
- If necessary, induce HhaII MTase expression with 0.5 mM IPTG when the OD≈0.15 for 1h. Centrifuge 1 mL for 3 min at 3000 rpm, pour off supernatant and recentrifuge briefly. *Skip the next step.*
- Select a late exponentially growing culture (OD_{600} around 0.6). Centrifuge 1 mL for 3 min at 3000 rpm, pour off supernatant and recentrifuge briefly.
- Aspire supernatant and resuspend the cell pellet in LB to a final OD of 25. Leave the aliquot on ice until use. *Do not wait more than 1 hour on ice before use.*

Note: arabinose concentrations are different for plasmidic expressions of GFP-Mrr or free GFP. Induction is done when cells reach an $OD_{600} \approx 0.4$ with 0.002% arabinose for 20-30 min only. Expression levels can vary a lot, which is why an alternative protocol for pad induction is proposed.

Preparation of agarose pads:

- Take an aliquot of 2% agarose and heat until melted in a dry bath at 95°C. Mix well before use.
- Take a round cover slip and place 65µl of the hot molten agarose in the center of the well so it forms a dome.
- Dry the agarose pad in the laminar hood for 20 min. *Less time and the pad will be wet and result in low density cells. More time and the pad will shrink below the level of the silicone resulting in multiple layers of cells.*
- Keep pads in a Petri dish with a cover. *Pads can be store just a few hours (3-4h in the microscopy room).*
- Place the ring around the agar place. It should be slightly higher than the silicone ring *Rings can be reused (4-5 times) as long as they keep sticking the cover slips.*
- Add 2 µl of bacterial suspension at a high density. Wait around 3-5 min (you should see a grainy surface and a gray ring).
- Place a poly-Lysine treated cover slip and press down gently in a circular motion (using a pipette with no tip for instance) until the pad breaks so that the cover slip sticks on the silicon rings.

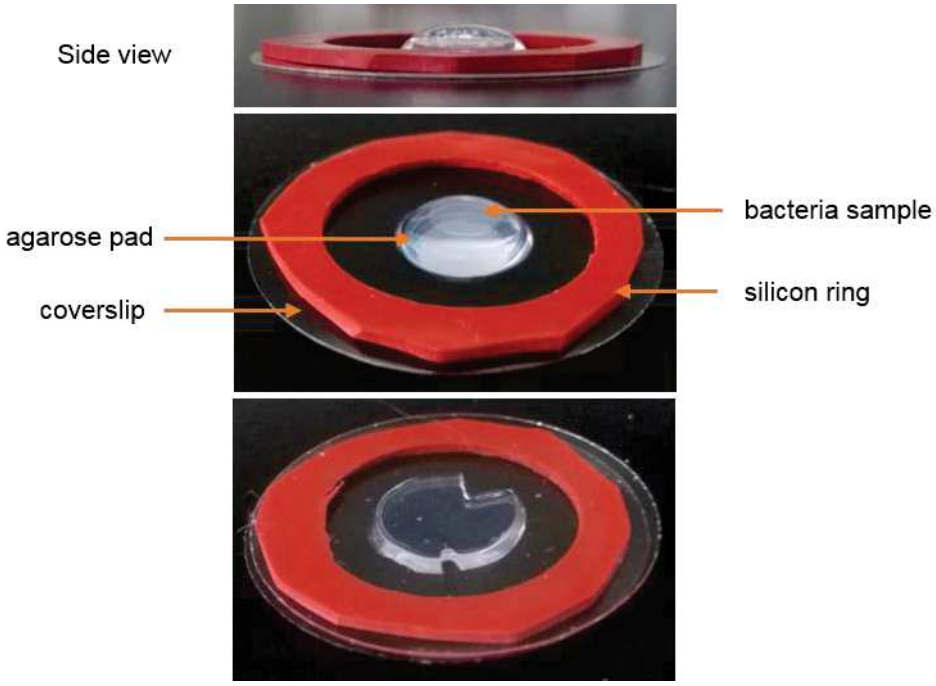

Pictures of 2% agarose pad. Cells are deposed on the agarose and squeezed between two glass cover slips.

High pressure treatment:

- Select a late exponentially growing culture (OD_{600} around 0.6). Centrifuge 2x1 mL for 3 min at 3000 rpm, pour off supernatant and recentrifuge briefly.

- Aspire supernatant and resuspend the cell pellet in LB to a final OD of 25 for one tube. Image it readily or leave the aliquot on ice until use. *Do not wait more than 1 hour on ice before use.*
- Aspire the supernatant of the second tube and resuspend the cell pellet in 50 µL of LB.
- Transfer in a pressure tube and close with the appropriate lid for the sample volume.
- Apply 100 MPa for 15min.
- Centrifuge sample for 3 min at 3000 rpm and aspire supernatant. Resuspend the cell pellet in LB to a final OD of 25. Image it immediately.

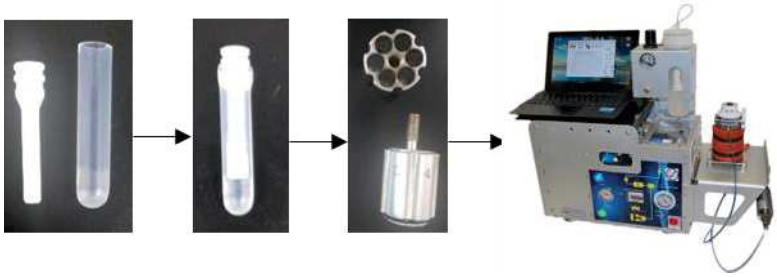

High pressure treatment process. 50 µL of high-density cells are transferred in a pressure tubes and then in the HUB pressure system. Pressure is applied for 15 min at 100 MPa.

7.3 Solution preparation

2% agarose:

- Weight 1g of agarose (ex: agarose 1000, Invitrogen) and put in a glass bottle of 250 mL with 50 mL of fresh M9 medium (filter sterilized) with no carbon source.
- Warm in a microwave until melted. *Remove as soon as it starts boiling and repeat until melted*
- Put in a 50 mL Falcon and eventually readjust the volume to 50 mL with sterile water
- Make aliquots of 1 mL in 1.5 mL tubes and keep at -20°C

M9 media:

M9 salts 10x 250mL:	*Amounts (g)*
Na2HPO4	15
KH2PO4	7.5
NaCl	1.25
NH4Cl	2.5

Dissolves salts into 200 mL of distillated H20 and bring to 250 mL in a graduate cylinder. Pour into a bottle and autoclave or filter sterilize. Store at 25°C.

Vitamin stock solution:	*Amount (g)*
Thiamine HCl	0.5
Biotin	0.1
Choline Cl	0.1
Folic Acid	0.1
Niacinamide	0.1
D-pantothenate	0.1
Pyrodoxal	0.1
Riboflavin	0.01

Dissolve vitamins into 100 mL distillated H_2O by stirring at room temperature. Note that dissolution of vitamins may not be complete. Solution should be yellow/orange. Filter sterilize after a reasonable amount of time using a 0.2 µm filter into an autoclaved bottle. Make aliquots of 1.25 mL and store at -20°C.

Metals stock solution 250,000x:	*Amount (g)*
$FeCl_3 \cdot 6H_2O$	0.48
$CuSO_4 \cdot 2H_2O$	0.27
$MnSO_4 \cdot H_2O$	0.31
$CoCl_2 \cdot 6H_2O$	0.081
$Na_2MoO_4 \cdot 2H_2O$	0.051
$NiCl_2 \cdot 6H_2O$	0.047

Dissolve metals into 40 mL distillated H_2O, filter sterilize using 0.2 µm filter into a 50 mL Falcon tube. To make a 1000x stock, take 400 µL of the 250,000-stock solution into 100 mL of distillated H_2O.

M9 Minimal Media 1 L:	*Volume (mL)*	*Final concentration*
M9 salt stock 10x	100	1x
MgSO4 1 M	2	2 mM
CaCl2 0.2 M	0.5	0.1 mM
Metal ions 1000x	1	1x
Vitamin mix	1	-
Glucose 30 %	13	0.4%

Autoclave the distillated H_2O into a 2 L flask cover with foil. When the water has cooled, add the above reagents.

7.4 Purification protocol for 1L of culture

7.4.1 Buffer solutions

Cell wash buffer 250 mL:	*Concentration (M)*	*Volume (mL)*	*Final concentration (mM)*
Tris pH7.5	1	2.5	10
NaCl	3	8.3	100

Lyse buffer 20 mL:	*Concentration (M)*	*Volume (mL)*	*Final concentration (mM)*
Sodium phosphate pH7	0.5	4	100
Na2SO4	0.5	5	125
MgCl2	1	0.05	2.5
DTT	1	0.01	0.5
NaCl	3	0.335	50

Wash buffer 1 L:	*Concentration (M)*	*Volume (mL)*	*Final concentration (mM)*

Tris pH8	1	100	100
NaCl	3	50	150
EDTA	0.5	2	1

Elution buffer 20 mL:	*Volume (mL)*	*Weight (g)*	*Final concentration (mM)*
Wash buffer	20	-	-
Destiobiotin	-	0.0109	2.5

All solutions are made in distillated H_2O and filter sterilized with a 0.2 µm filter.

7.4.2 Protocols

Glycerol stock:

- Re-isolate the strains from a plate or previous glycerol stock on LB-agar with appropriate antibiotics. Grow at 37°C ON.
- Inoculate 2 mL of LB medium antibiotics.
- When the culture is well grown (6-8 hours), add 1 mL of sterile glycerol 50% and mix well. *Use sterile filtered tips to avoid any risk of contamination.*
- Make 2-3 aliquots of 1 mL and store at -80°C.

Preculture (around 4pm):

- Inoculate 2 mL of LB medium containing 100 µg/mL Ampicillin with frozen stock and shake 2-3 hours at 37°C and 200 rpm.

Overnight culture (around 6pm):

- Inoculate 25 mL of M9 medium containing 100 µg/mL Ampicillin with 2 mL of preculture and shake ON at 37°C and 200 rpm.

Next day:

- Dilute 20 mL of ON culture in 1 L of fresh M9 containing 100 µg/mL Ampicillin and shake at 37°C and 200 rpm. Monitor the optical density at 600nm (OD_{600}) and induced with 1 mM IPTG when OD_{600} is around 0.6/0.7 for 3h at 30°C. *Take a 1 mL sample immediately before induction (non-induced control) and 1 mL sample before centrifugation (induced control) (resuspend pellet in blue for a SDS gel.* Centrifuge cells at 6000 rpm for 25 minutes at 4°C.
- Pour off supernatant and resuspend the pellet in 15 mL of cell wash buffer.

- Centrifuge at 4000 rpm for 10 minutes at 4°C. Pour off supernatant and keep the pellet at -80°C.

Lysate preparation:

- Defreeze pellet (Falcon tube in water) and resuspended it in 20 mL of lyse buffer. Freeze it at -80 °C and defreeze it again. Add 1 mL of Na2HPO4 0.5M, 30 µL of benzamidine 1M, 15 µL lysozyme 1 mg/mL and 15 µL DNase 1M. Leave it on ice 30 min. Sonicate 2x3 minutes (amplitude 60 and pulse 2/2s). *Take a 50 µL sample for an SDS gel.*
- Centrifuge 25 minutes at 18000 rpm and 4°C. Filter supernatant using a 0.4 µm filter (or 0.2 µm for prepack column). *Take a 50 µL sample for a gel.*

Purification using batch gravity flow column:

The column volume (CV) corresponds to 3 mL of Streptactin-superflow resin (IBA).

- Equilibrate column with 2 CVs Buffer W
- Add supernatant (volume should be in the range of 0.5 and 10 CVs). Leave it few minutes on the resin. *Collect flow through in case proteins is not attach and keep 50 µL for a gel.*
- Wash the column 5 times with 1 CV wash buffer after he cell extract has completely entered the column.
- Add 6 times 0.5 CVs Buffer E (usually 1 mL) and collect the eluate. Use 20 µL + 80 µL Buffer W for fluorescence measurement of each fractions. Pool fractions containing the protein if needed. *Take a 20 µL sample for a gel.*
- *Store aliquots at – 80°C.*

Resin regeneration:

Wash the column 3 times with 5 CVs regeneration buffer (Buffer R, IBA)(really red), overlay with 2 mL Buffer W or R for storage at 4°C. Remove Buffer R by washing with 2 times 4 CVs of Buffer W at pH 10.5 (better) and exchange with Buffer W at pH 8.

Gel filtration column:

Equilibrate the column (GE Healthcare, Superdex S200 HR10/300) with the gel filtration buffer (GF) at a flow rate of 0.5 mL/min. Inject 400 or 500 µL of sample and collect fraction of 400 µL. Measure fraction fluorescence on the TECAN using a 96 wells plate (Greiner) in a total volume of 100 µL (20 µL of fraction + 80 µL GF buffer).

Bibliography

1. Rampelotto,P.H. (2013) Extremophiles and extreme environments. *Life (Basel, Switzerland)*, **3**, 482–5.

2. Hazael,R., Meersman,F., Ono,F., Mcmillan,P.F. and Bains,W. (2016) Pressure as a Limiting Factor for Life. *Life*, **6**.

3. Lauro,F.M. and Bartlett,D.H. (2008) Prokaryotic lifestyles in deep sea habitats. *Extremophiles*, **12**, 15–25.

4. Sogin,M.L., Morrison,H.G., Huber,J.A., Mark Welch,D., Huse,S.M., Neal,P.R., Arrieta,J.M. and Herndl,G.J. (2006) Microbial diversity in the deep sea and the underexplored 'rare biosphere'. *Proc. Natl. Acad. Sci. U. S. A.*, **103**, 12115–20.

5. Aertsen,A. and Michiels,C.W. (2005) Mrr instigates the SOS response after high pressure stress in Escherichia coli. *Mol. Microbiol.*, **58**, 1381–1391.

6. Rivalain,N., Roquain,J. and Demazeau,G. (2010) Development of high hydrostatic pressure in biosciences: Pressure effect on biological structures and potential applications in Biotechnologies. *Biotechnol. Adv.*, **28**, 659–672.

7. Simonato,F., Campanaro,S., Lauro,F.M., Vezzi,A., D'Angelo,M., Vitulo,N., Valle,G. and Bartlett,D.H. (2006) Piezophilic adaptation: a genomic point of view. *J. Biotechnol.*, **126**, 11–25.

8. Regnard,P. (1884) Effets des hautes pressuons sur les animaux marins. *Seances Soc. Biol.*, **36**, 394–395.

9. Jebbar,M., Franzetti,B., Girard,E. and Oger,P. (2015) Microbial diversity and adaptation to high hydrostatic pressure in deep-sea hydrothermal vents prokaryotes. *Extremophiles*, **19**, 721–740.

10. Daniel,I., Oger,P. and Winter,R. (2006) Origins of life and biochemistry under high-pressure conditions. *Chem. Soc. Rev.*, **35**, 858.

11. Jannasch,H.W. and Taylor,C.D. (1984) Deep-sea microbiology. *Ann. Rev. Microbiol.*, **38**, 487–514.

12. Fang,J., Zhang,L. and Bazylinski,D.A. (2010) Deep-sea piezosphere and piezophiles: geomicrobiology and biogeochemistry. *Trends Microbiol.*, **18**, 413–422.

13. Oger,P.M. and Jebbar,M. (2010) The many ways of coping with pressure. *Res. Microbiol.*, **161**, 799–809.

14. ZoBELT,C.E., Johnson,F.H. and Zobell,C.E. (1949) The influence of hydrostatic pressure on the growth and viability of terrestrial and marine bacteria. *J. Bacteriol.*, **57**, 179–89.

15. Zhang,Y., Li,X., Bartlett,D.H. and Xiao,X. (2015) Current developments in marine microbiology: high-pressure biotechnology and the genetic engineering of piezophiles. *Curr. Opin. Biotechnol.*, **33**, 157–164.

16. Daniel,I. and Winter,R. (2006) Origins of life and biochemistry under high-pressure conditions young Earth. *Chem. Soc. Rev.*, **35**, 858–875.

17. Lauro,F.M., Chastain,R.A., Blankenship,L.E., Yayanos,A.A. and Bartlett,D.H. (2007) The unique 16S rRNA genes of piezophiles reflect both phylogeny and adaptation. *Appl. Environ. Microbiol.*, **73**, 838–45.

18. Russell,N.J. (1990) Cold adaptation of microorganisms. *Philos. Trans. R. Soc. Lond. B. Biol. Sci.*, **326**, 595–608, NaN-11.

19. Bartlett,D.H. (1999) Microbial Adaptations to the Psychrosphere/Piezosphere. *J. Molec. Microbiol. Biotechnol*, **1**, 93–100.

20. Fiala,G. and Stetter,K.O. (1986) Pyrococcus furiosus sp. nov. represents a novel genus of marine heterotrophic archaebacteria growing optimally at 100°C. *Arch. Microbiol.*, **145**, 56–61.

21. Whitman,W.B., Coleman,D.C. and Wiebe,W.J. (1998) Prokaryotes: The unseen majority. *Proc. Natl. Acad. Sci.*, **95**, 6578–6583.

22. Balny,C., Masson,P. and Heremans,K. (2002) High pressure effects on biological macromolecules: from structural changes to alteration of cellular processes. *Biochim. Biophys. Acta*, **1595**, 3–10.

23. Welch,T.J., Farewell,A., Neidhardt,F.C. and Bartlett},D.H. (1993) Stress Response of Escherichia coli to Elevated Hydrostatic Pressure. *J. Bacteriol.*, **175**, 7170–7177.

24. Fernandes,P.M.B., Domitrovic,T., Kao,C.M. and Kurtenbach,E. (2004) Genomic expression pattern in Saccharomyces cerevisiae cells in response to high hydrostatic pressure. *FEBS Lett.*, **556**, 153–60.

25. Vezzi,A., Campanaro,S., D'Angelo,M., Simonato,F., Vitulo,N., Lauro,F.M., Cestaro,A., Malacrida,G., Simionati,B., Cannata,N., *et al.* (2005) Life at Depth: Photobacterium profundum Genome Sequence and Expression Analysis. *Science (80-.).*, **307**, 1459–1461.

26. Campanaro,S., Vezzi,A., Vitulo,N., Lauro,F.M., D'Angelo,M., Simonato,F., Cestaro,A., Malacrida,G., Bertoloni,G., Valle,G., *et al.* (2005) Laterally transferred elements and high pressure adaptation in Photobacterium profundum strains. *BMC Genomics*, **6**, 122.

27. Vannier,P., Michoud,G., Oger,P. and Marteinsson,V. þór (2015) Genome expression of Thermococcus barophilus and Thermococcus kodakarensis in response to different hydrostatic pressure conditions. *Res. Microbiol.*, **166**, 717–725.

28. Valentine,R.C. and Valentine,D.L. (2004) Omega-3 fatty acids in cellular membranes: a unified concept. *Prog. Lipid Res.*, **43**, 383–402.

29. Delong,E.F. and Yayanos,A.A. (1986) Biochemical Function and Ecological Significance of Novel Bacterial Lipids in Deep-Sea Procaryotes. *Appl. Environ. Microbiol.*, **51**, 730–737.

30. Cossins,A.R., Beddard,G., West,M.A.A.R., Morns,G.J., Clarke,A. and Prosser,C.L. (1983) Adaptation to temperature in bacterial membranes. *Biochim. Biophys. Acta Proc. Natl. Acad. Sci. U.S.A. Biochim. Biophys. Acta Cossins J. Comp. Physiol. Fluoresc. Spectrosc. N. J. Biochem. SOC. Trans*, **4**, 39–80.

31. Allen,E.E., Facciotti,D. and Bartlett,D.H. (1999) Monounsaturated but not polyunsaturated fatty acids are required for growth of the deep-sea bacterium Photobacterium profundum SS9 at high pressure and low temperature. *Appl. Environ. Microbiol.*, **65**, 1710–20.

32. Allen,E.E. and Bartlett,D.H. (2002) Structure and regulation of the omega-3 polyunsaturated fatty acid synthase genes from the deep-sea bacterium Photobacterium profundum strain SS9. *Microbiology*, **148**, 1903–1913.

33. Bartlett,D., Wright,M., Yayanos,A.A. and Silverman,M. (1989) Isolation of a gene regulated by hydrostatic pressure in a deep-sea bacterium. *Nature*, **342**, 572–574.

34. Welch,T.J. and Bartlett,D.H. (1998) Identification of a regulatory protein required for pressure-responsive gene expression in the deep-sea bacterium Photobacterium species strain SS9. *Mol. Microbiol.*, **27**, 977–985.

35. Kato,C. and Qureshi,M.H. (1999) Pressure response in deep-sea piezophilic bacteria. *J. Mol. Microbiol. Biotechnol.*, **1**, 87–92.

36. Friedman,S.M. and Weinstein,I.B. (1965) Fidelity in protein synthesis: Proline miscoding in a thermophile system. *Biochem. Biophys. Res. Commun.*, **21**, 339–345.

37. Chilukuri,L.N., Fortes,P.A.G. and Bartlett,D.H. (1997) High Pressure Modulation ofEscherichia coliDNA Gyrase Activity. *Biochem. Biophys. Res. Commun.*, **239**, 552–556.

38. GROSS,M. and JAENICKE,R. (1994) Proteins under pressure. The influence of high hydrostatic pressure on structure, function and assembly of proteins and protein complexes. *Eur. J. Biochem.*, **221**, 617–630.

39. Royer,C.A. (1995) [16] Application of pressure to biochemical equilibria: The other thermodynamic variable. *Methods Enzymol.*, **259**, 357–377.

40. Papini,C.M., Pandharipande,P.P., Royer,C.A. and Makhatadze,G.I. (2017) Putting the Piezolyte Hypothesis under Pressure. *Biophys. J.*, **113**, 974–977.

41. Reed,C.J., Lewis,H., Trejo,E., Winston,V. and Evilia,C. (2013) Protein adaptations in archaeal extremophiles. *Archaea*, **2013**, 373275.

42. Vanlint,D., Rutten,N., Michiels,C.W. and Aertsen,A. (2012) Emergence and stability of high-pressure resistance in different food-borne pathogens. *Appl. Environ. Microbiol.*, **78**, 3234–3241.

43. R,M. and RE,M. (1973) Loss of bacterial motility under pressure. *Nature*, **246**, 525–527.

44. Landau,J. V. (1967) Induction, transcription and translation in Escherichia coli: A hydrostatic pressure study. *Biochim. Biophys. Acta - Nucleic Acids Protein Synth.*, **149**, 506–512.

45. Zobell,C. and AB.,C. (1964) Filament formation by Escherichia coli at increased hydrostatic pressures. *J Bacteriol*, **87**, 710–719.

46. Zobell,C.E. and Cobet,A.B. (1962) Growth, reproduction, and death rates of Escherichia coli at increased hydrosctatic pressures. *J. Bacteriol.*, **84**, 1228–1236.

47. Yayanos,A. and Pollard EC (1969) A study of the effects of hydrostatic pressure on macromolecular synthesis in Escherichia coli. *Biophys J*, **9**, 1464–1482.

48. Gross,M., Lehle,K., Jaenicke,R. and Nierhaus,K.H. (1993) Pressure-induced dissociation of ribosomes and elongation cycle intermediates. *Eur. J. Biochem.*, **218**, 463–468.

49. Paga,R. and Mackey,B. (2000) Relationship between Membrane Damage and Cell Death in Pressure-Treated Escherichia coli Cells : Differences between Exponential- and Stationary-Phase Cells and Variation among Strains. *Appl. Environ. Microbiol.*, **66**, 2829–2834.

50. Nishiyama,M., Sowa,Y., Kimura,Y., Homma,M., Ishijima,A. and Terazima,M. (2013) High hydrostatic pressure induces counterclockwise to clockwise reversals of the Escherichia coli flagellar motor. *J. Bacteriol.*, **195**, 1809–14.

51. Mota,M.J., Lopes,R.P., Delgadillo,I. and Saraiva,J.A. (2013) Microorganisms under high pressure — Adaptation, growth and biotechnological potential. *Biotechnol. Adv.*, **31**, 1426–1434.

52. Ishii,A., Sato,T., Wachi,M., Nagai,K. and Kato,C. (2004) Effects of high hydrostatic pressure on bacterial cytoskeleton FtsZ polymers in vivo and in vitro. *Microbiology*, **150**, 1965–1972.

53. Kumar,P. and Libchaber,A. (2013) Pressure and Temperature Dependence of Growth and Morphology of Escherichia coli : Experiments and Stochastic Model. *Biophys. J.*, **105**, 783–793.

54. Schulz,E., Lüdemann,H.-D. and Jaenicke,R. (1976) High pressure equilibrium studies on the dissociation—association of E. coli ribosomes. *FEBS Lett.*, **64**, 40–43.

55. Groß,M. and Jaenicke,R. (1990) Pressure-induced dissociation of tight couple ribosomes. *FEBS Lett.*, **267**, 239–241.

56. Gordon W. Niven,C.A.M. and B.M.M. (1999) The effects of hydrostatic pressure on ribosome conformation in Escherichia coli: an in vivo study using differential scanning calorimetry. *Microbiology*, **145**, 419–425.

57. Alpas,H., Lee,J., Bozoglu,F. and Kaletunç,G. (2003) Evaluation of high hydrostatic

pressure sensitivity of Staphylococcus aureus and Escherichia coli O157:H7 by differential scanning calorimetry. *Int. J. Food Microbiol.*, **87**, 229–237.

58. Macgregor,R.B. (2002) The interactions of nucleic acids at elevated hydrostatic pressure. *Biochim. Biophys. Acta - Protein Struct. Mol. Enzymol.*, **1595**, 266–276.

59. Aertsen,A., Vanoirbeek,K., De Spiegeleer,P., Sermon,J., Hauben,K., Farewell,A., Nyström,T. and Michiels,C.W. (2004) Heat Shock Protein-Mediated Resistance to High Hydrostatic Pressure in Escherichia coli. *Appl. Environ. Microbiol.*, **70**, 2660–2666.

60. Tiwari,S., Thakur,R. and Shankar,J. (2015) Role of Heat-Shock Proteins in Cellular Function and in the Biology of Fungi. *Biotechnol. Res. Int.*, **2015**, 132635.

61. Landini,P., Egli,T., Wolf,J. and Lacour,S. (2014) sigmaS, a major player in the response to environmental stresses in *E scherichia coli* : role, regulation and mechanisms of promoter recognition. *Environ. Microbiol. Rep.*, **6**, 1–13.

62. Malone,A.S., Chung,Y.-K. and Yousef,A.E. (2006) Genes of Escherichia coli O157:H7 That Are Involved in High-Pressure Resistance. *Appl. Environ. Microbiol.*, **72**, 2661–2671.

63. Aertsen,A., Faster,D. and Michiels,C.W. (2005) Induction of Shiga Toxin-Converting Prophage in Escherichia coli by High Hydrostatic Pressure Induction of Shiga Toxin-Converting Prophage in Escherichia coli by High Hydrostatic Pressure. **71**, 1155–1162.

64. Desmarais,D., Douglas,M. and Roberts,M.F. (2002) Solute accumulation in the deep-sea bacterium Photobacterium profundum. *Extremophiles*, **6**, 507–514.

65. W Bridgman,B.P. (1914) The coagulation of albumen by pressure. *Amer. Acad. Arts Sci.*, **19**, 511–5212.

66. Suzuki,K., Miyosawa,Y. and Suzuki,C. (1963) Protein denaturation by high pressure. Measurements of turbidity of isoelectric ovalbumin and horse serum albumin under high pressure. *Arch. Biochem. Biophys.*, **101**, 225–228.

67. Le Chatelier,H. (1884) Sur un énoncé général des lois des équilibres chimiques. *C. R. Hebd. Seances Acad. Sci.*, **99**, 786–789.

68. Sanfelice,D. and Temussi,P.A. (2016) Cold denaturation as a tool to measure protein stability. *Biophys. Chem.*, **208**, 4–8.

69. Privalov,P.L. and Makhatadze,G.I. (1990) Heat capacity of proteins: II. Partial molar heat capacity of the unfolded polypeptide chain of proteins: Protein unfolding effects. *J. Mol. Biol.*, **213**, 385–391.

70. Rouget,J.-B., Aksel,T., Roche,J., Saldana,J.-L., Garcia,A.E., Barrick,D. and Royer,C.A. (2011) Size and Sequence and the Volume Change of Protein Folding. *J. Am. Chem. Soc.*, **133**, 6020–6027.

71. Roche,J., Caro,J.A., Norberto,D.R., Barthe,P., Roumestand,C., Schlessman,J.L., Garcia,A.E., García-Moreno,B., Royer,C.A. and Baldwin,R. Cavities determine the pressure unfolding of proteins.

72. Mitra,L., Rouget,J.-B., Garcia-Moreno,B., Royer,C.A. and Winter,R. (2008) Towards a Quantitative Understanding of Protein Hydration and Volumetric Properties. *ChemPhysChem*, **9**, 2715–2721.

73. Ludovic Brun,‡, Daniel G. Isom,§, Priya Velu,§, Bertrand García-Moreno,§ and and Catherine Ann Royer*,‡ (2006) Hydration of the Folding Transition State Ensemble of a Protein†. 10.1021/BI052638Z.

74. Roche,J. and Royer,C.A. (2018) Lessons from Pressure Denaturation of Proteins. *J. Interdiscip. Sci.*, **in press**.

75. Imamura,H. and Kato,M. (2009) Effect of pressure on helix-coil transition of an alanine-based peptide: An FTIR study. *Proteins Struct. Funct. Bioinforma.*, **75**, 911–918.

76. Takekiyo,T., Shimizu,A., Kato,M. and Taniguchi,Y. (2005) Pressure-tuning FT-IR spectroscopic study on the helix–coil transition of Ala-rich oligopeptide in aqueous solution. *Biochim. Biophys. Acta - Proteins Proteomics*, **1750**, 1–4.

77. Neumaier,S., Büttner,M., Bachmann,A. and Kiefhaber,T. (2013) Transition state and ground state properties of the helix-coil transition in peptides deduced from high-pressure studies. **110**, 20988–20993.

78. Kitahara,R., Royer,C., Yamada,H., Boyer,M., Saldana,J.-L., Akasaka,K. and Roumestand,C. (2002) Equilibrium and Pressure-jump Relaxation Studies of the Conformational Transitions of P13MTCP1. *J. Mol. Biol.*, **320**, 609–628.

79. Yin,H., Feng,G., Clore,G.M., Hummer,G. and Rasaiah,J.C. (2010) Water in the polar and nonpolar cavities of the protein interleukin-1β. *J. Phys. Chem. B*, **114**, 16290–7.

80. Qvist,J., Davidovic,M., Hamelberg,D. and Halle,B. (2008) A dry ligand-binding cavity in a solvated protein. *Proc. Natl. Acad. Sci. U. S. A.*, **105**, 6296–301.

81. Nucci,N. V, Fuglestad,B., Athanasoula,E.A. and Wand,A.J. (2014) Role of cavities and hydration in the pressure unfolding of T4 lysozyme. *Proc. Natl. Acad. Sci. U. S. A.*, **111**, 13846–51.

82. Gekko,K. and Timasheff,S.N. (1981) Mechanism of protein stabilization by glycerol: preferential hydration in glycerol-water mixtures. *Biochemistry*, **20**, 4667–76.

83. Pappenberger,G., Saudan,C., Becker,M., Merbach,A.E. and Kiefhaber,T. (2000) Denaturant-induced movement of the transition state of protein folding revealed by high-pressure stopped-flow measurements. *Proc. Natl. Acad. Sci. U. S. A.*, **97**, 17–22.

84. Frye,K.J. and Royer,C.A. (1997) The kinetic basis for the stabilization of staphylococcal nuclease by xylose. *Protein Sci.*, **6**, 789–93.

85. Oliveira,A.C., Gaspar,L.P., Da Poian,A.T. and Silva,J.L. (1994) Arc Repressor will not Denature Under Pressure in the Absence of Water. *J. Mol. Biol.*, **240**, 184–187.

86. Silva,J.L. and Weber,G. (1993) Pressure Stability of Proteins. *Annu. Rev. Phys. Chem.*, **44**, 89–113.

87. Paladini,A.A. and Weber,G. (1981) Pressure-Induced Reversible Dissociation of Enolase. *Biochemistry*, **20**, 2587–2593.

88. Schmid,G., Ludemann,H.-D. and Jaenicke,R. (1979) Dissociation and Aggregation of Lactic Dehydrogenase by High Hydrostatic Pressure. *Eur. J. Biochem.*, **97**, 407–413.

89. Bonafe,C.F.S., Vital,C.M.R., Telles,R.C.B., Gonçalves,M.C., Matsuura,M.S.A., Pessine,F.B.T., Freitas,D.R.C. and Vega,J. (1998) Tobacco Mosaic Virus Disassembly by High Hydrostatic Pressure in Combination with Urea and Low Temperature. *Biochemistry*, **37**, 11097–11105.

90. Oliveira,A.C., Valente,A.P., Almeida,F.C.L., Lima,S.M.B., Ishimaru,D., GonçAlves,B., Peabody,D., Foguel,D. and Silva,L. (1999) Hydrostatic Pressure as a Tool to Study Virus Assembly: Pressure-Inactivation of Viruses by Formation of Fusion Intermediate States. In *High Pressure Molecular Science*. Springer Netherlands, Dordrecht, pp. 497–513.

91. Silva,J.L., Foguel,D., Da Poian,A.T. and Prevelige,P.E. (1996) The use of hydrostatic pressure as a tool to study viruses and other macromolecular assemblages. *Curr. Opin. Struct. Biol.*, **6**, 166–175.

92. Chalikian,T. V. and Macgregor,R.B. (2007) Nucleic acid hydration: a volumetric perspective. *Phys. Life Rev.*, **4**, 91–115.

93. Macgregor,R.B. (1998) Chain length and oligonucleotide stability at high pressure. *Biopolymers*, **38**, 321–328.

94. Macgregor,R.B. (2000) Effect of hydrostatic pressure on nucleic acids. *Biopolymers*, **48**, 253–263.

95. Amiri,A.R. and Macgregor,R.B. (2011) The effect of hydrostatic pressure on the thermal stability of DNA hairpins. *Biophys. Chem.*, **156**, 88–95.

96. Wu,J.Q. and Macgregor,R.B. (1993) Pressure Dependence of the Melting Temperature of dA*dT Polymers*. *Biochemistry*, **32**, 12531–12537.

97. Wu,J.Q. and Macgregor,R.B. (1995) Pressure dependence of the helix-coil transition temperature of poly[d(G-C)]. *Biopolymers*, **35**, 369–376.

98. Najaf-Zadeh,R., Wu,J.Q. and Macgregor,R.B. (1995) Effect of cations on the volume of the helix-coil transition of poly[d(A-T)]. *Biochim. Biophys. Acta - Gene Struct. Expr.*, **1262**, 52–58.

99. Royer,C.A., Weber,G., Daly,T.J. and Matthews,K.S. (1986) Dissociation of the lactose repressor protein tetramer using high hydrostatic pressure. *Biochemistry*, **25**, 8308–

8315.

100. Royer,C.A., Chakerian,A.E. and Matthews,K.S. (1990) Macromolecular binding equilibria in the lac repressor system: studies using high-pressure fluorescence spectroscopy. *Biochemistry*, **29**, 4959–4966.

101. Robinson,C.R. and Sligar,S.G. (1998) Changes in solvation during DNA binding and cleavage are critical to altered specificity of the EcoRI endonuclease. *Proc. Natl. Acad. Sci. U. S. A.*, **95**, 2186–91.

102. Robinson,C.R. and Sligar,S.G. (1994) Hydrostatic Pressure Reverses Osmotic Pressure Effects on the Specificity of EcoRI-DNA Interactions. *Biochemistry*, **33**, 3787–3793.

103. Refaee,M., Tezuka,T., Akasaka,K. and Williamson,M.P. (2003) Pressure-dependent Changes in the Solution Structure of Hen Egg-white Lysozyme. *J. Mol. Biol.*, **327**, 857–865.

104. Hite,B. (1899) The effect of pressure in the preservation of milk: a preliminary report. *West Virginia Agric. Exp. Stn.*, **58**.

105. Rastogi,N.K., Raghavarao,K.S.M.S., Balasubramaniam,V.M., Niranjan,K. and Knorr,D. (2007) Opportunities and Challenges in High Pressure Processing of Foods. *Crit. Rev. Food Sci. Nutr.*, **47**, 69–112.

106. Fabian,E., Bello,T., González,G., Nez,M., Klotz Ceberio,B.F., Rodrigo,D. and Martí Nez López,A. (2014) High Pressure Treatment in Foods. **3**, 476–490.

107. Strohalm,J., Kocurová,K., Totušek,J., Lefnerová,D., Tříska,J., Vrchotová,N., Fiedrleová,V., Holasova,M., Gabrovská,D. and Paulíčková,I. (2006) High pressure and foods—fruit/vegetable juices. *J. Food Eng.*, **77**, 386–398.

108. Borekt,E. and Ryan,A. (1958) The transfer of irradiation-elicited induction in a lysogenic organism. *Biochim. Biophys. Acta Nat.*, **16**, 13–17.

109. Witkin,E.M. (1969) Ultraviolet-Induced Mutation and DNA Repair. *Annu. Rev. Microbiol.*, **23**, 487–514.

110. Yeiser,B., Pepper,E.D., Goodman,M.F. and Finkel,S.E. (2002) SOS-induced DNA polymerases enhance long-term survival and evolutionary fitness. *Proc. Natl. Acad. Sci.*, **99**, 8737–8741.

111. Aertsen,A. and Michiels,C.W. (2006) Upstream of the SOS response: figure out the trigger. *Trends Microbiol.*, **14**, 421–423.

112. Veen,S. Van Der and Abee,T. (2011) Bacterial SOS response : a food safety perspective. *Curr. Opin. Biotechnol.*, **22**, 136–142.

113. Wu,H.-Y., Lu,C.-H. and Li,H.-W. (2017) RecA-SSB Interaction Modulates RecA Nucleoprotein Filament Formation on SSB-Wrapped DNA. *Sci. Rep.*, **7**, 11876.

114. Simmons,L.A., Foti,J.J., Cohen,S.E. and Walker,G.C. (2008) The SOS Regulatory

Network. *EcoSal Plus*, 10.1128/ecosalplus.5.4.3.

115. Kuzminov,A. (1999) Recombinational repair of DNA damage in Escherichia coli and bacteriophage lambda. *Microbiol. Mol. Biol. Rev.*, **63**, 751–813, table of contents.

116. Morimatsu,K. and Kowalczykowski,S.C. (2003) RecFOR Proteins Load RecA Protein onto Gapped DNA to Accelerate DNA Strand Exchange. *Mol. Cell*, **11**, 1337–1347.

117. Hegde,S.P., Qin,M.H., Li,X.H., Atkinson,M.A., Clark,A.J., Rajagopalan,M. and Madiraju,M. V (1996) Interactions of RecF protein with RecO, RecR, and single-stranded DNA binding proteins reveal roles for the RecF-RecO-RecR complex in DNA repair and recombination. *Proc. Natl. Acad. Sci. U. S. A.*, **93**, 14468–73.

118. Aertsen,A. and Michiels,C.W. (2005) SulA-dependent hypersensitivity to high pressure and hyperfilamentation after high-pressure treatment of Escherichia coli lon mutants. *Res. Microbiol.*, **156**, 233–237.

119. Cordell,S.C., Robinson,E.J.H. and Lowe,J. (2003) Crystal structure of the SOS cell division inhibitor SulA and in complex with FtsZ. *Proc. Natl. Acad. Sci. U. S. A.*, **100**, 7889–94.

120. Pennington,J.M. and Rosenberg,S.M. (2007) Spontaneous DNA breakage in single living Escherichia coli cells. *Nat. Genet.*, **39**, 797–802.

121. Echols,H. (1975) The y Protein Specified by Bacteriophage. *J. Biol. Chem.*, **250**, 7377–7387.

122. Oliver,D.B. and Goldberg,E.B. (1977) Protection of parental T4 DNA from a restriction exonuclease by the product of gene 2. *J. Mol. Biol.*, **116**, 877–881.

123. Malinin,A.I., Vostrov,A.A., Rybchin,V.N. and Svarchevskiĭ,A.N. (1992) Structure of ends of linear plasmid N15. *Mol. Gen. Mikrobiol. Virusol.*, **5**, 19–22.

124. Dillingham,M.S. and Kowalczykowski,S.C. (2008) RecBCD enzyme and the repair of double-stranded DNA breaks. *Microbiol. Mol. Biol. Rev.*, **72**, 642–671.

125. Đermić,D., Halupecki,E., Zahradka,D. and Petranović,M. (2005) RecBCD enzyme overproduction impairs DNA repair and homologous recombination in Escherichia coli. *Res. Microbiol.*, **156**, 304–311.

126. Niu,H., Raynard,S. and Sung,P. (2009) Multiplicity of DNA end resection machineries in chromosome break repair. *Gene Dev.*, **23**, 1481–1486.

127. Aertsen,A. and Houdt,R. Van (2004) An SOS response induced by high pressure in Escherichia coli. *J. …*, **186**, 6133–6141.

128. Loenen,W.A.M., Dryden,D.T.F., Raleigh,E.A., Wilson,G.G. and Murray,N.E. (2014) Highlights of the DNA cutters: a short history of the restriction enzymes. *Nucleic Acids Res.*, **42**, 3–19.

129. Loenen,W.A.M., Dryden,D.T.F., Raleigh,E.A. and Wilson,G.G. (2014) Type I restriction

enzymes and their relatives. *Nucleic Acids Res.*, **42**, 20–44.

130. Pingoud,A. and Jeltsch,A. (2001) Structure and function of type II restriction endonucleases. *Nucleic Acids Res.*, **29**, 3705–27.

131. Rao,D.N., Dryden,D.T.F. and Bheemanaik,S. (2014) Type III restriction-modification enzymes: a historical perspective. *Nucleic Acids Res.*, **42**, 45–55.

132. Loenen,W.A.M. and Raleigh,E.A. (2014) The other face of restriction: Modification-dependent enzymes. *Nucleic Acids Res.*, **42**, 56–69.

133. Horvath,P. and Barrangou,R. (2010) CRISPR/Cas, the immune system of bacteria and archaea. *Science*, **327**, 167–70.

134. Kennaway,C.K., Obarska-Kosinska,A., White,J.H., Tuszynska,I., Cooper,L.P., Bujnicki,J.M., Trinick,J. and Dryden,D.T.F. (2009) The structure of M.EcoKI Type I DNA methyltransferase with a DNA mimic antirestriction protein. *Nucleic Acids Res.*, **37**, 762–70.

135. Gupta,Y.K., Chan,S.-H., Xu,S.-Y. and Aggarwal,A.K. (2015) Structural basis of asymmetric DNA methylation and ATP-triggered long-range diffusion by EcoP15I. *Nat. Commun.*, **6**, 7363.

136. Sukackaite,R., Grazulis,S., Tamulaitis,G. and Siksnys,V. (2012) The recognition domain of the methyl-specific endonuclease McrBC flips out 5-methylcytosine. *Nucleic Acids Res.*, **40**, 7552–62.

137. Sibley,M.H., Raleigh,E.A. and Biolabs,N.E. (2018) Cassette-like variation of restriction enzyme genes in Escherichia coli C and relatives. *Nucleic Acids Res.*, **32**, 522–534.

138. Waite-Rees,P.A., Keating,C.J., Moran,L.S., Slatko,B.E., Hornstra,L.J. and Benner,J.S. (1991) Characterization and expression of the Escherichia coli Mrr restriction system. *J. Bacteriol.*, **173**, 5207–5219.

139. Raleigh,E.A., Murray,N.E., Revel,H., Blumenthal,R.M., Westaway,D., Reith,A.D., Rigby,P.W., Elhai,J. and Hanahan,D. (1988) McrA and McrB restriction phenotypes of some E. coli strains and implications for gene cloning. *Nucleic Acids Res.*, **16**, 1563–75.

140. Heitman,J. and Model,P. (1987) Site-specific methylases induce the SOS DNA repair response in Escherichia coli. *J. Bacteriol.*, **169**, 3243–3250.

141. Kelleher,J.E. and Raleigh,E.A. (1991) A Novel Activity in Escherichia coli K-12 That Directs Restriction of DNA Modified at CG Dinucleotides. *J. Bacteriol.*, **173**, 5220–5223.

142. Bujnicki,J.M. and Rychlewski,L. (2001) Identication of a PD- (D / E) XK-like domain with a novel conguration of the endonuclease active site in the methyl-directed restriction enzyme Mrr and its homologs. *Gene*, **267**, 183–191.

143. Ghosh,A., Passaris,I., Mebrhatu,M.T., Rocha,S., Vanoirbeek,K., Hofkens,J. and Aertsen,A. (2014) Cellular localization and dynamics of the Mrr type IV restriction

endonuclease of Escherichia coli. *Nucleic Acids Res.*, **42**, 3908–3918.

144. Shechter,N., Zaltzman,L., Weiner,A., Brumfeld,V., Shimoni,E., Fridmann-Sirkis,Y. and Minsky,A. (2013) Stress-induced condensation of bacterial genomes results in re-pairing of sister chromosomes: implications for double strand DNA break repair. *J. Biol. Chem.*, **288**, 25659–67.

145. Aertsen,A., Tesfazgi Mebrhatu,M. and Michiels,C.W. (2008) Activation of the Salmonella Typhimurium Mrr protein. *Biochem. Biophys. Res. Commun.*, **367**, 435–439.

146. Tesfazgi Mebrhatu,M., Wywial,E., Ghosh,A., Michiels,C.W., Lindner,A.B., Taddei,F., Bujnicki,J.M., Van Melderen,L. and Aertsen,A. (2011) Evidence for an evolutionary antagonism between Mrr and Type III modification systems. *Nucleic Acids Res.*, **39**, 5991–6001.

147. Orlowski,J., Mebrhatu,M.T., Michiels,C.W., Bujnicki,J.M. and Aertsen,A. (2008) Mutational analysis and a structural model of methyl-directed restriction enzyme Mrr. *Biochem. Biophys. Res. Commun.*, **377**, 862–866.

148. Brennan,R.G. (1993) The winged-helix DNA-binding motif: another helix-turn-helix takeoff. *Cell*, **74**, 773–6.

149. Sukackaite,R., Grazulis,S., Tamulaitis,G. and Siksnys,V. The recognition domain of the methyl-specific endonuclease McrBC flips out 5-methylcytosine. 10.1093/nar/gks332.

150. Combs,C.A. (2010) Fluorescence microscopy: a concise guide to current imaging methods. *Curr. Protoc. Neurosci.*, **Chapter 2**, Unit2.1.

151. Stokes,G.G. (1852) On the change of refrangibility of light. *Philos. Trans. R. Soc. London.*, **142**, 463–562.

152. Jabłoński,A. (1935) Über den Mechanismus der Photolumineszenz von Farbstoffphosphoren. *Zeitschrift für Phys.*, **94**, 38–46.

153. Vissier,A.J.W.G. and Rolinski,O.J. (2010) BASIC PHOTOPHYSICS.

154. Drummen,G. (2012) Fluorescent Probes and Fluorescence (Microscopy) Techniques — Illuminating Biological and Biomedical Research. *Molecules*, **17**, 14067–14090.

155. Shimomura,O., Johnson,F.H. and Saiga,Y. (1962) Extraction, Purification and Properties of Aequorin, a Bioluminescent Protein from the Luminous Hydromedusan,Aequorea. *J. Cell. Comp. Physiol.*, **59**, 223–239.

156. Prasher,D.C., Eckenrode,V.K., Ward,W.W., Prendergast,F.G. and Cormier,M.J. (1992) Primary structure of the Aequorea victoria green-fluorescent protein. *Gene*, **111**, 229–233.

157. Tsien,R.Y. (1998) The green fluorescent protein. *Annu. Rev. Biochem.*, **67**, 509–544.

158. Alaraby Salem,M. and Brown,A. (2015) Two-photon absorption of fluorescent protein chromophores incorporating non-canonical amino acids: TD-DFT screening and classical dynamics. *Phys. Chem. Chem. Phys.*, **17**, 25563–25571.

159. Patterson,G.H., Knobel,S.M., Sharif,W.D., Kain,S.R. and Piston,D.W. (1997) Use of the green fluorescent protein and its mutants in quantitative fluorescence microscopy. *Biophys. J.*, **73**, 2782–90.

160. Heim,R. and Tsien,R.Y. (1996) Engineering green fluorescent protein for improved brightness, longer wavelengths and fluorescence resonance energy transfer. *Curr. Biol.*, **6**, 178–82.

161. Cormack,B.P., Valdivia,R.H. and Falkow,S. (1996) FACS-optimized mutants of the green fluorescent protein (GFP). *Gene*, **173**, 33–38.

162. Minsky,M. (1988) Memoir on inventing the confocal scanning microscope. *Scanning*, **10**, 128–138.

163. Göppert-Mayer,M. (1931) Über Elementarakte mit zwei Quantensprüngen. *Ann. Phys.*, **401**, 273–294.

164. Kaiser,W. and Garrett,C.G.B. (1961) Two-Photon Excitation in Ca F 2 : Eu 2 +. *Phys. Rev. Lett.*, **7**, 229–231.

165. Xu,C., Williams,R.M., Zipfel,W. and Webb,W.W. (1996) Multiphoton excitation cross - sections of molecular fluorophores. *Bioimaging*, **4**, 198–207.

166. Magde,D., Elson,E. and Webb,W.W. (1972) Thermodynamic Fluctuations in a Reacting System—Measurement by Fluorescence Correlation Spectroscopy. *Phys. Rev. Lett.*, **29**, 705–708.

167. Berland,K.M., So,P.T.C. and Gratton,E. (1995) Two-Photon Fluorescepce Correlation Spectroscopy : Method and Application to the Intracellular Environment. *Biophys. J.*, **68**, 694–701.

168. Elson,E.L. (2011) Fluorescence Correlation Spectroscopy: Past, Present, Future. *Biophys. J.*, **101**, 2855–2870.

169. Guia,S., Jaeger,B.N., Piatek,S., Mailfert,S., Trombik,T., Fenis,A., Chevrier,N., Walzer,T., Kerdiles,Y.M., Marguet,D., *et al.* (2011) Confinement of Activating Receptors at the Plasma Membrane Controls Natural Killer Cell Tolerance. *Sci. Signal.*, **4**, ra21-ra21.

170. Ruprecht,V., Wieser,S., Marguet,D. and Schütz,G.J. (2011) Spot variation fluorescence correlation spectroscopy allows for superresolution chronoscopy of confinement times in membranes. *Biophys. J.*, **100**, 2839–45.

171. Remaut,K., Lucas,B., Braeckmans,K., Sanders,N.N., De Smedt,S.C. and Demeester,J. (2005) FRET-FCS as a tool to evaluate the stability of oligonucleotide drugs after intracellular delivery. *J. Control. Release*, **103**, 259–271.

172. Petrásek,Z., Hoege,C., Mashaghi,A., Ohrt,T., Hyman,A.A. and Schwille,P. (2008)

Characterization of protein dynamics in asymmetric cell division by scanning fluorescence correlation spectroscopy. *Biophys. J.*, **95**, 5476–86.

173. Balakrishnan Kannan,†, Lin Guo,†, Thankiah Sudhaharan,§, Sohail Ahmed,§, Ichiro Maruyama,‖ and and Thorsten Wohland*,† (2007) Spatially Resolved Total Internal Reflection Fluorescence Correlation Microscopy Using an Electron Multiplying Charge-Coupled Device Camera. 10.1021/AC0624546.

174. Wiseman,P.W., Squier,J.A., Ellisman,M.H. and Wilson,K.R. (2000) Two-photo image correlation spectroscopy and image cross-correlation spectroscopy. *J. Microsc.*, **200**, 14–25.

175. Chen,Y., Müller,J.D., So,P.T. and Gratton,E. (1999) The photon counting histogram in fluorescence fluctuation spectroscopy. *Biophys. J.*, **77**, 553–67.

176. Digman,M.A., Dalal,R., Horwitz,A.F. and Gratton,E. (2008) Mapping the Number of Molecules and Brightness in the Laser Scanning Microscope. *Biophys. J.*, **94**, 2320–2332.

177. Digman,M.A., Wiseman,P.W., Choi,C., Horwitz,A.R. and Gratton,E. (2009) Stoichiometry of molecular complexes at adhesions in living cells. *Proc. Natl. Acad. Sci.*, **106**, 2170–2175.

178. Nagy,P., Claus,J., Jovin,T.M. and Arndt-Jovin,D.J. (2010) Distribution of resting and ligand-bound ErbB1 and ErbB2 receptor tyrosine kinases in living cells using number and brightness analysis. *Proc. Natl. Acad. Sci. U. S. A.*, **107**, 16524–9.

179. Hellriegel,C., Caiolfa,V.R., Corti,V., Sidenius,N. and Zamai,M. (2011) Number and brightness image analysis reveals ATF-induced dimerization kinetics of uPAR in the cell membrane. *FASEB J.*, **25**, 2883–97.

180. Ross,J.A., Digman,M.A., Wang,L., Gratton,E., Albanesi,J.P. and Jameson,D.M. (2011) Oligomerization state of dynamin 2 in cell membranes using TIRF and number and brightness analysis. *Biophys. J.*, **100**, L15-7.

181. Presman,D.M., Levi,V., Pignataro,O.P. and Pecci,A. (2012) Melatonin inhibits glucocorticoid-dependent GR–TIF2 interaction in newborn hamster kidney (BHK) cells. *Mol. Cell. Endocrinol.*, **349**, 214–221.

182. Hinde,E., Pandz,E., Gratton,E. and Gaus,K. (2016) Quantifying the dynamics of the oligomeric transcription factor STAT3 by pair correlation of molocular brightness. *Nat. Commun.*, 10.1038/ncomms11047.

183. Hennen,J., Hur,K.-H., Saunders,C.A., Luxton,G.W.G. and Mueller,J.D. (2017) Quantitative Brightness Analysis of Protein Oligomerization in the Nuclear Envelope. *Biophys. J.*, **113**, 138–147.

184. James,N.G., Digman,M.A., Gratton,E., Barylko,B., Ding,X., Albanesi,J.P., Goldberg,M.S. and Jameson,D.M. (2012) Number and brightness analysis of LRRK2 oligomerization in live cells. *Biophys. J.*, **102**, L41-3.

185. James,N.G., Digman,M.A., Ross,J.A., Barylko,B., Wang,L., Li,J., Chen,Y., Mueller,J.D., Gratton,E., Albanesi,J.P., *et al.* (2014) A mutation associated with centronuclear myopathy enhances the size and stability of dynamin 2 complexes in cells. *Biochim. Biophys. Acta*, **1840**, 315–21.

186. Moutin,E., Compan,V., Raynaud,F., Clerté,C., Bouquier,N., Labesse,G., Ferguson,M.L., Fagni,L., Royer,C.A. and Perroy,J. (2014) The stoichiometry of scaffold complexes in living neurons – DLC2 functions as a dimerization engine for GKAP. *J. Cell Sci.*, **127**, 3451–3462.

187. Golebiewska,U., Johnston,J.M., Devi,L., Filizola,M. and Scarlata,S. (2011) Differential response to morphine of the oligomeric state of μ-opioid in the presence of δ-opioid receptors. *Biochemistry*, **50**, 2829–37.

188. Ferguson,M.L., Le Coq,D., Jules,M., Aymerich,S., Declerck,N., Royer,C.A., Le,D., Jules,M., Aymerich,S., Declerck,N., *et al.* (2011) Absolute quantification of gene expression in individual bacterial cells using two-photon fluctuation microscopy. *Anal. Biochem.*, **419**, 250–259.

189. Ferguson,M.L., Le Coq,D., Jules,M., Aymerich,S., Radulescu,O., Declerck,N. and Royer,C.A. (2012) Reconciling molecular regulatory mechanisms with noise patterns of bacterial metabolic promoters in induced and repressed states. *Proc. Natl. Acad. Sci. U. S. A.*, **109**, 155–60.

190. Guiziou,S., Sauveplane,V., Chang,H.-J., Cler E,C., Declerck,N., Jules,M. and Bonnet,J. (2016) A part toolbox to tune genetic expression in Bacillus subtilis. *Nucleic Acids Res.*, **44**, 7495–7508.

191. Dorsey,S., Tollis,S., Cheng,J., Black,L., Notley,S., Tyers,M. and Royer,C.A. (2018) G1/S Transcription Factor Copy Number Is a Growth-Dependent Determinant of Cell Cycle Commitment in Yeast. *Cell Syst.*, **6**, 539–554.e11.

192. Brown,C.M., Dalal,R.B., Hebert,B., Digman,M.A., Horwitz,A.R. and Gratton,E. (2008) Raster image correlation spectroscopy (RICS) for measuring fast protein dynamics and concentrations with a commercial laser scanning confocal microscope. *J. Microsc.*, **229**, 78–91.

193. Rossow,M.J., Sasaki,J.M., Digman,M.A. and Gratton,E. (2010) Raster image correlation spectroscopy in live cells. *Nat. Protoc.*, **5**, 1761–1774.

194. Digman,M.A., Sengupta,P., Wiseman,P.W., Brown,C.M., Horwitz,A.R. and Gratton,E. (2005) Fluctuation Correlation Spectroscopy with a Laser-Scanning Microscope: Exploiting the Hidden Time Structure. *Biophys. J.*, **88**, L33–L36.

195. Blattner,F.R., Iii,G.P., Bloch,C.A., Perna,N.T., Burland,V., Riley,M., Collado-vides,J., Glasner,J.D., Rode,C.K., Mayhew,G.F., *et al.* (1997) The Complete Genome Sequence of Escherichia coli K-12. *Science (80-.).*, **277**, 1453–1462.

196. Bourges,A.C., Torres Montaguth,O.E., Ghosh,A., Tadesse,W.M., Declerck,N., Aertsen,A. and Royer,C.A. (2017) High pressure activation of the Mrr restriction endonuclease in Escherichia coli involves tetramer dissociation. *Nucleic Acids Res.*, **45**, 5323–5332.

197. Ferguson,M.L., Le,D., Jules,M., Aymerich,S. and Radulescu,O. (2012) Reconciling molecular regulatory mechanisms with noise patterns of bacterial metabolic promoters in induced and repressed states. *Proc. Natl. Acad. Sci.*, **109**, 155–160.

198. Ferguson,M.L., Le Coq,D., Jules,M., Aymerich,S., Declerck,N. and Royer,C.A. (2011) Absolute quantification of gene expression in individual bacterial cells using two-photon fluctuation microscopy. *Anal. Biochem.*, **419**, 250–259.

199. Schmidt,T.G. and Skerra,A. (2007) The Strep-tag system for one-step purification and high-affinity detection or capturing of proteins. *Nat. Protoc.*, **2**, 1528–1535.

200. Gratton,E. and Muller,J.D. (2003) High-Pressure Fluorescence Correlation Spectroscopy. *Biophys. J.*, **85**, 2711–2719.

201. Nicolini,C., Celli,A., Gratton,E. and Winter,R. (2006) Pressure tuning of the morphology of heterogeneous lipid vesicles: a two-photon-excitation fluorescence microscopy study. *Biophys. J.*, **91**, 2936–42.

202. Horton,J.R., Nugent,R.L., Li,A., Mabuchi,M.Y., Fomenkov,A., Cohen-Karni,D., Griggs,R.M., Zhang,X., Wilson,G.G., Zheng,Y., *et al.* (2014) Structure and mutagenesis of the DNA modification-dependent restriction endonuclease AspBHI. *Sci. Rep.*, **4**, 4246.

203. Horton,J.R., Mabuchi,M.Y., Cohen-Karni,D., Zhang,X., Griggs,R.M., Samaranayake,M., Roberts,R.J., Zheng,Y. and Cheng,X. (2012) Structure and cleavage activity of the tetrameric MspJI DNA modification-dependent restriction endonuclease. *Nucleic Acids Res.*, **40**, 9763–73.

204. Horton,J.R., Wang,H., Mabuchi,M.Y., Zhang,X., Roberts,R.J., Zheng,Y., Wilson,G.G. and Cheng,X. (2014) Modification-dependent restriction endonuclease, MspJI, flips 5-methylcytosine out of the DNA helix. *Nucleic Acids Res.*, **42**, 12092–101.

205. C. Shuyan Chen,§, André White,‖, John Love,⊥, John R. Murphy,⊥ and and Dagmar Ringe*,‖,# (2000) Methyl Groups of Thymine Bases Are Important for Nucleic Acid Recognition by DtxR†,‡. 10.1021/BI0009284.

206. Pace,C.N., Fu,H., Fryar,K.L., Landua,J., Trevino,S.R., Shirley,B.A., Hendricks,M.M., Iimura,S., Gajiwala,K., Scholtz,J.M., *et al.* (2011) Contribution of hydrophobic interactions to protein stability. *J. Mol. Biol.*, **408**, 514–28.

207. Yu,J., Zhou,Y., Tanaka,I. and Yao,M. (2010) Roll: a new algorithm for the detection of protein pockets and cavities with a rolling probe sphere. *Bioinformatics*, **26**, 46–52.

208. Horton,J.R., Mabuchi,M.Y., Cohen-karni,D., Zhang,X., Griggs,R.M., Samaranayake,M., Roberts,R.J., Zheng,Y. and Cheng,X. (2012) Structure and cleavage activity of the tetrameric MspJI DNA modification-dependent restriction endonuclease. *Nucleic Acids Res.*, **40**, 9763–9773.

209. Schneider,S., Paulsen,H., Reiter,K.C., Hinze,E., Schiene-Fischer,C. and Hübner,C.G. (2018) Single molecule FRET investigation of pressure-driven unfolding of cold shock protein A. *J. Chem. Phys.*, **148**, 123336.

210. Hashimoto,H., Shimizu,T., Imasaki,T., Kato,M., Shichijo,N., Kita,K. and Sato,M. (2004) Crystal Structures of Type II Restriction Endonuclease EcoO109I and Its Complex with Cognate DNA*. 10.1074/jbc.M411684200.

211. Sasnauskas,G., Zagorskaitė,E., Kauneckaitė,K., Tamulaitiene,G. and Siksnys,V. (2015) Structure-guided sequence specificity engineering of the modification-dependent restriction endonuclease LpnPI. *Nucleic Acids Res.*, **43**, 6144–55.

212. Murchie,A.I.H. and Lilley,D.M.J. (1989) Base methylation and local DNA helix stability: Effect on the kinetics of cruciform extrusion. *J. Mol. Biol.*, **205**, 593–602.